Novel Methods for Improving Fault Protection & Health Management within Advanced Aircraft Electrical Power Systems

Rory Telford

A thesis submitted for the degree of Doctor of Philosophy to

Institute for Energy and Environment

University of Strathclyde

April 2017

This thesis is the result of the author's original research. It has been composed by the author and has not been previously submitted for examination which has led to the award of a degree.

The copyright of this thesis belongs to the author under the terms of the United Kingdom Copyright Acts as qualified by University of Strathclyde Regulation 3.50. Due acknowledgement must always be made of the use of any material contained in, or derived from, this thesis.

Signed:

Date:

ABSTRACT

The more-electric aircraft (MEA) concept is widely viewed as the next evolutionary step towards enabling the industry goal of developing optimised, fuel efficient aircraft. MEA have an increased dependency on electrical energy for distribution to secondary systems and, in order to service this increased dependence, the electrical power systems (EPS) are more complex with increased voltage distribution levels, power conversion stages and safety critical components compared with their conventional counterparts. These complexities will only increase in future platforms as they further embrace the MEA concept - the migration to increasingly novel, critical and complex EPS will incur several development and integration challenges.

This thesis considers the fundamental challenge of maintaining high reliability standards within future aircraft EPS through the development of accurate and discriminative real-time protection systems which will react during fault conditions. Specifically, the thesis researches novel methods that improve real-time aircraft EPS protection and health management systems by 1) accurately diagnosing *degraded* faults before their progression to *critical* failure and 2) diagnosing faults that are difficult to detect using only conventional protection methods – in particular, series arc faults are considered.

Within future aircraft EPS, the volume of operational data is expected to significantly increase beyond that of the conventional systems; consequently, the thesis focuses on the use of data-driven, machine learning based methods, to enable these extended functionalities of the EPS protection and health management systems. The types of machine learning modelling techniques that were chosen are explained and justified. Conventional protection methods are described, including a discussion on the difficulties in using them to detect both degraded fault modes and arcing conditions. The necessity to detect these types of faults in an accurate and timely manner is also discussed.

One of the main contributions of the thesis is the proposal of the *EPSmart* method that can autonomously diagnose and isolate a multitude of degraded faults within an aircraft representative EPS. These degraded faults include intermittent and incipient conditions, which, in comparison to overcurrent faults, often lack the energy to be detected by conventional means. Early, and accurate, detection of these conditions will improve overall system health management and reliability and ensure safe operation of the aircraft.

Further contribution is the design of the *IntelArc* method that can detect series arc faults within direct current supplied systems. Accurate detection of series arc faults is extremely

challenging as, despite their presence being a serious fire hazard, they result in a decrease of load current. Although methods do exist for diagnosis of series arcing, there remain challenges with regards to accurate detection across different system configurations and operating conditions. The thesis shows the potential for IntelArc to provide accurate detection across a variety of configurations and operating conditions.

While the thesis only describes the initial development of these novel methods, the significant conclusions are that application testing has shown the potential for them to enhance real-time network protection, fault tolerance and health management of aircraft EPS through detection of degraded fault and arcing conditions.

TABLE OF CONTENTS

LIST OF FIGURES

LIST OF TABLES

GLOSSARY OF ABBREVIATIONS

AC	Alternating Current
ADAPT	Advanced Diagnostic and Prognostic Testbed
ADL	ADAPT Lite
AEA	All-Electric Aircraft
AFCB	Arc Fault Circuit Breaker
AFD	Arc Fault Diagnosis
ANN	Neural Network
APU	Auxiliary Power Unit
BIC	Bayesian Information Criterion
BN	Bayesian Network
BPCU	Bus Power Control Unit
BTB	Bus Tie Breaker
CB	Circuit Breaker
CDF	Cumulative Distribution Function
CF	Constant Frequency
CSD	Constant Speed Drive
CT	Current Transformer
DC	Direct Current
DGM	Directed Graphical Model
DWT	Discrete Wavelet Transform
ECS	Environmental Control System
ELCU	Electronic Load Control Unit
EM	Expectation Maximisation
EMI	Electromagnetic Interference
EPS	Electrical Power System
FDI	Fault Diagnosis and Isolation
FFT	Fast Fourier Transform
FPA	Fault Parameter Algorithm
FT	Fourier Transform
FTC	Fault Tolerant Control
GCB	Generator Circuit Breaker
GCU	Generator Control Unit
GMM	Gaussian Mixture Model
HMM	Hidden Markov Model
HMS	Health Management Systems
HVDC	High Voltage Direct Current
LL	Log Likelihood

MAP	Maximum a Posteriori
MEA	More-Electric Aircraft
MEE	More-Electric Engine
ML	Machine Learning
MTBF	Mean Time Between Failure
PE	Power Electronics
PMG	Permanent Magnet Generator
POA	Power Optimised Aircraft
PPDS	Primary Power Distribution System
QTA	Qualitative Trend Analysis
RAT	Ram Air Turbine
RMS	Root Mean Square
RPDU	Remote Power Distribution Unit
SCADA	Supervisory Control and Data Acquisition
SPDS	Secondary Power Distribution System
SSPC	Solid State Power Controller
SVM	Support Vector Machine
TRU	Transformer Rectifier Unit
UAV	Unmanned Aerial Vehicles
VA	Viterbi Algorithm
VF	Variable Frequency
WT	Wavelet Transform

ACKNOWLEDGEMENTS

I would like to firstly thank Dr Stuart Galloway for giving me the opportunity to undertake this PhD. His guidance throughout is much appreciated, and the anecdotal asides and random conversations that ensued most of our meetings has helped to keep sanity in check.

Sincere gratitude also goes out to colleagues past and present within the AES group for making this much more enjoyable than it otherwise would have been. Particular thanks go to the long standing members of the aircraft electrical systems team as well as Dr Bruce Stephen and Dr Ian Elders for their help throughout various stages of this work.

The biggest thank you of all is reserved for Susie – if it wasn't for your encouragement throughout the years this thesis would never have been completed.

Last, but not least, I wish to thank my parents, David and Laura, for their support and for allowing me to study for all these years.

1. Introduction

Since the notion of utilising machines to fly was first realised, designers and engineers have continually strived to advance and improve the air vehicles, or *aircraft*, that enable this capability. The 20th century saw significant development and evolution of aircraft, from pioneers the Wright brothers developing the first successful heavier than air machine in 1903, through to the inception of the jet engine during World War II, and the subsequent dawn of the jet age and rise in commercial aviation in the 1950's. The latter part of the century saw a shift of focus, from increasing the speed and distance of flight, towards an evolution of aircraft design, manufacturing techniques and avionics.

Economic and social incentives, coupled with enabling technology, have been the main drivers for the mass changes that have occurred within aircraft since the jet age. Such factors have culminated in modern aircraft, most notably *Airbus' 380* (A380) and *Boeing's 787 Dreamliner* (B787), being able to carry up to 850 passengers with flight ranges of 15,700 km and wingspans of 80m. During 2012, civilian aircraft transported an estimated 2.9 billion passengers worldwide [1].

Evidence of the next progression in development can be found when considering the reformed secondary power system architectures of Airbus' and Boeings' flagship aircraft. The conventional form of providing secondary power through combinations of pneumatic, hydraulic and electrical energy has been converted in the A380 and B787 to a system that is

more dependent on utilising electrical energy for distribution to aircraft subsystems. This alternative method of power distribution means such aircraft can be termed a *more-electric aircraft* (MEA) [2, 3, 4].

Figure 1-1 illustrates the electrical generator power ratings of various aircraft along with their associated maximum take-off weights (ToW). The A380 and, in particular, the B787 have a greater total generating capacity than their predecessors; with consideration to ToW, it could be surmised that the A380 is *partially* more-electric whereas the B787 has made significant advancements. Nevertheless, the migration from constant frequency (CF) to variable frequency (VF) systems, as well as higher operating voltages, has meant that both aircraft have gained more-electric status. The A380 and B787 are revolutionary in that they are the first civil MEA to enter service and, in so doing, confirmed that the future for aircraft is electrical.
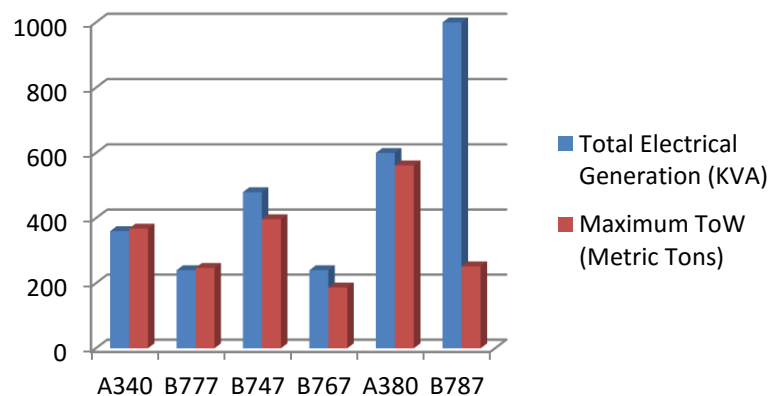
Figure 1-1: Electrical Generator rating and Maximum ToW of various commercial aircraft

The MEA principle is not a new idea – indeed, looking as far back as World War II, military aircraft used electrical power for functions that, according to conventional wisdom, would be powered by other means [5]. Despite this precedent, the lack of electrical power generation capabilities and the volume requirements of the power conditioning equipment meant that efforts were focused on providing secondary power on civil aircraft with a combination of sources. Up to the late 1970's, electrical power was restricted to avionics and utility functions, with hydraulics used for most actuation functions and pneumatics for air conditioning/pressurisation and ice protection.

However, increasing pressure on airline economics due to rising fuel prices and increased competition through low cost carriers, incentivised manufacturers to further optimise the operational efficiency of aircraft. The conventional secondary systems posed a number of challenges with respect to optimisation, mainly due to the complexities and

interdependencies that existed within the hybrid networks. These issues, coupled with technological advancements in power electronics (PE), fault tolerant electrical machines and electrically driven primary flight control actuator systems [6, 7] have enabled the MEA concept to begin to be realised within the B787 and A380.

There are various reasons *why* MEA are desirable, including; improved fuel consumption and efficiency; elimination/reduction of inefficient and costly pneumatic and hydraulic systems [8]; improved reliability [9]; and an increased potential for global optimisation of the secondary power system. The main, high-level objectives of aircraft system design are to reduce overall weight, reduce operational cost and increase reliability - the MEA option is widely viewed as the most viable and attractive option for meeting such objectives.

A number of research projects dedicated to addressing the challenge of meeting these objectives have been established in both Europe and the United States, including; Northrop/Grumman′s MADMEL project [10], the Power Optimised Aircraft (POA) programme [11] and the Totally Integrated More Electric Systems (TIMES) programme [12]. POA confirmed the feasibility of MEA and showed more focus had to be placed on management of electrical loads and enabling technologies. The TIMES programme integrated the outputs of various standalone generation, actuation and load enabling technology programmes to formulate their collective impact at a system level. The objective of MADMEL was to design and demonstrate an advanced electrical generation and distribution system for MEA; the project developed a ground demonstrator that highlighted a particular architecture that provides fail-op fault tolerance for mission critical loads.

The perceived benefits of the MEA lead to the logical conclusion that eventually the *all-electric aircraft* (AEA) will be implemented i.e. secondary distribution networks that are fully composed of electrical systems [13]. While this eventuality is realistic, the relatively static nature of the aerospace industry dictates that such advancements, at least within civil aircraft, would not be likely for at least another three generations [14]. The increasing trend of unmanned aerial vehicles (UAV) for military applications, and the less stringent safety standards they entail, has facilitated deeper opportunities for the AEA concept to be developed, implemented and tested [43]. This aids the acceleration of the technologies and architectures that will eventually be implemented within such concepts.

1.1 More Electric Aircraft Development and Integration Challenges

Migrating to increasingly novel, complex and critical EPS architectures will incur several development and integration challenges. This thesis considers two fundamental research challenges pertinent to the MEA:

1. Maintaining reliability standards in EPS with increased complexity and diversity of fault modes.

2. Fault protection in higher voltage, DC systems.

The MEA/AEA future poses significant challenges in terms of developing electrical systems that fulfil the unique functions required by aircraft. Reliability is at the forefront of system development, and it is essential that components, both individually and collectively, perform with minimal probability of failure. Aircraft reliability standards [15] dictate that safety critical systems on-board civil aircraft have a probability of failure in the order of 1×10^{-9} per flight hour, equating to a mean time between failure (MTBF) for an aircraft fleet of 1 billion flight hours.

The MEA has led to a greater dependence on electrical distribution for the provision of power to such safety critical systems. Accordingly, the complexity of electrical power systems (EPS) has increased, with a diversity of power conversion stages and more demanding loads now present [16]. As future aircraft will further utilise EPS to meet functionality, this complexity and dependence will continue to increase. A key challenge associated with the increased dependency on electrical energy in aircraft is how the EPS health management system (HMS), which monitors and responds to undesirable network conditions, can be enhanced to enable fault tolerance [17] within more diverse and demanding systems. Greater EPS complexity will not only increase the number of failure modes which have to be managed but also introduce new faults which were not readily considered within conventional EPS. Also, the manner in which HMS manage, process and interpret the increased volumes of system data[1] is imperative for the real-time detection of system faults and trends, implementing control system reconfigurations and, generally, providing optimally reliable and secure electrical systems [18]. This motivates research for challenge 1.

In considering the second challenge, EPS protection and control is a critical aspect of HMS. The MEA evolution has led to growing research in the protection domain, particularly in the areas of direct current (DC) protection and solid-state power controllers (SSPC). DC protection is inherently more difficult to achieve than alternating current (AC) protection, as the lack of a natural voltage or current zero crossing affects circuit breaker (CB) operation during fault conditions [35]. SSPC technology is seen as the preferred option for the replacement of electromechanical circuit breakers (CB), which offer poor performance at higher levels of DC voltage [19].

---

[1] The B787 transmits 28 times more data than the B777 and it is estimated there will be a 14,000% increase in the total amount of data being transmitted from global fleets by 2030 [18].

The issue of DC arc fault protection has also become prevalent in the aerospace industry with the migration to higher magnitude DC voltages and the fact that traditional overcurrent protection practices do not detect such anomalies [36]. Electrical arcing is a product of the breakdown of wire insulation - breakdown can occur with exposure to moisture, vibration and chafing against other wires/hard surfaces or simply through the ageing process where wires become brittle and crack. Damaged wiring is extremely difficult to detect, and the resulting arcs and electromagnetic emissions pose a major concern to aircraft safety. Two separate fatal accidents – *Swissair 111* near Nova Scotia in 1998 and *TWA 800* off Long Island in 1996 – attributed faulty wiring as the cause for both aircraft grounding [37].

Traditional CBs are heat sensitive elements that trip only when a large current passes through the circuit long enough to heat the element. The duration of arcing faults may only be 1.25 milliseconds (ms), with a series of events lasting 25-30ms, and are invariably too fleeting to trip ordinary CBs despite having the ability to cause catastrophic local damage to wires - fires have been known to break out with the breaker still intact [38]. Arc Fault Circuit Breaker (AFCB) technology has been developed [19]. AFCB operation involves the use of sophisticated electronics to sample the current flow through wires at sub-millisecond intervals and extract arc fault signatures using both time-domain and frequency domain filtering. Despite this technology improving security levels and limiting the damage caused by arcing, these devices suffer similar monitoring and control problems as the CB, and can only be applied within AC power distribution systems.

Arc fault detection issues highlight that, with the migration to alternative methods of electrical power distribution throughout aircraft which utilise higher operating voltages and place greater emphasis on DC systems, there is the requirement to develop advanced protection methods that can overcome shortfalls in conventional practices. This motivates research on Challenge 2.

1.2 Intelligent Fault Diagnosis and Isolation for Aircraft EPS

With these two research challenges in mind, this thesis researches methods that advance EPS protection systems and maintain the high overall reliability standards through autonomous and accurate identification of various aircraft EPS faults. In particular, the thesis develops and evaluates the use of new, *intelligent* fault diagnostic and isolation (FDI) methods [39] to:

1) Diagnose multiple degraded fault conditions prior to their progression to critical failure – this includes autonomous diagnosis of intermittent and incipient faults, as well as distinguishing between faults in the monitored system and sensor failures.

2) Diagnose 'difficult to detect' series arc faults within DC supplied systems – diagnosis methods should be generalised to react to such faults across a range of operating conditions.

Fundamentally, intelligent methods have the ability to perform tasks normally requiring human cognition and knowledge. There is a wide variety of relevant intelligent FDI applications within the general EPS domain. Typical applications comprise:

- The condition monitoring, diagnostics and prognostics of transformers [21], electrical machines [22] and rotating plant assets [23].

- Real-time health monitoring of distribution systems with automated anomaly detection and diagnosis using supervisory control and data acquisition (SCADA) telemetry data [24, 25].

With respect to aircraft EPS, intelligent systems have previously been proposed to monitor system behaviour and aid both real-time network operation [20, 26] and the initial design process [27]. Various stages of aircraft operation have to be considered with the integration of intelligent FDI systems, which include: flight operation, maintenance, logistics and fleet management. In order to positively impact each stage of operation, there is a variety of top-level requirements that intelligent FDI based systems have to meet. These requirements are outlined as follows:

- *Minimise false alarm rates* – this is critical if an FDI method is to be effective. Even low false alarm rates will induce an extra burden due to the need to evaluate the alarm while also dealing with recovery options.

- *Specific fault identification/location* – this is essential for efficient allocation of the resources needed to confirm and rectify a fault.

- *Earliest warning of failure* – information on the likelihood of impending failure is desirable.

- *Minimise information overload* – it is essential for FDI methods to eliminate frequent fault messages, or large blocks of alternate messages. In this sense, some form of prioritizing and filtering is required. An intelligent method will also need to distinguish between critical and non-critical faults over both immediate and long-term time frames. The need to distinguish between hardware faults in the monitoring system itself (i.e. sensors) and faults within the base system is another necessity.

Theoretically, the extension of intelligent FDI to aircraft EPS is based on techniques that can automatically isolate the source(s) of system malfunction. Techniques typically collect information on system behaviour using measurements, tests and other information sources

(e.g. observed symptoms), and then analyse this information to determine *if* and *why* system anomalies are present. Various methods exist for collating and analysing the information; methods are usually classified as either model based [29] or data based [28].

This thesis concentrates on the data based intelligent FDI methods. More specifically, the application of *machine learning* techniques [30] to the domain of aircraft EPS health monitoring is considered. The thesis focuses on intelligent data based methods as they have the potential to simplify health management in EPS that produce large amounts of operational data. Critically, the thesis attempts to evaluate how intelligent FDI methods based on machine learning techniques can enhance the understanding of complex EPS dynamics throughout normal and faulted operating conditions to improve health management and fault protection.

1.3 Research Objectives

With the ever growing complexity and criticality of aircraft EPS, there comes the need to consider the development of intelligent FDI methods which will aid system health monitoring and real-time protection as well as automatically interpret system status through the analysis of data. The objectives of the research described in this thesis were to determine if, and how, intelligent data based FDI methods operating within the unique aircraft EPS context can:

1. Manage historical system data to develop protection systems that can accurately detect and diagnose both critical and degraded system anomalies to supplement and improve the protection of aircraft EPS. The diagnosis of degraded faults has the potential to improve system reliability by ensuring corrective remedies are pursued prior to the development of critical network failures.

2. Handle a multitude of both nominal operating and complex system failure modes in order to quickly detect anomalies and therefore aid both understanding of network conditions and fault management. This includes the implementation of scalable intelligent methods that can be updated to handle additional fault modes.

3. Fill the gap where conventional electrical protection practices fall short in order to produce optimally reliable, fault tolerant MEA EPS with highly accurate FDI. Specifically, the detection and isolation of intermittent and self-sustained DC arc faults are considered.

Intelligent FDI methods that have the potential to meet these objectives can be based on an array of different data based machine learning techniques. These include artificial neural networks (ANN) [31], support vector machines (SVM) [32], Bayesian networks (BN) [33]

and hidden Markov models (HMM) [34]. The majority of these techniques are classically applied for speech, handwriting and gesture recognition [40, 41]. However, further theoretical evolution and exposure has seen applications expand to mechanical, electrical and process engineering fields [34, 42]. The thesis will consider machine learning techniques that would be most suitable to meet the objectives described above.

The form of data used for the development of novel methods proposed within the thesis included both EPS test bed datasets as well as datasets synthesised through model simulations. A significant development issue is the extraction of unique fault signatures from the data. This *feature extraction* stage is imperative for accurate fault discrimination, particularly when multiple fault modes exist. As such, a further objective of the research is to determine optimum features from data for accurate fault diagnosis.

The ultimate objective of the work was to develop accurate and scalable intelligent EPS FDI methods which can assist health management and improve real-time network protection through the diagnosis of critical and degraded fault modes as well as faults which are difficult to detect using conventional protection practices.

1.4 Summary of Key Contributions

A number of contributions are made within the thesis. These are outlined as follows.

1) Degraded EPS fault conditions, such as intermittent and incipient failures, often lack the energy to be detected by conventional protection methods. Detection and diagnosis of these faults prior to critical failure is important for maintaining reliable operation as well as improving health management and maintenance scheduling. This thesis describes the design and development of *EPSmart*, a novel FDI method that provides autonomous diagnosis of multiple degraded system faults, including sensor failures, within compact, hybrid AC/DC aircraft EPS. A published journal article [44] is an outcome of this contribution.

2) Despite the catastrophic damage series arc faults have the potential to cause, the reduction of electrical current during such events means that traditional protection methods and overcurrent protection devices generally do not detect their occurrence. This thesis describes the design and development of a novel series DC arc FDI method, *IntelArc*, for application to aircraft DC systems. The thesis demonstrates that IntelArc is capable of accurately discriminating between arc fault onset and normal network transients. The method is generalised to be implemented in systems

where a variety of DC voltage distribution levels, sources and loads are present. An accepted journal article [45] is an outcome of this contribution.

3) Resolving discriminative features is fundamental to the design of accurate series arc FDI methods that minimise false positive/negative diagnoses. This thesis determines discriminative time-frequency domain and time domain features that are used within IntelArc to optimise diagnostic accuracy. Features were selected through analysing and comparing the distribution of extracted features across different nominal and faulted system conditions.

4) The relative lack of historical fault data poses a significant problem throughout the development of data-driven FDI methods. This thesis demonstrates feature extraction and sensor fusion techniques that enable EPSmart to provide accurate FDI of multiple system anomalies when fault data is limited. Explorative analysis of multi-dimensional sensor data enabled significant fault features to be maintained for system development. This analysis was also used to identify and discard redundant features within the data, thus simplifying both method development and application.

5) The thesis establishes the shortcomings of conventional protection methods for diagnosis of degraded and series arc fault conditions and outlines the requirement for intelligent methods to improve real-time protection and health management systems. A comprehensive review of existing intelligent FDI techniques and methods is provided in the thesis, with specific focus on their application to diagnosing faults within an aircraft system domain.

6) Construction of a DC series arc fault simulation model is described in the thesis. The model was utilised for the generation of synthetic data for use in development of the series DC arc fault detection system. The model captures the complex characteristics of series arcing phenomenon and can be implemented within any DC electrical system model. Model accuracy was validated by comparing model outputs with previous studies described in the literature.

1.5 Thesis Outline

There are a total of 7 chapters in the thesis. An introduction to the work has been provided in this chapter.

Chapter 2 introduces aircraft EPS architectures, components and technologies which will be referred to throughout the thesis. Conventional protection practices during fault conditions, including the devices used to isolate faults, are described. A discussion on EPS fault formation, and the different types of faults within aircraft EPS, is provided. The difficulties in protecting against a variety of degraded faults and arc faults using only the conventional protection methods are established. The chapter emphasises the motivation for development of intelligent FDI methods within MEA EPS to detect these types of faults and improve overall network protection and health management.

Chapter 3 describes intelligent FDI concepts and techniques. The chapter summarises model based and data based FDI before going on to discuss machine learning techniques in detail. Attributes of machine learning techniques are compared and the reasons for selecting certain techniques to meet the research objectives of this thesis are outlined. A review of previous aircraft FDI methods proposed within the literature, including systems applied to NASAs ADAPT network, is provided. Relevant machine learning based FDI methods applied to the general EPS domain are also summarised.

Chapter 4 describes arc faults in significant detail. This includes a description of their electrical characteristics through a summary of numerous previous studies that have attempted to define the complex phenomenon. A series DC arc fault simulation model that was developed using MATLAB′s *Simulink* and used for generation of synthetic fault data is described. This model is validated by comparing its outputs with the previous studies and models. A review of existing arc fault detection methods is then provided, including the benefits and limitations of each.

Chapter 5 details the two novel FDI methods that are the main outcome of the work of this thesis. EPSmart is developed for autonomous FDI of a multitude of critical and degraded fault modes, while IntelArc is developed for FDI of series DC arc faults. The main aspects, and challenges, of developing each method are discussed, including; describing EPS data used throughout development; data processing and analysis; feature extraction and selection; overcoming a lack of available fault data; sensor fusion; on-line application issues; and model training. Alongside the proposition of the two FDI methods, another main contribution of Chapter 5 is the determination of optimal time-frequency domain features for accurate diagnosis of series DC arc faults.

Chapter 6 outlines four separate case studies that were used to test the application and accuracy of EPSmart and IntelArc. The first case study describes applying EPSmart for autonomous FDI within NASA′s ADAPT network; this includes testing its ability to diagnose intermittent and incipient fault modes as well as discriminate between faults in the underlying system and sensor faults. The second case study describes application testing of IntelArc for FDI of sustained series DC arc fault events while the third case study describes testing the ability of IntelArc to diagnose intermittent arcing events. The fourth case study experimentally validates IntelArc on a DC testbed. Results of each case study are presented and analysed, and recommendations for practical application of the proposed methods are provided.

Finally, Chapter 7 draws together the conclusions, describes possible avenues for future work and highlights the contributions of this thesis.

1.6 Publications

The following publications have been completed during the course of this PhD:

Journal Articles

R. Telford, S. Galloway, B. Stephen and I. Elders, 'Diagnosis of series DC arc faults: A machine learning approach', IEEE Transactions on Industrial Informatics, Advance Online Publication, doi: 10.1109/TII.2016.2633335

R. Telford and S. Galloway, 'Fault classification and diagnostic system for unmanned aerial vehicles based on hidden Markov models', IET Electrical Systems in Transportation, vol. 5, no. 3, pp. 103-111, September 2015

Conference Papers

R. Telford, C. Jones, P. Norman and G. Burt, 'Analysis tool for initial high level assessment of candidate more-electric aircraft architectures', *SAE Technical Paper*, September 2016

R. Telford, S. Galloway and G. Burt, 'Evaluating the reliability and availability of more-electric aircraft power systems', in *Universities Power Engineering Conference*, London, UK, Sep. 2012, doi: 10.1109/UPEC.2012.6398542

2. AIRCRAFT ELECTRICAL POWER SYSTEMS: ARCHITECTURES, TECHNOLOGIES & PROTECTION

The requirement for future aircraft designs to have optimal operational efficiency, and the proposed migration to MEA (and eventually AEA) as a means of fulfilling this requirement, will inevitably result in more complex, demanding and safety critical EPS. This chapter introduces aircraft EPS and familiarises the reader with system designs and the elements that compose such systems.

The chapter begins with a general overview of aircraft secondary power systems, where conventional topologies through to present day more-electric distribution topologies are discussed. A review is then provided of MEA enabling technological advances in electrical generation sources, loads, power conversion, and how these sub-systems combine to form advanced EPS distribution architectures.

The chapter also reviews conventional methods for ensuring fault tolerance within EPS, with discussions on the HMS in general as well as the conventional philosophies and devices used to protect the network throughout fault conditions. Fault formation and the various types of network faults that impact operation are also described and the chapter concludes by

elaborating on the difficulties of using conventional methods to detect and isolate particular faults.

2.1 Aircraft Secondary Power System Overview

The majority of power – or 'primary power' - on an aircraft is used in the form of fuel to produce the required thrust from the engines to propel the aircraft. 'Secondary power' refers to all other non-propulsive power systems on board aircraft. Conventionally secondary power systems are driven by a combination of different energy sources including hydraulic, pneumatic, electrical and mechanical [46]. Secondary power is drawn from the aircraft's main engines[2] in two forms:

1) Bleed air is tapped from one or more points along the engine compressor to provide pneumatic power.

2) Drive Shafts, from the engines high-pressure shaft, drive an accessory gearbox where electrical generators and hydraulic pumps are mounted.

A simplified schematic of a generic twin engine conventional secondary power distribution system (SPDS) is shown in Figure 2-1. This form of distribution, with three separate types of power, was standardized in both civil and military aircraft when the increasing speed and size of aircraft meant that 'power' functions, which previously could be manually operated by pilots, had to be automated [48]. In these conventional SPDS, hydraulics is generally used for most actuation functions, pneumatics for air conditioning/ pressurisation and electrics for avionics and utility functions.

---

[2] When the main engines are non-operational, power can also be supplied by an auxiliary power unit (APU), an external ground power unit (GPU) or a ram-air turbine (RAT).
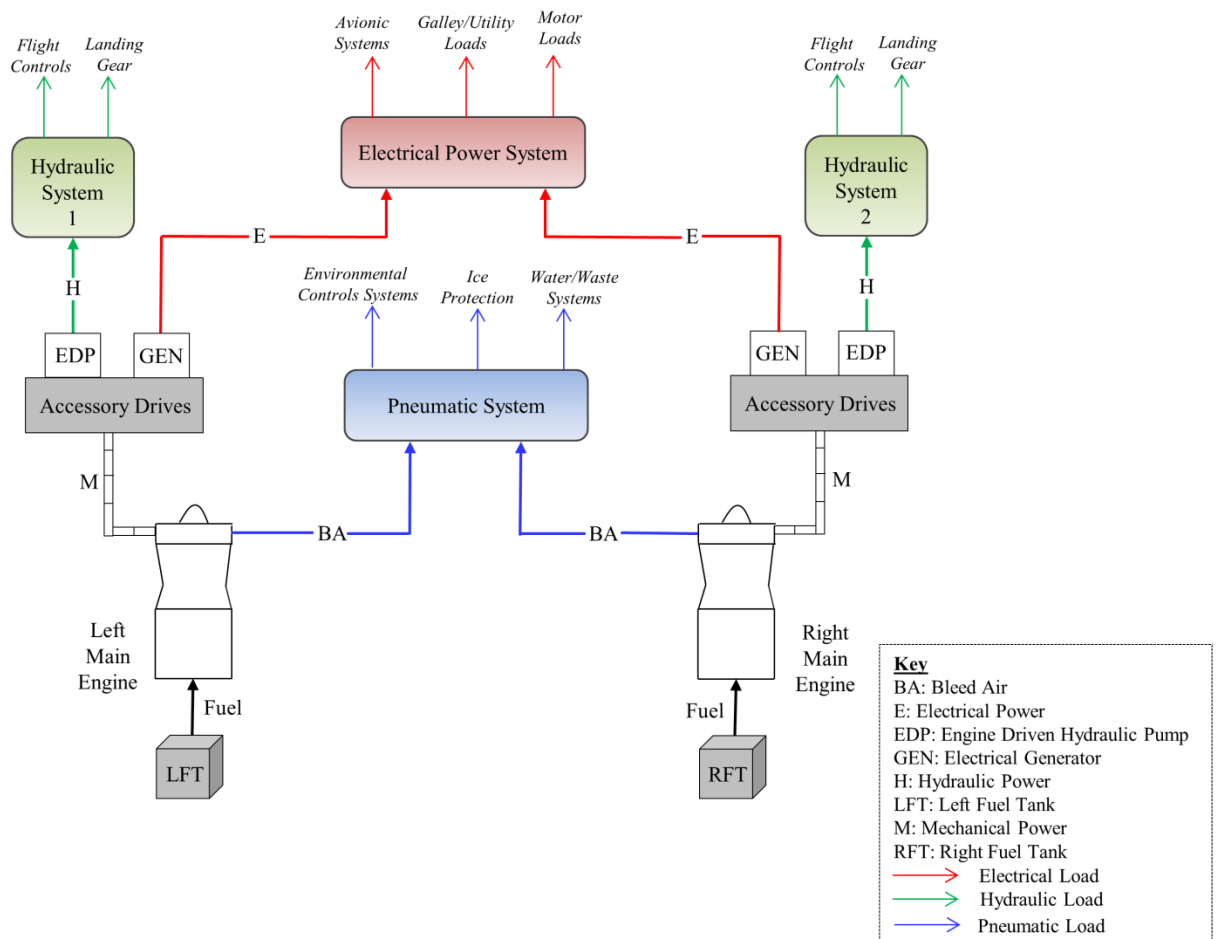
Figure 2-1: Simplified Schematic of a conventional Aircraft Secondary Power Distribution System

The hybrid distribution system illustrated in Figure 2-1 shows the main users of secondary power throughout the aircraft, which include:

- Environmental Control Systems
- Ice & Rain Protection
- Landing Gear
- Primary and Secondary Flight Controls
- Avionics (e.g. navigation and communication systems)
- Galley loads (e.g. entertainment systems)

The pneumatic and hydraulic systems within conventional SPDS are summarised in Appendix D. The following section describes aircraft EPS to highlight the various features unique to the aircraft environment. A summary of the main drivers and circumstances that have dictated a shift from conventional to more-electric SPDS is also provided in Section 2.3.1.

2.2 Electrical Distribution System

There has been significant evolution of electrical distribution systems since the beginning of the jet age. Typical systems of the 1940s and 50s's comprised 28VDC levels distributing ~12kW of power from two separate engines. The changes since this period have been marked, with an overall increase in both voltage distribution levels and power extracted from the main engines – as an example, the A380 has four main engine driven generators rated at 150 kVA each.

The next electrical system evolution has come in the form of the MEA, where significant changes, in terms of both demand and architecture, have been implemented within the EPS. This sub-section provides an introduction to aircraft EPS and describes both system elements and the main users of electrical power. Building upon this introduction, the various motivations and drivers for MEA adoption and the resultant EPS advancements that will entail, are outlined.

2.2.1 Conventional Aircraft EPS

The design and operation of Aircraft EPS is split into four inter-connected sub-systems [46]:

- Power Generation
- Primary power distribution and protection
- Power conversion and energy storage
- Secondary power distribution and protection

A generic EPS architecture in terms of each constituent sub-system is illustrated in Figure 2-2. A summary of each sub-system is provided in the following. Refer to Appendix D for a detailed example of the Boeing 777 EPS.
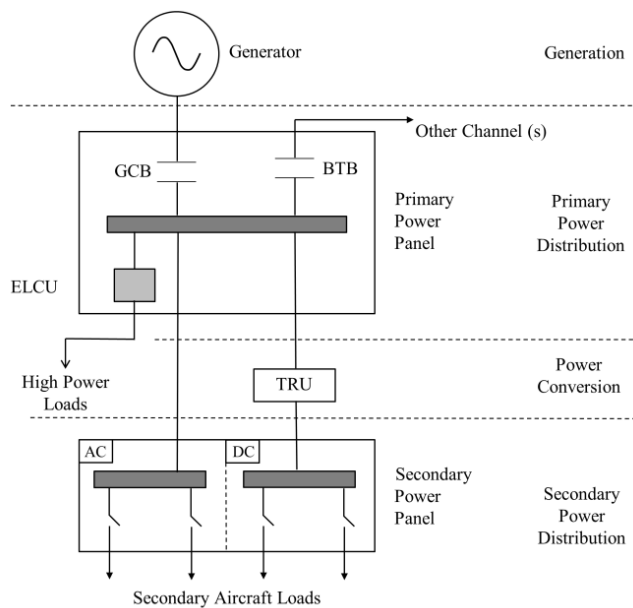
Figure 2-2: Generic Conventional Aircraft EPS architecture

2.2.1.1 Power Generation

Electrical power can be generated in both DC and AC forms. DC generators are typically self-excited, where energy is generated using electro-magnets, and supply a regulated 28VDC output via an electrical commutator. DC generation is only preferable within smaller aircraft with minimal power requirements and, as such, was phased out with the introduction of larger scale aircraft.

AC generation is favoured within larger, more power demanding vehicles. AC generators are driven from the aircraft's main engines and provide sine waves of rated voltage and constant frequency (CF) [47]. Nominally, AC power is three-phase with phase voltage levels of 115VAC (200VAC line-to-line, star connected) at 400Hz. CF voltage is attained using compound generators, where variable frequency, variable voltage power is converted into regulated CF constant voltage power. Compound generators contain several complex conversion stages. These stages include raw power being generated directly from the engine's variable speed drive using permanent magnet generators (PMG). This raw power is then used to provide DC excitation current, from which a frequency regulated AC voltage is induced, and used to supply the aircraft systems. Other means of providing CF power include integrated drive generators (IDG)[48], where the variable speed engine shaft is converted to constant speed using automatic gearboxes. The constant speed shaft then directly drives an electrical generator, which outputs CF electrical power.

The various sources of electrical power are described in Appendix D.

2.2.1.2 Primary Power Distribution System

The primary power distribution system (PPDS) accepts the electrical generation sources as input. In civil aircraft, these sources include: the main engine driven generators, alternate backup generators in the event of failure, APU and ground power, and the RAT generator in emergency situations. These sources supply power to a primary distribution busbar. The PPDS manages and controls the input to the primary busbar by using magnetically latched power contactors (generator circuit breakers (GCB)) to switch between alternate sources either during generator fault conditions, or when paralleling generators throughout normal operating periods.

The PPDS also controls the supply of power to high rated loads (typically defined as > 7 kVA) which are connected to the primary busbar. Electronic load control units (ELCU) are connected between the busbar and loads for undertaking the high current switching. The ELCUs also perform protection functions, using current transformers to detect and isolate the loads from overcurrents.

2.2.1.3 Power Conversion and Energy Storage

The PPDS functions not only to supply high power loads, but also to further distribute energy to secondary distribution systems. To supply loads throughout the aircraft that operate with different power ratings, it is necessary to convert the power distributed by the PPDS from one level to another. The PPDS is directly supplied with 115VAC from the main generators within the aircraft. Generally, this voltage is converted to different levels with the use of converting units. Such operations are generally described as follows:

- Conversion from 115VAC to 28VDC using transformer rectifier units (TRU)[49]. TRU's convert three phase AC power to DC power. Often, the output voltage is not regulated to 28VDC, and voltage may deviate depending on load requirements.
- Conversion from 115VAC to 26VAC. This AC conversion stage uses auto transformers to step-down the voltage.

Further power conversion functions involve the charging of, and energy extraction from, the battery system. The battery acts as an electrical storage medium which is independent of the primary generation sources [50]. It provides additional power for both system start-up and during emergency conditions while alternative sources are brought online. It also assists in damping load transients to enhance power quality during normal switching events. Battery chargers maintain the state of charge throughout flight. The chargers are similar to TRU's, where 115VAC is converted to the 28VDC charging voltage.

When acting as a source of start-up and/or backup power, conversion of the 28VDC battery output back to 115VAC is required. Inverter units undertake this DC-AC conversion stage, where a single phase AC voltage is output - in civil applications, this backup AC power is used as a source for critical flight instruments. Inverter technology development has meant that conversion is now realised with semi-conductors rapidly switching to produce a synthesised AC waveform [51].

2.2.1.4 Electrical Secondary Power Distribution System

The electrical SPDS ensures the correct provision of power from the secondary busbars to medium and low rated electrical loads. This includes both the switching of power to meet the systems functional requirements and the protection of circuits in the event of electrical overloads. Relays are used for switching operations in the electrical SPDS where currents do not exceed 20A – these operate in a similar manner to the high power contactors in the PPDS although are lighter, simpler and less expensive. In low power applications, where load current is <<20A, simple switches may be used for switching functions.

Circuit breakers (CBs) protect the loads from over currents. These are graded to trip according to the current carrying capacity of nominal operation within each circuit, and there may be as many as 500-600 utilised throughout the aircraft [46]. The CBs operate by mechanically opening contacts when an overcurrent is detected, thus ensuring power is removed from the circuit. Solid state power controllers (SPPC), which combine the function of relays and CBs, are deemed as viable alternatives for the provision of both load switching and protection functionality [19]. Higher trip accuracy and the elimination of mechanical switching are the main advantages of SSPC over the traditional CB and relay.

The various types of electrical loads within conventional EPS are described in detail in Appendix D.

2.3 More Electric Aircraft Concepts and Technologies

The operation and design of conventional aircraft SPDS, which consist of combinations of pneumatic, hydraulic and electrical forms of distribution, have been described. The MEA has also previously been briefly discussed. This section aims to fully introduce the MEA in terms of why the concept has been pursued, how MEA SPDS differ from the conventional systems, and what are the main advantages of its adoption.

2.3.1 Why the need for Change?

Transportation as a whole is estimated to be responsible for over 20% of the world's CO_2 emissions. The Intergovernmental Panel on Climate Change claims that global aviation contributes 2% of total CO_2 discharges caused by human activities [52]. Despite the relatively small output caused by aviation, emissions from high altitude are deemed to have a particularly damaging effect on the environment. Accordingly, the Advisory Council for Aeronautics Research in Europe has set several goals to be achieved by 2020 for air transportation [53]. These include: a 50% reduction of CO_2 emissions through decreased fuel burn, an 80% reduction in N_2O emissions; a 50% reduction of external noise, and a green product life cycle in terms of design, manufacturing, maintenance and disposal [54]. These targets have resulted in the aerospace industry facing significant challenges to drastically improve aircraft fuel efficiency and emissions [55].

In order to address these challenges and meet designated targets, the conventional design and operation of aircraft is no longer deemed viable for future generations of aircraft, and alternative solutions are required. Although the primary propulsion system of an aircraft consumes ~ 40MW power, improving non-propulsive SPDS efficiency, which consumes a comparatively less ~ 1.7MW of power[3] [56], is still vital to achieving these targets. A promising solution to the improvement of aircrafts SPDS efficiency is to remove the need for on-engine hydraulic power generation and bleed air off-takes. Hydraulic power systems tend to be complex, heavy and maintenance intensive while the use of bleed air increases fuel consumption as high-speed air, primarily used for producing thrust from the engines, is diverted for environmental control system (ECS) and anti/de-icing functions.

This significant SPDS redesign would require all power off-takes to be electrical in nature – hence the term *all electric aircraft*. As mentioned in Chapter 1, the AEA concept is not new and was previously considered by military aircraft designers in World War II. However, until recently, the lack of electrical generation capability and volume of power conditioning equipment which is required rendered the concept unfeasible. Since the 1980's and the introduction of a variety of research projects [13, 57, 58] advancements in enabling technology have allowed incremental steps towards the AEA goal. As such, the B787 and A380 MEA are examples where bleed air off takes and hydraulic generation have been reduced, but not entirely eliminated.

It should be considered at this point that the AEA/MEA notion is not simply organising the aircraft in a different manner. The concept aims to implement more energy efficient methods

---

[3] Power consumption figures for aircraft relative to the size of A330 or B777.

of converting and distributing power across all non-propulsion subsystems – realising this will have a far reaching effect upon overall aircraft performance [59].

2.3.2 Benefits of Electrical Power

Historically there has been a desire to use electrical power as the motive force for all non-propulsion systems [46]. The disadvantages of hydraulic and bleed air power distribution were briefly discussed in the previous section. This section outlines why utilising electrical power to a greater extent throughout the aircraft has the potential to improve global aircraft efficiency. The high level benefits are apparent when considering the replacement of centralised hydraulic networks and bleed air systems with electrically powered systems– the advantages of having only one distribution system as opposed to three, each with their own redundancy, is clear in terms of simplicity of design, maintenance and optimisation potential.

Specific advantages of aircraft having greater dependency on electrical energy include [9, 60] :

- Electrical wires are lighter than hydraulic pipes. Specific weight gains may not be immediately apparent with the introduction of large generators and power convertors. However, electrical systems tend to offer more flexibility than hydraulic systems for further weight savings.

- This greater design flexibility of electrical systems allows further, and perhaps continual, opportunity to enhance operational performance/system efficiency.

- Losses in electrical wires are lower than those in hydraulic and pneumatic piping.

- Switching within electrical systems means they function only when required. Hydraulic systems remain energised throughout the entire flight despite the fact that larger users of hydraulic power, such as landing gear and secondary flight control, only require power for short periods at a time.

- Electrical systems can be designed to provide the exact quantity of energy to each load. This is not the case in hydraulic and pneumatic systems, where excess/insufficient power is often supplied to loads.

- Elimination of inefficient air pre-coolers and hydraulic restrictors will reduce fuel burn.

- Hydraulic fluid leaks are difficult to locate leading to increased aircraft downtime, maintenance and ground support.

- Elimination of high temperature air ducts and flammable hydraulic fluids required in traditional aircraft.

These factors have culminated in the design of modern SPDS being more electrically based and it is anticipated that technological evolution will enable future aircraft generations to further embrace this concept.

2.3.3 MEA SPDS

The conventional design of SPDS previously described in Section 2.1 will be altered to accommodate the greater dependency on electrical distribution. The extent to which SPDS are transformed over time is conditional on the maturity of the enabling technology. Figure 2-3 illustrates a time line of expected advancements within the SPDS.
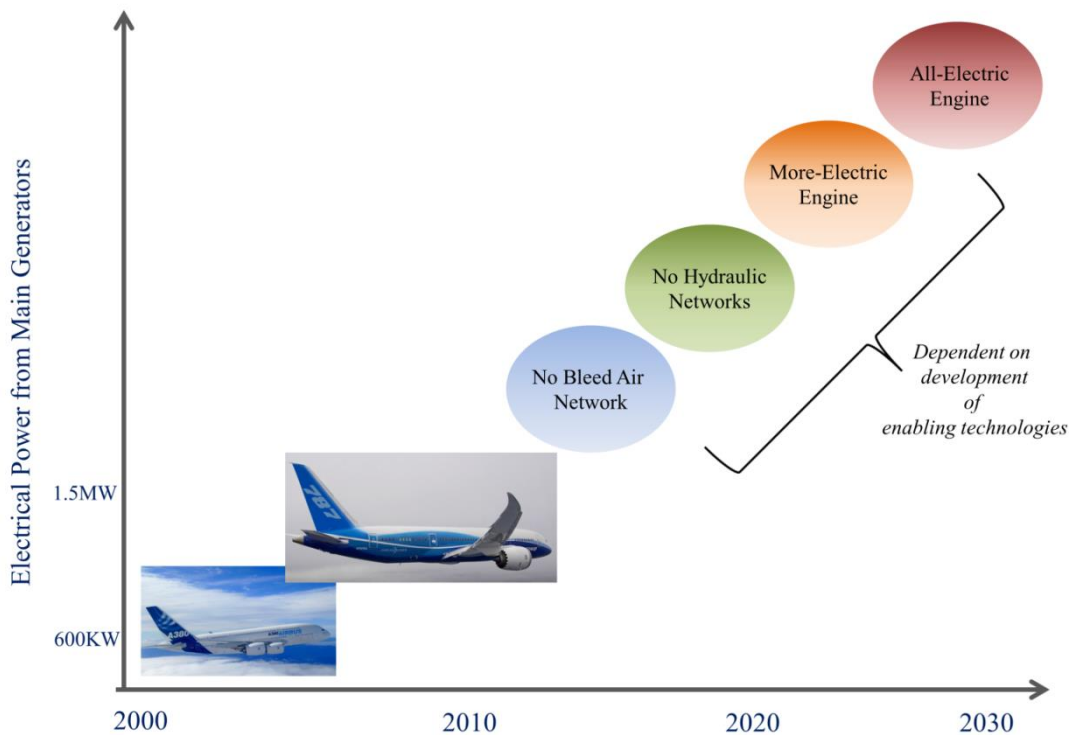
Figure 2-3: Time line of SPDS advancements [61]

The B787 and A380 are MEA presently in service. The B787 has eliminated the bleed air network whilst the A380 has focused on a more de-centralised hydraulic system design utilising remote, electrically controlled hydraulic actuators. Figure 2-3 shows that future advancements include the complete elimination of both hydraulic and pneumatic systems and the development of the *more electric* and *all electric* engines. Figure 2-4 demonstrates how power demands differ between conventional and more-electric SPDS. The MEA will depend on ~ 1MW of electrical power - a five-fold increase in comparison to conventional levels.
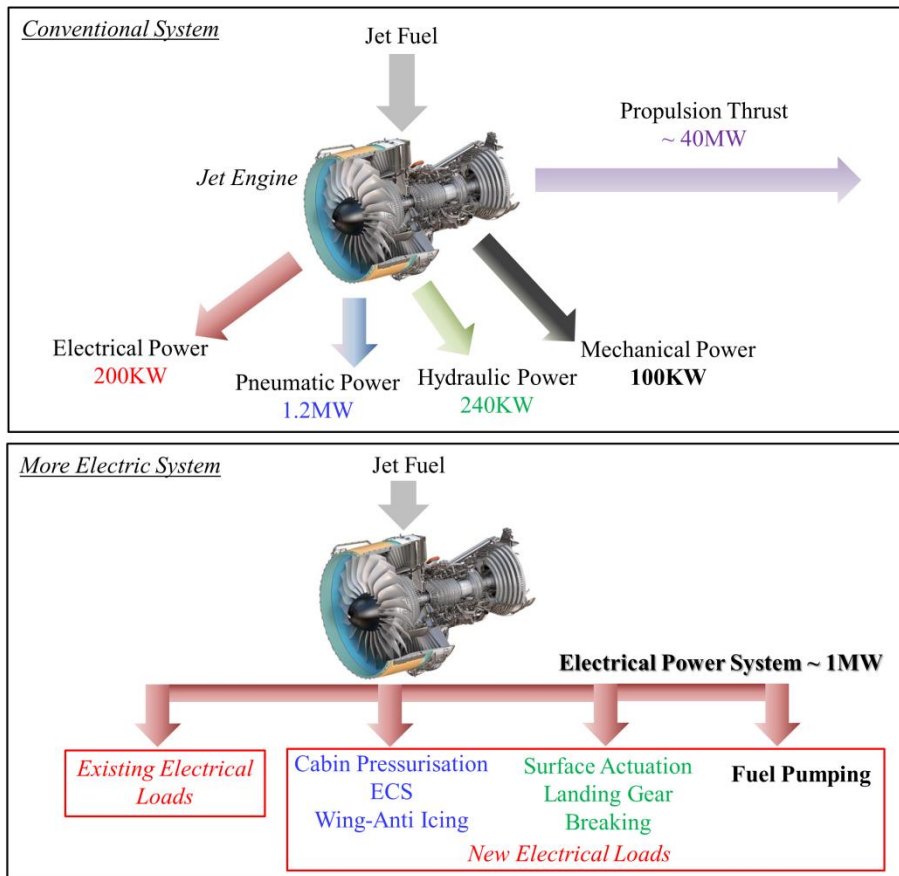
Figure 2-4: Comparison of power demands between conventional and more-electric SPDS

It is the purpose of this section to detail the evolution of electrical system technology which has enabled current MEA, spanning generation, conversion and distribution architectures. Appendix D provides detailed examples of A380 and B787 EPS to illustrate these changes within a system wide context. Novel MEA loads are also discussed in Appendix D.

2.3.3.1 Power Generation

Significant changes in electrical generation strategies of MEA include an increase in power and voltage ratings and the migration from a constant to variable AC frequency output. The increased power/voltage ratings are relatively self-explanatory – the higher electrical demand within MEA dictates greater power availability from the primary generators. Higher generation capability is evident in the B787, which has four main engine driven 250kVA generators with 230VAC output – double that of the conventional 115VAC levels, with a significantly higher power output.

Moving to a variable frequency (VF) generator output is a consequence of the inefficiencies of IDG constant speed drives (CSD) (described previously in Section 2.2.1.1). The CSD is a gearbox that maintains constant speed of the generator shaft to produce a constant 400 Hz frequency output, where engine speeds vary at a 2:1 ratio between maximum power and ground idle. The main drawbacks of the CSD are its space and intensive maintenance requirements. The rationale behind a move to VF systems was that power conversion technological improvements would eradicate the necessity for CSDs.

VF output from generators is generally in the range 380-760 Hz. The frequency of power provided to the primary distribution bus is dependent on the conversion stage between generator and busbar. For example, the VF can be converted back to CF using DC link methods or cyclo-converter units [46], or even rectified directly to DC for primary distribution. Table 2-1 summarises the generation strategies of various aircraft, including the B787 and A380.

Table 2-1: Main electrical power generation of various aircraft [46]

Generation Type	Civil Application		Military Application	
IDG/CF [115VAC / 400Hz]	B777	2 x 120kVA	Eurofighter	
	A340	4 x 90kVA		
	B737	4 x 90kVA		
	B747	4 x 120kVA		
	B717	2 x 40kVA		
	B767	2 x 120kVA		
VSCF Cyclo-converter [115VAC / 400Hz]			F-18 C/D	2 x 45kVA
			F-18 E/F	2 x 65kVA
VSCF (DC Link) [115VAC / 400Hz]	B777 (backup)	2 x 20kVA		
	MD-90	2 x 75kVA		
VF [115VAC /380-760Hz]	A380	4 x 150kVA	Boeing JSF X-32	2 x 50kVA
	Horizon	2 x 25kVA		
VF 230VAC	B787	4 x 250kVA		
270VDC			F-22 Raptor F35	2 x 70kVA

The migration to MEA has given significant scope to redesign and optimise the aircraft's engines. The *power optimised aircraft* (POA) programme was initiated to address and integrate technologies for a more efficient aircraft [62]; in doing so, the programme demonstrated the feasibility of the *more electric engine* (MEE). The MEE essentially replaces the current hydraulic, pneumatic and lubrication system with electrical systems, where the main features include:

- An electrical machine mounted on the high pressure shaft functions as both a generator and an engine start unit, while the main generator is connected to the low pressure shaft.
- All oil, fuel and hydraulic pumps are driven by electric motors
- No external gearbox

A comprehensive overview of the MEE design and features is provided by Hirst *et al.* [63].

2.3.3.2 Power Conversion

There is a critical requirement for power conversion within MEA EPS. Increased voltage distribution levels and VF output from the main generators means that the number of conversion stages in MEA is significantly higher. It is widely accepted [46, 51, 55, 64] that conversion technology, particularly in the power electronics domain, has given significant impetus to the growth of the MEA. Advances in power electronic conversion systems have enabled a more efficient and reliable means of converting capability.

An example of power conversion importance is illustrated using the MEA EPS distribution system in Figure 2-5.
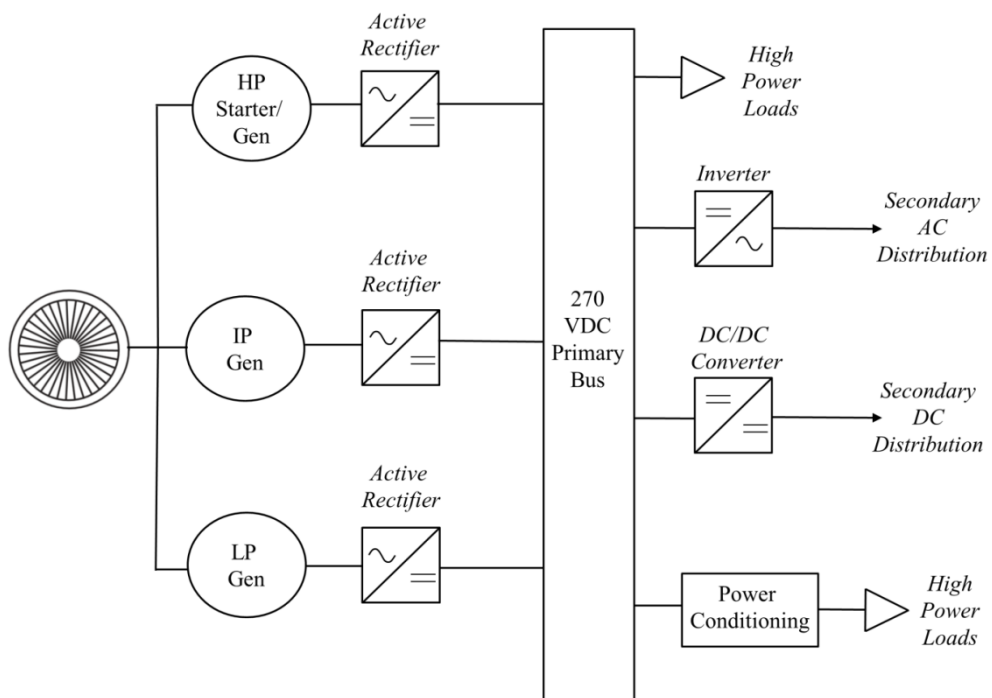
Figure 2-5: Potential Future MEA EPS architecture [55]

This example is a potential future trend, with power off-takes from each engine shaft and load sharing between the high voltage DC primary buses. The three phase active rectifiers allow paralleling of generators operating with different frequency and voltage on the DC

side. The DC primary bus can drive high power loads either directly or with further power conditioning. Inverters convert the DC voltage to AC for distribution and DC/DC converters are used to step down the DC voltage. The number of conversion stages in such a topology is in marked contrast to the conventional topologies described in Section 2.2.1. This highlights that, in order to distribute energy more efficiently throughout the EPS, converters are essential components to achieving this.

In general, the role of converters within MEA is to:

- Convert higher voltage distribution levels (DC/DC; DC/AC; AC/DC) to conventional levels for supply to legacy loads
- Convert generated AC voltage to higher magnitude 270 VDC for primary power distribution
- Control frequency and voltage supply to accessory AC electrical motor loads using DC/AC inverters
- Convert power to/from battery and energy storage systems

Despite the significant advances made in power electronic converter technology, further refinement is required in: mitigating electromagnetic interference (EMI); improving power quality by reducing harmonic distortion; reducing the reliance on passive components; and developing fault-tolerant topologies. The addition of heat to the aircraft system as a result of their implementation also has knock-on effects to SPDS efficiency through increasing ECS requirements. In general, though, the development of converter technology has been vital to MEA development.

2.3.3.3 High Voltage DC Systems

Higher operating voltages in both AC and DC distribution systems are beneficial in terms of reduced cable sizes and reduced electrical losses [65]. The higher levels of voltage allow a decrease in current whilst still maintaining the same quantity of power. Lower current magnitudes enable smaller cable diameters and a minimisation of I^2R losses – desirable characteristics for the development of energy efficient systems with significant electrical power demand.

In particular, there has been growing interest around the development of high voltage DC (HVDC) distribution systems. HVDC power distribution of 270VDC provides a mass and volume advantage over three phase AC systems as the number of feeders can be reduced from three to one. Also, as discussed in the previous section, the use of DC primary distribution allows generators to operate at variable frequency before being converted to DC, as well as paralleling and load sharing between generators.

US military agencies extensively researched and developed HVDC systems over a number of years. The initial deployment of these systems within combat military platforms [66] enabled the progression to the civil sector, where the B787 now utilises this form. Challenges do still remain with the integration of HVDC architectures. The increased voltage levels require greater insulation thickness to avoid the risk of partial discharge. Also, the inherent problems involved in protecting DC circuits with no natural current zero crossing have already been discussed – this problem is amplified in higher voltage systems. In general, there are significant challenges surrounding DC protection systems. These range from the development of advanced, less bulky contactor/switching/circuit breaking technology to the determination of DC fault characteristics and behaviours. IntelArc, the novel method described as part of the work of this thesis addresses the challenge of detecting series arc faults in HVDC systems.

The benefits of HVDC should be viewed from a system wide context. For example, reducing the weight of electrical wires does not necessarily result in a global system weight reduction when considering the increased insulation required and reliance on power converters. Managing the various design trade-offs in terms of both the integrated system and the individual components is vital to realising the benefits of HVDC implementation. What is certain is that, as the amount of electrical power to be distributed is of the order of MW, the use of HVDC will increase the potential for system optimisation.

2.3.3.5 Distributed System Architecture

In conventional aircraft designs the EPS has a centralised architecture of the form illustrated in Figure 2-6 (a) [8]. Primary and secondary distribution units are situated in a main electrical/electronics (E/E) bay which is located at the front of the aircraft. Cables transfer power from the main generators to the E/E bay upon which all load feeders have to leave their respective distribution units to service the various loads throughout the aircraft.

(a)   **(b)**
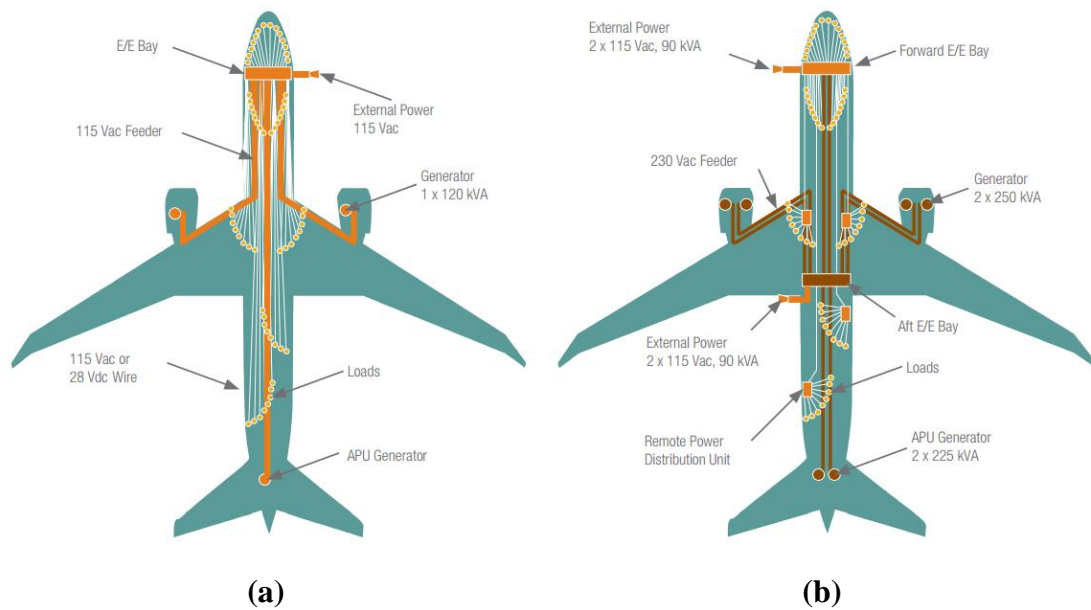
Figure 2-6: Centralised v Distributed EPS Networks [8]

Also, all control wires for the contactors and switches have to be joined together in the forward bay. This conventional design is sub-optimal in terms of space and weight as heavy cables have to be routed over the large distances between distribution centres and load terminals.

In contrast, MEA support a more physically distributed form of generation, where the aircraft is divided into different zones according to location (Figure 2-6 (b)). This distributed form features two (E/E) bays– one in the front and one in the aft. A limited number of higher power loads are supplied directly from the E/E bays with the majority of power being further distributed to various remote power distribution units (RPDU) throughout the aircraft. The RPDUs contain SSPCs instead of thermal CBs/relays and can be remotely controlled, allowing them to be strategically located to minimise aircraft wiring, weight and cost. Other advantages include higher redundancy in primary power distribution paths and decreased voltage drops, and hence lower losses, across the shorter feeders [7].

2.4 Fault Tolerant EPS and Protection Methods

This section reviews current practices for protecting and managing aircraft EPS during fault conditions. This includes a discussion on the limitation of conventional protection methods for diagnosing certain types of fault and emphasises the motivation for the work undertaken in this thesis.

The safety critical nature of aircraft requires the design, operation and reliability of all sub-systems to conform to strict certification standards and directives [33]. As such, a hierarchy

27

of sub-system criticality is established in order to determine optimal network designs which maximise reliability through increased redundancy of supply and components, whilst also considering the associated weight impact of redundancy measures.

In the event of system failures, a redundant system design has to be complemented with accurate and robust real-time health monitoring, protection and control systems so as to maintain highly reliable, fault tolerant EPS. A significant challenge concerns the development of real-time monitoring systems for operation within more complex MEA EPS. Greater EPS complexity is a result of increased generation, loads, variation of distribution levels and volume of conversion technology – these factors will not only increase the number of failure modes which have to be managed but also introduce new faults which were not readily considered within conventional EPS.

The following sections introduce various aspects of EPS monitoring and protection systems which detect and react during system failures – this includes a discussion on power management, state-of-the art health management systems, protection devices and methods and fault types.

2.4.1 Power Management Systems

Power management functions ensure that the power generated in any instant in time is equal to the consumed power. The various elements of a power management system include [67]:

- Load Management - The control of electrical loads. Electrical loads can at least be cut-off or reconnected and some may be regulated continuously or incrementally. The demand for a set of loads can be split across several bus bars.
- Source Management – The control of multiple electrical sources where primary bus bars can asynchronously accept power inputs from multiple sources.
- Energy storage devices, if available, providing/absorbing power.

Source management is undertaken using generator control units (GCU) and bus power control units (BPCU). GCUs control the operation of the main generator circuit breaker and can thus open the CB in the event of a non-tolerable overload. The bus power control unit (BPCU) closes or opens bus tie breakers (BTB) and auxiliary power breakers to connect two bus bars together.

The load management system involves the greatest complexity in terms of balancing load demand with available generation. Each controllable load has a fixed, pre-determined priority depending on its criticality to flight safety and mission function. In civil aircraft, loads are classified as vital, essential and non-essential and are connected to specific busbars according to their classification. Safety certification dictates that electrical loads should

conform to specific levels of reliability. Reliability levels vary between aircraft type and mission and are typically quantified in terms of failure rates (number of failures/hour) for an entire fleet of components/sub-systems. Reliability objectives for civil and military aircraft are summarised in Table 2-2 [71, 72, 73].

Table 2-2: Civil and military aircraft electrical load reliability targets

Aircraft Type	Load Classification	Probability of Failure (Qualitative)	Probability of Failure (Quantitative)
Civil	Vital	Extremely Improbable	$< 1x10^{-9}$
	Essential	Improbable	$< 1x10^{-5}$
	Non-Essential	Probable	$> 1x10^{-5}$
Military	-	Improbable	$< 1x10^{-6}$
		Remote	$< 1x10^{-3}$
		Occasional	$< 1x10^{-2}$
		Probable	$< 1x10^{-1}$
		Frequent	$> 1x10^{-1}$

A simple load hierarchy in civil aircraft is illustrated in Figure 2-7. The Load Management system will load shed in accordance with the load classifications; non-essential loads will be shed first to ensure that as many possible essential loads are powered. In the event of there still being power imbalance, the essential loads will be shed in turn to ensure as many vital loads as possible can get power. Prior to systems with automatic hierarchical disconnection of loads, CB boards were used which had to be reconnected via manual checklist.
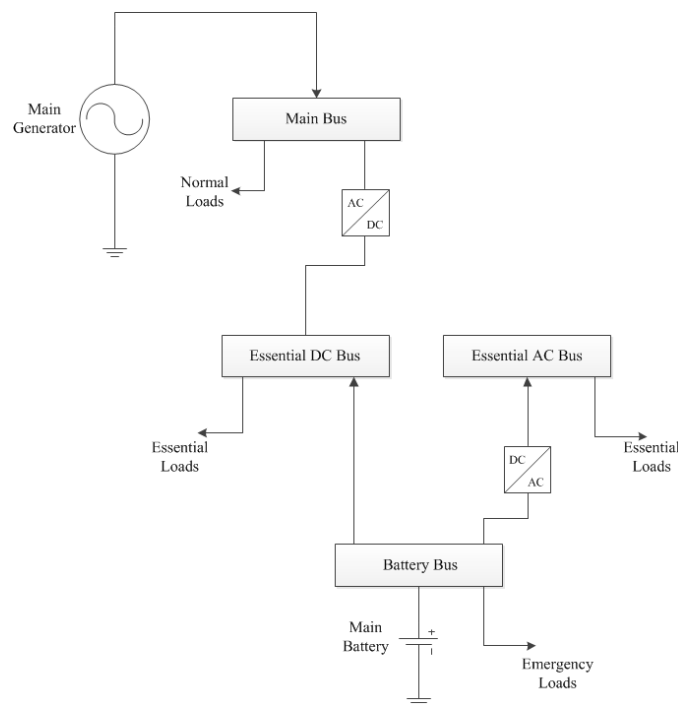
Figure 2-7: Simple electrical load hierarchy for civil aircraft

Advanced systems which integrated power distribution and load management were first introduced in the B777 [46]. The B777 load management system uses seven different power panels. Three primary power panels distribute to and protect higher power loads. The remaining four power panels distribute and protect loads for the left, right and standby channels and ground handling services. These four panels each have modular electronic units which receive data[4] regarding the availability of functions throughout the entire aircraft. The ability to receive real-time system data enables a sophisticated load management system which can configure the loads to give optimum distribution of available power throughout nominal and emergency operational periods.

2.4.2 Health Management Systems

Real-time data transference is also pivotal to the development of state-of-the-art HMS which detect and diagnose system anomalies [18, 69]. HMSs consist of an aircraft condition monitoring system which records data from the on-board systems and engines, including variations of flight and operating conditions. The HMS combines data and information into an integrated decision support tool for:

- Real-time fault management - communicates in-flight faults/alarms from the aircraft to the ground, allowing real-time operational decisions regarding maintenance.
- Performance monitoring – analyses and trends cruise performance data e.g. fuel efficiency and emission levels.

The availability of system data can aid fault management in both real-time and maintenance scheduling. However, there are associated challenges involved in accurately detecting, diagnosing and classifying faults within growing volumes and complexities of system data [70]. Part of the work of this thesis was to design novel methods that autonomously, and accurately, diagnose faults within large volumes of data.

2.4.3 EPS Protection

The protection system is an integral component of HMS that detects the occurrence of system faults and acts accordingly to mitigate potentially catastrophic events. Fundamentally, the main objectives of a protection system are to be [75]:

- Reliable – Accurately detect fault conditions and only operate when required.
- Selective – Minimise disruption to healthy portions of system by only tripping CBs required for isolating the fault.

---

[4] Digital data is transferred between each electronic unit using a data bus system – the system is designed so that each terminal can transmit data to, and receive data from, every terminal connected to the bus [68].

- Fast acting – Isolate faults as quickly as possible to reduce damage.
- Dependable – Ensure that the system will operate when required, and at the designed speed, when a fault is detected.

Systems are based on either *Non-Unit* or *Unit* methods [35]. Before summarising each method, the protection devices that physically isolate network faults in conventional systems [77] are briefly described. SSPC technology is also summarised, including the advantages it offers to the protection of future EPS.

2.4.3.1 Protection Devices

Electrical faults are generally characterised by an increase in system current. The current carrying capacity of cables[5] is determined by length and cross sectional area; cable size is therefore designed around rated current values of each circuit. Throughout normal service life, cable abrasion can cause insulation to degrade, exposing open conductors and enabling potential low resistance paths to ground (the aircraft frame) or between other conductors. Low resistance paths cause current to increase, possibly beyond rated values, resulting in increased heat and eventually fire. Protection against this, whilst also considering normal overcurrent transients, is vital to aircraft safety.

Fuses

Fuses are wire links connected in series with loads. Current carrying capacity for each fuse is pre-determined and the wire will melt and break the circuit when this capacity is reached. Fuses are typically encased within glass or ceramic with end caps providing the fusing point to cables - they should be located close to source to maximise the length of protected wire. Materials determine the speed at which the wire melts, and introduce a form of time delay within each device. Time graded settings in this sense are generally referred to as *energy let through* or I^2t protection [78], where the device will trip if energy exceeds a threshold. Despite being relatively low cost items, fuses can only be used once and have to be replaced once blown.

Circuit Breakers

CBs are electromechanical devices which interrupt and isolate a circuit in the event of excessive current. Unlike fuses, CB's can be manually reset once a fault condition has been cleared. In conventional systems, CB's are located in the forward bay and are the most common wire protection device in the 28VDC and 115VAC systems.

---

[5] Distinction should be made between wires and cables. A wire is a single solid conductor while cables are two or more wires contained within the same insulation sheath.

Relays control the operation of CBs. Relay settings coordinate times at which each CB in the system trips to maintain supply to healthy sections of the network - overcurrent relays typically have an inverse time current setting [75], where trip time is inversely proportionate to current.

There are significant drawbacks of CBs in terms of their deployment in MEA. These include:

- Limitation to localised control. This requires all CBs to be located in centralised front electronic bays and hence requires long runs of heavy load feeders. Within the last decade, this issue has been overcome with the development of remote control circuit breakers (RCCB) [74] that are controlled using a lightweight signal wire that runs to the cockpit. This means they can be placed closer to the system they are protecting to limit load feeder weight.

- The fundamental electromechanical feature of CBs is a significant hurdle to their implementation in future high voltage DC systems [77]. There is no natural zero crossing in the fault current waveform of a DC system and as such, the increased size and weight necessary for breaking higher current magnitudes means CBs are impractical for DC application above conventional levels.

- Traditional CBs cannot detect arc faults [19]. AFCB technology, which can protect against the arc fault, has been developed. These devices are limited in application to AC systems only and cannot be implemented in DC based systems. Arc faults are discussed in Section 2.4.5.3 and also extensively in Chapter 4. Chapter 5 describes *IntelArc*, a novel DC arc fault detection method and is one of the main outcomes of the work of this thesis.

Solid State Power Controllers

The development of solid state power controller (SSPC) technology [79] has been a major driver towards the realisation of the MEA. SSPCs are based on power semiconductors such as MOSFETs and IGBTs and effectively combine the function of load switching and wire protection within one device. The principle of switching operation is based on software control of electronic gate signals to the semiconductor within the device.

Significant advantages of SSPC over conventional protection devices include [19]:

- Their application to high voltage DC systems as a result of solid state switching as opposed to mechanical switching - SSPCs can be connected directly between a 270VDC bus and load.

- Remote control of multiple load switching and circuit protection. This enables distributed system architecture as SSPCs can be located closer to loads.

- Reduced switching time of ~3μs, compared to ~10ms for CBs.
- Built in I^2t time grade settings for wiring protection.
- Lower weight in comparison to relay and CB combinations.
- Lower susceptibility to in-flight vibrations and the reduction of bounce effect produced in the contacts of conventional contactors.
- Increased number of switching life cycles (~50000 compared to ~1000 for CB).

Issues do still remain with EMI causing instant shutdowns and affecting downstream loads. However, the advantages outlined show that SSPC technology will enable greater design flexibility and improve operational performance of aircraft EPS.

2.4.4 Conventional Protection Methods

Conventional Methods for detecting and isolating faults are classified as either non-unit or unit protection. Non-unit protection aims to correctly isolate faults by determining the thresholds at which multiple protection devices across the entire network should trip – determining correct thresholds is referred to as protection settings. In contrast, unit protection protects a clearly bounded zone and will only operate for faults within that respective zone. Each method is briefly summarised.

2.4.4.1 Non-Unit Protection

Current and/or voltage measurements are assessed from a single point in the network. The operation of the protection device at each point depends on a comparison of measurements with a pre-determined threshold setting. Protection settings throughout the system are designed so that only devices closest to a fault will trip to isolate that portion of the network and minimise disruption to the rest of the network. Non-Unit methods include overcurrent, rate of change of current, distance and loss-of-mains protection [76].

Overcurrent protection is illustrated in Figure 2-8. Faults further upstream and hence closer to supply will induce greater current magnitudes. Inverse current time relay settings enable CBs closer to supply to have a higher threshold and CBs further downstream to have lower current thresholds, thus maximising supply to healthy sections during fault events. Within compact aircraft EPS with shorter cable lengths, it is often difficult to correctly determine overcurrent protection settings as current magnitudes may be similar for faults at different locations. Shorter cable lengths also mean distance protection methods are unfeasible for aircraft EPS application.
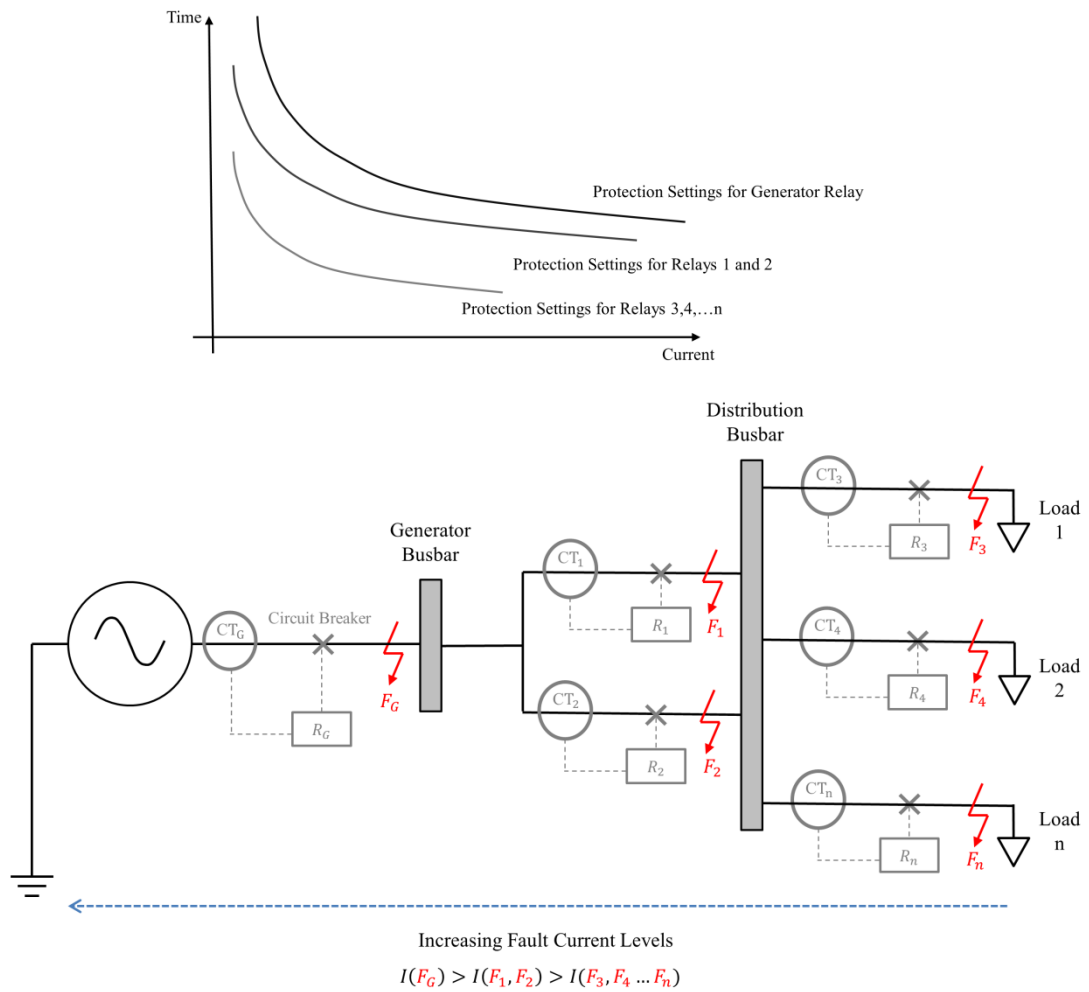
Figure 2-8: Simple example of non-unit overcurrent protection method. Relays with different protection settings isolate only the faulted section of the network to minimise disruption to healthy sections. *Top*: Examples of different inverse current-time relay settings. Settings for each relay are dependent on proximity to the electrical source.

2.4.4.2 Unit Protection

Protects a clearly bounded zone and will not operate for faults external to the zone. This method is commonly referred to as 'differential protection' as it principally detects a difference between currents entering and leaving a specified zone. Figure 2-9 illustrates unit protection of a generator feeder and busbar.

Measurements are taken at the boundaries of the zone using current transformers (CT) – CT_2 at the generator busbar and CT_1 at the earth return. In the event of a short circuit fault to earth, a (large) portion of current would flow directly to earth and not flow through CT_2 to the load feeder. This results in a difference between current supplied to the load (leaving the zone) and current returning through earth to the generator through CT_1 (entering the zone).

In this event, the GCU will trip the CB to avoid overheating. In contrast, if the fault is outside the protected zone (Figure 2-9 (b)), the same current magnitude (albeit greater than rated load current) would flow through each CT and the GCU would not trip the CB. Unit protection of the generator feeder and busbar is implemented in aircraft EPS.
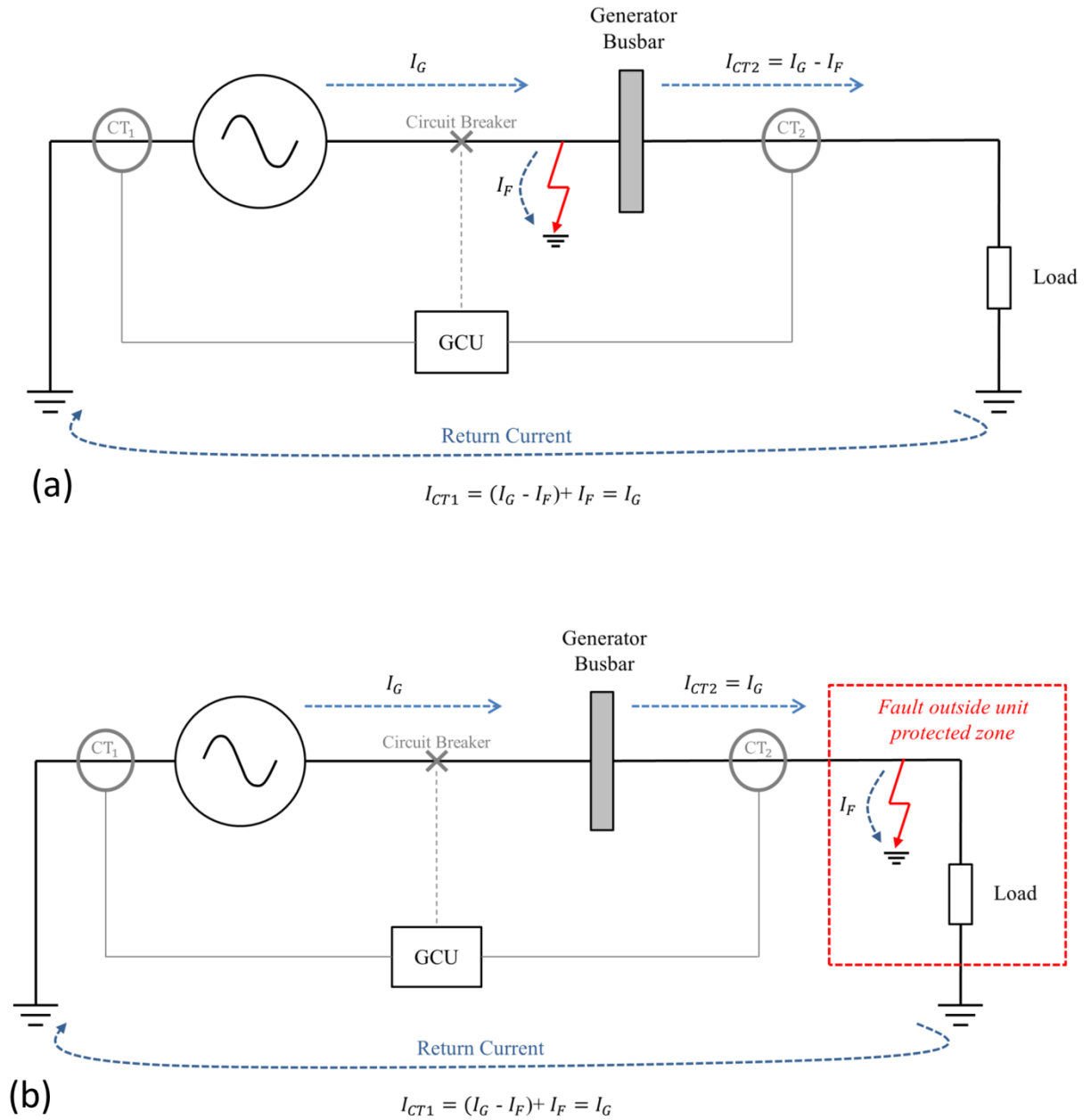
Figure 2-9: Examples of unit protection of a generator feeder and busbar for (a) A fault inside the protected zone and (b) A fault outside the protected zone.

2.4.5 EPS Faults – Limitations of Conventional Protection Methods

The limitations of conventional protection methods in detecting certain types of faults are described in this section. In Section 2.4.3.1 EPS faults were generally characterised by an increase in system current through live conductors directly contacting either earthed conductors or other phase conductors. The systems protecting against such *hard faults* are designed around detecting and isolating significant increases in system current. This section further describes system faults, including variations which, despite not resulting in sudden increases in sustained current, still have the potential to be equally catastrophic. Challenges with regard to protecting against electrical faults and the design of health monitoring and fault detection systems in the context of MEA are also elaborated throughout.

2.4.5.1 Fault Types

Adverse events can be categorised into five classes [80]:

- Incipient Fault – characterised by an extremely slow degradation and is very difficult to detect.
- Slow progression fault – gradual degradation in performance.
- Intermittent fault – faults that do not degrade but instead manifest themselves in a recurring fashion.
- Cascading fault – has a single root cause but progresses to create faults in other systems, sub-systems or components.
- Fast progression fault – faults that have limited detection signature but show rapid degradation.

Note that this thesis considers a slow progression fault to be of similar class to an incipient fault and any further reference throughout to an incipient fault should be considered to be either an extremely slow degradation or a gradual degradation. Furthermore, a cascading fault is referred throughout the thesis as a multiple fault condition while a fast progression fault is henceforth considered as an overcurrent fault.

In many cases, overcurrent faults begin as incipient low current faults [81]. Cables may be bundled and secured to the aircraft structure, which also acts as the electrical ground, for support. Insulation prevents metal-to-metal contact; this insulation may degrade causing high impedance paths to be established. It is desirable to detect faults in the high impedance/ incipient stage prior to their progression to an overcurrent condition. High impedance fault current levels are typically too low to trip overcurrent relays/fuses.

On-board EPS are exposed to harsh operating conditions, and in-flight vibrations can cause intermittent fault contact between two conductors or between loose terminal connections.

The intermittent nature means there is not enough sustained energy to trip protection devices and they may go undetected by ground maintenance as they cannot be replicated out-of-flight.

Despite these types of degraded faults not having enough energy to trip conventional protection devices, they are typically accompanied with electrical arcing, which is a potential fire hazards - see Section 2.4.5.3. Thus, detection is imperative for real-time fault tolerance and long term aircraft safety, particularly in more complex EPS. Chapter 5 of this thesis proposes EPSmart, a novel intelligent FDI method which detects a range of degraded failure types.

2.4.5.2 Fault Locations

US Air Force data [82], illustrated in Figure 2-10, reveal the distribution of electrical systems and components which fail in aircraft. The data were recorded for military aircraft between 1989 and 1999 – similar data were recorded between 1986 and 1989 and published in [83].

The majority of component failures occur in interconnecting cables, connectors and generators. Interestingly, for many years, the only attention given to electrical systems on aircraft was limited to key avionics and control systems [84]. The extended service of both military and civil platforms due to the retrofitting of new sub-systems resulted in a greater attention to the health of the interconnecting system. In particular, arcing as a consequence of wiring and interconnecting failures has fatal consequences [37]. Migrating to higher voltage (where arcing is more likely to occur) and DC systems (where arcing events are sustained and more difficult to detect than AC systems) requires the development of accurate and discriminative detection systems. Arcing faults are described in the following section.

Overall, the distribution of failures in the EPS highlights the necessity for autonomous, and scalable, FDI methods that can accurately detect failures of various components of the system – the EPSmart method, described as part of the work of this thesis in Chapter 5, is highly scalable and designed to autonomously detect a range of fault types at different locations.

Distribution of Electrical Faults by System
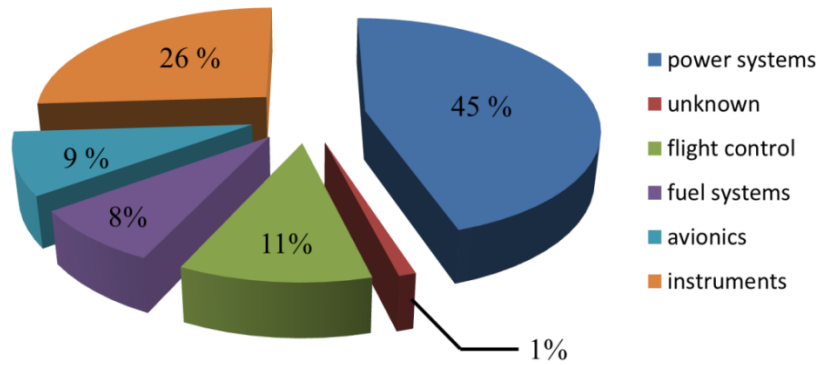
Distribution of Electrical Faults by Component
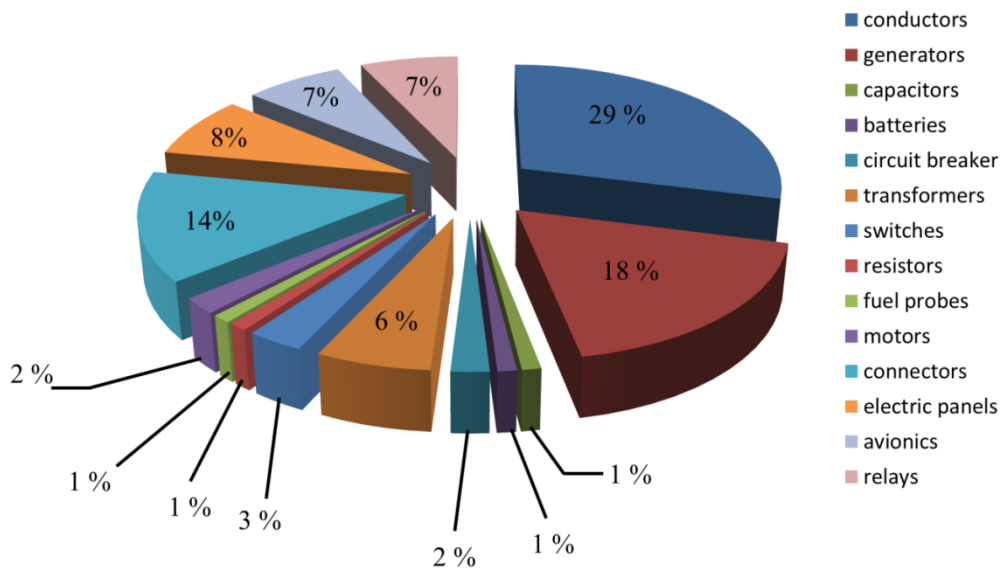
Figure 2-10: Distribution of aircraft electrical system failures across both systems (top) and components [82]

2.4.5.3 Arc Faults

Most faults will include arcing at some stage, typically at the point of fault and between the contacts of CBs which isolate the fault. Arc faults are defined as current flow through ionized gas between two ends of a broken conductor or at: a faulty contact or connector; between two conductors supplying a load; or between a conductor and ground [85]. Normal arcing events occur during mechanical switching operation of circuit breakers and contactors [169] – these devices are designed to withstand arc formation and normal arcing is typically highly transient and unsustainable. Conversely, arc current through ionized gas during fault events may be fully sustained; the high heat generated can lead to partial volatilization of the conductors and increases the risk of fire to surrounding insulation [170].

There are many conditions which may cause an arc fault, including [84]:

- Chemical, electrical and mechanical deterioration of wiring and interconnections.
- Presence of moisture or fluids on the insulation enabling leakage currents to create small electrical discharges across voids to other conductors (referred to as *wet arc tracking* [86]).
- Loose terminal connections.
- Wiring damaged during routine maintenance e.g. nails or staples through insulation.

Arc faults are categorised as either *parallel* or *series*.

- Parallel Arc Fault
  Parallel arcing involves the flow of current through ionised air (or other dielectric medium) between either two phase conductors, or a phase conductor and ground, as illustrated in Figure 2-11. These are typically the result of wet arc tracking formed when two conductors are brought into close proximity, or by degraded insulation. The fault is parallel to the electrical load and is considered a form of high impedance short circuit. The arc current levels are reduced by the impedance of both the system and the ionised path which forms the arc, which typically exhibits higher impedance in comparison to regular short circuit events. The high impedance nature of parallel arcing events often results in conventional protection devices not detecting their occurrence due to fault current levels being below the trip curve of the relays.
- Series Arc Fault
  Series arcing, illustrated in Figure 2-12, often begins with either chemical corrosion in pin-socket connections or loose connections in series with electrical loads. In-flight vibration causes intermittent connection/disconnection cycles within loose terminals. These cycles begin with small voltage drops which can eventually pyrolize the surrounding media and induce small arcs across the gap as the contacts

move away from each other. Single arc cycles will only dissipate a small amount of energy. However, if the vibrations produce many broken connections within a sufficiently short duration, the voltage will increase to create a build-up of localized dissipated energy and hence rapid temperature increase. Such instances produce a serious risk of fire within the surrounding insulation. A significant detection issue with the series arc fault is the fact that, because it is in series with the load, fault current actually decreases below load rated current and therefore well below relay trip curves.

Arc fault characteristics for both AC and DC systems, detection difficulties and arc fault modelling are all discussed extensively throughout Chapter 4. IntelArc, a novel series DC arc fault detection method is proposed in Chapter 5.
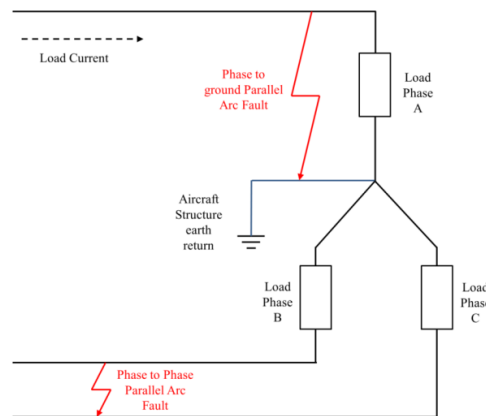
Figure 2-11: Illustration of phase-phase and phase-ground parallel arc faults
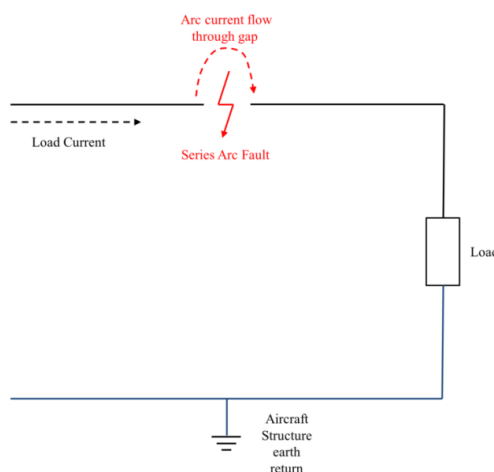
Figure 2-12: Illustration of a series arc fault

2.6 Protection and Health Management Issues Addressed in this Thesis

According to the various faults described, the protection and health management issues specific to this thesis include:

- Real-time monitoring and detection of faults where current levels either do not trip conventional circuit protection (incipient and intermittent faults) or actually fall below rated current (series arc faults)
- The development of scalable health management systems which can autonomously detect and diagnose a range of faults through analysis of large volumes of data

These challenges become more pertinent within MEA architectures, where there is:

- A general increase in safety-critical electrical systems
- An increase of PE components which affect fault behaviour [87]
- A greater emphasis on higher voltage, DC distribution

The remainder of this thesis describes the initial development of advanced methods which address these issues to enhance protection and health management. This includes the proposal of two novel FDI methods in Chapter 5: EPSmart, which diagnoses multiple critical and degraded faults within hybrid AC/DC networks, and IntelArc, which provides generalised detection and isolation of series DC arc faults.

2.7 Chapter 2 Conclusions

The chapter outlined the basis of the research by emphasising the motivation for development of advanced methods to improve protection and health management systems within aircraft EPS. In order to describe specific fault detection and management issues, the chapter described both conventional and MEA secondary power systems, not only to highlight the differences between them, but also to illustrate the specifics of aircraft based EPS. An understanding of these aspects enables comprehension of the importance and difficulty of detecting certain types of intermittent, incipient and arcing faults, as well as to reasons that the traditional protection approaches do not always suffice. The chapter identified and described various degraded fault modes that the remainder of the thesis will focus on and which novel methods for their detection are proposed in Chapter 5 – these include incipient, intermittent and arc faults. This chapter lays the groundwork for Chapter 3 to discuss advanced intelligent techniques that have the potential to enable accurate fault detection and diagnosis of these fault types within aircraft EPS.

3. INTELLIGENT FAULT DIAGNOSIS: THEORY & APPLICATION TO AIRCRAFT EPS

The necessity for advanced intelligent fault diagnostic methods to detect degraded and arcing faults that may not be identified using conventional protection methods was emphasised in Chapter 2. Detection and diagnosis of degraded fault conditions before their potential progression to critical failure will improve overall aircraft health management. This chapter builds on Chapter 2 and introduces intelligent fault diagnosis.

The topic is extensive, and intelligent diagnostic methods can be based on a variety of models, concepts and techniques which are summarised in this chapter. The methods proposed in this thesis for diagnosing aircraft EPS faults are based on machine learning (ML) techniques and these techniques are discussed in more detail. The attributes of each ML technique are summarised, and the motivations for selecting certain techniques to meet the objectives of this thesis explained. Previous applications of intelligent diagnostic methods to the aircraft EPS domain are described to place in context the contribution of this research.

3.1 Fault Diagnosis – A Definition

It is important to understand the general idea of fault[6] diagnosis before introducing intelligent fault diagnosis in more detail. The semantics of the subject can easily result in confusion as often there are a variety of accompanying terms, including: *fault detection*; *fault tolerant control*; *fault classification*; and, *fault isolation*.

Fekih [88] states that "Fault Diagnosis is the primary stage of fault tolerant control systems. Its goal is to perform two main decision tasks: fault detection, consisting of deciding whether or not a fault has occurred, and fault isolation, consisting of deciding which element of the system has failed." Fenton [39] summarises that "Fault diagnosis isolates the source (s) of a system malfunction by collecting and analysing information on system status using measurements, tests and other information sources (e.g. observed symptoms)".

These two statements summarise fault diagnosis rather well; definitions of the various terminology are provided, and a description of the processes involved, including means of achieving diagnosis, are succinctly described. Essentially, a system that has the capacity to detect, classify (or *identify*) and isolate a fault is termed a fault diagnosis system [89].

This thesis defines an intelligent fault diagnostic system as one that extends the functionality of traditional EPS protection systems (described in Chapter 2) by using more advanced methods for decision making. For clarity, intelligent fault diagnosis and isolation (FDI) is used throughout the thesis to describe advanced methods that enable systems to provide combinations of fault detection, classifying and isolating functionalities.

The thesis focuses more so on diagnosis, although it is important at this elementary stage to also briefly summarise *prognosis*. Prognostics are concerned with calculating or predicting the future through rational study and analysis of system data. While diagnosis is the process of detecting and diagnosing a failure mode within a system or sub-system once it has occurred, prognosis is the process of generating a rational estimation of the remaining useful life and/or remaining performance until complete failure occurs. For further information on prognostics please refer to the review provided by Lee *et al.* [125].

---

[6] A fault is defined as a departure from an acceptable range of an observed variable, or a calculated parameter, associated with a process.

3.2 Fault Diagnosis & Fault Tolerant Control – General Process

This section considers the general environment in which fault diagnosis systems operate, including how they combine with other system elements to detect, diagnose and isolate failures.

Fault diagnosis is often married with the concept of Fault tolerant control (FTC) - FTC reflects the ability to generate reconfigurable control action within systems in the presence of fault conditions. This is a necessity in safety critical systems such as aircraft EPS. A generic FTC process is illustrated in Figure 3-1 - the importance of fault diagnosis in this process is conveyed.

The four main components in Figure 3-1 are:

- The monitored plant, including sensors and actuators.
- The fault diagnosis system.
- The feed-forward controller.
- The supervision system.

Potential faults can occur within the plant, the sensors and the actuators. The fault diagnosis system utilises information provided by the sensors to inform the supervision system about the onset, location and severity of any faults. Based on this information, and the system inputs and outputs, the supervision system will reconfigure the sensor set and/or actuators to isolate the faults and adapt the controller to accommodate the fault effects [89, 90].

A conventional feedback control system without means of fault diagnosis may be less reliable, as the supervision and control system will not detect and reconfigure the system after the occurrence of malfunctions in sensors, actuators and other plant components [92].
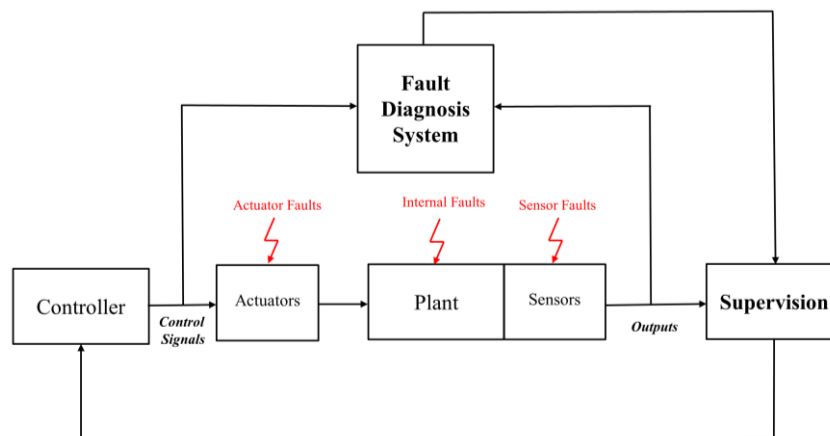
Figure 3-1: Generic FTC Process [89]

3.3 Fault Diagnosis – Desirable Characteristics

The importance of fault diagnosis systems for detecting and isolating faults, and generally maintaining reliable operation of a monitored system, was emphasised in the previous section. However, an inaccurate and poorly designed diagnosis system has the potential to negatively impact the reliability of the monitored system [91]. In order to avoid this scenario, there are various desirable characteristics a diagnosis system should possess that optimise operation and performance. These characteristics are summarised as follows:

- Quick detection and diagnosis – a real-time diagnosis system should respond quickly in detecting and diagnosing failures. One issue with a system designed for quick detection is that it is more susceptible to noise; the probability of false alarms during normal operation is therefore increased.

- Provision of fault classification/discrimination – should have the ability to distinguish between different failures.

- Ability to identify multiple-faults – an important, but difficult, requirement as different faults may interact making accurate identification of multiple anomalies highly complex.

- Robustness – system should be robust to noise and uncertainty.

- Classification error estimate – system should have the ability to quantify the reliability of diagnostic decisions. Ideally, this would include the probability of a prescribed fault.

- Adaptability – should maintain accurate performance throughout changing operating conditions.

- Explanation facility – besides the ability to identify the source of failure, a diagnostic system should also provide explanation on how the fault originated and propagated to the current situation.

- Modelling requirements – the modelling stage should be minimised for fast and easy deployment of real-time diagnostic systems.

- Computational requirements – quick, real-time solutions typically require algorithms and implementations which are computationally less complex.

The development of methods that enable diagnostic systems to possess all characteristics would be, if not unrealistic, extremely difficult. The novel intelligent FDI methods proposed in Chapter 5 were designed in an attempt to maximise these desirable characteristics - this is elaborated on throughout Chapter 5.

3.4 Intelligent Fault Diagnostic Methods – A Summary

This section discusses the methods that intelligent fault diagnostic systems use to analyse available information and detect and isolate system faults. There is a broad range of methods for diagnosing faults. The classification of each method can vary throughout literature - the categorisations provided in this section seem to be the most common.

Existing FDI methods and techniques are summarised in Figure 3-2.
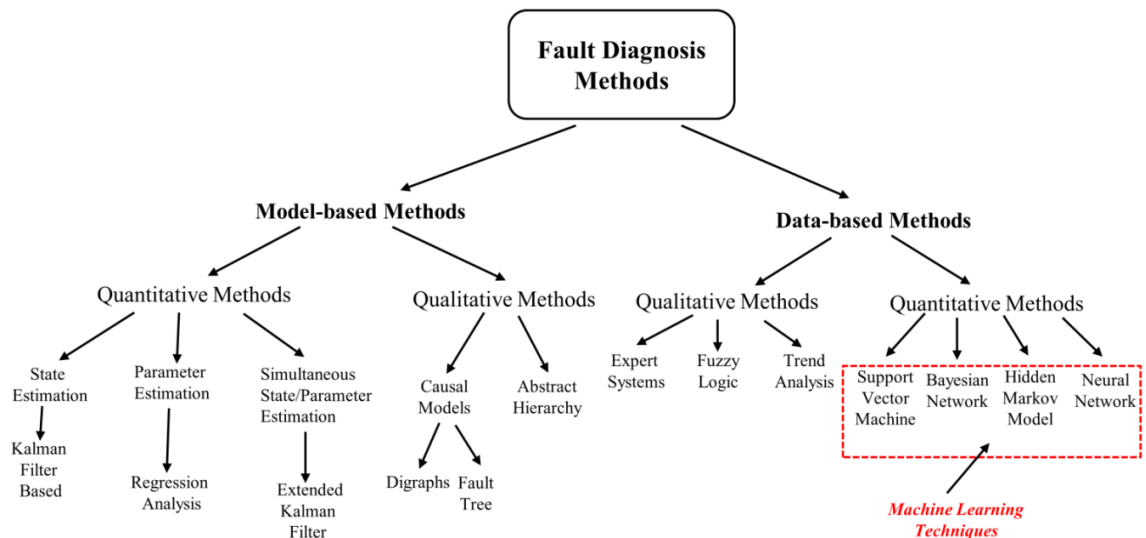
Figure 3-2: Summary of FDI Methods [91]

Methods are generally classified into two categories: model based and data based. The distinction between these two groups is summarised in the following sections.

3.5 Model Based Methods

Model based approaches can be broadly defined as either quantitative [91] or qualitative [97].

3.5.1 Quantitative Models

A quantitative model is usually developed based on some understanding of the physics of the monitored system. This understanding is expressed in terms of mathematical functional relationships between the inputs and outputs of the system. The models are usually discrete black-box system models or state space models [91], and assume linearity of the plant. Using quantitative models to diagnose faults usually requires two steps. Within the first step, inconsistencies are generated throughout fault conditions between actual, observed,

behaviour and expected normal behaviour from the model - these inconsistencies are known as 'residuals'. Residuals are close to zero throughout nominal conditions, and increase only during fault conditions.

The second step involves the development of decision rules for classifying faults in the presence of residuals. For example, residual generation within state-based models concerns divergence from expected values of state variables and/or model parameters. Classification is then determined by observing what state variables or model parameters have significant residuals.

Quantitative models have been used extensively within the aerospace domain. In particular, the Kalman filter, a form of state based model, has been applied for diagnosis of actuator failures [93, 94] and flight control during failures [95]. The main disadvantages of a quantitative modelling approach are that several factors render it very difficult, even impractical, to develop an accurate mathematical model of the system. These factors include system complexity, non-linearity, and high dimensionality. Consequently, they are not considered within this thesis.

3.5.2 Qualitative Models

The relationships between system inputs and outputs in qualitative models are expressed in terms of qualitative functions for the different sub-systems/components of the monitored system. For example, phrases that *describe* behaviour are used for detection, and model variables are usually binary with minimal discrete values. Qualitative modelling is often used to represent *deep knowledge* of a system [98], as they simplify systems that contain numerous variables and also reduce computation – this is in contrast to *shallow knowledge* based diagnosis which only captures the relationships between observed abnormalities and the associated fault, and does not contain detailed information on the underlying physics of the monitored system. Qualitative models can be classified as either causal or abstraction hierarchy [97].

Causal models are formed using signed digraphs [39]. Digraphs contain 'nodes', which represent system events or variables, and 'edges', which represent the relationship between the nodes. They provide an excellent means of representing models graphically and describe the effect or influence that certain entities (e.g. variables, faults) have on other entities. Fault diagnosis is performed by combining the observed system deviations and relating the combinations to a root cause. Studies within literature [96] describe the use of fault trees, a form of digraph, for fault diagnosis.

Within abstraction hierarchies, the monitored system is broken into a hierarchy of separate sub-systems and components. This decomposition allows a general representation of the functionality of a system in terms of the inputs and outputs of the constituent sub-systems. Fault diagnosis is a top down approach from a higher, sub-system level abstraction to a lower, component level abstraction. Each node in the hierarchy represents the intended function of each subsystem/component in the hierarchy. Comparison of the current performance of each node with the intended function enables the diagnosis of anomalies.

The main limitation of qualitative models is that they require detailed *a priori* knowledge of the monitored systems structure, components and functionality. Expert knowledge may not be available and, even if it is, the elicited knowledge may be specific to exact system conditions and configurations. Such specific knowledge will complicate the development of generalised models.

3.6 Data Based FDI

In contrast to model-based approaches, which require *a priori* knowledge (either quantitative or qualitative) about the monitored system, the data based approaches require sufficient volumes of system data [28] to be available. Raw data of this type can subsequently be transformed in a variety of ways and presented to the diagnostic systems as knowledge – this process is known as 'feature extraction'.

Similar to model based fault diagnosis, data based approaches can also be classified as either quantitative or qualitative. As part of this thesis, special consideration is given to ML techniques, a form of quantitative data based approach, as the novel FDI methods proposed in Chapter 5 of this thesis utilise these techniques. This discussion includes detail on their design and operation, as well as motivation for their adoption within the proposed methods. Particular issues with the design and development of data based FDI methods for application to an aircraft system domain are also discussed in Section 3.10.

3.6.1 Qualitative Data Based FDI

Forms of qualitative methods include; expert systems [99, 100, 101]; fuzzy logic [105]; and qualitative trend analysis (QTA) [108]. The development, operation and application of these methods are summarised in the following sections.

3.6.1.1 Expert Systems

An expert system is a specialised system that solves diagnostic problems in a narrow domain of expertise [28]. These systems apply expert knowledge to system data in an autonomous and programmatic manner to provide FDI. Application of expert knowledge is typically in the form of a rule based method, which analyses the data and classifies anomalies using prescribed rules. Expert systems are based on shallow knowledge, as only knowledge surrounding faults within the system is required [98].

Knowledge elicitation, where knowledge of the domain expert is gathered through some form of direct interaction, is pivotal to system development. The systems are designed in two principal parts: the knowledge base and the reasoning, or inference, engine. The knowledge base contains both factual and heuristic knowledge. Factual knowledge is commonly agreed upon within the domain community - i.e. well known, documented facts. Heuristic knowledge is more a result of the expert's experiences, and is therefore largely individualistic. The inference engine analyses and processes the rule base. Essentially, the inference engine traces its way through a grouping of rules to arrive at a conclusion [102].

Expert systems are advantageous for fault diagnosis systems as they:

- Possess vast quantities of domain specific knowledge to minute detail;
- Have a high explanation capability where reasoning can be reviewed and decisions explained;
- Can provide high quality performance in solving difficult programs as, or better than, human experts.

Expert systems have been developed and proposed for application within the aerospace domain for real-time fault diagnosis of aircraft engine failures [99], fuel system failures [100] and the diagnosis of problems immediately after the manufacturing process of combat aircraft [101]. In each case they have shown potential for accurate and efficient fault diagnosis within their respective applications. However, in all applications, the limitations of an expert system approach are relatively self-explanatory: knowledge based systems developed from expert rules are very system-specific and they are often difficult to update and generalise [28].

3.6.1.2 Fuzzy Logic

An important feature of expert systems is their ability to deal with incorrect or uncertain information [103]. Uncertainty within expert systems can manifest in two forms: linguistic

uncertainty and evidential uncertainty. Linguistic uncertainty occurs when there are vague statements to describe the data (e.g. "*the value is near 20*"), while evidential uncertainty occurs if the relationship between an observation and a conclusion is not entirely certain. Evidential uncertainty is commonly handled using conditional probability [103]. Linguistic uncertainty is commonly handled using fuzzy set theory [104].

Fuzzy set theories assume that the transition between different classes of a system is gradual rather than abrupt. Fuzzy logic quantifies this concept by using the qualitative data to define the probability of the system being in a certain class and arrive at a diagnostic conclusion. These concepts enable expert systems to deal with ambiguous observations and are often important to their application – fuzzy logic based expert systems have been developed for transformer fault diagnosis [106]. With respect to the aerospace domain, an expert system utilising fuzzy logic for FDI on the Airbus 340 was proposed by Wu [105].

3.6.1.3 Qualitative Trend Analysis

QTA represents measured time-series signals as a sequence of basic symbols [107]. The simplest qualitative representation of a signal uses three symbols: *increasing*, *constant* and *decreasing*. These symbols correspond to the derivatives of the signal - more complex symbols based on second derivatives, such as *sharp increase*, can also be used. The symbols are often termed 'primitives'.

The basic idea of QTA is to represent the measured signal as a trend using the primitives. QTA involves two main processes [108]:

1) *Trend extraction* – this involves fitting either a constant, first-order or second order polynomial function (in that order) to a period of data. The period of data in which the function is fitted is determined by comparing the noise in the signal to the fit error. If the error is significant in comparison to noise, the interval is halved until an acceptable limit is reached. A primitive is assigned to the period based upon the sign of the first and second order derivatives of the function. This process is applied to the remainder of the data until the entire signal is transformed into a sequence of primitives.

2) *Trend matching* – QTA for fault diagnosis involves matching the trend extracted from the current window of time-series data to previously determined abnormal trends. This includes matching both the trends of single sensors within the monitored system, and also trends of all sensors throughout the complete system.

The main benefits of QTA include its simplicity and its ability to provide quick fault diagnosis. However, the increased computational complexity and requirement for multiple sensor deployment prohibits its real-time application for very large scale plants.

3.6.2 Quantitative Data Based FDI

This section introduces quantitative data based approaches to fault diagnosis before going on to discuss ML techniques in more detail.

The quantitative methods are often summarised as being a pattern recognition problem where the main goal is to classify new data points into a pre-determined class of the monitored system [28]. Monitored systems tend to exhibit stochastic behaviour and, as such, quantitative methods usually adopt a probabilistic approach. Generally, utilising such an approach involves data observations during normal system operation having a certain distribution. During fault conditions, these distributions will change – fault diagnosis involves determining when, and how, the distributions change.

When a parametric distribution is used, the probability distributions are characterised by their parameters - for example, the parameters of a Gaussian distribution are its mean and standard deviation. During on-line system monitoring, changes in these parameters can be indicative of fault conditions. Methods that observe changes in distribution parameters are usually classified as statistical.

This thesis focusses on ML based FDI methods. ML combines the ideas of pattern recognition and learning, probabilistic methods and statistics for development and application of diagnostic systems.

One of the main reasons for this thesis focusing on ML based FDI is that the volume of data that future aircraft EPS will generate is expected to increase significantly in future platforms [18]. It is imperative that this additional information is utilised efficiently, and does not impede the reliable operation of these systems. The employment of intelligent ML based methods for interpreting the behaviour/condition of the system through analysis of data will ensure that efficient and reliable operation of future aircraft EPS will be maintained, if not enhanced.

The following sections discuss these ideas in more detail.

3.7 Machine Learning

Murphy [30] defined ML as "a set of methods that can automatically determine patterns in data, and then use the uncovered patterns to predict future data, or to perform other kinds of decision making under uncertainty". This section describes some of these methods as well as the general design and operation of ML based FDI methods.

Murphy's definition covers the basic aspects of such methods. Automatically determining patterns in data is essentially *training* models using historical system data. Predicting future data refers to using the trained models to diagnose new system data. ML methods rely on using cases or examples to solve a diagnostic problem, rather than using a predefined mathematical model of the monitored system or a set of rules.

The development and application of ML based FDI methods are summarised in Figure 3-3.
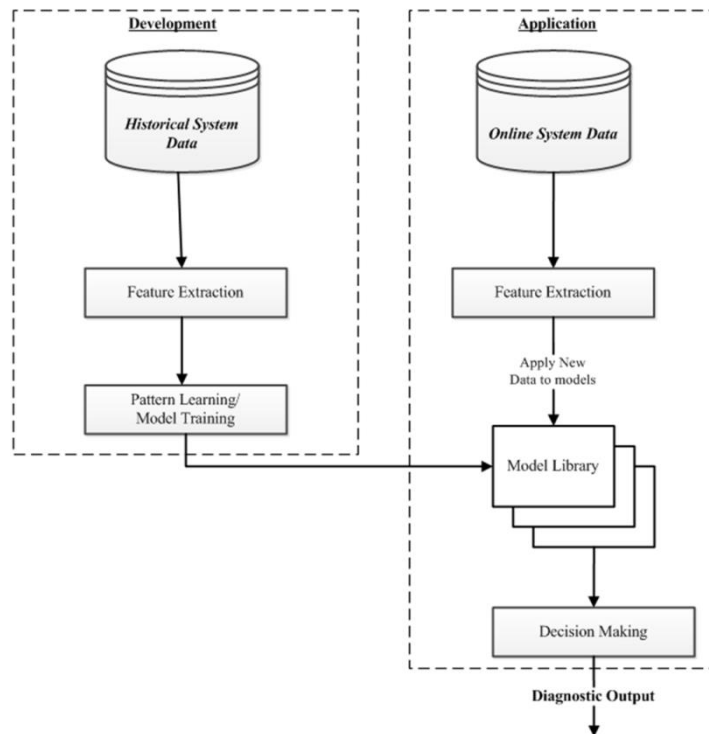
Figure 3-3: Development and application processes of ML based FDI methods

Methods are developed using historical system data - alternatively, system data generated using representative test beds and/or software models of the monitored system may also be used [109]. Data used throughout development is termed *training data*. Feature extraction from system data is a significant aspect of development – this process extracts the most significant features, in terms of discriminatory power, from raw system data. Feature

extraction is extremely important for the development of accurate methods, and is discussed further in Section 3.7.1.

The next stage of development involves using the extracted features to learn patterns, or signatures, of various system conditions. The process of pattern learning depends upon the type of modelling technique utilised – different ML modelling techniques are discussed in Section 3.8. The learning stage results in either a single model relating to nominal system condition, or a library of models corresponding to different nominal and fault conditions. The learning process is also dependent on the type of approach used. The two main learning approaches are *supervised* and *unsupervised* – these are described in Section 3.7.2.

Fault diagnosis is determined by comparing online behaviour with the modelled behaviour of each condition. Measures for these comparisons are again dependent on the modelling techniques used, and are discussed throughout Section 3.8. Interpretation of these comparisons is performed using some form of decision making tool or algorithm. Such tools may involve expert knowledge and/or fuzzy logic.

3.7.1 Feature Extraction

Feature extraction is the transformation of raw data from its original form to a new form from which suitable information can be extracted. This process ensures that fault diagnostic systems can be trained to realise significant features within data that relate to certain conditions. As discussed in the previous section, feature extraction is important for accurate diagnosis as it simplifies operation (by focusing only on a subset of the data) and increases discriminatory power.

Features may be directly extracted from the original data (e.g. using statistical measures such as RMS values) or from a transformed domain (e.g. Fourier and Wavelet Transforms). The Fourier transform (FT) [156] extracts the frequency components of time-domain data and has been used for discriminating between fault conditions that exhibit different frequency bands [85]. The advantage of the Wavelet transform (WT) [163] over the FT is that it provides both time and frequency information about a signal (i.e. what frequencies occur and at what time) – this is ideal for extracting information from highly transient signals.

A significant challenge involved with development of FDI methods is determining the features that optimise accuracy and discrimination – this process is often termed *feature selection*. Chapter 5 discusses feature extraction and selection for the novel FDI methods proposed as part of the work of this thesis.

3.7.2 Supervised and Unsupervised Learning

Learning patterns in data (or extracted features) using the various ML modelling techniques can be useful in two contexts. In the first context, the patterns of a specific, and known, condition described within the training data is learned - knowledge of these patterns can then be used in future to determine the presence of the same condition. This is termed as *supervised* learning as the features presented for learning relate to a known system condition.

In the second context, patterns within data that does not describe a *known* system condition are learned. This is termed *unsupervised* learning, where the goal is to discover interesting patterns that could have potential meaning – this is a less defined problem, as it is difficult to determine what the patterns relate to and there is no obvious error metric (unlike supervised learning where predictions of system conditions can be compared to the known condition).

The EPSmart and IntelArc FDI methods designed as part of the work of this thesis were developed using a supervised learning approach. This approach required examples of system data throughout different system conditions to be both available and labelled. This aspect of development is discussed further in Chapter 5.

3.8 Machine Learning Modelling Techniques

A selection of ML modelling techniques utilised for pattern learning are outlined in this section. The selected techniques include:

- Hidden Markov models (HMM)
- Bayesian networks (BN)
- Artificial Neural networks (ANN)
- Support vector machine (SVM)

The ways in which these techniques can detect and diagnose faults are elaborated. The attributes of each technique are discussed in Section 3.9. The motivation for using certain techniques over others, to meet the objectives of this thesis, is also explained in Section 3.9.

3.8.1 Hidden Markov Model

A HMM [127] is a statistical Markov model, in which the system being modelled is assumed to be a Markov process [110] with unobserved (*hidden*) states. They also assume that the system data is a noisy observation of this process. HMM are trained by extracting information from existing data and developing stochastic models of the signals. They can be used to solve classification problems associated with time series input data such as speech

signals, and can provide an appropriate solution by means of their modelling and learning capability, even though they do not have exact knowledge of the problems [42]. Traditional applications of HMM are in areas such as speech, handwriting and gesture recognition [30]. More recently, HMMs have been applied in classifying patterns in process trend analysis [111] and machine condition monitoring [112].

3.8.1.1 Elements of HMM

Usually HMM contain a finite number of states, where each state generates an observation at a certain point in time. The hidden state is characterised by two sets of probabilities: a transition probability and an observation probability distribution. The initial state distribution (i.e. the probability of the modelled process beginning in each of the hidden states) has to also be defined. In summary, the complete specification of an HMM includes the following elements [41]:

- set of hidden states:

$$S = \{S_1, S_2, \ldots, S_N\},$$

(3.1)

where N is the number of states in the model;

- state transition probability distribution:

$$A = \{a_{ij}\},$$

(3.2)

where $a_{ij} = P[q_{t+1} = S_j | q_t = S_i]$, for $1 \le i, j \le N$. q is the hidden state sequence throughout time: q_t represents the hidden state at time t and q_{t+1} represents the hidden state at time $t+1$;

- set of observations:

$$V = \{v_1, v_2, \ldots, v_M\},$$

(3.3)

where M is the number of observations per state. These observations relate to the physical output of the system being modelled, and each hidden state produces an associated set of observations;

- observation probability distribution which maps observations to hidden states:

$$B = \{b_j(k)\}, \tag{3.4}$$

where $b_j(k) = P[v_k \ at \ t|q_t = S_j]$ for $1 \le j \le N, 1 \le k \le M$. In continuous density HMM, B represents a particular continuous distribution (e.g. Gaussian distribution) over the set of observations, V, for hidden state j;

- initial state probability distribution:

$$\pi = \{\pi_i\}, \tag{3.5}$$

where $\pi_i = P[q_1 = S_i]$, for $1 \le i \le N$.

For convenience an HMM can be represented by the notation:

$$\lambda = (A, B, \pi), \tag{3.6}$$

to indicate the complete parameter set.

The HMM elements are illustrated in Figure 3-4 using a directed graphical model (DGM)[7].
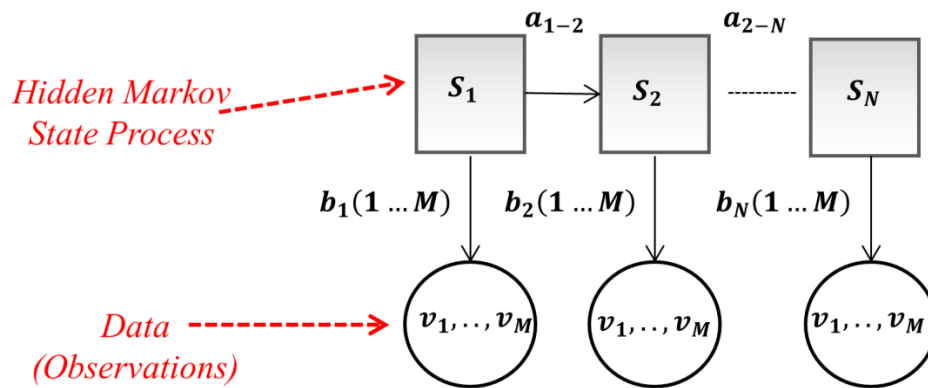
Figure 3-4: Graphical representation of HMM elements

---

[7] A DGM is a way to represent joint probability distributions of system/model variables by making assumptions about the conditional independence of each variable. See reference [30] for further detail.

Figure 3-4 illustrates the relationships between the HMM state and observation variables – the observational data is dependent on the (hidden) system state, while the current system state is dependent only on the previous system state. The observations in an HMM can be discrete or continuous. If they are discrete, it is common for the observation model to be an observation matrix. If they are continuous, the observation model will usually be a conditional Gaussian [30]. Please refer to [41] for further reading on HMM theory.

3.8.1.2 HMM Parameter Training

Training refers to the characteristics of the input patterns to be modelled by the set of parameters $\lambda = (A, B, \pi)$. A HMM is applied to a classification problem under the assumption the model parameters can be determined given the observation data. The complexity of this problem means this is difficult to achieve. However, it is possible to find local optima through maximum likelihood estimation [42]. The Expectation-Maximization (EM) algorithm [113] is used to solve the training problem and determine the likelihood of the parameters, given an observation sequence.

3.8.1.3 Expectation-Maximisation Algorithm

The EM algorithm [113], also known as the Baum-Welsh algorithm, is used in statistics for finding maximum-likelihood estimates of parameters in probabilistic models, where the models depend on hidden variables. The algorithm can compute maximum-likelihood estimates of the HMM parameters when given only a set of observation training data. The algorithm involves two steps: an Expectation, or E step, and a Maximization, or M step. The general EM algorithm is summarised in the following.

Given a joint distribution $P(V, Q|\lambda)$ over observed variables V and latent variables Q, governed by parameters λ, the goal is to maximize the likelihood function $P(V|\lambda)$ with respect to λ.

The algorithm can be generalised as follows:

1. Choose an initial setting for the parameters λ^{old}.

2. E step - Evaluate $P\left(Q|V, \lambda^{old}\right)$ (3.7)

3. M step - Evaluate λ^{new} given by
$$\lambda^{new} = argmax_\lambda Q(\lambda, \lambda^{old})$$ (3.8)

Where

(3.9)

57

$$Q(\lambda, \lambda^{old}) = \sum_{Q} P(Q|V, \lambda^{old}) \ln P(V, Q|\lambda)$$

4. Check for convergence of the log likelihood. If the convergence criterion is not satisfied, then let

$$\lambda^{old} \leftarrow \lambda^{new} \tag{3.10}$$

and return to Step 2.

3.8.1.4 Using Trained HMM for FDI

HMMs can be trained to diagnose unlabelled sequential data. In many applications [42] it is popular to establish several trained HMM models corresponding to the different conditions under consideration. Within such an approach, the unlabelled data would be applied to each trained HMM. Classification would regard choosing the model that gives the maximum probability (or, more specifically, the log-likelihood) of the observational data, given the trained parameters. That is, network condition, C, can be classified by

$$C = argmax(\ln P(V|\lambda_s)) \qquad 1 \le s \le H \tag{3.11}$$

where H is the number of network conditions considered within the FDI system - *argmax* refers to the model with parameters λ_s that provides the maximum LL value and *not* the maximum value itself.

A general framework of this method is illustrated in Figure 3-5.
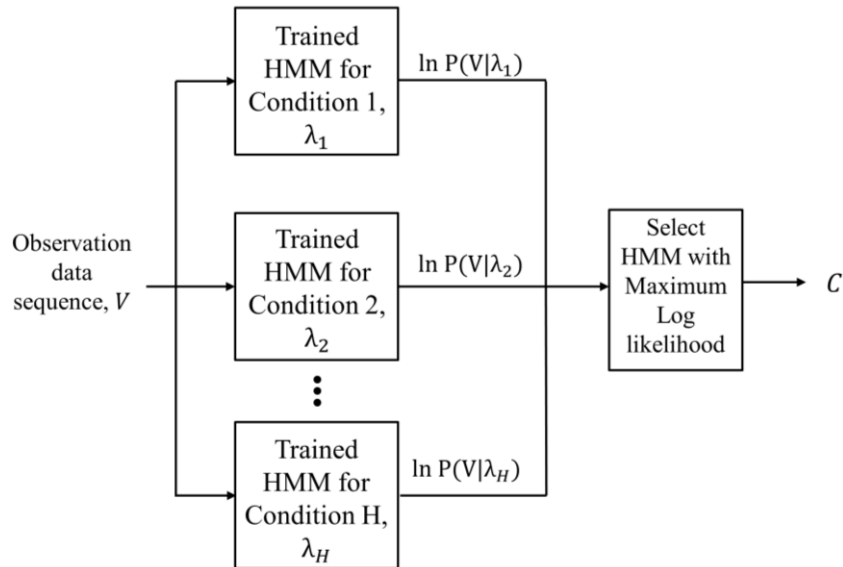
Figure 3-5: Framework of HMM based FDI system

The Viterbi algorithm (VA) [30] can be used for inferring from an observation sequence the most likely sequence of hidden underlying states that might have generated it. For each observation point in the sequence, an associated hidden state can be determined. HMM may be trained in a context where the hidden variables represent physical quantities of interest, such as specific fault states. In this context, the VA may be used for FDI by using the observational data to infer the sequence of physical states in which the monitored system has evolved. However, often HMM are trained in the context where the hidden states have no physical meaning and diagnosis is achieved by using the framework illustrated in Figure 3-5 (see, for example, references [78-81]).

For reasons outlined in Section 3.9, the novel FDI methods proposed in Chapter 5 are based on HMM. Consequently, Section 3.11.3 provides a review of HMM based FDI methods described within the literature.

3.8.2 Bayesian Networks

A BN is a form of directed graphical model used to represent the joint probability distribution of variables within a system. In Section 3.5.2 there has already been a discussion on qualitative causal graphs, that model the interaction of system variables using qualitative relationships and deep knowledge. BNs are similar to this concept, although they use system data to learn both graph structure and the joint probability distributions that quantify the relationships between system variables. BN's include both observed and hidden variables, and can be used to combine observed data with the joint distributions to infer hidden variables [114].
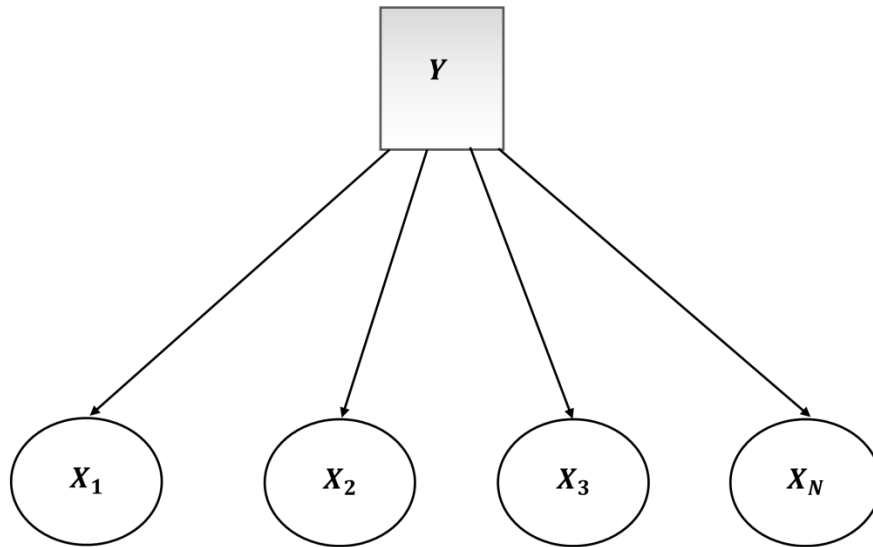
Figure 3-6: Basic structure of a naive BN

The most simplistic form is the naïve BN [30], illustrated in Figure 3-6. This form assumes the observed variables, X_1 to X_N, are all independent and conditional on the hidden class variable, Y – thus, in terms of diagnosis, the hidden variable can be inferred by considering each of the observed variables separately. This type of BN is termed naïve as it does not assume any relationship between observed variables – a more advanced form of BN would model correlation between the observed variables. There may also be correlation between multiple hidden variables (if they exist). Development of advanced BNs that capture these correlations requires sufficient domain/system knowledge. Application is widespread in the medical diagnostics domain [115]. Engineering based applications include fault diagnosis of rotating machines [116] and road vehicles [117]. Examples of BN based FDI methods for application to aircraft EPS are discussed in Section 3.11.2.

3.8.3 Artificial Neural Networks

ANNs are non-linear, multivariable models which are developed using a set of input/output training data. They were originally inspired by the neural circuitry of the human brain, which has billions of interconnected cells [39]. ANNs are represented by a set of nodes with connections between them. The connections have weights associated that represent the strength of each connection between the nodes. In the training phase, the weights between each node are learned. Within a supervised approach the labelled training data is used to attribute specific combinations of learned weights to particular conditions/faults.

ANNs are organised into different layers [118]. The 'input' layer relates to observable data, where each node represents a single variable/feature. The input nodes are connected to multiple hidden nodes in the 'hidden' layer. The hidden nodes perform a non-linear mapping from the input space into a new space – these nodes are connected to output nodes in the 'output' layer. The output of the network is a linear combination of the hidden nodes. This architecture is illustrated in Figure 3-7. Inference of new data is determined through the status of output nodes. Each output node, which relates to a specific system condition, has a binary output [119] – an output of 1 indicates presence of the condition.
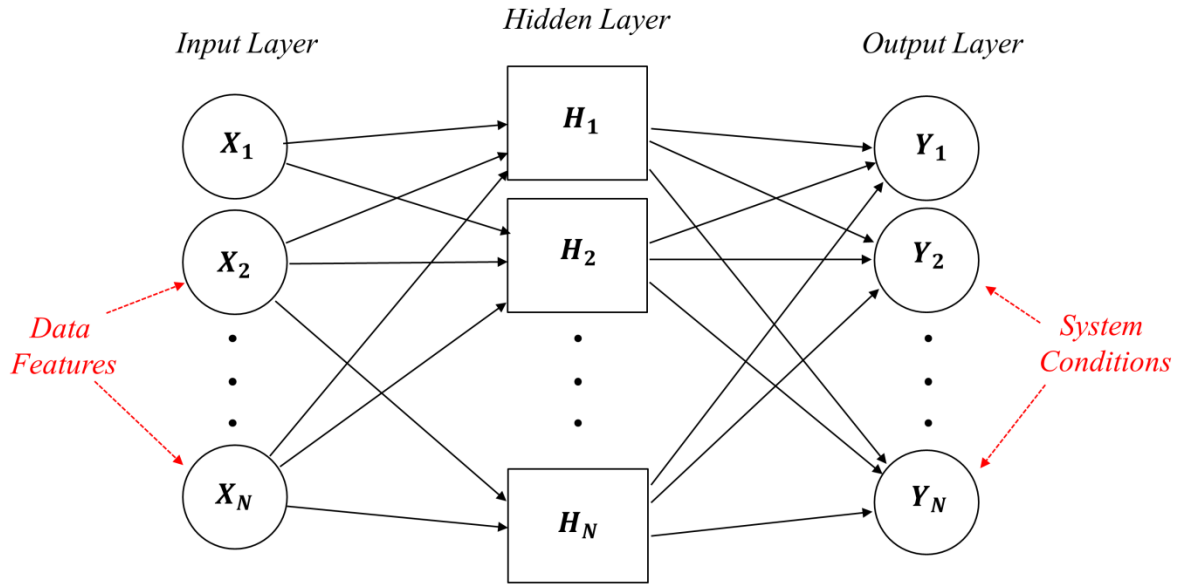
Figure 3-7: General architecture of an ANN

ANN's have been extensively applied for diagnosis of power quality problems within the general EPS domain [39, 119, 120]. Examples of their application to EPS within aircraft and shipboard systems are described in Section 3.11.2.2.

3.8.4 Support Vector Machines

SVMs are a relatively new supervised machine learning technique [126]. SVM learn the location of decision boundaries, or *hyperplanes*, that produce optimal separations of classes within observed data. Finding the optimal separation of linearly separable data is relatively simple – essentially the SVM searches for the optimal hyperplane that correctly classifies the data. This concept is illustrated in Figure 3-8 (a). Determining the optimal hyperplane is equivalent to maximising the distance separating each class, as shown in Figure 3-8 (b). The support vectors are training data points that lie on the margin. These are the most significant

61

points, as classification of new data points involves determining their position relative to the support vectors.
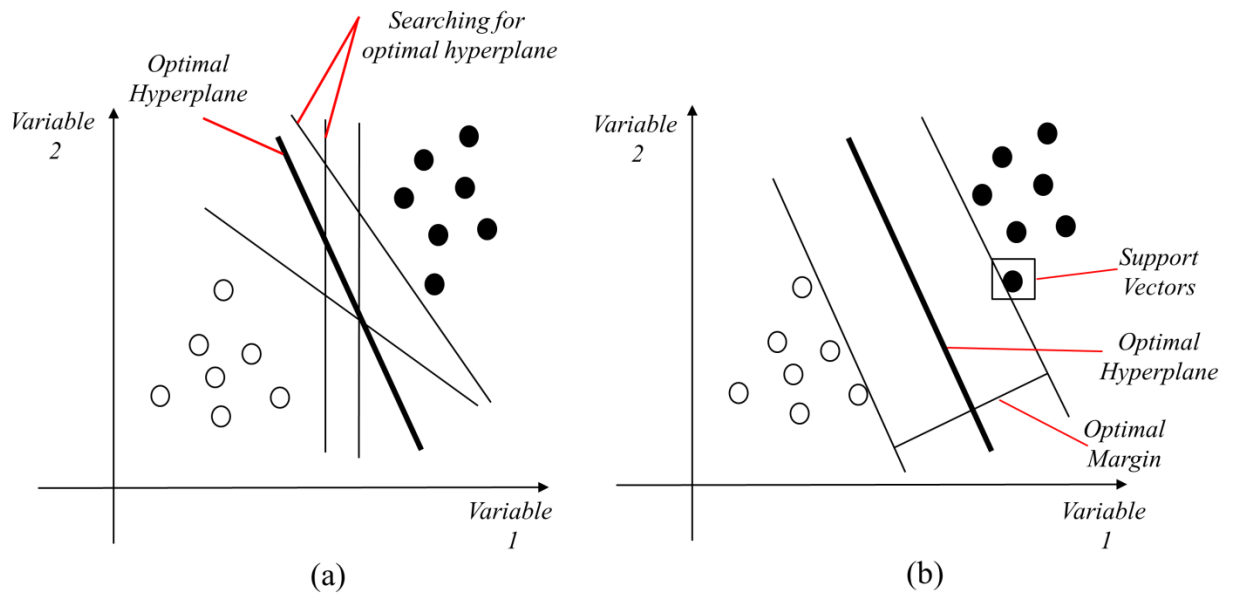
Figure 3-8: (a) Searching for optimal hyperplanes between two linearly separable classes of data (b) Optimal margin criteria for determining hyperplane

SVM can also be extended to classify data that is not linearly separable. In this extension, training data is mapped into a high dimensional feature space using kernel functions. Transformation to an alternative feature space enables linear separation of classes - [121] provides more information on this process and SVM in general.

SVM have been proposed for fault diagnosis in series compensated electrical transmission lines [122] and high voltage circuit breakers [123]. Applications particularly relevant to this thesis include their use for high impedance fault/arc fault detection [124] (this is described further in Chapter 4), and FDI and prognosis of aircraft engine degradations [164].

3.9 Comparison of Machine Learning Modelling Techniques

Section 3.8 described various ML modelling techniques that utilise system data to diagnose system faults. Each technique has the potential to be applied for fault diagnosis within an aircraft EPS environment – indeed, as is elaborated in Section 3.11.2, various techniques have previously been applied in this context.

The main objectives of the novel aircraft EPS FDI methods proposed in this thesis are to:

- Autonomously, and accurately, detect a multitude of fault conditions.

- Detect the onset of degraded fault conditions (i.e. intermittent and incipient faults) in an appropriate timeframe.
- Detect series arc faults in DC supplied systems that are difficult to detect using conventional protection methods.

The following section outlines the attributes of the potential ML techniques that could be applied to meet these objectives. Summarising these attributes helps to explain the motivation for the choices that were made.

3.9.1 Attributes of Machine Learning Techniques

The various attributes of the selected ML techniques are summarised in Table 3-1 [125, 129].

It was explained in Section 3.8.1.4 that the novel FDI methods proposed as part of the work of this thesis would be based on the use of HMM to infer the presence of faults using system data. Each potential technique outlined in Table 3-1 has associated advantages and disadvantages. According to the aims outlined in the previous section, the main motivations for basing the FDI methods on HMM include:

- Their suitability for detection of transient signals – this makes them ideal for series DC arc faults which exhibit highly transient, non-stationary behaviour.
- Their ability to provide a log-likelihood metric that quantifies the probability of various fault hypotheses. This form of diagnostic explanation means HMMs are more suitable for multiple fault diagnosis than ANNs, which only provide a binary decision.
- HMM based FDI methods are highly scalable and can be readily updated to include models of emergent system conditions.
- SVM can provide excellent fault diagnostic accuracy. However, they are usually suitable for classifying between only two system conditions and thus multiple fault diagnosis is complicated.
- The accuracy of naïve BN classifiers is debatable. To improve accuracy, more advanced BNs can be developed, although this requires significant *a priori* system/domain knowledge.
- ANN training is complicated by the fact there is no standard method for determining network structure. In comparison, the number of hidden states within HMM can be determined through simple plotting and visualisation of the training data.

Table 3-1: Attributes of various ML modelling techniques [125]

Technique	Advantages	Disadvantages	General Accuracy	Speed of Learning	Speed Of Classification	Explanation Ability	Capability to Generalise	Multiple Fault Handling	Tolerance to Noise
HMM	-Appropriate for multiple fault diagnosis. -Good for detection of degradations within non-stationary/transient signals.	- Need sufficient training data for accurate modelling. - Issues with over fitting training data.	Very Good	Good	Excellent	Good	Good	Very Good	Excellent
BN	– Visualises dependency links between system variables. - Naïve networks do not require iterative parameter learning algorithms and can be applied to large feature sets.	- Learning unknown structures can be complex. - Rely on certain amount of *a priori* domain knowledge. - Naïve networks not optimally accurate.	Average	Excellent	Excellent	Excellent	Good	Naturally Extended	Very Good
ANN	- Suitability for complex, non-linear systems. - Require minimum knowledge about variable and class relationships. - Successful on several real world applications.	- Lack of diagnostic explanation ability/metric. -No standard method to determine network structure.	Very Good	Average	Excellent	Average	Average	Naturally Extended	Good
SVM	-Requires minimal training examples. -Less prone to over fitting than other techniques. - Maximised decision boundary improves overall accuracy.	- Lack of diagnostic explanation ability/metric. - No standard method to choose kernel function. -Difficulty in extending to multiple fault diagnosis.	Excellent	Average	Excellent	Average	Average	Only Binary Classifier	Good

64

The main drawbacks of HMM are their susceptibility to over fitting, as well as the requirement for relatively large volumes of training data. Approaches do exist that can minimise these drawbacks. A lack of training data can be compensated by selection of features from the data that generalise fault conditions and do not focus on intricacies of the specific training examples. Over fitting can be minimised with the use of the Bayesian Information Criterion (BIC) [30] – the BIC essentially optimises the number of parameters in a model to ensure the fit is not overly representative of the training examples. These issues are described throughout Chapter 5. ANNs suffer with regards to generalisation as there are no such formalisms for ensuring models are not over fitted.

Overfitting and generalisation are relative in that a model that is over-fitted to the training examples will perform poorly at providing a generalised diagnosis. This relationship is simplistically illustrated in Figure 3-9 – as generalisation improves, the fit of the model is reduced. Generalisation is dependent not only on the particular modelling technique but also on the features of the data that are presented for detection. Hence, a technique that theoretically can improve generalisation may in practice perform poorly at inference of new examples as a result of poor feature selection. The issues of feature selection for the methods proposed as part of the work of this thesis are also described throughout Chapter 5.
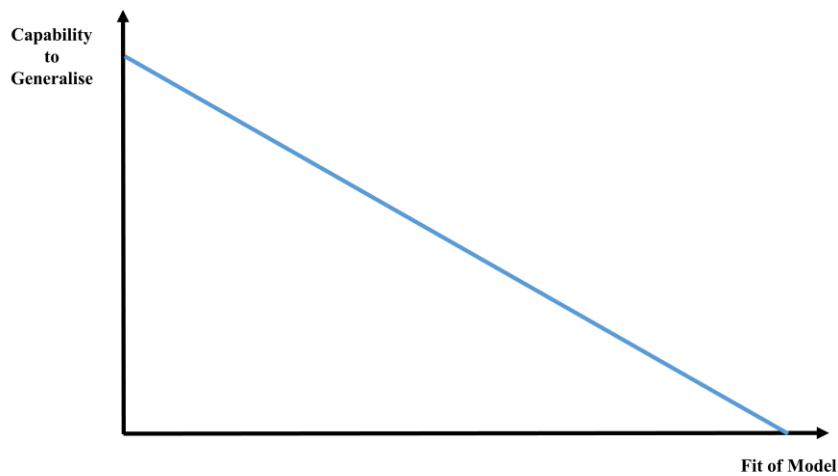
Figure 3-9: Relationship between generalisation and model fit

3.10 Domain Considerations

This section discusses specific issues for FDI within aircraft systems. These issues are not wholly unique and some are shared with most real world operation domains. There does though remain the necessity to adapt FDI methods to suit domain considerations – the most pertinent considerations for aircraft systems are described in the following:

Sensor Failure – In highly engineered systems, such as aircraft EPS, the sensors are often more likely to fail than the monitored system itself. Hence, a FDI method needs to be able to identify sensor failures and to distinguish such failures from faults in the underlying system. Systems may employ a 3-fold sensor redundancy to identify sensor failure, although this approach is expensive in terms of weight and maintenance. *Sensor fusion* [128] is another viable solution that merges and interprets information from multiple sensors. Chapters 5 and 6 highlight the ability of the EPSmart method to utilise sensor fusion techniques to accurately identify sensor failures.

Fleet Variation – Aircraft EPS operate in extreme, highly variable environments. These extremities mean that specific vehicles in a fleet of aircraft may develop individual nominal and faulty behaviour. Additionally, maintenance inspection and repair standards may diverge from standards, potentially introducing new faults or altering the signature of nominal operating modes. Variations within conceptually identical systems emphasises the requirement for generalised FDI methods that can accurately operate across different operating conditions.

System Transients – Nominal transients are inevitable in aircraft EPS. Transients are typically a result of: inductances generating large voltage excursions when circuits are switched on and off; in-rush currents during the start-up of electrical motors; and, nominal load changes causing potentially large, and sudden, changes in current magnitude. FDI methods must be robust to nominal transients and have the ability to discriminate between true faults and normal system dynamics. The potential for the IntelArc method to be robust against nominal system transients is described in Chapters 5 and 6.

Mode Drift – Any complex system can be subject to drift in observables associated with single operating modes. In aircraft systems, the majority of drifts in observables during nominal conditions are a result of sensor degradation/ageing. A FDI method must identify these conditions to avoid false trips. Also, they should deal with the potential for fault modes to fall within the extended normal mode operations, and thus not be detected.

Multiplicity of Modes – A variety of flight phases and functional requirements means that aircraft systems have multiple nominal operating modes. FDI methods must account for

different modes of operation to maintain accuracy. Multiple modes may also experience drift which may mask true operational conditions. The multiple model approach of the novel FDI methods proposed in Chapter 5 of this thesis will improve a health management systems realisation of different modes.

These issues reveal some of the challenges involved with applying accurate FDI methods within an aircraft EPS environment. The methods proposed in this thesis, despite only being at a conceptual/prototype stage of development, address these challenges.

3.11 Review of Significant Literature

The chapter, so far, has described various FDI methods, where particular focus was given to data driven ML methods. The attributes of different ML techniques were described, and the motivations for basing the FDI methods proposed as part of the work of this thesis on HMM were explained. The previous section elaborated on the specific challenges of applying accurate FDI methods within an aircraft systems domain.

Building on these discussions, this section reviews FDI methods available within the literature that have previously been proposed for application to aircraft systems. This begins with a general review, before going into greater detail on aircraft EPS FDI methods. The section also reviews HMM applications; this includes a brief discussion on their use in solving more traditional problems [41], as well as how they have been adopted for FDI within engineering systems.

This review of previous work contextualises the contributions of this thesis.

3.11.1 FDI Methods for Application to Aircraft Systems

The majority of FDI within the aircraft systems domain is centred on assessing hardware faults in the flight control surfaces. There are numerous methods described within the literature for detection of:

- locked ailerons [130];
- sensor failures in accelerometers [131] and internal navigation systems [132];
- failure of electromechanical control surfaces [133];
- tail and wing damage [134].

The rise in UAV has seen an increase in diagnosis of communication link failures [135]. All of these methods use a variety of model based and data based approaches, which have been summarised in Sections 3.4 - 3.8. Reference can be made to the extensive review in [136] for further reading on FDI methods for general aircraft system applications.

Although a number of methods have been proposed in the literature, there still remains a wide gap between state-of-the-art intelligent FDI research and industry practice [136]. Aircraft fault diagnosis and protection methods are usually part of an integrated vehicle health management system that relies on either hardware redundancy or simple limit checking of sensor outputs with threshold values fixed on the basis of recorded flight data.

Clearly, such approaches would not meet the objectives for FDI of degraded and arcing faults outlined in this thesis. Also, in general, there is a distinct lack of FDI methods proposed for application to aircraft EPS, possibly due to the perceived impact on certification. Considering the fact that EPS will become more critical for safe flight (see Chapter 2), there will be an increased requirement within future platforms for EPS faults/degradations to be diagnosed quickly and accurately.

The following section describes FDI methods for specific application to aircraft EPS.

3.11.2 FDI Methods for application to Aircraft EPS

The majority of aircraft system FDI research has been focused on flight control surfaces and communication failures, with limited development of EPS specific methods. Within the general EPS domain, numerous intelligent FDI methods have been developed [39]. However, EPS deployed on aircraft, and other similar environments such as shipboards, exhibit different challenges to that of typical land based systems. Such unique challenges include harsh operating environments, a hybrid AC and DC distribution, and high penetration of power electronic conversion technology.

In an effort to support and accelerate the research of aircraft EPS health management technologies in a real world setting, NASA Ames Research Center developed the advanced diagnostic and prognostic test bed (ADAPT) [137]. The ADAPT is an EPS test bed that incorporates off-the-shelf components connected in a system topology that provides the functions typical of aerospace EPS. The test bed is capable of controlled insertion of faults in repeatable failure scenarios. The development of a diagnostic framework enabled various algorithms to be tested and compared and, in 2009, the First International Diagnostic Competition (DXC09) [138] used this framework to test FDI methods applied to the ADAPT. The competition was run again in 2010 (DXC10) [139]. The EPSmart method proposed in Chapter 5 was developed using data that was released by DXC10 – Chapter 5 can be referred to for further information on ADAPT. Section 3.11.2.1 discusses a variety of methods that were proposed in DXC09 and DXC10.

The review is not limited to discussion on methods for application to ADAPT. Significant aircraft EPS FDI methods previously described, including a dedicated program for such research, are discussed in Section 3.11.2.2. The discussion is extended to include FDI methods for EPS that have similar topologies, and challenges, as those deployed on aircraft, such as shipboard systems.

3.11.2.1 FDI on ADAPT

This section summarises selected FDI methods for application to the ADAPT. These systems were entered into the DXC09 and DXC10 diagnostic competitions.

Daigle *et al.* [140] described a methodology that combined qualitative and quantitative models for fault diagnosis and classification. Primarily, a quantitative observer model based on extended Kalman filters and bond graphs generates residuals for fault detection by comparing actual and predicted system behaviours. After the detection of a fault, a qualitative model employing symbolic representations of changes in impedance (similar to the QTA concept described in Section 3.6.1.3 is used for fault classification. The main advantage of this method is its ability to diagnose both AC and DC faults. A particular benefit is the detection of AC faults using sensors with only limited sampling frequency. The main issue with the proposed methodology is the requirement for extensive *a priori* knowledge of the ADAPT system, as the bond graphs model the physical connections of all components in the system. Also, the method was not extended for the detection of incipient fault conditions.

Narasimhan and Brownston [137, 141] proposed the hybrid diagnosis engine (HyDE), a form of model based diagnosis. The complete model contained 86 separate electrical component models connected according to the configuration of ADAPT. Component models consisted of variables (e.g. voltage/current/relay positions), different operating modes, and transitions between different modes. Updating the parameters of each component model using sensor observations enabled HyDE to infer system behaviour. This reasoning engine involved maintaining a set of fault candidates that are consistent with observations. Each candidate is tested for consistency as new observations become available. The drawbacks of HyDE are fairly self-explanatory – developing component models requires significant effort and knowledge. Also, the accuracy of HyDE in diagnosing incipient and intermittent faults was reduced by a high false positive rate.

Mengshoel *et al.* [33] developed a probabilistic approach based on BNs and arithmetic circuits (ACI). The ADAPT topology was primarily described using a novel high-level modelling language; a program then automatically converted the high-level specification into a BN. The BN of the ADAPT network had 503 discrete nodes (sensor observations were discretised) and 579 edges. Nodes included health and evidence nodes. The BN was compiled into an ACI – converting to an ACI reduces the computational resources required during on-line inference, as the number of parameters and nodes are minimised. All of these stages were conducted off-line. Online FDI is achieved by clamping evidence to observed nodes and inferring the probability of various health nodes. The proposed method showed excellent diagnostic coverage over a range of fault types. However, once again, development involved detailed knowledge of system structure. Also, component failure rates, required for implementation of their approach, may not always be available.

Gorinevsky *et al.* [142] developed a mathematical model based method for diagnosis of sensor and DC load faults on the ADAPT. The linear model combined state equations and observation equations. The state equations were modelled using Kirchhoff's voltage and current laws; the observation equations were modelled using the voltage and current observations. Fault vectors are used in the state and observation equations to model the impact of load and sensor faults respectively - online FDI involves estimating these fault vectors. Testing results showed overall high diagnostic accuracy with an average time to diagnosis of 20ms. However, there were issues with incorrect diagnoses as a result of power converter dynamics. This suggests that the mathematical model may have to be extended to include nominal system transients.

Other methods proposed for fault diagnosis on the ADAPT include *SystemicsC* and *TARDEC* [139]. *SystemicsC* combined a system model with case based reasoning for

inference – the method is based on the General Diagnostic Engine described by de Kleer and Williams [143]. The model generates conflicts when observed behaviour is not consistent with model behaviour. The hypotheses for generation of such conflicts are refined by mapping known conflicts to known faults.

TARDEC is a two-tier method which primarily utilises statistical models to categorise sensor faults. All detected sensor faults and other sensor observations are aggregated and a rule based system then infers the most likely cause of a fault. Fault parameters are also estimated to determine fault severity. Unfortunately, the nature of the *TARDEC* method - it was developed by a branch of the US Army - means that detailed information surrounding its operation is not in the public domain.

While each method had associated benefits, the main overarching drawback of the majority of methods was the requirement for significant *a priori* knowledge on the topology and components of the ADAPT – none of the systems were entirely developed using system data alone. The novel EPSmart and IntelArc methods proposed in Chapter 5 of this thesis address this issue as development and application does not require such *a priori* knowledge and only system data is required.

3.11.2.2 General Review of Aircraft and Shipboard EPS Fault Diagnosis

A summary of relevant FDI methods proposed in the literature is described in this section. The section discusses the application of FDI methods to other compact, power dense EPS; such systems include general spacecraft and shipboard EPS.

The aircraft electrical power systems prognostics and health management program [144] was developed by Dual Use Science and Technology and sponsored by the Air Force Research Laboratory. The objective of the program was to demonstrate health management technologies that ease real-time and maintenance issues to improve mission readiness of military aircraft, and dispatch reliability of commercial aircraft. The first phase of the program addressed FDI of electrical actuators, fuel pumps/valves and arc faults. The second phase addressed faults within the generation systems. A major objective of the program was to identify the data required to accurately diagnose fault conditions and retain a desired level of health management. This involved researching the generation of fault data using laboratory tests and the integration of diagnostic and prognostic algorithms into health management systems.

Diagnostic systems for 135VDC brushless motor actuators and 270VDC supplied fuel pumps were developed based on the analysis of vibration and frequency signatures.

Integrating traditional off-line arc fault FDI methods into the power distribution units for online application was proposed. A prototype of this method was demonstrated for the detection of series and parallel DC arcing – Chapter 4 can be referred to for detailed discussions on arc fault diagnosis. Overall, the program stressed the requirement for intelligent FDI methods within aircraft EPS and researched ways in which this can be practically achieved [144].

Liu *et al.* [145] proposed an intelligent built-in-test system based on wavelet analysis and ANN. Built-in-test [146] provides an on-board, automated test capability to detect, diagnose and isolate faults – the general idea is similar to the health management system described in Chapter 2, Section 2.4.2. Essentially, it enables faults to be diagnosed without the requirement for external test equipment. The system proposed by Liu *et al.* used the WT for feature extraction and an ANN for classification of various generator and converter faults within an MEA representative EPS. Initial testing results showed the proposed system had an average accuracy of 98%.

Cao *et al.* [147] proposed the combination of fault trees and an expert system for aircraft EPS fault diagnosis. Fault tree models of the power supply systems were developed. At the detection of a failure, or *top event*, the expert system is used to analyse the most probable cause of the fault. The limitations of expert systems were discussed in Section 3.6.1.1.

FDI within a general EPS spacecraft system was proposed by Gonzalez *et al.* [152]. They outlined an intelligent power controller prototype with the ability to protect the EPS from degraded and overcurrent faults. To minimise real-time constraints, the proposed method acts as primary protection for degraded faults and backup for overcurrent faults. The method was developed for the 'space station module power management and distribution breadboard', a NASA DC test bed representative of a space station power system. A model of the test bed system was developed using Kirchhoff's current law to determine current values throughout the network under a range of nominal scenarios. The model is used for FDI by analysing and applying expert knowledge following discrepancies between expected and observed system current values. The paper summarised tests which showed the methods ability to accurately isolate faults and enable recovery of power to critical loads if required. The paper also highlighted the requirement for global control of the system - where a single controller receives all sensor measurements – as opposed to local control, for FDI of degraded faults.

Akin to the trend of MEA, shipboard systems have become more focused on the use of electrical energy for distribution to secondary sub-systems. Increasing dependence on electrical energy has resulted in a range of FDI methods being proposed for shipboard EPS.

Liu *et al.* [148] proposed a multi-agent system, where each agent monitors separate components within the EPS. Each agent in the system utilises model based diagnosis to determine both sensor and component faults. The paper also discusses the use of separate agents for different tasks (such as power quality monitoring, load shedding and network reconfiguration) to ensure reliable and optimal operation.

A FDI method for medium voltage multi-terminal DC shipboard systems was proposed by Weillin *et al.* [149]. Similar to the method proposed for aircraft EPS described in [145], the method is based on WT for feature extraction and ANN for feature classification. The paper emphasises the challenges involved with FDI in multi-terminal DC systems - challenges include diagnosis of faults within compact networks with different distribution zones, as well as the overall higher safety requirements within such networks. The method proposed within the paper is developed to diagnose short circuit faults on the main DC bus and AC side of a rectifier and ground faults within the high-resistance grounded network. Energy levels of the extracted WT coefficients were selected as suitable input features for the ANN to classify. The method was trained using data from a real-time digital simulator, and was tested online using an experimental test bed. Testing showed high accuracy. The lack of explanation capabilities from the binary ANN output (see Section 3.9) is one limitation of the multiple fault diagnostic method.

Weillin *et al.* [149] also give an excellent overview of proposed fault detection method for medium voltage DC networks - this includes discussion on other ANN based methods [150], active impedance estimation [151], and the use of power electronic converters for detecting and isolating short circuit faults [153].

3.11.3 HMM Applications

The EPSmart and IntelArc FDI methods proposed as part of the work of this thesis are based on HMM. Consequently, this section briefly reviews previous HMM applications described within literature.

HMM theory was first introduced by Baum and Petrie [161] in the late 1960's, and the technique was first implemented for speech processing applications by IBM [162] in the early 1970's. However, the fact that the theories were both difficult to apply in practice and confined to purely mathematical journals, meant that it was not until the mid-1980's that they became a popular tool for solving a variety of problems. The more traditional applications of HMM are in areas such as speech, handwriting and gesture recognition [40, 41, 154]. The tutorial by Rabiner [41] is recommended for a complete description of the use of HMM in these applications.

Attractive features, including: their inherent scalability; potential to infer the probability of multiple hypotheses; and, suitability for classifying time series input data under minimal computational burden, inevitably resulted in their application to other domains. Examples of some applications include:

- Rotating machine condition monitoring [42, 155].

- Classifying patterns in process trend analysis [111].

- Anomaly detection in nuclear reactor cores [157].

HMM based methods particularly relevant to this thesis are outlined in references [34, 158-160]. These methods were all developed for FDI within either transmission or distribution network line disturbances. Each system is briefly described as follows.

Abdel-Galil *et al.* [34] proposed a multiple-model HMM approach, where a separate HMM is trained for each class of power quality disturbance (similar to the framework illustrated in Figure 3-5). Disturbances included sags, swells, and transients within land based distribution networks. An unrecognised disturbance sequence is matched to each of the trained models. Classification is determined by the HMM which attains the highest score in the matching process. The paper describes the use of a discrete-density HMM, where a vector quantisation technique is used to discretise either WT or FT continuous feature vectors. The authors claim the discretisation process enables the system to distinguish between both slow and fast transient phenomena. They also claim the HMM based system is advantageous in terms of the minimal computation time, and the lack of re-training required (as a new disturbance class can be included readily in the classification procedure with the addition of a new HMM). The paper compared using FT and WT for extracting features from network voltage data. While both transformations provided high accuracy, they concluded that the WT was more suitable.

Perrera and Rajapaske [158] also proposed a multiple-model HMM based method developed to determine if the presence of transients observed in transmission networks were a result of fault conditions. Training data was generated using simulations of a 765kV transmission network, and two separate HMM were trained corresponding to fault and non-fault transient conditions respectively. Fault transients included various phase-phase and phase-ground conditions. Non-fault transients included line switching, load switching and transformer in-rush. The classification system uses a range of WT decomposition and approximate coefficients as discriminative features. Application of the proposed system was tested in a hardware environment using a real-time playback waveform generator. Results showed 100% accuracy for non-fault test cases and 88% accuracy for fault test cases.

Average response time of the system was 6ms, although the majority of this time was calculating wavelet coefficients.

Chung *et al.* [159] outlined a wavelet-packet based HMM method to diagnose fast capacitor switching, normal capacitor switching and impulse disturbances in a 7.2kV distribution line. Wavelet packet is an extension of the WT, where additional coefficients are extracted to obtain extra time-frequency information. The proposed method used wavelet packet coefficients extracted throughout each disturbance to train a separate HMM – a total of 11 HMM were trained for each condition. The system was tested using over 500 actual disturbance events recorded on a digital fault recorder – average accuracy across all tests was 98.7%.

These methods are important in the context of this thesis as they have shown the potential for HMM to accurately diagnose faults and classify disturbances in EPS. There was concern within the diagnostic community that applying HMM in less traditional application environments would yield less accurate systems. However, these papers have shown that high accuracy can be achieved on top of the benefits they have over other potential techniques (see Section 3.9).

While the papers described in this section are important for highlighting their application to EPS, they only described diagnosis of AC based systems. Aircraft EPS have hybrid distribution and, as described in Chapter 2, DC is likely to become more prevalent. Chapter 5 of this thesis describes EPSmart and IntelArc, HMM based methods for FDI of both intermittent and incipient faults within hybrid distribution environments and series arc faults within DC supplied systems. Utilising HMM for solving such problems has not previously been researched.

3.12 Chapter 3 Conclusions

This chapter introduced the theory of fault diagnostic systems based on intelligent FDI methods. This included a general description on the main objectives of fault diagnostic systems and the different methods that enable such objectives. The increased volume of EPS data expected to be generated within MEA has resulted in the thesis focusing on quantitative, data driven methods. The chapter emphasised that intelligent FDI methods based on ML techniques have the potential to efficiently, and reliably, interpret network behaviour/condition through analysis of the extensive volumes of generated data. The attributes of various ML techniques were compared, and the chapter summarised why HMM were selected as the basis for the FDI methods proposed in this thesis.

Existing FDI methods applied to an aircraft EPS domain were reviewed to help place in context the contributions of this thesis. This review established that there is a lack of FDI methods specific to this domain and the majority of EPS still rely on local control and basic overcurrent fault protection methods. The review focused on methods developed and applied to NASAs ADAPT test bed, which was designed to accelerate development of diagnostic algorithms for aircraft EPS - the EPSmart method proposed in Chapter 5 this thesis was validated using data from the ADAPT. The majority of methods reviewed were model based, which have the specific disadvantage of requiring *a priori* knowledge of system topology and components - data based methods are beneficial in this sense as they do not require this form of *a priori* knowledge. FDI methods for application to shipboard and other similar microgrid topologies were briefly discussed. The chapter also reviewed HMM based methods applied for FDI and disturbance classification within the general EPS domain; these methods were all developed for main grid transmission and distribution applications, and thus focused only on AC distribution. The FDI methods proposed as part of the work of this thesis are developed for both hybrid AC/DC aircraft EPS and for series DC arc fault diagnosis.

Overall, the chapter has described important theories of FDI methods based on data driven ML techniques, particularly HMM. This facilitates easier understanding of the EPSmart and IntelArc methods proposed in Chapter 5.

4. ARC FAULT CHARACTERISTICS, MODELLING & DETECTION

The arc fault was introduced in Chapter 2. The main causes of such events occurring in aircraft and difficulties in protecting against them were outlined. The *IntelArc* method described in Chapter 5 is proposed specifically for diagnosis of series arc conditions and, to provide further insight into this particular type of fault, this chapter fully elaborates on them. This includes:

- A description of their electrical characteristics. Present knowledge of arcing has been largely developed based on the observation and analysis of electrical measurements during test conditions. The electrical characteristics are essential to defining the complex arcing phenomenon in power systems [165]. Numerous studies, spanning decades of research, are available in literature – the main studies relevant to this research are summarised within the chapter.

- The description, and validation, of a series DC arc fault model. The model was used for generation of synthetic current and voltage data during simulated arcing events. Appreciation of electrical characteristics of arcing described within literature is necessary for validation of model accuracy.

- A summary of existing arc fault detection methods.

Synthetic data generated from the fault model was used throughout development of the IntelArc method, and fault model validation is necessary to confirm the accuracy of simulated arc fault data. The discussion on existing detection method enables deeper understanding of the IntelArc method proposed as part of the work of this thesis.

4.1 The Arc Fault

An arc fault is a self-sustaining luminous discharge of electricity through conductive ionized gas across a gap in a circuit or between conductors. This process is simplistically illustrated in Figure 4-1. Arc faults are initiated when there is sufficient ionisation of the air gap between two conductors such that their voltage difference exceeds the dielectric breakdown voltage.
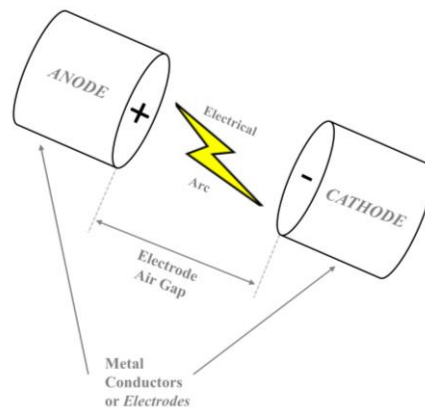
Figure 4-1: Arc fault across an air gap between conductors
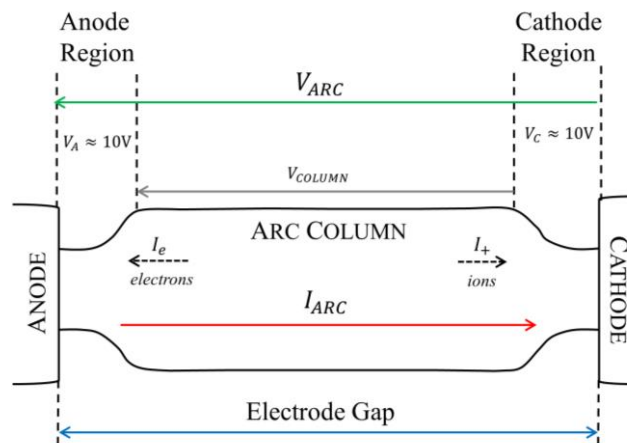
Figure 4-2: Ionisation in the column as a result of increased temperature frees electrons from atoms. Free electrons flow to the anode and positively charged ions flow to the cathode. The anode and cathode regions are accumulations of electrons and ions respectively – they are typically about 0.01mm with a potential difference of 10V. Arc current in the form of positive ions in the gas is transitioned to the metal conductor cathode where current flow is in the form of electrons.

Electrical properties of an arc are illustrated in Figure 4-2 [166]. The arc consists of three regions: the anode region, the plasma column, and the cathode region. The electrode regions form the transition regions between the gaseous plasma cloud and the solid conductors. Thermal ionisation within the gas column frees electrons from atoms that, under the force of an electric field (voltage), create a flow of current between the conductors [167].

The voltage profile across an arc consists of voltage drops across the anode and cathode regions and across the column itself. Voltage across the arc column depends on the arc length – as convection forces the conductive plasma to bow upwards, arc length will usually be longer than the electrode gap itself [165].

Arc faults are usually initiated when two conductors are separated[8] and a large electric field appears across the small air gap. 'Normal' arcing occurs during mechanical switching operation of CBs and contactors [169]. These devices are designed to withstand arc formation and normal arcing is typically highly transient and unsustainable.

Conversely, arc current through the gas column during fault events may be fully sustained between two separated conductors. High heat generated during fault events often leads to partial volatilization of the conductors and increases the risk of fire [170].

The separation of conductors can occur in a variety of ways and, accordingly, arc faults are classified as follows [171]:

- *Constant Speed Fault* – Electrodes are separated at a constant speed with incrementally increasing distance.
- *Fixed Distance Fault* – Constant speed fault where the electrode gap eventually dwells at a fixed distance.
- *Accelerated Fault* – Fast separation of electrodes e.g. a conductor physically breaking.

Arc faults are also classified in terms of their location with respect to load.

Series arc faults occur in series with loads at unintended points of discontinuity within an electrical circuit [84]. These circuit imperfections often emerge as a contact separation or loose connection– in aircraft, vibration often results in series arcing being intermittent. These faults are particularly difficult to detect as low values of arc resistance produce only minimal changes in system current and voltage levels [171] – the novel IntelArc method is designed to detect these faults and is a main contribution of this thesis.

---

[8] In the case of wet arc tracking [168], conductors may not have to contact at any point

Parallel arc faults occur between two conductors in parallel with the load. These can be a result of wet arc tracking, or of wires with damaged insulation temporarily contacting. These events primarily lead to a high impedance arc that melts and carbonises the insulator. This forms a low impedance path between the conductors [172] and effective short circuit of the load.

4.1.1 Comparison of AC and DC arc faults

Behaviour throughout arcing events is dependent on the nature of the electrical source. AC power has a natural current and voltage zero. In the time-domain, a distinct characteristic of an AC arc is the arc extinguishing after current zero. This feature is illustrated in the current waveforms in Figure 4-3.

Zero current flows in the time between arc extinguishing and re-ignition. Duration of zero-current flow depends mainly on electrode gap distance and the condition of the plasma itself. Plasma resistivity decreases in the presence of previous arcing, resulting in a decreased re-strike voltage and therefore shorter current gaps. Highly inductive loads reduce the duration of the current gap through limiting the rate of change of current through the gap [173].

Re-strike voltage is also dependent on the distance between electrodes – increased electrode distance usually requires a greater voltage to re-ignite the arc. Arc re-ignition involves steep current edges, where rate of change depends on current gap duration and on the connected load.

In series AC arcing (Figure 4-3 (b)), where the electrode gap is usually much smaller, current flow may not be interrupted during current zeros as drops of molten copper from the previous arc may bridge the gap [173]. Also, rate of change of current after re-ignition is less stable in comparison to parallel faults.

In DC supplied systems, there is no natural current zero. As a result, arcing conditions are more sustainable and, potentially, more dangerous [174, 175]. A typical arc current waveform in a DC system is illustrated in Figure 4-4 where arcing over a sustained period is evident.

Natural arc extinction in DC systems is usually a result of:

- Excessive cooling of the plasma under high-voltage, low current conditions.
- Increase in distance between electrodes.
- Increase of arc voltage above supply voltage.

The accurate detection of arcing events in both AC and DC systems is vital to minimising the risk of fire to surrounding insulation or other flammable materials.
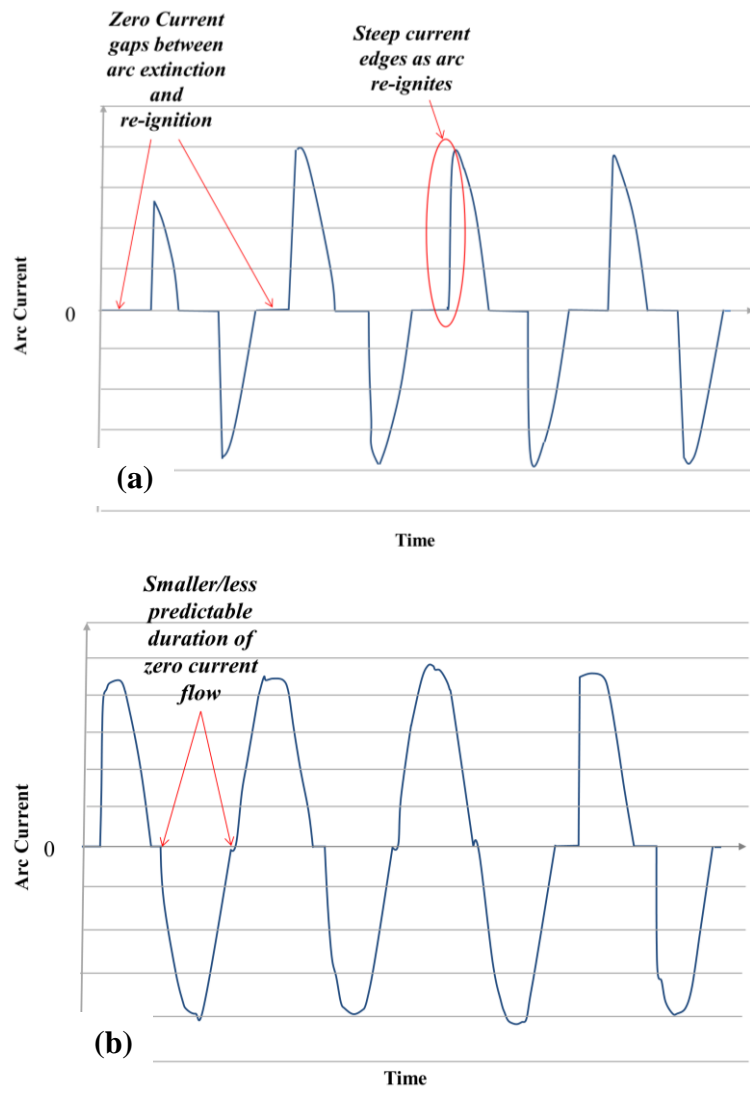
Figure 4-3: Typical arc current waveforms for AC faults of (a) Parallel fault and (b) Series fault
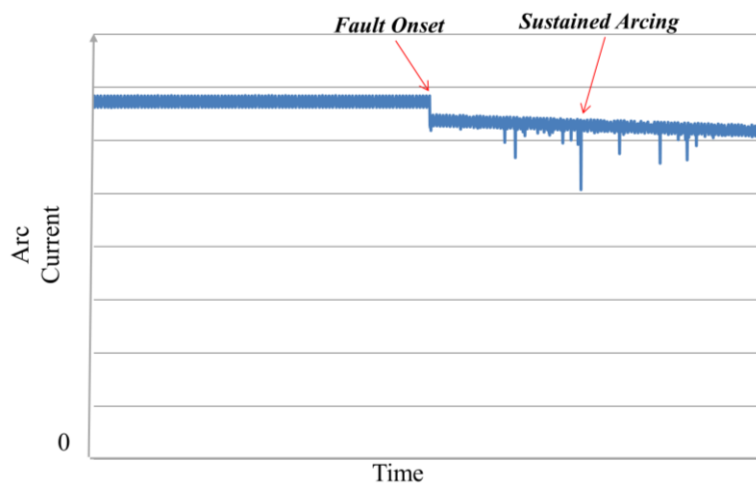
Figure 4-4: Typical arc current waveform for a series DC fault

81

4.1.2 Detection Issues within Aircraft EPS

Current magnitudes of series and parallel arc faults relative to typical nominal load current ratings are illustrated in Figure 4-5. Series arc fault current is limited by load impedance and is therefore within the range of rated current and significantly below relay thresholds. Parallel arc fault current is usually characterised by a high impedance (lower fault current) stage preceding the formation of a low impedance short circuit path.
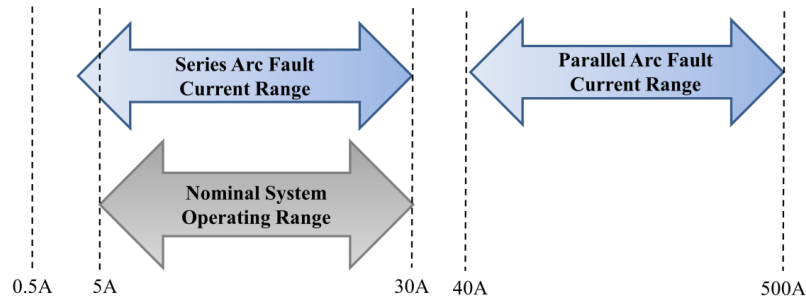
Figure 4-5: Fault ranges for parallel and series arc faults [176]. Lower current magnitudes often result in traditional overcurrent protection devices (CB's and relays) not detecting arc faults

Fault current levels, particularly during series events, highlight the detection challenges. Fault current magnitudes being within, or even below, rated values leads to the requirement for detection methods to discriminate between fault events and normal load transients. In conventional aircraft EPS, this challenge is theoretically simplified as the majority of loads on a given circuit are fixed by design and transient variations are minimised [85]. This is not the case for MEA EPS, where loads are likely to be more dynamic to meet varying demand throughout flight phases.

Altitude impacts the nature of arcing events, particularly in DC systems. High altitude reduces the number of gas molecules in the arc column and induces rapid diffusion of the localised, high-temperature ionized gases needed to sustain the arc. This results in arcs extinguishing at shorter gap lengths at lower pressure, and therefore greater difficulty in detection [192]. Less sustainable, intermittent series arcing in DC systems can also be a result of in-flight vibrations.

With respect to parallel arcing, the absence of a neutral conductor within aircraft means arcing to ground is particularly difficult to detect. AFCBs [85], which detect arcing shorts from line-to-line, have been developed. AFCB devices monitor line voltages and currents to detect parallel arcing signatures and incorporate the signatures of normal transient events such as arcing at motor brushes/CBs, inrush starting currents and load changes to minimise false detection rates of arcing events. However, AFCB's are limited to application in AC distribution systems.

This limitation highlights the importance of developing arc fault diagnostic methods that can be applied accurately within DC systems. Aircraft will increasingly rely on DC distribution. Technology that can determine the presence of difficult to detect, and potentially dangerous, events within this form of distribution is critical to its evolution.

This research focuses, as one of its objectives, on the design and development of IntelArc, a series DC arc FDI method. Some of the challenges of meeting this objective have been outlined. Section 4.3 describes a validated series DC arc fault model that was used throughout development of IntelArc.

To validate the simulation model, it is necessary to first outline arcing characteristics and models that have previously been defined within literature.

4.2 Arc Fault Electrical Characteristics and Modelling

Arc faults are modelled in terms of either their underlying physical processes [177] or their electrical characteristics [165]. Physics based models combine electromagnetic, fluid dynamic and thermodynamic equations to form systems of differential equations. The physics of arcing phenomenon is complex and the constants are hard to define for real-world arcing faults in power systems.

Electrical based models [178] capture arc effects on electrical circuits and are developed around electrical characteristics that have been defined through observation of empirical data [171]. They are more simplistic and useful in the power system context in comparison to physics based models.

Usually a 'black box'[9] technique is used, where the arc is modelled as an equivalent electrical circuit/component, usually impedance. This technique often adopts a heuristic approach [171], where mathematical relationships are used to correlate V-I model outputs with empirical observations.

This section summarises both the electrical characteristics of arc faults and various electrical models that have been developed.

4.2.1 Electrical Characteristics

Arcs existing at fault points are described as 'long arcs in still air' [169] that exhibit highly complex, non-linear behaviour.

In general, electrical characteristics of arcs depend on a variety of factors, including:

- Length of electrode gap

---

[9] A black box model is viewed in terms of only its inputs and outputs and the internal processes of the model are not required for use/application.

- Electrode material
- Ambient conditions (e.g. air pressure and type of gas)

Arcs are commonly associated with a voltage profile across the arc plasma that is dependent on the length of the arc. Voltage gradients (*Volts/Arc length*) were defined by Strom [179] for various arc currents - these are outlined in Table 4-1. Limited variation in voltage gradients across large ranges of currents led many researchers to the conclusion that it is essentially independent from arcing current.

Table 4-1: Average voltage gradients defined by Strom

Arc Current	Average Voltage Gradient
< 5kA	12.2 – 13.0V/cm (31-33V/in.)
10 kA – 20 kA	15.0V/cm (38V/in.)
68 A – 21.75kA	13.4V/cm (34V/in.)

However, extensive research has proven that V-I behaviour for fixed length gaps is both inverse and non-linear at very low current levels.

4.2.1.1 Arc V-I Relationships

Figure 4-6 illustrates the general V-I characteristic for an arc with fixed length electrode gap.
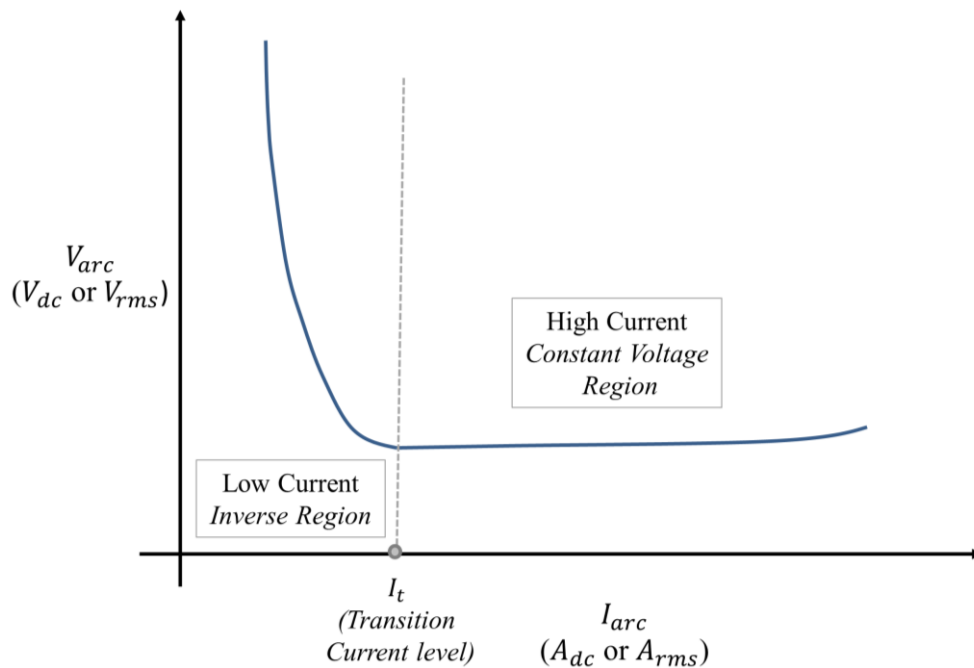
Figure 4-6: V-I characteristic for arc with fixed electrode gap. Note the two distinct regions and the current transition level that marks the boundary between the regions.

Two distinct regions exist in the V-I characteristic:

1) Inverse region – at lower current magnitudes, the voltage drops as arc current increases.

2) Constant Voltage region – at higher current magnitudes, voltage increases slightly as arc current increases (in agreement with Strom's theory).

Within the inverse region, arc power remains relatively constant. In the constant voltage region, power increases with arc current. Indeed, instantaneous arc power tends to exhibit greater stability in comparison to arc current and voltage. Voltage and current can fluctuate significantly – a minor fluctuation in arc voltage is accompanied by an opposite fluctuation in current delivered by the power supply. However, when power is taken as the measure, the voltage and current instabilities are cancelled out, and the measure is more constant.

Differences in V-I behaviour at low and high values of arc current are mainly attributed to the dominance of natural convection forces at lower current levels being overtaken by magnetic convection at higher current levels [180, 184]. Stokes [180] quantified the transition level, I_t, between low current behaviour and high current behaviour as:

$$I_t = 10 + 0.2E_{gap}$$

<div align="right">(4.1)</div>

Where E_{gap} is the distance between electrodes in millimetres (mm). For shorter gap lengths ($\approx$ 0.01 to 30mm), the current transition level is $\approx$ 10-13 Amps. This level is in agreement with Solver [165], who determined that, for shorter gap lengths, arc voltage is almost entirely dominated by the anode and cathode voltage drops, and therefore exhibits constant magnitudes for a range of currents above roughly 10A.

Other research [181, 182] determined the transition level to be higher ($\approx$ 50-100A), and not related to electrode gap. Tendency to overemphasise inverse V-I characteristics was probably a consequence of the difficulty for early researchers to measure high current arcing. The availability of low-power supplies meant most studies were conducted in low current ranges and results read across to higher current scenarios.

Other factors affecting V-I behaviour includes:

- Electrode material – different materials affect overall arc voltage. Minimum voltage required for stable arcing is also dependent on electrode material.

- Electrode configuration – horizontal and vertical arcs in air are affected differently by convection forces.

V-I characteristics derived from the research cited within this section are summarised in Section 4.2.2.

4.2.1.2 Impedance Characteristics

The majority of experimentation (see Section 4.2.2) observed near simultaneous changes in arc current and arc voltage. This indicates that arc impedance is mostly *resistive* in nature. The main characteristics of arc impedance include:

- Non-linear resistance-current (R-I) behaviour, with significantly increased resistance at lower current levels.
- Near constant resistance for a given electrode gap at high current magnitudes.
- For a given arc current, arc resistance increases linearly with electrode gap.

These characteristics are illustrated in Figure 4-7.

Arc resistance for current levels above and below a transition level, were quantified by both Stokes [180] and Paukert [181]. These are described in Section 4.2.2. Comparison between these empirically derived arc resistance formulas and arc resistance from the developed MATLAB Simulink [227] fault model is also provided in Section 4.3.3.3.
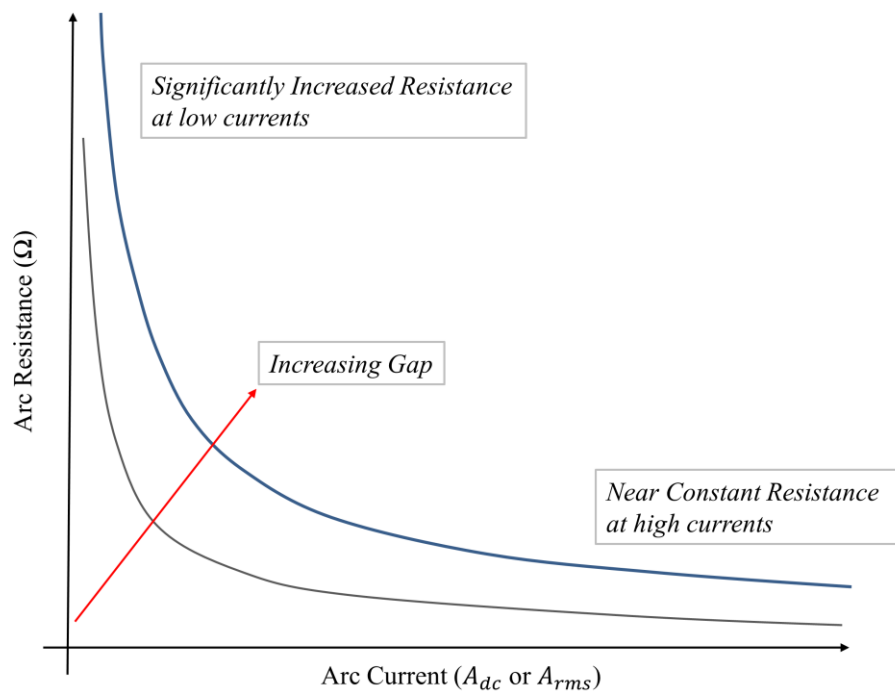
Figure 4-7: Arc R-I characteristics

4.2.1.3 Time & Frequency Domain Characteristics

Time domain examples of AC and DC arcing current were illustrated in Figures 4.3 and 4.4 respectively. These simple examples highlight the chaotic and random behaviour of arcing events, particularly in DC systems. In AC systems, natural current zeros result in more consistent, even periodical, time domain signatures. DC arcing behaviour is characterised by random unsuccessful arc quenches [171, 174] throughout more sustained arcing periods. Arc voltages and currents are often highly unstable, where voltage spikes and current notches represent unsuccessful quenching.

Such chaotic time domain features translate to arcing events exhibiting an expansive frequency range, which extends from the lowest DC components up to radio, microwave, infrared and light spectra. Numerous detection methods are based on the identification of high frequency components which may be indicative of arcing events. These are discussed further in Section 4.4.4.2. An excellent discussion on the frequency domain characteristics of arcs is provided in [183].

4.2.2 Significant Arc Fault Studies & Models

Table 4-2 summarises some of the key studies that have contributed to knowledge of electrical characteristics of arcing and determined specific equations and models. The summary includes a description of the types of experiments conducted within each study.

The majority of studies outlined in Table 4-2 are particularly relevant to this research as they included DC arcing conditions. Other models based on electrical characteristics have been developed, most notably Cassie and Mayr models [218]. Mayr assumed a constant power loss in the arc, while Cassie assumed a constant arc voltage. The research in this thesis is focused on series DC arc faults, where contacts are drawn apart. Changing arc length means both arc voltage and power are not constant. The Cassie and Mayr models are therefore not suitable for the considered fault cases.

Within the described studies, only Uriarte [171] designed test conditions exclusively concentrating on both DC and series arc faults. Consequently, the Simulink fault model that was developed for generation of synthetic arc current and voltage data was significantly based on Uriarte's derived model.

The following section describes the fault model and validates its output against the other studies.

Table 4-2: Outline of Key Selected Arc Fault Studies and Models

Study (Year)	Experiments	Arcing Characteristics	Derived Models
Ayrton (1902) [185]	Arcs initiated between carbon electrodes separated by a few mm. Formulated first known equation to model electrical properties of arc. All early arc models [24] were based on a limited number of low-current tests.	Early research assumed empirical constants affect arcing behaviour. This was later disproved [25] in research that showed constants are in-fact dependent on arc conditions.	$$V_{arc} = A + BL + \frac{C + DL}{I_{arc}}$$ Where A is electrode voltage drop, B is voltage gradient, L is arc length and C and D are the empirical constants that model the non-linear characteristic.
Hall, Myers & Vilicheck [182] (1978)	Evaluated arc faults on DC trolley systems used in the mining industry. Over 100 tests using 300VDC supply with currents ranging from 300-2400A and electrode gap widths from 4.8 to 152mm	Non-Linear V-I characteristic. Voltage remained constant at ≈ 50V for arcing currents over 800A. Once an arc was established, gap increased sufficiently to self-extinguish. Current and voltage contained high frequency components. Inductance in circuit reduced high frequencies in current.	Modelled V-I characteristic with inverse behaviour below 500A and extremely inverse behaviour below 200A.
Stokes & Oppenlander [180] (1990)	Arc current and voltage recorded for vertical and horizontal DC arcs burning with exponentially decaying current from 1000 to 0.1A and 50Hz AC arcs with currents ranging from 20kA to 30A. Voltage supply ranged from 6kV to 100kV.	Significant fluctuations in arc current and voltage. Inverse V-I characteristic below a transition current, which is determined by electrode gap and is ≈ 10-12A for small gaps - arc voltage increase slightly for currents above the threshold. Formulated minimum arc voltages required for stable arcing.	$$V_{arc} = (20 + 0.534 E_{gap})I_{arc}^{0.12}$$ $$R_{arc} = \frac{20 + 0.534 E_{gap}}{I_{arc}^{0.88}}$$ Where I_{arc} > transition current
Paukert [181] (1993)	Compiled published arcing fault data from seven researchers who conducted a wide range of DC and AC tests. Arcing currents ranged from 0.3A to 100kA and electrode gaps ranged from 1 to 200mm.	Inverse V-I and R-I characteristics across the range of electrode gaps for lower current values (<100A). Transition arc current of ≈ 100A, at which characteristics become positive.	Formulated arc-voltage and arc resistance equations for various electrode gap widths. Two sets of equations- one for arcing currents below transition value and the other for above.
Uriarte *et.al.* [171, 188] (2012)	Staged series arc faults on a DC microgrid at voltage levels up to 1kV and currents in excess of 100A.	At fault onset, initial arc voltage is equal to the anode and cathode voltage drops – as electrode gap increases, voltage across the arc column also increases. Several voltage spikes are observed in the voltage trajectory which represents unsuccessful arc quenches. Eventually, a critical gap distance is reached, and the arc extinguishes.	Modelled the dynamic components of arc voltage and current with a hyperbolic approximation, which represents contacts separating, and a rectangular pulse, which represents the electrode voltage drops.

4.3 DC Series Arc Fault Model – Design and Validation

The fault model described within this section is based on the empirically derived model developed by Uriarte et al. [171]. The mathematical model (detailed in [171]) was developed to correlate its output with experimental observations. Experimental data was generated through the staging of faults on a DC microgrid test bed [188, 189]. The horizontal series faults were initiated through the separation of two conductors that were previously contacting - this is a method commonly applied within literature [190] and is recommended in arc fault detection standard UL1669B [191]. Voltage and current trajectories from the numerous faults staged on the test bed were used to develop a generalised fault model that showed consistency across various source and load conditions.

This section describes the development of a fault model in MATLAB Simulink that was based on the mathematical equations determined by Uriarte *et al*. Comparison of the developed fault model with the other arc models described in Section 4.2.2 allowed validation of model accuracy.

4.3.1 Summary of Empirically Derived Model

The arc model is essentially a hyperbolic approximation of the dynamic arc voltage and current. Basic elements of the model - voltage, current, and resistance - are illustrated in Figure 4-8 and described in the following.
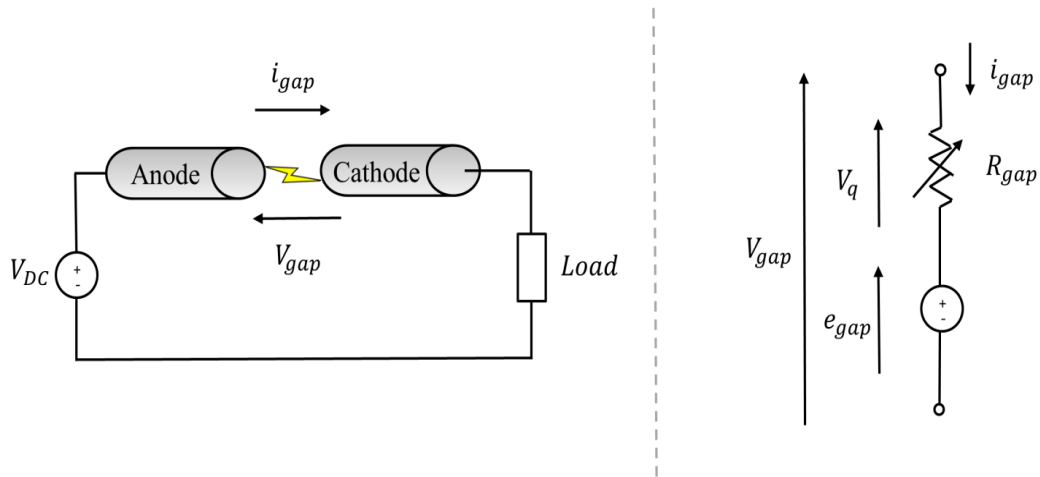
Figure 4-8: Basic elements of arc fault model

4.3.1.1 Gap Voltage

Gap voltage, V_{gap} is decomposed into a non-linear hyperbolic tangent function V_q and an electromotive force (EMF) pulse term, e_{gap}:

$$V_{gap} = V_q + e_{gap} \qquad (4.2)$$

The decomposition of V_{gap} is shown in Figure 5-9. The contribution of both the hyperbolic function and EMF pulse to total gap voltage is dependent on a distance ratio, q, where:

$$q = \frac{X_{gap}}{X_{critical}} \qquad (4.3)$$

X_{gap} is the electrode gap and $X_{critical}$ marks the boundary between the arcs burning and quenching stages. At the point where $X_{gap} = X_{critical}$, $q = 1$, and the arc quenches.
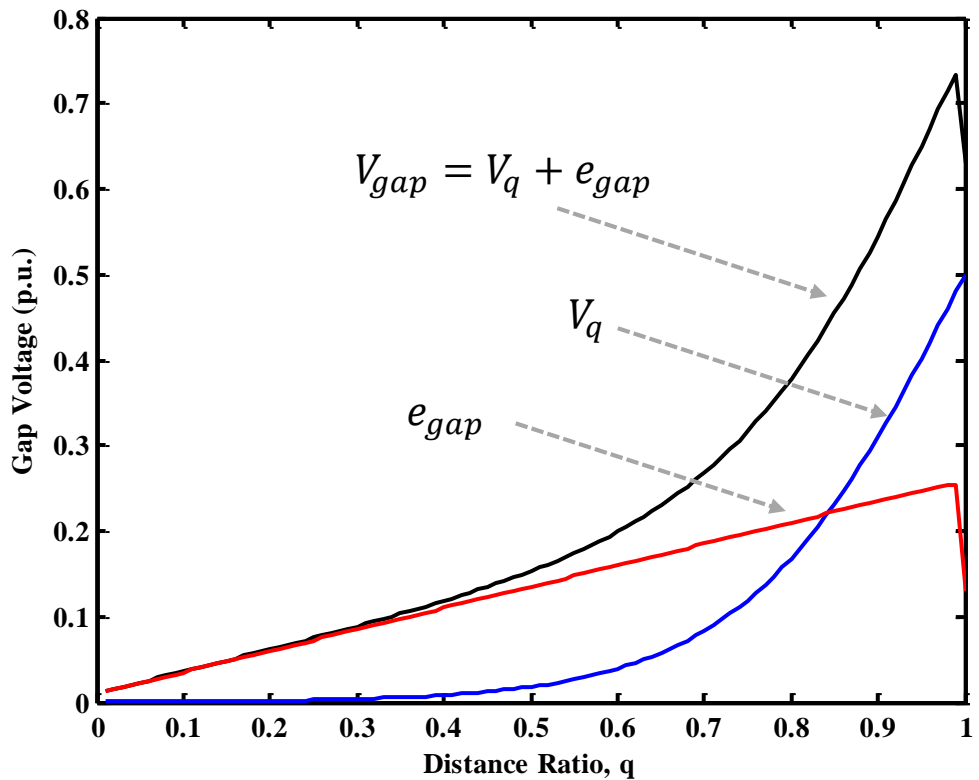
Figure 4-9: Decomposition of V_{gap}

V_{gap} is dominated initially by e_{gap} – as q increases and the arc begins to collapse, the voltage profile then becomes dominated by V_q. In this sense, e_{gap} represents the electrode voltage drops while V_q represents voltage across the column increasing as the electrode gap increases.

Both V_q and e_{gap} are modelled mathematically and are dependent, not only on distance ratio, but also on supply voltage, V_{dc} :

- V_q is approximated with a hyperbolic tangent function

$$V_q = V_{dc} \left(\frac{1}{2} + \frac{1}{2} \tanh(\alpha(q-1)) \right) = V_{dc} \left(\frac{e^{2q\alpha}}{e^{2\alpha} + e^{2q\alpha}} \right)$$ (4.4)

where α is a variable that controls the slope of V_q.

- e_{gap} is approximated as a rectangular pulse of amplitude $a + bX_{gap}$:

$$e_{gap} = \frac{1}{2}(a + bX_{gap})(\tanh(\lambda q) - \tanh(\lambda(q-1)))$$ (4.5)

where λ controls the rate at which e_{gap} rises and decays.
A description on modelling the voltage functions in Simulink, as well as suitable values for the control variables α and λ, is provided in Section 4.3.2 and Appendix A.

4.3.1.2 Gap Current

Gap current, i_{gap}, is similarly decomposed into a non-linear hyperbolic tangent function, i_q, and a step function j_{gap}, where:

$$i_{gap} = i_q - j_{gap}$$ (4.6)

These components are illustrated in Figure 4-10.
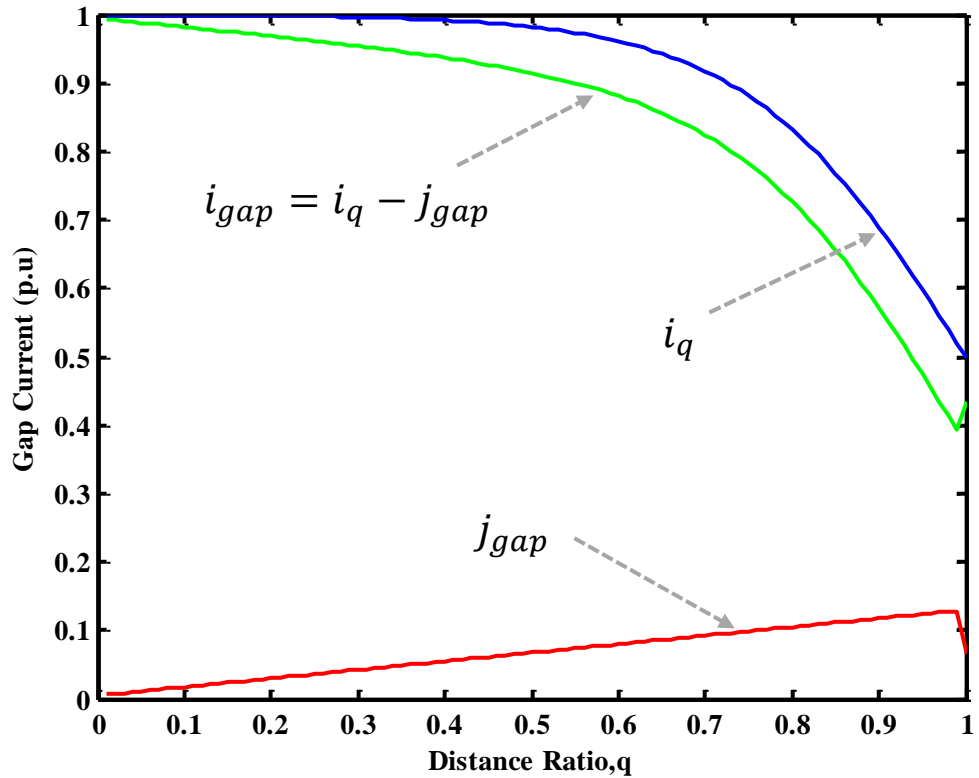
Figure 4-10: Decomposition of i_{gap}

i_{gap} exhibits an opposite effect to v_{gap}, where current decreases with increasing distance ratio. Accordingly, i_q, is approximated with a negative hyperbolic function:

$$i_q = I_{load}\left(\frac{1}{2} - \frac{1}{2}\tanh(\alpha(q-1))\right) = I_{load}\left(\frac{1}{1 + e^{2\alpha(q-1)}}\right) \tag{4.7}$$

where I_{load} is load current prior to the fault.

j_{gap} models the decrease in current as a result of e_{gap} and is approximated by:

$$j_{gap} = \frac{e_{gap}}{(R_{gap} + R_{load} + R_{system})} \approx \frac{e_{gap}I_{load}}{V_{dc}} \tag{4.8}$$

where R_{gap} is the gap impedance and R_{system} is the generator and line impedances. R_{load} is significantly greater than both R_{gap} and R_{system}, allowing j_{gap} to be fully approximated by load current and supply voltage.

4.3.1.3 Gap Impedance

R_{gap} is resistive and is approximated by:

$$R_{gap} = \frac{V_q}{i_{gap}} = \frac{V_q}{i_q - j_{jap}} \approx \frac{V_{dc}}{I_{load}}e^{2\alpha(q-1)} \tag{4.9}$$

The influence of j_{gap} in R_{gap} was found to be negligible, allowing a much simpler expression without loss of accuracy. Note, from Figure 4-8, R_{gap} only considers the non-linear impedance and not the impedance associated with the EMF pulse term.

4.3.1.4 Arc Randomness

Non-intermittent fluctuations in both V_{gap} and i_{gap} are a result of unsuccessful arc quenches (see Figure 4-12). The unsuccessful arc quenches result in a sudden increase in arc voltage and a corresponding decrease in arc current. These fluctuations are modelled by randomising the distance ratio, q, to produce rapid changes in voltage and current. As the electrode gap is a measurable distance, randomising q essentially randomises the critical distance at which the arc quenches (where successful arc quenching is modelled if $q \geq 1$).

Details on modelling a random q value in Simulink are provided in the following section and in Appendix A.

4.3.2 Simulink Series DC Arc Fault Model

An outline of the arc fault model developed in Simulink is provided in Figure 4-11.
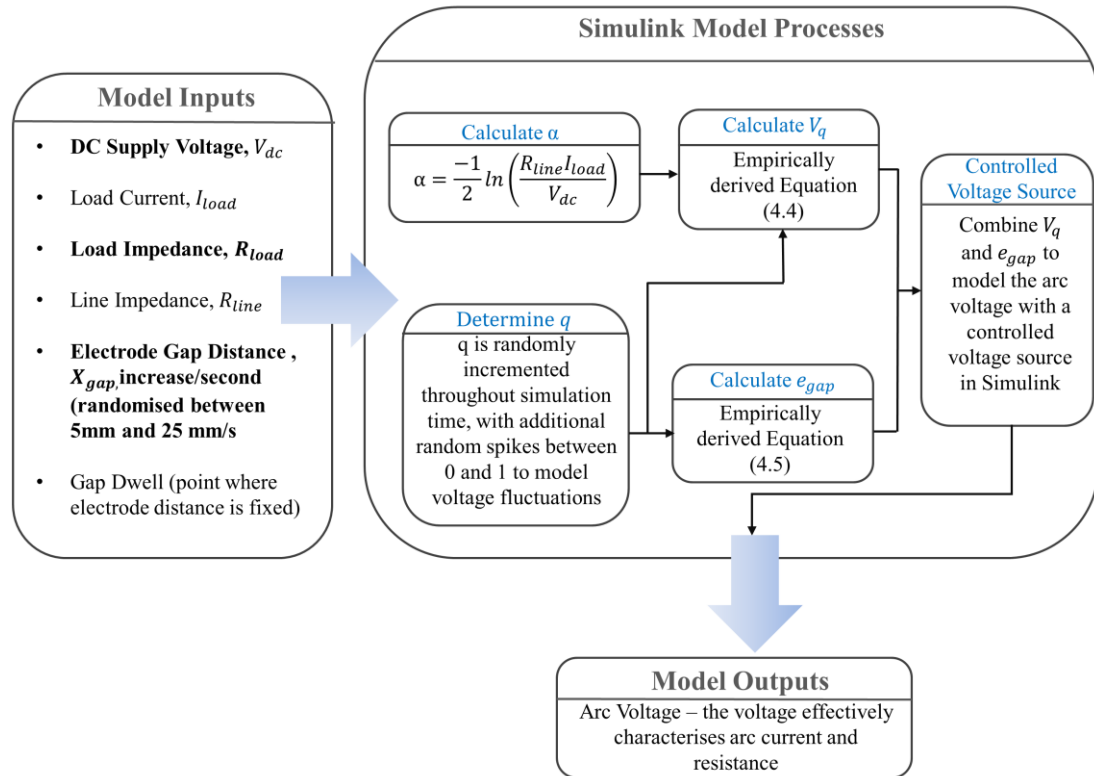
Figure 4-11: Outline of Simulink arc fault model

The model accepts user inputs of various electrical system and arc fault parameters – these are used to calculate V_q and e_{gap}, which are combined to model the arc voltage. The arc is modelled solely as a voltage - the arc current and resistance can be effectively deduced from the voltage. The model process is updated at each simulation time step to model the highly dynamic arc voltage.

The Simulink model is described fully in Appendix A.

4.3.2.1 Model Outputs

An example of modelled voltage during a fixed distance arc fault is illustrated in Figure 4-12 (a). Corresponding arc current and power are shown in Figure 4-12 (b) and 4-12 (c).

Prior to the series fault developing, voltage across the conductor represents line impedance losses – voltage loss is usually < 0.001 p.u.. At fault onset, the development of a conductive gap within the conductor results in an arc voltage of 0.05 - 0.1 p.u.. This voltage gradually increases as the electrodes separate – the rate of increase is relative to speed of electrode separation. As the electrodes dwell at a fixed distance, voltage remains at a constant base

level, with spikes representing unsuccessful arc quenches. When the arc extinguishes, the gap becomes an open circuit, and supply voltage (1 p.u.) is impressed across the gap.

A distinct arc current feature is the reduction in current at fault onset. The series nature of arc faults means that arc current and load current are the same entity. Before a fault develops, current is limited by load and line impedance, and current is ≈ 1 p.u. At fault onset, current decreases in proportion to the arc voltage increase across the gap – the arc current notches represent the unsuccessful arc quenches, and are simultaneous to the arc voltage spikes. With the arc becoming an open circuit upon extinction, current ceases to flow through the gap.

Arc power is a product of arc voltage and arc current. The corresponding increase and decrease of these elements results in arc power being limited – typically arcs will not be sustained beyond 0.25 p.u. range although this level may slightly increase with the presence of reactive elements providing stored energy to the arc.

The arc voltage, current and power features described are typical of the model output. However, it should be noted that the features illustrated in Figure 4-12 are just one example – the random elements in the model mean that, whilst maintaining the same general characteristics, certain model outputs (e.g. duration of arc, frequency of quenching) vary between separate simulations.

The general characteristics of the model are validated in the following section.
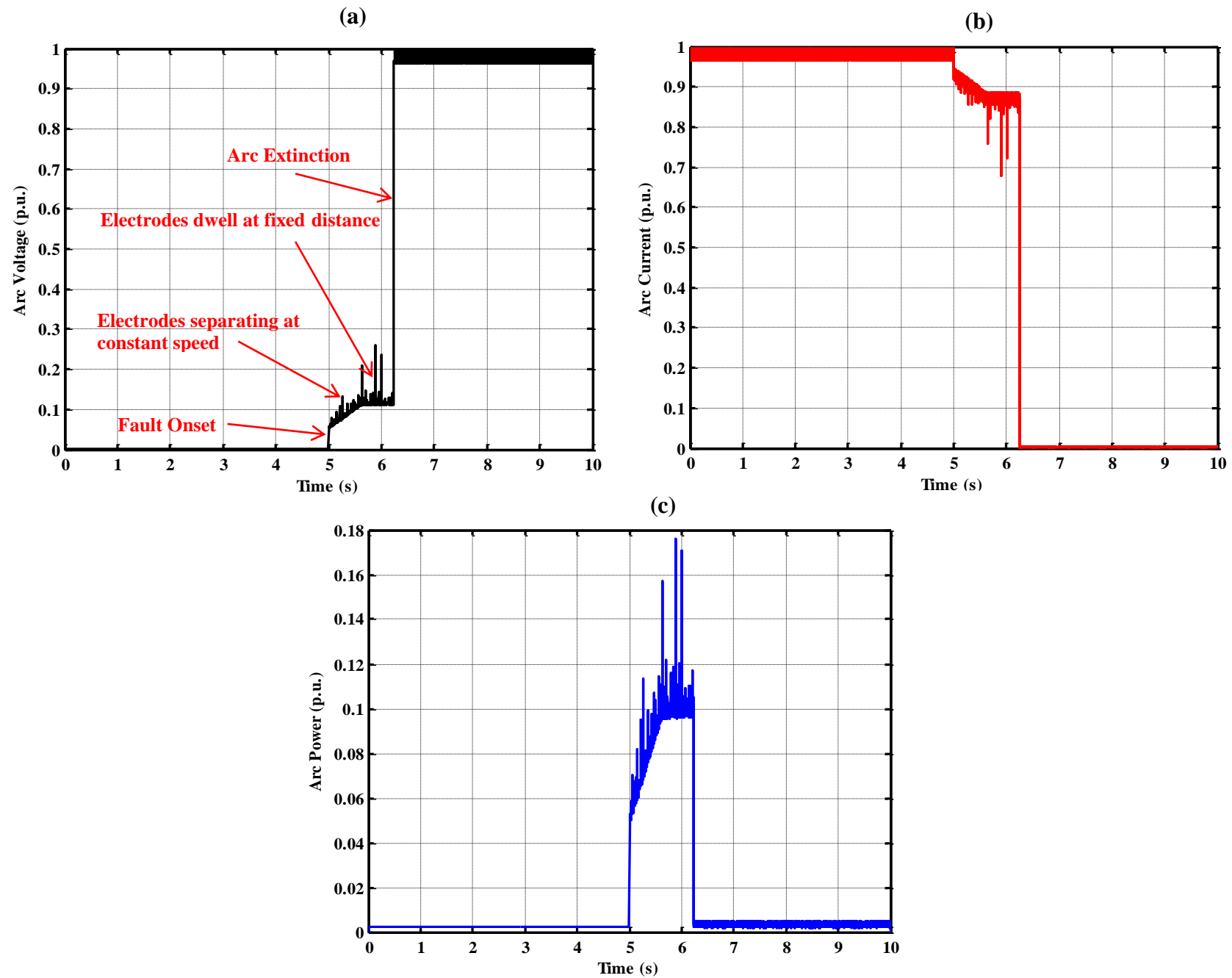
Figure 4-12: Plots of simulated fixed distance arc fault data. (a) Arc Voltage (b) Arc Current (c) Arc Power

4.3.3 Simulink Arc Fault Model Validation

Model validation is necessary to confirm the accuracy of fault data generated from the model. Previous arc fault models were outlined in Table 4-2 – this section compares those models (and others) with the developed Simulink model to validate accuracy.

4.3.3.1 Voltage Gradient

Arc voltage gradients were defined by both Strom (Table 4-1) and Browne [184]. Strom defined an average voltage gradient in the arc column of 13.4V/cm while Browne determined arc column voltages of 12V/cm above an arc current transition level. Figure 4-13 illustrates a comparison of these levels against the average voltage gradient of the developed Simulink model.
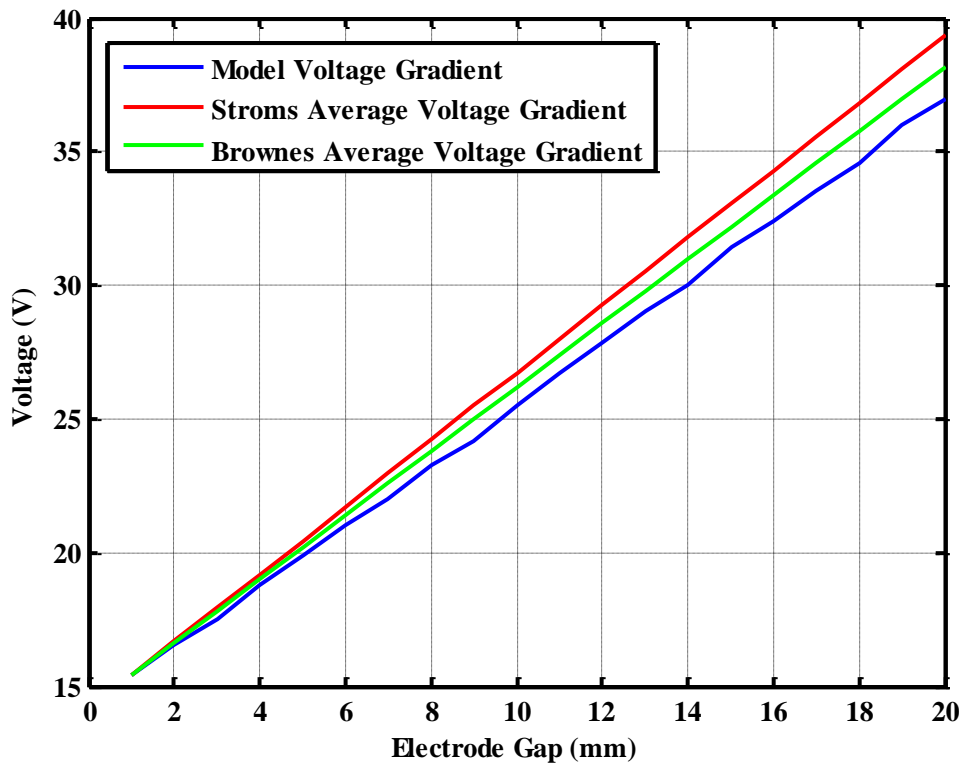
Figure 4-13: Comparison of model voltage gradient against gradients defined by Strom and Browne

Average voltage gradient of the model was ≈ 10V/cm. Despite exhibiting slightly lower values, there is good agreement with both Browne and Strom's models, particularly for smaller electrode gaps.

4.3.3.2 V-I Characteristics

V-I characteristics of fixed length arcs were described as having inverse non-linear behaviour below a current transition level; for currents above this level, voltage increased only minimally with current. Conflicting transition values were defined in the literature (see Table 4-2). Stokes and Solver defined this value to be in the region of 10-13A for small electrode gaps, while other research determined levels significantly higher.

Evaluation of model V-I behaviour showed minimal agreement with the lower arc current characteristics - non-linear inverse behaviour was not evident below a current transition level. In general, arc voltage remained relatively stable across increasing current ranges for fixed electrode gaps.

Figure 4-14 outlines model V-I outputs; voltage stability across the range of current levels is illustrated. Although it does not possess inverse non-linear behaviour at low current levels, the model does still accurately characterise voltage for higher current ranges. In this sense, an associated caveat of the model is that voltage output at currents below roughly 10A are less accurate.

This would be a significant issue if gaps sufficiently greater than 30mm were being considered (as current transition level would be $\gg$ 10A – see Equation (4.1)). As such, the model should ideally be used for conditions with arcing current greater than 10A and electrode gaps limited between 1 to 30mm.
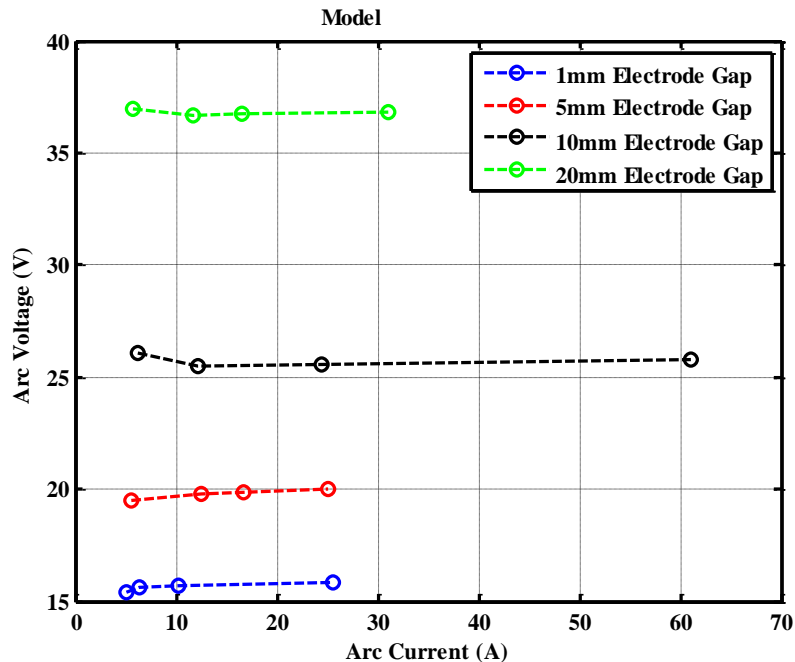
Figure 4-14: Model V-I Characteristics

4.3.3.3 Arc Impedance

Arc impedance characteristics were outlined in Section 4.2.1.2. Paukert [181] and Stokes [180] defined models that quantified the arc impedance. Comparisons between model impedance and Paukert and Stokes formulas for various electrode gaps are provided in Figures 4-15 and 4-16 respectively.
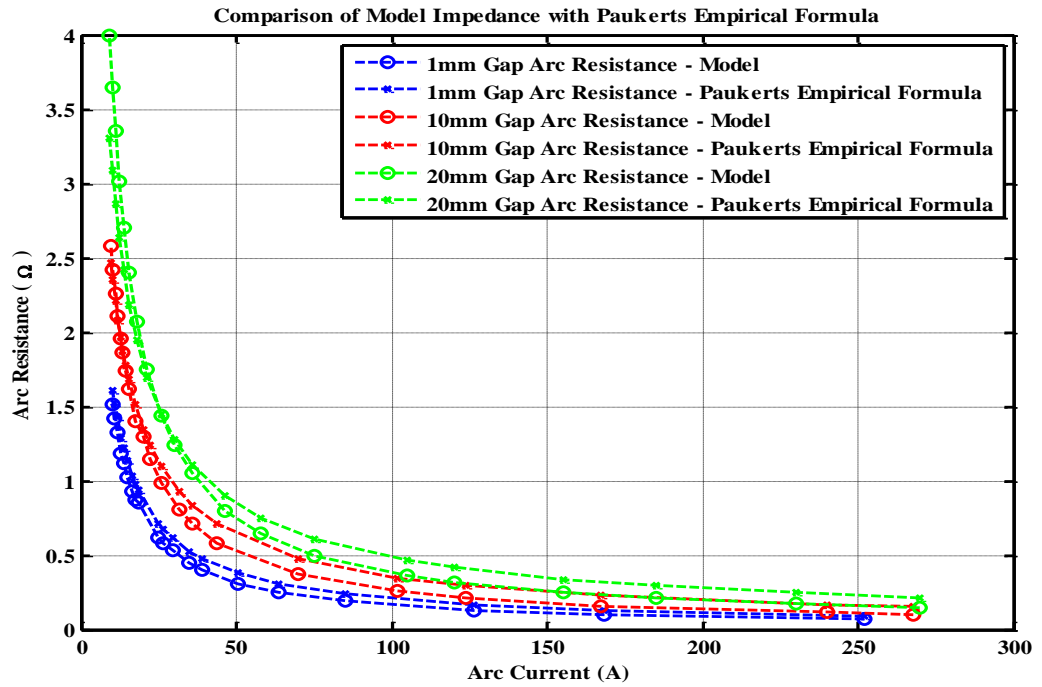
Figure 4-15: Comparison of Model Impedance with Paukert's Empirical Formula
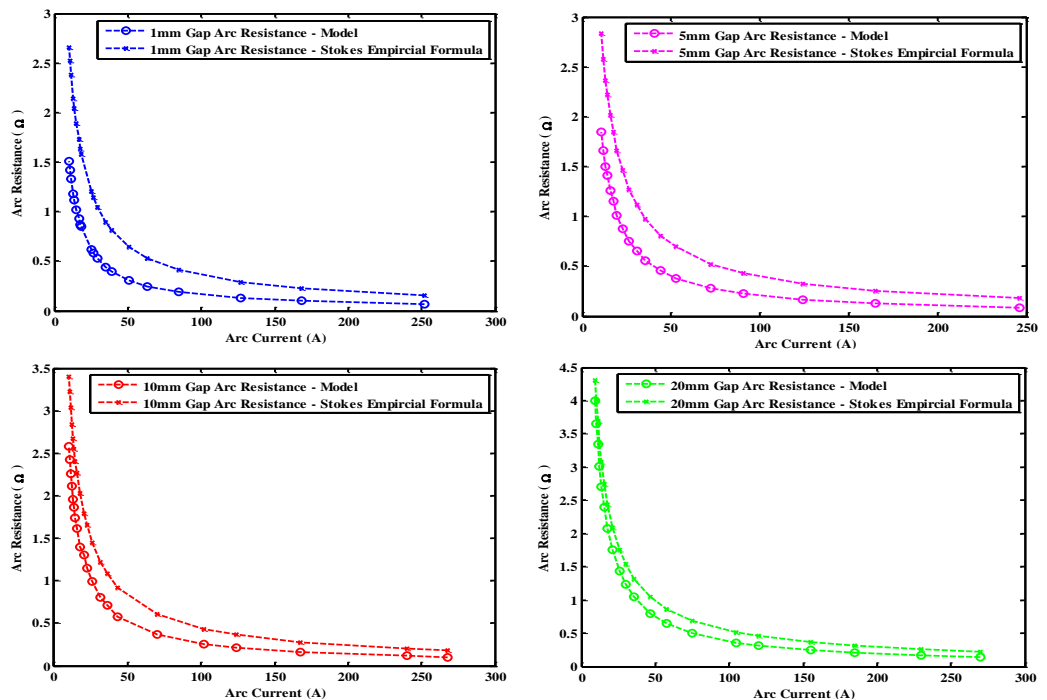
Figure 4-16: Comparison of Model Impedance with Stokes' Empirical Formula

The general non-linear characteristic of arc impedance is captured within the model - resistance increases significantly at lower current values and becomes almost constant at higher currents levels. There is also acceptable agreement with both Paukert and Stokes' empirical models, albeit with modelled resistance lower for corresponding current magnitudes. A lower resistance suggests that arc voltage magnitude is slightly lower than the empirical formulas propose.

As resistance was calculated across fixed electrode gaps, the contribution of e_{gap} to overall arc voltage is likely smaller than expected. In other words, electrode voltage drops are underestimated in the model, which results in a slightly reduced arc resistance. However, overall, the modelled arc resistance provides a relatively good representation.

4.3.3.4 Frequency Characteristics

Arc current and voltage signals exhibit an expansive frequency range spanning from DC up to MHz range (see Section 4.2.1.3). To understand the frequency components of the developed arc fault model, a fast Fourier transform (FFT) [222] was applied to generated arc current data. Frequency spectra in the range 0-200kHz for a variety of arcing conditions are illustrated in Figure 4-17.

The DC nature of the model results in:

- Fundamental frequency being equal to zero.
- Greater energy content in the lower harmonics, where energy decreases inversely with harmonic frequency.

The main point of interest is the energy content at higher frequencies under arcing conditions. There is significant increase in higher frequency energy in comparison to nominal background noise. Indeed, there is roughly a 25dB disparity at a frequency as low as 10 kHz.

These results show that the contribution of high harmonic energy is significantly increased under arcing conditions. Arc current frequency spectra output from the model are consistent with those described in literature. Readers should refer to a comprehensive study undertaken on DC arcing spectra by Johnson [192] for further information.

4.3.3.5 Validation Summary

Comparison of the Simulink fault model outputs with various arc characteristics and models defined within literature has, on the whole, validated model accuracy. The main

inconsistency concerned V-I characteristics at low current levels. However, voltage gradients, arc impedance and frequency characteristics showed relatively good agreement.

The validated model was used for the generation of accurate series DC arc fault data. This data was used to develop the IntelArc FDI method, described in Chapter 5.
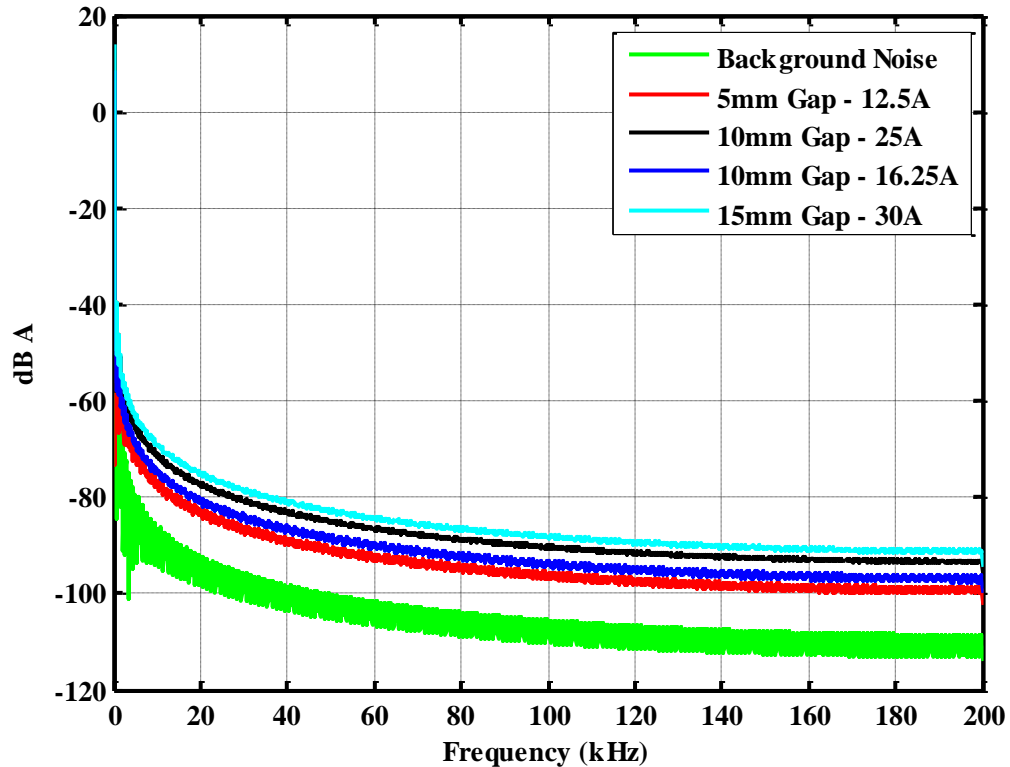
Figure 4-17: Examples of arc fault current frequency spectra. Nominal noise is illustrated in green

4.4 Arc Fault Diagnosis & Isolation Systems

Challenges involved with the detection of arc faults within aircraft were outlined in Section 4.1.2. Numerous detection methods have been developed to attempt to overcome these challenges. Such methods are generally classified in terms of the extracted arc features utilised for detection. This section introduces the different types of detection methods, before discussing in more detail systems specifically related to detection of series DC faults.

4.4.1 Classification of Arc Fault Detection Methods

Figure 4-18 summarises the various types of arc FDI methods [193].
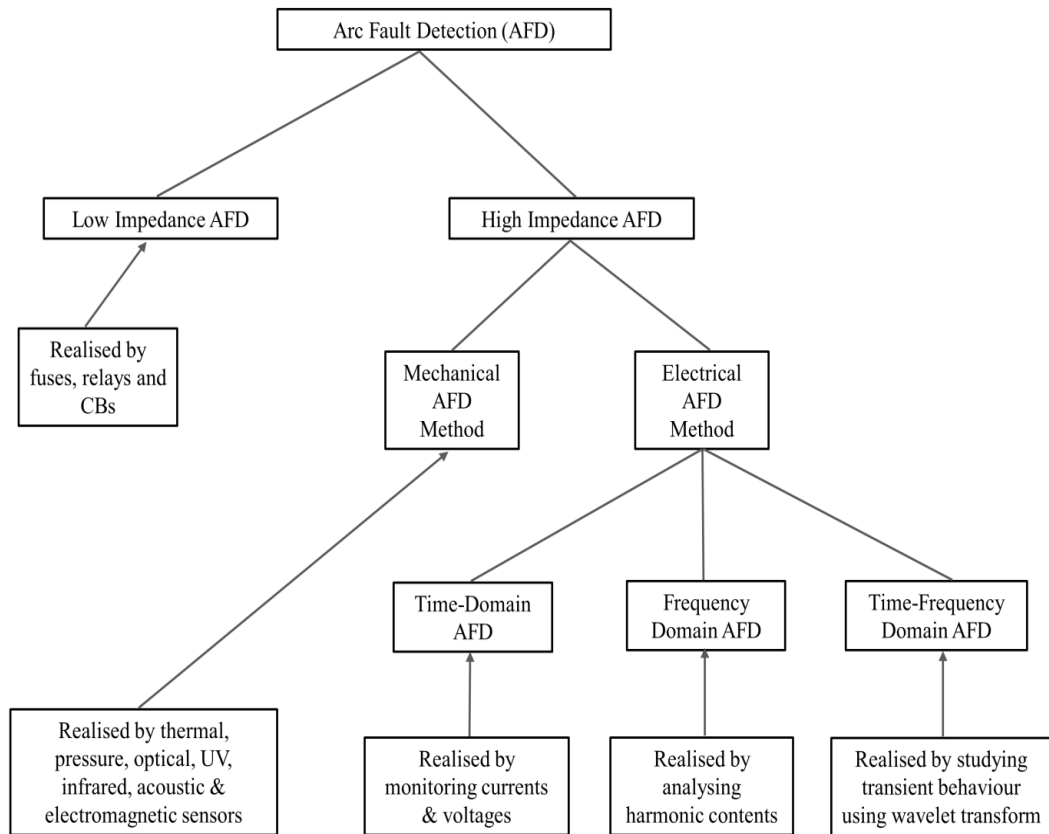
Figure 4-18: Classification of arc fault detection methods

Low impedance arc FDI can be realised with conventional protection devices. However, low impedance parallel arc faults are typically preceded by a high impedance, low fault current stage. It is desirable to detect and isolate arc faults *before* the development of high system currents – this means conventional protection devices are not suitable for arc FDI purposes.

High impedance arc fault detection is based on either mechanical or electrical methods. Electrical based methods extract arc fault features either in the time, frequency or time-frequency domains and algorithms analyse the extracted features to determine the presence of arcing events. Mechanical and electrical arc FDI methods, including examples, are summarised in Sections 4.4.3 and 4.4.4.

Before specific methods are described, the main objectives of arc FDI in aircraft systems are outlined.

4.4.2 Arc FDI Objectives

Understanding the objectives of arc FDI in aircraft systems further emphasises the development challenges. The high level objective of arc FDI in aircraft is to have high

accuracy and sensitivity to arc fault events in order to maintain system reliability and minimise interruption to safety critical loads. This includes the minimisation of false alarms.

With respect to series arc conditions, where faults are often highly intermittent and current levels actually decrease, this general requirement poses a significant development challenge. Being able to discriminate between true fault events and normal system transients within increasingly dynamic aircraft EPS is another significant challenge.

These objectives and challenges motivate the need for advanced arc FDI methods (see Section 4.4.5). More simplistic methods which assign constant thresholds for fault detection are not suitable as determining threshold values which account for normal transient behaviour, as well as provide accurate fault detection coverage, is very difficult.

Advanced arc FDI methods should possess the following characteristics:

- *Effective* – the ability to detect, and locate, faults accurately without any false alarms or non-detection.
- *Non-Intrusive* – should not disturb normal operation.
- *Real-Time* – detect and locate faults online before overcurrent faults occur.
- *Low-cost* – should be inexpensive while computation burden for data acquisition and signal processing should not be too heavy.

The novel IntelArc method proposed in Chapter 5 aimed to meet these objectives and address the challenges.

4.4.3 Mechanical Arc FDI Methods

Mechanical methods determine fault conditions through the use of special sensors which detect thermal and pressure rises [194] or specific light/infrared radiation [195]. Pressure and photo sensors have been extensively deployed for detection of switchboard arc faults on board US Navy submarines [196].

The main limitations of mechanical methods include:

- High installation and maintenance costs incurred from specialised sensors.
- Impracticality for complete system coverage as sensors must be set near arc location for reliable detection.
- Susceptibility to noise increases the probability of false detection.

An in depth discussion on mechanical arc FDI methods is out with the scope of this thesis.

4.4.4 Electrical Arc FDI Methods

Arc FDI systems based on electrical methods, which detect faults according to abnormality in current and voltage signals, are more relevant to this thesis. Time, frequency and time-

frequency domain features of electrical signals were outlined in Figure 4-18. Methods may be based on algorithms that analyse the extracted features directly to determine fault presence, while other, more advanced methods, are based on the development of models of normal and/or fault conditions for detection.

Further discussion on arc FDI methods, that utilise various features of electrical signals, is provided in this section.

4.4.4.1 Time Domain Arc FDI

Numerous time domain arc FDI methods have been presented in the literature [193]. These methods tend to involve analysis of three-phase current imbalance [197], voltage imbalance along a feeder [198], differential current [199] and arc fault energy [200]. Analysis of phase current imbalance and differential current characteristics is only applicable for the detection of parallel arc faults (and mainly confined to AC systems). Also, the lack of a neutral conductor within aircraft EPS increases the difficulty in detection of parallel arcing to ground.

Series arc fault detection and location methods [198] that monitor voltage across a feeder require multiple voltage sensors across a single conductor – associated weight increases result in such systems not being ideal for aircraft application. An off-line non-contact series arc fault diagnosis device was developed for aircraft wiring systems, which comprises capacitive probes measuring voltages across a conductor at two reference points [201].

A method for the detection of DC parallel arcs [202] was developed, based on averaging multiple current measurements over a specific time period - averaged measurements across consecutive time periods are compared and a fault is detected if the difference in measurements exceeds a pre-determined threshold.

SSPC based protection from arcing faults has also been described [203, 204]. Each SSPC protects its own downstream load – dynamic load characteristics are pre-programmed and the SSPC trips if measured load current is outside an allowable signature range.

The main limitations of time-domain arc FDI include difficulty in:

- Determining threshold values.
- Finding features that accurately distinguish between true arcing events and mimicking events (such as load inrush and switching transients).

4.4.4.2 Frequency Domain Arc FDI

Frequency characteristics of arc events were discussed in Sections 4.2.1.3 and 4.3.3.4 – frequency domain arc FDI methods exploit unique features of arc voltage and current spectra to determine the presence of faults. The FFT provides a computationally efficient method for mapping time-domain signals to the frequency domain. Analysis of harmonic content enables discrimination between normal transients and faults.

Scott *et al*. [85] described a method for application to aircraft EPS based on determining the presence of broadband noise in the load current of a monitored circuit - if a broadband spectrum is evident, the energy level of harmonics in a predetermined range of frequencies indicates fault presence. A similar method that focused on the order of harmonics relative to supply frequency is proposed in [205], while Kwon *et al.* [206] described a high impedance fault detection method based on even order harmonics only.

Frequency bands that contain all essential information for discrimination of arc events were extensively discussed by Parker *et al.* [183]. Within the discussion, Parker suggests that frequency-domain based arc FDI methods focus on sub-bands that are either too narrow or in higher frequency ranges which are more susceptible to radio interference. Indeed, it is suggested that fractal sub-bands in the 200-3500Hz range, below voice frequency range, may be more suitable for frequency based arc FDI.

The main disadvantage of using the FFT to map the frequency spectrum of a signal is the inability to decipher the time at which certain harmonic frequencies are present. It is therefore ideal for fault events that are continuous and stationary. However, in aircraft EPS, arcing faults are likely to be highly intermittent in nature. High intermittence will result in the energy content of particular arc signature harmonics being attenuated across the entire sampled signal.

These disadvantages of frequency domain methods highlight the attributes of time-frequency domain arc FDI.

4.4.4.3 Time-Frequency Domain Arc FDI

Time frequency domain methods determine how the frequency behaviour changes over time. The WT (refer to Chapter 3) can provide the frequency of a signal, as well as the time associated with each frequency – this makes it ideal for dealing with non-stationary, highly transient signals.

High impedance fault detection methods utilising WTs for feature extraction from current and voltage data are described in [207, 208]. A major challenge associated with WT based

detection methods is evaluating the generated wavelet coefficients to decide if faults are present. Often systems will use advanced, intelligent, models and techniques to determine the probability of fault presence from WT features.

4.4.5 Intelligent arc FDI methods

Combining extracted electrical signal features with advanced models and probabilistic classifiers enables more effective discrimination between arc faults and normal transient events. Intelligent methods have been developed that are based on combinations of: harmonic feature extraction and Kalman filters [209]; time-domain features and neural networks [210]; and WT coefficients and support vector machines [124]. Various adaptive expert algorithms have also been developed [211]. Detection methods based on advanced electrical models have been described. Yaramasu [212] utilised a transmission model (or *ABCD model*) to derive both nominal and fault models for AC and DC aircraft EPS - this modelling method is limited to parallel arc fault detection.

These methods are by no means 100% accurate. They also involve significant development challenges. However, the potential for increased detection accuracy in comparison to more simplistic algorithms or threshold systems makes advanced arc FDI methods an attractive option for aircraft systems.

The IntelArc system proposed as part of the work of this thesis in Chapter 5 combines time domain and time-frequency domain features with HMM.

4.4.6 Series DC Arc FDI

Previous sections provided a general discussion on arc FDI methods. The discussion did not necessarily distinguish between detection of parallel or series faults or between AC and DC supplied systems.

The IntelArc method proposed in Chapter 5 is applied specifically for detection of series DC arcing conditions. As such, this section discusses significant research of, and methods developed for, the detection of series DC arc faults. Previous methods have been developed based on time, frequency and time-frequency domain features.

Guo *et al.* [175] defined a method that identifies a period of time between a sudden drop in load current and arc ignition as an arc precursor time. Detection of precursor events, which typically only last tens of microseconds, theoretically enables isolation before the presence of arcing. The detector circuit uses a toroidal inductor, which outputs a sharp voltage increase, and hence fault alarm, when current suddenly decreases. The requirement for additional hardware circuitry is one limitation of the proposed method. Discriminating

between true arcing events and normal drops in load current in such short time frames is also extremely difficult using this method.

Kilroy *et al.* [202] developed a method based on averaging load current signal values over multiple time periods. Series arc faults are detected by determining if the difference in average values across the multiple time windows is greater than a pre-determined threshold. Observation of current features over multiple time periods enables higher discrimination between normal transients and arcing events although there is trade-off between increased detection accuracy and detection time.

Dargatz *et al.* [213] developed a series arc FDI method for Photovoltaic (PV) systems. Current and voltage at the output terminal of a power converter are sampled and analysed for potential arc fault signatures. Rapid changes in current slope (≈ 0.1 amp/microsecond) are indicative of fault conditions - normal transients typically have a slower rate of change of current.

Zeurcher *et al*. [214] detected series faults through analysing load current after a sudden decrease. In this sense, load current is actually momentarily turned off after the sudden decrease – if current magnitude is at a similar level as when it was turned off, it is concluded some other phenomenon was a result of the sudden decrease. However, an arc fault is diagnosed if current has further decreased or has returned to a nominal value. The application of this method to aircraft EPS is unsuitable as power may be unnecessarily interrupted to critical loads.

In terms of frequency domain methods, Kojori *et al.* [215] developed a method that used a sliding window FFT to extract, in real-time, the DC component of load current. Amplitude variation of the DC component across each window indicated series arc fault presence – level of variation was determined by counting the number of maxima over a certain period and comparing with a threshold. The method also measured non-stationary changes in load current for detection - statistical analysis of inter-harmonics and high frequency components quantified the degree of load current distortion. Consideration of DC component amplitude and current distortion increased the potential for accurate fault detection. A similar method based on frequency spectrum characteristics is proposed by Ohta [216].

Momoh [217] proposed an intelligent detection method that used spectral energy from nominal and fault events to train separate artificial neural networks (ANNs) - the fault data was collected on a test rig with voltage supply in the range 50-150VDC. Elementary testing proved real-time fault detection across a variety of conditions. The main drawback of using ANNs for arc fault detection concerns the difficulties associated with model development and, in particular, determining the type and structure of neural network [220]. Also, a

significant disadvantage of frequency domain feature extraction is the lack of time resolution – this is particularly the case when extracting features of highly transient signals, such as series DC arc faults (see Section 4.4.4.2).

In theory, time-frequency domain signatures provide increased discrimination capability. Yunmei *et al.* [221] analysed time-frequency signatures of series arc fault current data using the WT. The data was recorded throughout experiments on a 28VDC network. Their research determined that calculation of the energy values of five consecutive wavelet coefficients enabled discrimination between series arc faults and normal load transients.

Yao *et al.* [219] developed a method based on time and time-frequency domain features for application to representative DC microgrid networks. The detection algorithm calculated statistics from 25ms windowed time domain arc current data; statistics included maximum and minimum current levels and the difference between them. These measures were coupled with calculation of the RMS values of wavelet coefficients within the 25-50 kHz fractal sub-band. When both current difference and RMS values exceed a threshold value, a flag is raised indicating a potential series arc fault. One issue of the method surrounded setting the number of consecutive flags to accurately indicate a fault and also avoid nuisance trips. The authors concluded that four consecutive flags would enable this for the system under test – it was inconclusive if four is an optimal number that generalises across a variety of system configurations and normal transients.

4.4.6.1 Remaining Challenges

Various methods for FDI of series DC arc faults have been described. Despite the development of multiple methods, major challenges still exist with regards to accuracy of fault detection, not least within aircraft EPS. Increasing detection accuracy is the primary goal of any fault detection method. However, the development of highly accurate and discriminative series arc FDI methods within an aircraft EPS context is particularly challenging as:

- Decreased current levels make it difficult to discriminate between fault current and nominal current transients/load switching.
- High intermittence, as a result of in-flight vibration, results in decreased fault duration and greater likelihood of non-detection.
- PE circuits/converters introduce high frequency electromagnetic interference that may result in false tripping.

Ideally, a *generalised* detection method can handle these challenges across a variety of network configurations, voltage levels and loads. The issue of generalisation highlights the

problem with algorithms that rely on more simplistic statistical analysis of extracted features. Methods developed around basic statistical analysis and associated thresholds have proven to be accurate within limited network configurations and test conditions; nevertheless, the ability to define threshold values for generalised detection performance is extremely difficult, if not impossible.

The development of intelligent arc FDI methods should increase the potential for generalised, accurate and discriminative performance. The development of intelligent systems is not trivial, and performance is based on utilisation of correct features for model training. Chapters 5 and 6 describe the development and testing of the IntelArc method that is proposed to address the challenges outlined.

4.5 Chapter 4 Conclusions

The chapter described a validated Simulink series DC arc fault model that was used for the generation of fault data. Model accuracy was validated by comparing the model outputs (arc voltage, arc current, arc resistance and frequency spectra) to electrical characteristics defined in literature. There are numerous studies that attempt to characterise the arc. The chapter summarised the main studies relevant to DC arcing, including electrical models and relationships that have been derived from empirical data. Overall, there was relatively good agreement between the Simulink model outputs and the derived models described in literature.

The chapter also discussed challenges in detecting series DC arc faults within aircraft – these include dealing with fault current that decreases below nominal rating, high intermittence and discriminating between true fault events and normal transients. Existing detection methods developed to meet these challenges were discussed, including benefits and limitations of each. Overall, it was concluded that there is a requirement for the development of advanced, and generalised, detection methods to discriminate series DC faults within a variety of system architectures and configurations.

The novel IntelArc method, described in the following chapter, aimed to meet these objectives. The method is designed and tested using data generated from the validated Simulink arc fault model.

5. NOVEL FDI METHODS TO SUPPORT PROTECTION & HEALTH MANAGEMENT OF AIRCRAFT EPS

This chapter proposes two novel FDI methods that have the potential to support protection and health management of aircraft EPS through the diagnosis of various fault conditions. The first novel method, *EPSmart,* is proposed for FDI of intermittent, drift and abrupt and sensor faults within a general aircraft EPS environment. Design and testing of EPSmart has been published in [44]. The second novel method, *IntelArc,* is proposed for FDI of series arc faults in DC supplied systems. Design and testing of IntelArc has been published in [45]. The difficulties of detecting these fault types using conventional protection methods have been described in Chapters 2 and 4. These two methods vary in terms of feature extraction and are thus described in turn throughout this chapter. Both methods are based on ML techniques, specifically HMM. EPSmart and IntelArc are the main contributions of this thesis.

5.1 EPSmart – FDI of Abrupt, Intermittent & Incipient Faults

The EPSmart method is proposed to detect a range of fault types within an aircraft EPS environment. Within this thesis, the ability of EPSmart to autonomously detect, classify and diagnose the severity of diverse EPS faults is validated with its application to NASAs advanced diagnostic and prognostic test bed (ADAPT), a representative aircraft EPS [137]. EPSmart is a data-driven HMM based FDI method and, in this case, network data from the ADAPT is used for both HMM training and application testing.

The main objectives of EPSmart are to:

- Improve EPS network protection and health management through autonomous diagnosis of multiple critical and degraded fault modes

- Accurately discriminate between faults in the underlying system and sensor failures

These objectives are both broad and demanding. The capability of autonomously, and accurately, isolating a range of degraded and critical faults will enhance both real-time protection and overall system health management. As the majority of failures in aircraft systems are accredited to faults in the sensors themselves, it is also important to identify 'true' faults in the monitored system to eliminate unnecessary interruption of supply to system loads.

Section 5.1.1 describes the ADAPT in more detail, including network topology and characteristics of the faults injected into the testbed. A general outline of the EPSmart method is provided in Section 5.1.2. Further details on the method, including HMM training, feature extraction, and severity diagnosis algorithms are provided in Section 5.1.3.

5.1.1 ADAPT Network – Topology and Fault Modes

The NASA ADAPT [139] is a unique facility designed to test, measure, evaluate and help mature diagnostic and prognostic health management technologies. The ADAPT is representative of the topology of an EPS vehicle system, in that it provides energy generation/conversion, energy storage, power distribution and power management functions. A schematic of the ADAPT network is shown in Figure 5-1. It is a hybrid architecture and delivers DC and AC power to the electrical loads. Within an aerospace vehicle contextualisation of ADAPT, typical loads would include appropriate sub-systems such as avionics, propulsion, life support, environmental controls and science payloads. The DC loads in APADT are directly powered from the 24VDC battery. An inverter converts the 24VDC power to 120VAC to power the AC loads. There are multiple redundant paths connecting the three batteries to the two load banks.

A data acquisition and control centre commands the test bed into different configurations using the circuit breakers (CBs), and records data from system variables such as voltages, currents, temperatures and switch positions. The system is limited by the data collection rate at which these variables are monitored – sampling rates are low and range from 2-10 Hz.
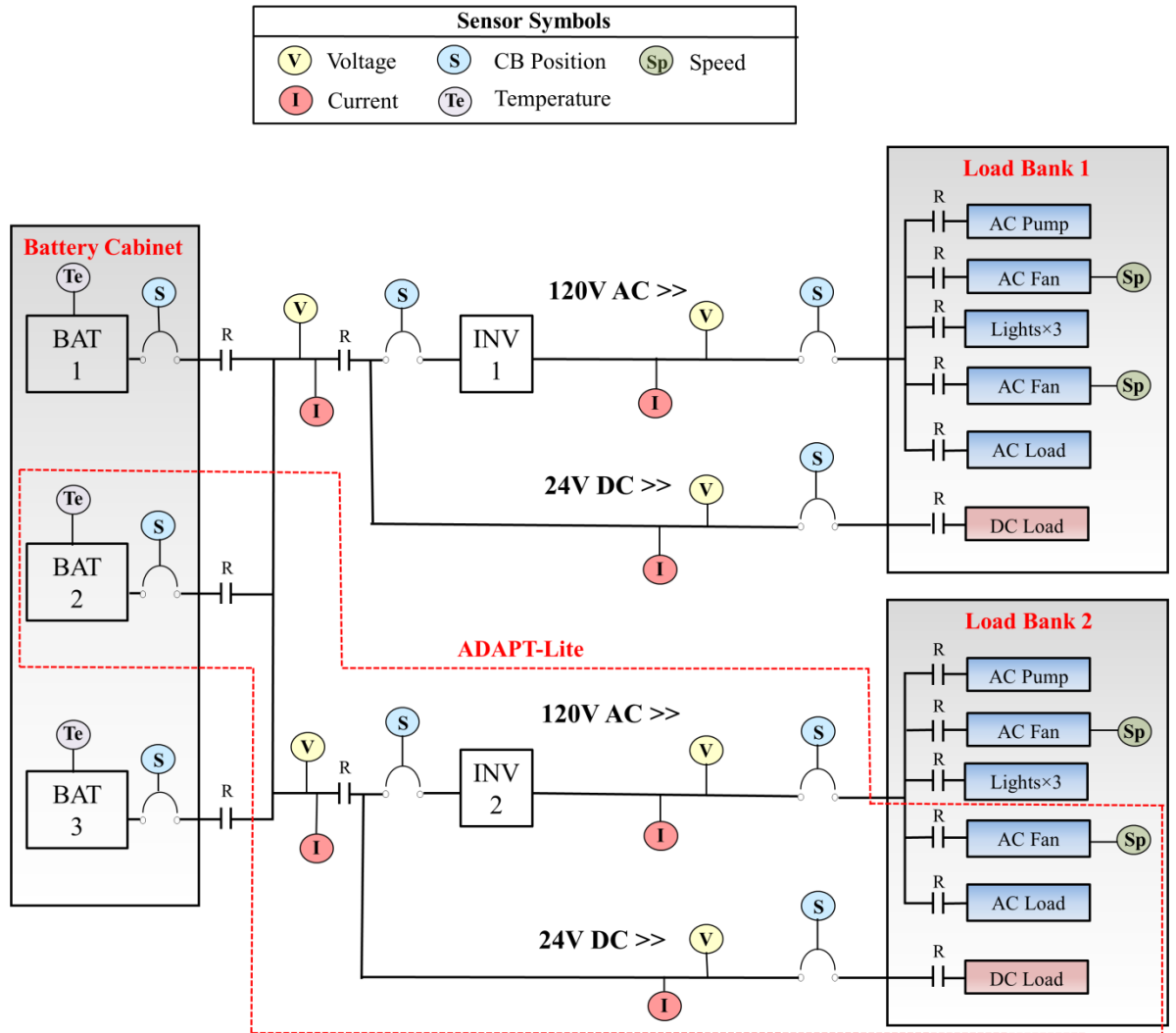
Figure 5-1: Simplified schematic of the ADAPT network with sub network ADAPT-Lite highlighted

A subset of the ADAPT network, the ADAPT-Lite (ADL), was used for validating the proposed EPSmart method as only single faults occurring throughout any observed period of system operation are being considered at this stage. The ADL subset is highlighted in Figure 5-1. The network is a non-redundant configuration of the ADAPT and includes a single battery, two AC loads, one DC load, an inverter and associated sensor and control circuitry. EPSmart was designed and tested using ADL data which was publicly distributed by the DXC10 competition [139].

EPS data (voltage and current levels) was recorded by NASA AMES research centre throughout individual controlled experiments on the ADL. Within a number of these experiments, failure scenarios were included. In the absence of true fault conditions this was captured by injecting representative fault behaviour into the network [137].

5.1.1.1 ADL Fault Modes

The injected failure scenarios on the ADL network were characterised by the location of the fault and the fault mode. Faults were injected to all components within the network, including sensors. Fault modes included abrupt, intermittent and incipient failures. The severity of the injected fault was classified by two conditions: either network critical or degraded. Examples of ADL fault characteristics are illustrated in Figure 5-2.
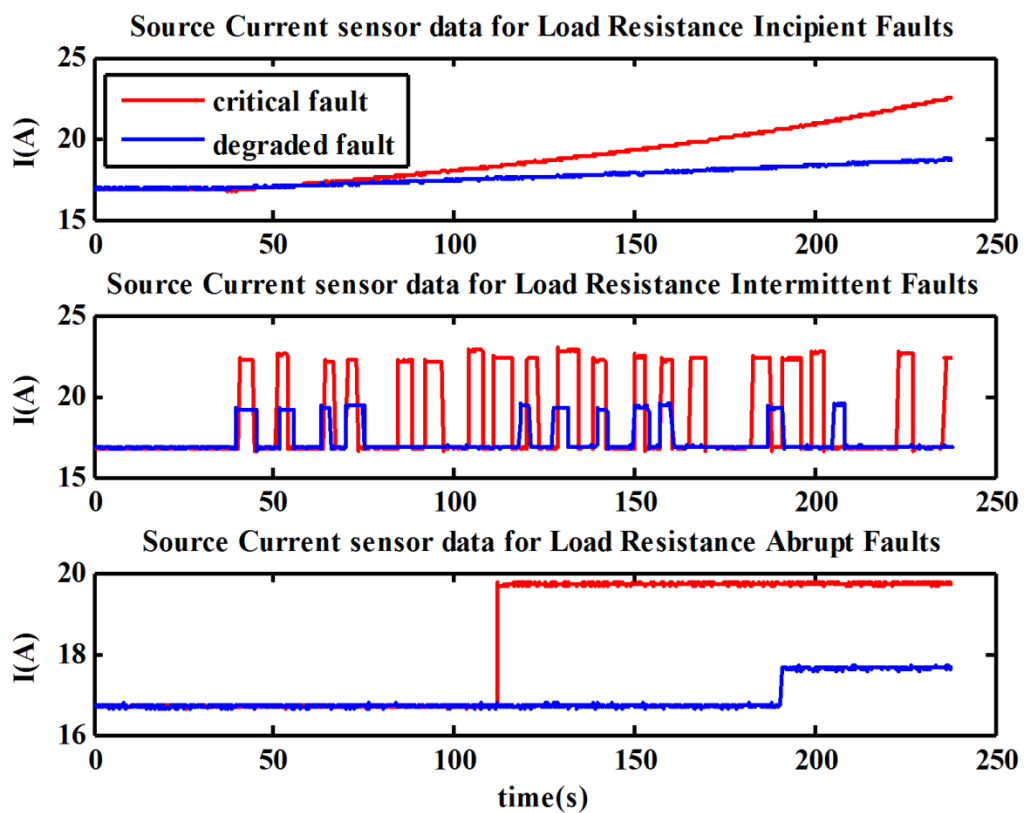
Figure 5-2: Outline of faults injected into the ADL network. Faults are characterised by their mode, location and severity.

Faults were injected into the ADL using both software and hardware techniques. For example, the incipient resistance load faults were simulated using software to apply an offset to sensor data that starts at zero and grows linearly with time. An abrupt load fault is injected by applying a constant offset to the true data value. Faults physically injected into the

hardware include; inverter faults, where the power settings are manually adjusted; and various load and sensor faults, where the connecting load feeders/control wires are short circuited or disconnected.

Sensor data recorded during each experiment by NASA on ADL was used to develop and validate EPSmart. Data from each experiment was labelled with fault location and mode, which enabled a supervised learning approach to be used (see Chapter 3, Section 3.7.2).

In designing EPSmart, the aim was to have the ability to accurately and autonomously detect, diagnose and classify a variety of critical and degraded AC load, DC load and converter faults. Furthermore, the system should also have the ability to discriminate between underlying system faults and sensor failures. The following sections describe the methodology of EPSmart for meeting these challenges.

5.1.2 EPSmart Method Outline

The EPSmart method is outlined in Figure 5-3. There are two distinct stages of the method: Stage 1 classifies network condition, and, once the network condition has been classified, Stage 2 diagnoses the severity of any fault that may have occurred. This section describes these stages in the context of applying the EPSmart to the ADL. This application highlights the potential for the method to differentiate between multiple EPS network conditions and identify both critical and degraded fault modes.

Stage 1 – Fault Classification

A framework of multiple trained HMM corresponding to separate conditions within the ADL network enables the classification of candidate system data. For application of EPSmart to the ADL network, a total of 15 conditions, described in Table 5-1, are modelled within the framework. A decision on network condition is made by primarily calculating the log-likelihood (LL) of the input data, given each models trained statistical parameters; classification then involves selecting the labelled model that returns the highest LL. This form of framework with multiple HMMs was described in Chapter 3, Section 3.8.1.4. The 15 ADL conditions outlined in Table 5-1 include 1 nominal and 14 fault conditions - sensor stuck and failed off faults are akin to abrupt faults.

In the event of multiple faults occurring simultaneously, the LL of the associated models will exhibit higher levels in comparison to other models within the framework across the observed time period. To handle such occurrences, a suitable LL threshold may be set; any labelled model that outputs higher levels than this threshold will be used as evidence that such condition(s) are currently present on the system.
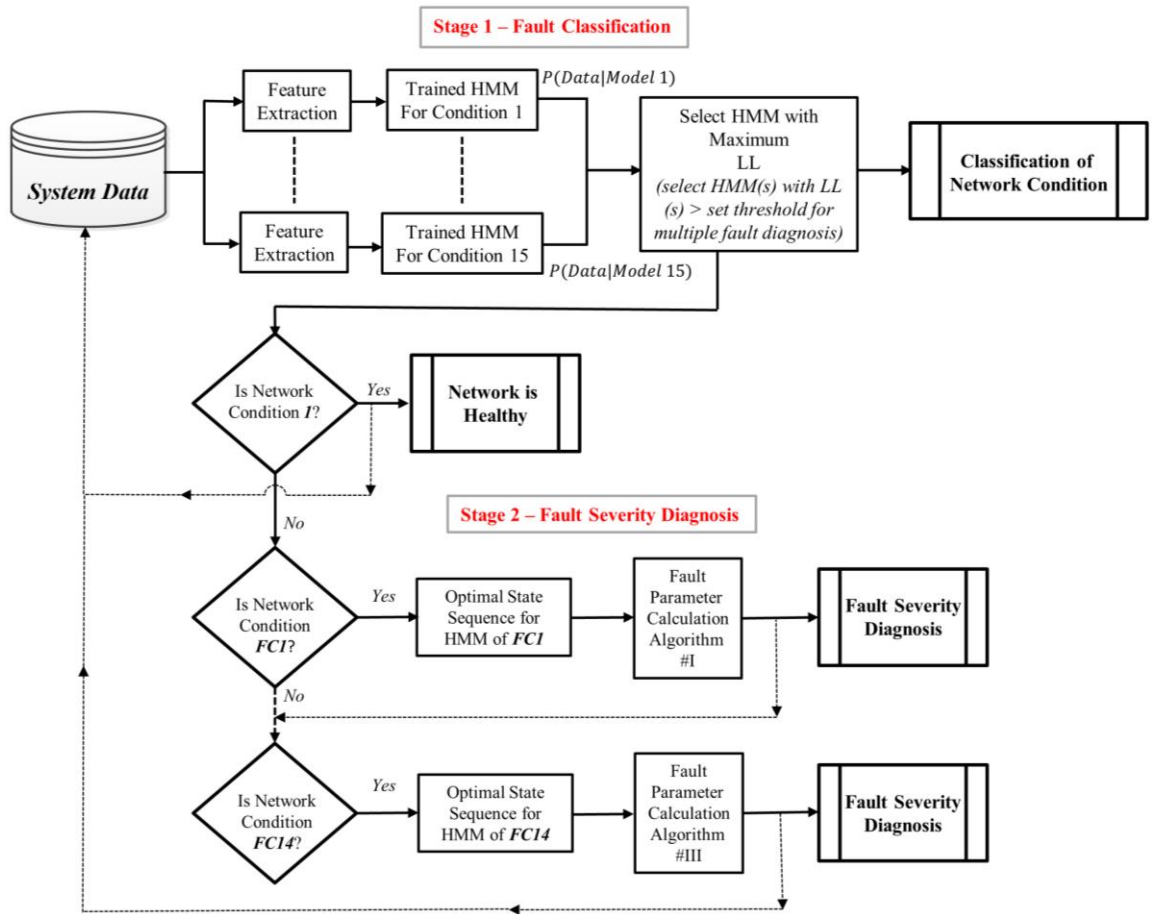
Figure 5-3: Two-stage EPSmart method

Table 5-1: Conditions modelled within EPSmart applied to the ADL network The FPA utilised for each condition is detailed. For clarity, Abrupt fault mode FPA is titled #I, Intermittent fault mode FPA is titled #II and Incipient mode FPA is titled #III.

Network Conditions Modelled		Condition #	FPA #
Location	*Mode*		
No Fault	Nominal	1	N/A
	DC Load Abrupt Resistance Offset	FC1	I
DC Load Faults	DC Load Intermittent Resistance Offset	FC2	II
	DC Load Incipient Resistance	FC3	III
	AC Load Abrupt Resistance Offset	FC4	I
AC Load Faults	AC Load Intermittent Resistance Offset	FC5	II
	AC Load Incipient Resistance	FC6	III
	Fan Load Failed Off	FC7	I
Inverter Faults	Inverter Failed	FC8	I
	Stuck	FC9	I
Voltage Sensor Faults	Intermittent	FC10	II
	Incipient	FC11	III
	Stuck	FC12	I
Current Sensor Faults	Intermittent	FC13	II
	Incipient	FC14	III

Stage 2 – Fault Severity Diagnosis

Stage 2 operates on the basis that a fault has been classified from Stage 1; hence, if a nominal condition has been classified after Stage 1, there is no requirement for the implementation of severity diagnosis. However, in the event of a fault being classified, it is necessary to determine the impact the presence of the classified fault has on the reliable operation of the system.

Calculating fault parameters enables the severity of any fault to be quantified. Fault parameter calculation algorithms (FPA) were developed that use the HMMs' optimal state sequence, calculated using the VA (see Chapter 3, Section 3.8.1.4), to determine the parameters. The set of parameters required for the quantification of fault severity is dependent on the mode of fault that has been classified. Hence, three separate FPA's were developed corresponding to the three modes of fault (abrupt, intermittent and incipient) within the ADL network, as outlined in Table 5-1. The FPA algorithms are discussed in Section 5.1.3.4.

As an example of operation, if FC1 is classified after Stage 1, the optimal state path for the particular HMM of this fault condition will be calculated and then, considering FC1 relates to an abrupt fault mode, the FPA for calculating parameters for an abrupt fault would be initialised. State transitions occur within HMM when there are changes within the observed data. The optimal state path attributes each data point in an observation sequence to a particular hidden state – transitions between hidden states are a result of non-stationary dynamics within the data. Further discussion and illustration of these points are provided in Section 5.1.3.4. The algorithms essentially utilise the optimal state path sequence to detect points in time where the condition of the system changes. Deciphering points of state changes enables fault parameters to be calculated.

After fault parameters have been calculated, the severity of the fault, and its impact on system reliability, can be determined.

5.1.3 EPSmart: HMM Training, Feature Extraction & Severity Diagnostic Algorithms

This section describes various aspects of EPSmart including: the implementation of HMM for EPS FDI; feature extraction and sensor fusion; HMM training; and the FPA severity diagnostic algorithms.

5.1.3.1 HMM for EPS FDI

HMM were introduced in Chapter 3. The following discussion describes how they have been implemented within EPSmart for EPS fault diagnosis. Particular focus is given to the training of HMM using ADL data, however, the general ideas discussed are not limited to ADL application and can be extended to similar hybrid, compact EPS.

The ADL sensor data is an example of multivariate time series data [233] where non-stationary periods define the presence of fault/transient conditions. The ability to determine the latent physical state responsible for such changes in the data is the main goal of data driven FDI. Relating observational data to latent variables is a fundamental concept of HMM. This relationship involves non-stationary periods in the data representing transitions between latent states and, conversely, stationary periods in the data representing some form of latent state. It is therefore vital to have the capability to model data in a way that certain temporal aspects are explicit. Modelling the distribution of system data and then detecting shifts in its characteristics would enable such changes to become explicit.

There are a number of distribution functions that can be used for modelling the probability distribution of observed variables. Typically, the 'simplest' function applied for continuous density observations assume Gaussian distributions per latent state [30]. Considering the multidimensional nature of the ADL data, approximating the distribution with a single Gaussian function would provide an overgeneralised fit [110]. A solution to this is to approximate the unknown density with a mixture of simple density functions. The general form of a variable x of dimension d using M mixture components is given by

$$P(x) = \sum_{i=1}^{M} P(\theta_i) P_i (x|\theta_i) \tag{5.1}$$

where θ_i are the parameters of the ith simple density used as a mixture component. The most widely used mixture model is the Gaussian mixture model (GMM) [157], where each base distribution is a Gaussian with parameters $\theta_i = \{\mu_i, \Sigma_i\}$ comprising the mean vector μ_i and covariance Σ_i of the i-th mixture component. The likelihood of an observation for each mixture component is given by

$$p(x|\theta_i) = \frac{1}{\sqrt{2\pi^d \det (\Sigma_i)}} \exp \left\{ -\frac{1}{2} (x - \mu_i)^T \Sigma_i^{-1} (x - \mu_i) \right\} \tag{5.2}$$

Changes in observation distribution can be detected by testing which base mixture component returns the highest likelihood for a given observation where each distribution comprising the GMM represents a latent class conditional density within the HMM. The relationship between latent states and observational data is illustrated in Figure 5-4 which shows both the hidden Markov temporal dynamics and the GMM representation of the observation space. A Markov model assumes that the presently active state has been generated by the previous n states it has been in, where n is the model order. A HMM

abstracts time series observation data into a state based form and uses a first order Markov chain to model the dynamics of the hidden state sequence [157].

The example in Figure 5-4 shows sensor data for electrical current during a basic load resistance offset fault within the ADL network. The GMM has two base densities representing the distribution of the data. Regions in the data where the current remains constant are modelled by a single mixture component which in turn can be mapped to certain states within the hidden sequence.
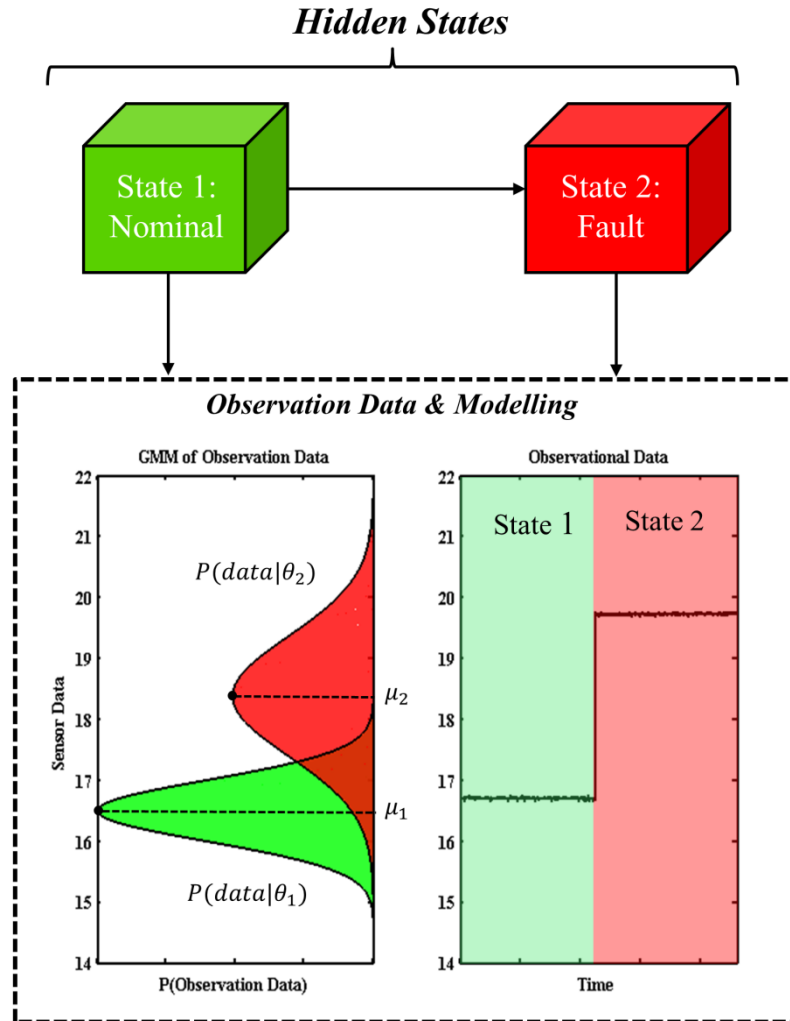
Figure 5-4: Illustration of relationship between latent states and observational data that form HMM. Data (right-hand side) is modelled by a GMM (left-hand side). Shifts in dominant mixture distributions indicate hidden state transitions.

At fault onset, current magnitude increases; the increase in current corresponds to a change in the most likely mixture component represented by the increased current value, resulting in a change of state in the HMM. The changes in mixture distributions, and hence state, are what the HMMs use to characterise different fault conditions within the proposed EPSmart method.

Inference of the state evolution in a HMM for a given observation period can be undertaken using a number of different methods [30]. A maximum a posteriori (MAP) estimation infers the most probable state sequence in chain structure models; in the context of HMM, the MAP estimation is known as Viterbi decoding [223]. The VA computes

$$s^* = \underset{s_{1:T}}{argmax}\, p(s_{1:T}|x_{1:T}) \tag{5.3}$$

The VA enables the optimum underlying system state sequence, s^*, to be inferred across the observation period, $x_{1:T}$, where all possible state sequences, $s_{1:T}$, are considered. In Figure 5-4, it can be inferred from the data that the ADL is in a nominal condition until the point in time where the change in current magnitude enhances the likelihood of the network being in a faulted condition.

An additional property of HMM concerns the probability of their statistical parameters yielded through training. These are a measure of how well a model has fitted the training examples presented to it through its parameters. A framework that contains multiple HMM permits the classification of candidate observation sequence by inferring the probability of the sequence being generated by a given model. This measure can be used to select the model which returns the highest likelihood and in doing so allows it to be classified with a label associated with the model.

With respect to the work of this thesis, within the EPSmart method, separate HMM are trained based on different input data sets, each representing unique system conditions. Each HMM uses a GMM to model the observational data and enables the dynamics specific to each condition to be characterised by the HMM parameters. New data is classified by applying it to each of the models, with the model returning highest probability of generating the data, or LL, assumed to be the closest match and therefore the most likely condition of the system.

5.1.3.2 Feature Extraction and Sensor Fusion

Training of each HMM within the EPSmart framework is critically dependent on the quality and volume of training data and the selection of features presented to the learning algorithms. Training a HMM on inappropriate data will result in an inadequate representation of the generalised behaviour of the modelled condition, and produce a model that will perform poorly at the inference stage.

Feature extraction, which was introduced in Chapter 3, is used to determine features within the data that optimise the discrimination capabilities of the system. Extracting unique

signatures for each condition is integral to the EPSmart method proposed within this thesis, especially when attempting to discriminate between a large set of network conditions.

Throughout training EPSmart for application to the ADL network, the limited sampling rate of the ADL sensors meant that basic statistical features were extracted for each modelled condition. Figure 5-5 (a) provides an example of the feature extraction process from load current sensor data throughout an intermittent fault condition. The sensor data is de-noised using wavelet analysis and then normalised to a notionally common scale. Normalising emphasises the dynamics within the data and also improves the generalisation capabilities of the trained HMM.
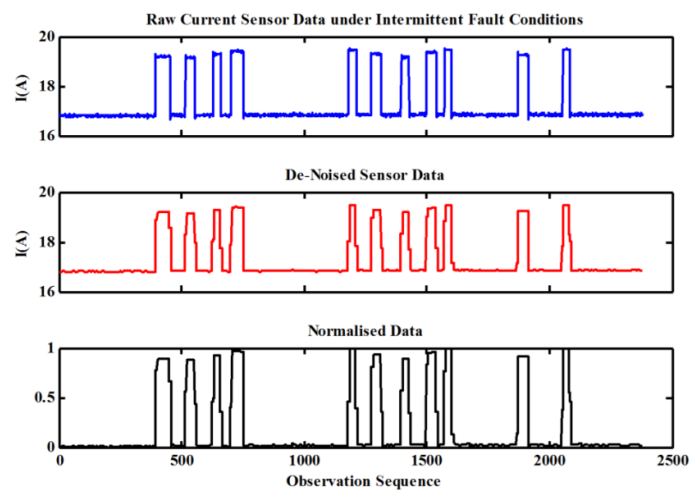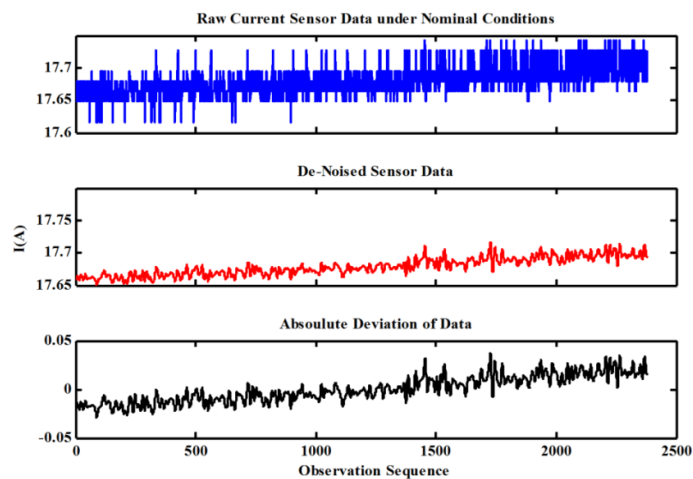
Figure 5-5: Illustration of features extracted from data for HMM training. Raw data was de-noised using wavelet analysis. For data describing nominal conditions, extraction involved calculating the absolute deviation. For fault conditions, a normalisation process was used.

In contrast, Figure 5-5 (b) shows the feature extraction process used for modelling nominal conditions. In this case, normalising the load current data to a common scale would undesirably magnify slight changes in the data. As such, the absolute deviation of the nominal data was extracted to maximise the constancy associated with nominal conditions.

EPSmart uses a global control structure to detect, diagnose and classify faults - i.e. data from multiple sensors within the network are combined to accurately identify and discriminate between faults. In a similar vein to the feature extraction processes, 'sensor fusion' [128] is necessary to determine the network sensors that optimise the discrimination capabilities of the system.

Within the ADL network there are a total of twelve sensors. The sensor fusion process determines dependencies that exist between these sensors throughout certain system conditions. Identifying these dependencies not only increases the discrimination powers of the EPSmart method but also eliminates any redundant information used throughout HMM training and reduces the dimension of the observation space.

Capturing dependencies within the multivariable ADL training data was achieved through simple plotting and analysis. Within systems more complex than the ADL, dependencies can be determined using more formalistic approaches (for example, principal component analysis [224]). Table 5-2 outlines the ADL sensor data used to train the HMM models for each network condition within EPSmart. A simplified schematic of the ADL showing only main components and labelled sensors is provided in Figure 5-6. Note that determination of the sensors used for training each condition is dependent only on the *location* of the fault, and not the mode.

Of the twelve sensors illustrated in Figure 5-6, the maximum number used to train a single network condition model is three (the maximum of three sensors is specific to the ADL and will change from network to network through analysis of dependencies captured between variables – sensors that react in a similar fashion across different fault conditions, and therefore result in ambiguous diagnoses, may be discarded altogether). This reduction of the observation space significantly simplifies the training process. The nominal model uses data from all three current sensors – current levels are relatively constant throughout nominal operation and any dynamic change in current magnitudes may be indicative of fault conditions. AC and DC load fault models use data form both the source current sensor, I_1, and their respective feeder current sensors, I_2 and I_3, for training.

The inverter fault model is trained using current and voltage data from feeders both upstream and downstream from the device. Detection of sensor failures is achieved through fusion of various sensors throughout the ADL network. Sensor failures are characterised by

isolated changes in sensor data, whereas faults in the underlying system will have a more widespread effect on sensor observations.

As a result of the feature extraction and sensor fusion processes, the data applied to each HMM for training are feature vectors describing sensor data for a variety of sensors sensitive to the specific network condition being modelled.

Table 5-2: Sensor data used to train each HMM

ADL Network Conditions	Sensor Data for HMM training
Nominal	I_1, I_2, I_3
AC Load Faults	I_1, I_2
AC Fan Load Faults	I_1, I_2, S_p
DC Load Faults	I_1, I_3
Inverter Fault	I_1, V_2
I_1 Sensor Fault	I_1, I_2, I_3
I_2 Sensor Fault	I_1, I_2, V_2
I_3 Sensor Fault	I_1, I_3
V_1 Sensor Fault	V_1, I_1
V_2 Sensor Fault	V_2, I_2
V_3 Sensor Fault	V_3, I_3
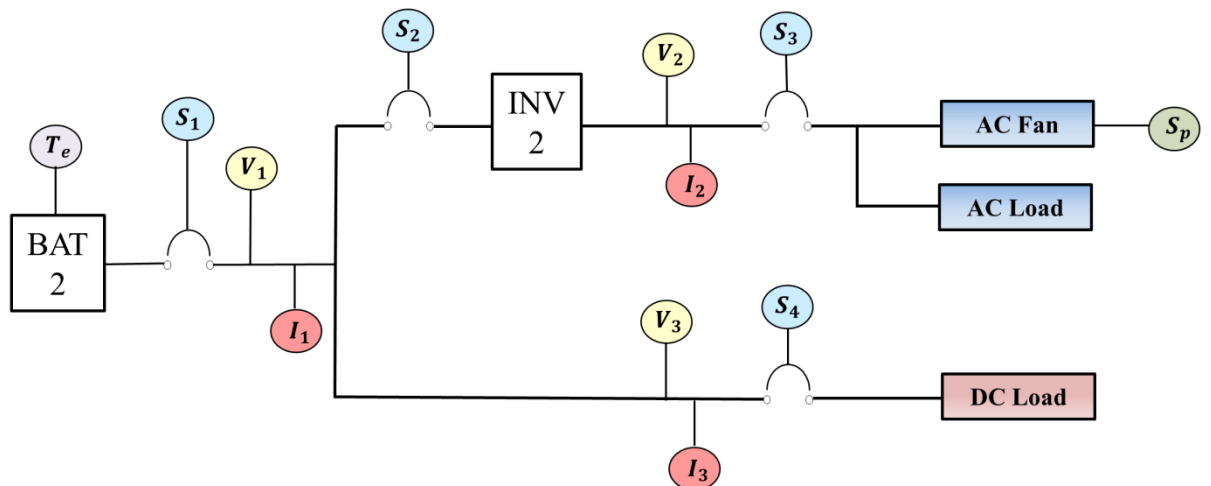
Figure 5-6: Simplified schematic of the ADL network showing main components and sensors: T_e donates a temperature sensor at the battery; S_n donates a circuit breaker sensor; V_n donates a voltage sensor; I_n donates a current sensor; and S_p donates a speed sensor at the fan load.

5.1.3.3 HMM Training & Model Selection

A significant EPSmart development issue concerns determination of the number of hidden states and mixture components of each trained HMM. This is an inherent issue with ML models, and this section describes the processes required to optimise these model parameters.

Modelling the observation space of HMM with a GMM captures non-stationary intervals through changes in dominant mixture distribution and thus changes in latent state [157]. However, the degree to which non-stationary periods are measured depends upon the number of mixtures that represent the distribution due to the fact that some non-stationary behaviour is absorbed into changes within the dominant mixture component as opposed to changes between distributions.

Although increasing the number of states and mixture components will implicitly capture a finer degree of non-stationary behaviour, the computational complexity of the model will increase. This modelling flexibility poses the problem of determining the cardinality of parameters, for example, how many states to use and how many mixture components will be present in the observation model. The quantity of training data also has to be considered with respect to learning the parameters of the models and whether the set of training data is sufficient to specify a set of parameters that suitably model the condition.

When fitting HMM to data using the expectation maximisation (EM) algorithm [225], increasing the cardinality of states and mixture components will increase the likelihood of the trained parameters. The problems associated with doing this are that models can become over-fitted to the training examples presented to them. Over fitting [110] is a phenomenon in which the models learn features pertinent only to the training set, and which will therefore perform poorly at inferring new, unseen data. A solution to overcome such problems is to introduce terms in the model selection criteria that punish model complexity, but still take into account model fit [157].

One such technique that considers model likelihood but retains a term to punish model complexity is Bayesian information criterion (BIC) [30], which is defined formally as

$$BIC(X, \theta) = \sum_{n=1}^{N} logP(x_n | \theta) - \frac{N_m}{2} logN \tag{5.4}$$

where X is the training data set, θ is the maximum likelihood estimate (MLE) of the model, N is the dimension of the training set and N_m is the number of degrees of freedom (parameters) of the model. Minimising the BIC value will optimise the number of parameters in terms of both model fit and complexity. Consequently, for each of the 15 modelled conditions within the ADL network (see Table 5-1 in Section 5.1.2), the BIC was used in determining model selection.

Throughout development of EPSmart for the ADL network, the relatively limited volumes of training data, particularly with regard to fault conditions, meant the number of model

parameters considered was limited [41]. Accordingly, when training each HMM within the Stage 1 framework, BIC ratings were calculated by increasing the number of states from two through to five and separate training examples describing each condition from one through to five (where possible, as some fault conditions did not have five separate training examples). Varying the number of states between two through to five was the result of analysing plots of the training examples. Fault current magnitude during intermittent and fault conditions can vary significantly - models with more than two states were required to capture these dynamics although it was decided to limit model complexity to a maximum of five hidden states. The training examples presented for each condition was limited to five so as to ensure there was sufficient test examples. Table 5-3 shows optimal trained models within EPSmart for selected ADL conditions, chosen by minimising the model BIC. The LL details the degree to which the parameters of the trained HMM described the training examples provided, with a value closer to zero detailing a 'better' model fit. The BIC considers all model elements, and determines if there is necessity to either increase or decrease cardinality. Table 5-3 highlights the state variability among selected HMM within the framework, where some modelled conditions require a greater number of states to achieve model optimality, compared with others.

Table 5-3: Optimal HMM Parameterisation within EPSmart for selected ADL conditions

ADL Network Condition Model	Training Examples	States	Log-[10]Likelihood	Bayesian Information Criterion
1 - Nominal	5	3	-2732.3	5526
FC2 – DC load abrupt resistance offset	2	4	-3346.8	6804
FC4 – AC load abrupt resistance offset	2	2	-1815.6	5704
FC6 – AC load incipient resistance	3	3	-2831.7	3646

5.1.3.4 Fault Parameter Calculation Algorithms

This section describes the development of the FPAs within Stage 2 of EPSmart, which were introduced in Section 5.1.2. The FPA utilise hidden state changes within the HMM to

---

[10] Log-likelihood is the natural log of the joint probability of all data points in an observation training sequence being generated by a model with certain parameters. Across a large data sequence, the joint probability is intuitively going to be a small number (the product of numbers < 1). LL ranges from zero (where all probabilities are 1) to minus infinite (where all probabilities are zero).

determine points in time where there is a significant change in network data. However, the fact that each of the 15 trained HMM in the classification framework have a different number of hidden states (as described in the previous section), there is a requirement to establish how they should be interpreted. Essentially, the FPA's only utilise the times where there is a *change* in hidden state within the optimum sequence – the raw sensor data is then analysed at these specific times to determine the severity of these changes. Note that the optimal state sequence of a particular HMM will only be calculated once that condition has been classified (refer to Section 5.1.2).

The best way to describe these concepts is with the use of an example. Figure 5-7 shows both the raw current sensor data for an AC load intermittent resistance fault and the associated optimal sequence within the related four state HMM of that condition. At the beginning of the observed sequence, the HMM is in State 1; at intermittent fault onset, the state sequence alters between States 3 and 4 and, when the system returns to a nominal condition, the state sequence also returns to State 1. The FPAs assume that the initial state within an observation sequence relate to a nominal condition; any divergence from this state indicates the point of fault onset.

Three FPAs were developed corresponding to each fault mode. Table 5-4 outlines the parameters calculated by each FPA. The FPA algorithm for an abrupt mode fault is outlined in Algorithm FPA I below.
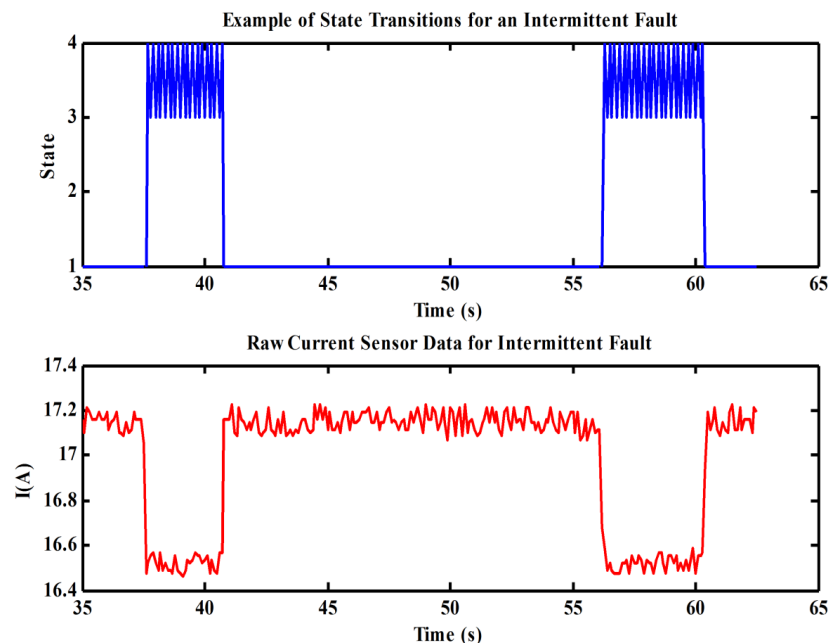
Figure 5-7: Example of optimal state sequence when ADL intermittent fault data is applied to a four state intermittent fault HMM

Table 5-4: Fault parameters required for determination of fault severity

FPA I – Abrupt mode fault	FPA II- Intermittent mode fault	FPA III – Incipient mode fault
1) Time of Fault Onset	**1)** Time of Fault Onset	**1)** Time of Fault Onset
2) Power Offset	**2)** Power Offset	**2)** Drift Gradient
	3) Average time in fault condition	
	4) Average time not in fault condition	

Algorithm 5-1: Abrupt Mode FPA1 Algorithm.

Algorithm FPA I Abrupt Mode Fault
1. **Inputs** Optimal State Sequence of HMM (*state*)
2.   Raw Data observation sequence (*raw*)
3. **for** i = 2:size(*state*) **do**
4.   **if** i ≠ *state*(1) **then**
5.   Fault Time = (i)
6.   Fault Level =*raw*(i) – *raw*((i-1))
7.   **else**
8.   *No change in optimal state*
9.   **end if**
10.**end for**

The algorithm determines the time of optimal state change to be the point of fault onset. Fault level, or power offset, is determined by calculating the change in current levels between the point of fault onset and the current level prior to fault onset. The intermittent mode FPA calculates these two parameters as well as the average intermittent fault time across the observational period. The incipient mode FPA also calculates the time of fault onset from the state change; the drift gradient is calculated by subtracting current magnitude at this point from the current magnitude at the end of the observation period.

5.1.4 EPSmart - Summary

The EPSmart method has been proposed as part of the work of this thesis to detect a variety of abrupt, intermittent and incipient fault modes across different locations throughout a hybrid AC/DC aircraft EPS. The aims of EPSmart are to diagnose different critical and degraded modes of operation as well as discriminate between sensor failures and faults in the underlying system; meeting these aims will improve overall EPS network protection and control. Two separate stages of the method – fault classification using an HMM framework,

and diagnosis of fault severity using HMM optimal state sequences – were described throughout this section.

For the purposes of this thesis, EPSmart was developed using data from the NASA ADAPT network. EPSmart application is not limited to ADL. The methodology may be applied to various forms of compact hybrid EPS networks: the main prerequisite for wider application is the availability of training data for nominal and faulty conditions. The variety of ADL fault modes described within the data was outlined. To validate the system, a case study, outlined in Chapter 6, uses ADAPT data, separate to data that was used for EPSmart development, to test the methods accuracy.

5.2 IntelArc – FDI of Series DC Arc Faults

The series DC arc fault phenomena was described in detail in Chapter 4. Faults of this type remain a problem in both utility and micro grid applications [170]. However, detection and diagnosis of these network events within aircraft is particularly challenging as:

1) Fault current reduces below nominal load current, meaning conventional overcurrent protection devices do not usually detect and isolate them.

2) In-flight vibration may result in highly intermittent faults between loose terminals/connections, where typical duration is less than 50ms.

Despite the considerable research and development effort over a number of years on detection systems and methods for arc faults, issues still remain surrounding the discrimination of fault events from nominal transient events [219]. This becomes particularly difficult when attempting to develop generalised fault detection methods[11].

This thesis puts forward a novel series DC arc fault diagnosis (AFD) method, *IntelArc*, which can provide accurate coverage across a range of network conditions, and also classify highly intermittent fault events. The proposed method combines time and time-frequency domain extracted fault features with HMM. Data generated from the validated arc fault model, described in Chapter 4, will be used for IntelArc development and testing. The ultimate goal of IntelArc is to improve aircraft EPS network protection against potentially dangerous series arc events through accurate fault detection and diagnosis.

The novel IntelArc AFD method presented here is one of the key research outputs of this thesis.

This section begins by outlining IntelArc. Off-line development of IntelArc is then described in Section 5.2.2 and on-line application is discussed in Section 5.2.3. The determination of characteristic arc fault features for use within IntelArc is discussed in Section 5.2.4. HMM training is also described in Section 5.2.5. Two applications relating to arc faults on aircraft systems are presented in Section 5.2.6.

5.2.1 IntelArc - Method Outline

The IntelArc method utilises a framework of trained HMM relating to different network conditions – this is similar to the methodology of Stage 1 of the EPSmart system, described in Section 5.1.2. Figure 5-8 outlines the basic IntelArc method.

---

[11] A generalised detection method can accurately (and autonomously) detect faults within a variety of system conditions and topologies.

For brevity, only three trained HMM are shown in Figure 5-8 – the three HMM relate to series arc fault, nominal steady-state and nominal transient conditions respectively. Practically, further HMM relating to different system transient conditions would be trained and implemented within the framework.

During on-line application, windows of load current data are applied to each HMM within the framework. Each load current window covers a particular period, X ms, of EPS operation. Each HMM outputs a LL measure which quantifies the similarity of on-line data with the trained parameters of the HMM (see Chapter 3, Section 3.8.1.4). An AFD algorithm within IntelArc analyses the LL output of each HMM every X ms. IntelArc outputs an alarm if there is sufficient evidence to suggest the presence of arc fault conditions. This process is repeated as new system data becomes available.

The general design of IntelArc is similar to that of the EPSmart method. The main difference is that IntelArc only uses the LL outputs of the HMM every X ms to diagnose arc fault conditions – there is no requirement for optimal state paths to be calculated. However, there is the requirement for development of an AFD algorithm to analyse the various outputs of each HMM. Also, IntelArc uses time-frequency domain feature extraction techniques for detection as opposed to only time-domain features used within EPSmart.
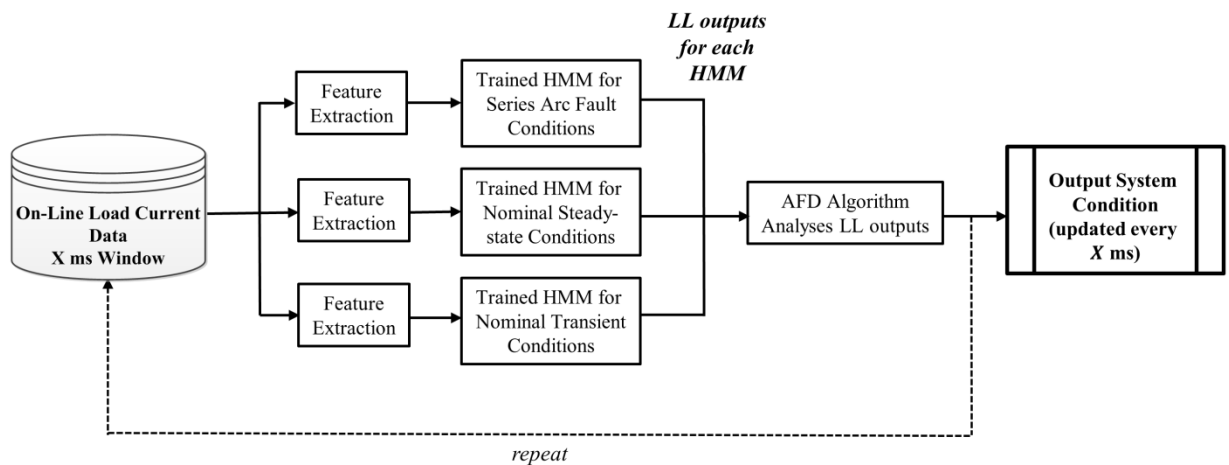
Figure 5-8: Basic Outline of IntelArc method.

5.2.2 IntelArc – Off-line Development

Development of IntelArc centred on the use of EPS network data to train HMMs. Multiple HMMs corresponding to different network conditions were identified and trained. These corresponded to:

1) Nominal steady-state behaviour

2) Nominal transient behaviour

3) Series DC arc fault behaviour

Each HMM was trained in a supervised manner [226] using labelled data corresponding to each of the three conditions. Several steps were undertaken to ensure correct processing of the generated training data and to determine optimal feature extraction for series DC arc fault discrimination. The main off-line development processes are shown in Figure 5-9 and summarised as follows:

- Data Generation – Synthetic data generated using a software model (or similar)

- Data Analysis – plotting, formatting and labelling synthesised data

- Feature Extraction from Data – Features extracted from data in time and time-frequency domains

- Machine Learning Model Development – HMM trained using feature extracted data

- Algorithm Development – Algorithms diagnose network condition through analysis of HMM LL outputs
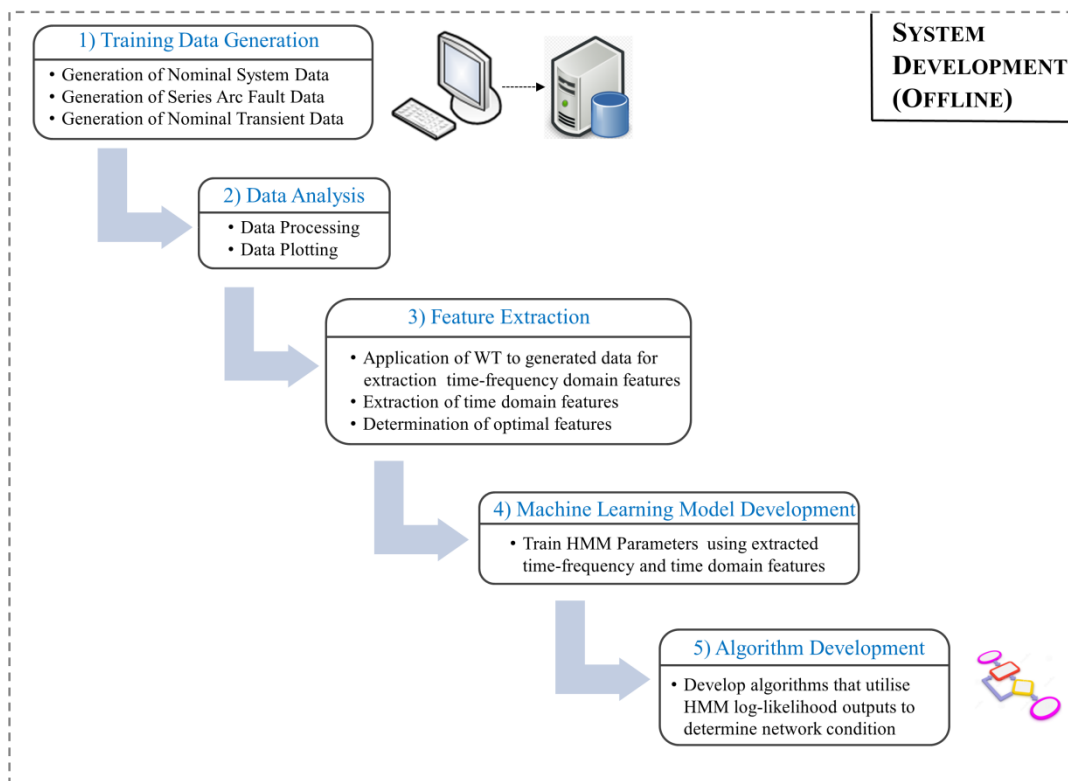
Figure 5-9: IntelArc off-line development processes

Training data was generated and labelled for all three conditions using Simulink and SimPower Systems [227] model simulations. Nominal steady-state data was captured during stationary periods of system operation, while nominal transient behaviour data was captured during load switching events; series DC arc fault behaviour was captured using the Simulink fault model, which was described and validated in Chapter 4. Randomised instances of the fault model were used for generating fault training data: speed of electrode separation was randomised between 5 and 25mm/s and the distance at which the electrodes dwell was randomised between 1 and 15mm.

IntelArc uses load current data to determine fault presence. Use of load current signatures for detection ensures the system is non-intrusive and there is no further hardware requirement beyond load current sensors.

Data processing was required for correct formatting and labelling of data. Explorative data analysis through graphical plots allows visualization of data and yields understanding of relationships throughout different network conditions.

IntelArc uses both time-frequency and time domain extracted features for fault detection. The Wavelet Transform (WT) was used for time-frequency domain extraction of the load current data, while statistical measures were used for time domain extraction. The feature extraction process is non-trivial, and determining optimal features is important for the development of an accurate and discriminative diagnostic method. This is discussed in detail in Section 5.2.4.

The extracted time-frequency and time domain features were used to train each HMM. Model training used the presented training data features to determine the model parameters through the use of the Expectation Maximisation (EM) iterative algorithm [30]. There was also the requirement to specify both the number of hidden states in the hidden state space, and the number of mixture distributions for the observation space. These processes are described in Section 5.2.5.

The AFD algorithm determines network condition (i.e. healthy, faulted) through analysis of the HMM LL outputs. The LL measure of a given HMM quantifies the likelihood that new, unseen network data has been generated by the said HMM. Mathematically, this is defined as:

$$LL_m = p(Data|Parameters_m) \qquad (5.5)$$

where LL_m is the log-likelihood that network data, *Data,* was generated from the mth model with trained parameters, $Parameters_m$.

AFD Algorithm development involved setting LL values that prove sufficient evidence to return a decision on network condition.

5.2.3 IntelArc – On-Line Application

The IntelArc method developed as part of this thesis is applied to diagnose series DC arc faults in real-time. Load current data is input to IntelArc in the form of windowed data streams. The method processes and extracts features from each window of load current data. These extracted features are applied to each of the trained HMM, and the AFD algorithm analyses the LL outputs of each model to infer network condition at that point in time. These processes were illustrated in Figure 5-8. They are discussed in further detail in the following sections.

5.2.3.1 Types of Data Window

Sampling frequency, window length and window type impact system operation. Two separate applications of the IntelArc method relating to arc faults on aircraft are presented in this thesis. One application is for generalised sustained arc fault diagnosis across a range of voltage distribution levels. The other application is for the detection of intermittent series arc fault events.

The main, and essentially only, differences between these two applications are the sampling frequency and type of window. Figures 5-10 and 5-11 highlight the differences in load current data windows between each application.

Figure 5-10 illustrates the consecutive window technique utilised in the sustained fault detection application. This technique uses data windows of load current in consecutive time frames of length ∆t – a frame length of 50ms was used in both applications to reduce the probability of transient behaviour causing false diagnoses and to allow fault isolation prior to excessive electrode heating (thus reducing the risk of fire). This frame length is not binding and may be altered in separate applications of IntelArc. Each window is consecutively input to IntelArc to infer network condition.

The main difference between the consecutive window technique and the sliding window technique, utilised for intermittent arc fault detection, and illustrated in Figure 5-11, is the overlap between windows. Despite ∆t being equal in both techniques for the examples considered here, the overlap means that only 10ms of new data is analysed within each window. This is advantageous for detection of intermittent arc events, as there is increased

potential for the detection of changes in fault current across smaller time intervals. Examples of IntelArc being applied for generalised diagnosis of both sustained arcing events and intermittent arcing events are provided in Section 5.2.6.
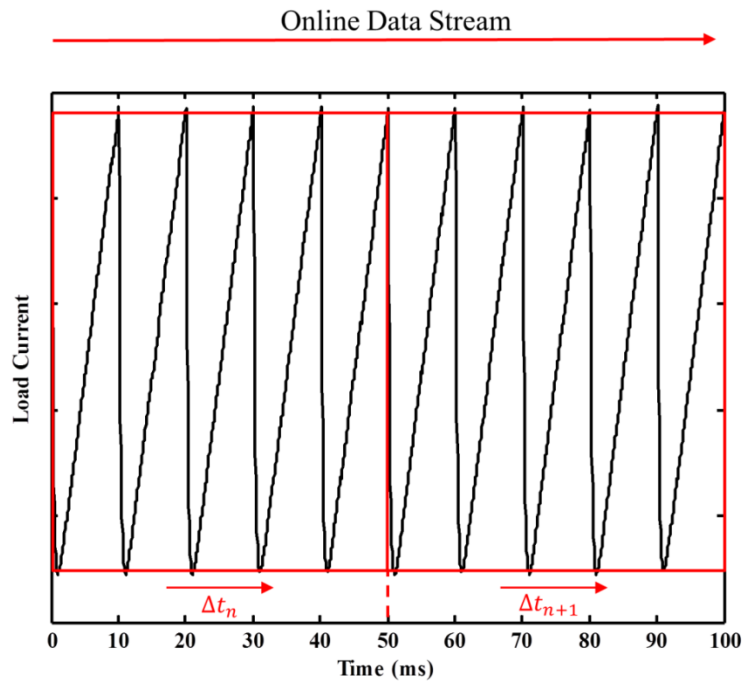
Figure 5-10: Consecutive windowing technique utilised in the sustained arc fault application
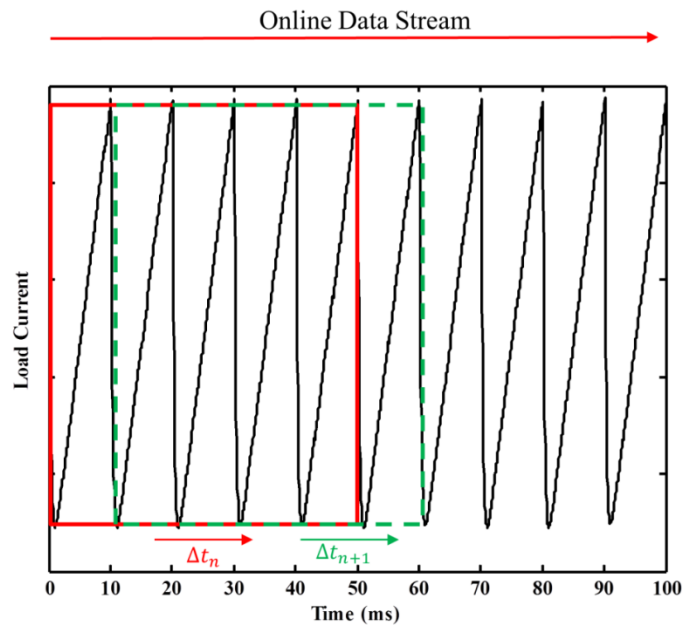
Figure 5-11: Sliding window technique utilised in the intermittent arc fault application

5.2.3.2 Application Overview

Figure 5-8 illustrated the on-line method of IntelArc. Each stage of this process is briefly described in the following.

- **Online EPS Data**

  System data is in the form of windowed batches covering a particular time period of load current, Δt_n, where n is the nth time window. Load current is sampled at frequency, f_s, meaning that, for any time window, n, the number of samples, s_n, is:

  $$s_n = f_s \times \Delta t$$
  (5.6)

- **Feature Extraction**

  Features are extracted from each data window using the WT (for time-frequency domain features) and statistical measures (for time domain features). These extracted features are then applied to each of the trained HMM. Feature extraction is described in detail in Section 5.2.4.

- **Apply to Trained Models**

  Extracted features of data window, n, where $n \in (1, 2, \ldots, N)$ and $N \in \mathbb{R}$, are applied to each of the three trained HMM to determine the LL that each model generated the data.

- **AFD Algorithm**

  The algorithm uses the LL of each HMM to infer network condition. The algorithms for both sustained and intermittent fault detection applications are presented in Section 5.2.6.

The application process, in terms of receiving load current windows and using them to update inference of network condition is illustrated in Figure 5-12. Time between updates is dependent on the length of window Δt, and whether a consecutive or sliding window technique is used. Section 5.2.3.1 outlined that IntelArc updates network condition every 50ms – this length of time was deemed sufficient to safely diagnose and isolate arcing

conditions, and also decrease the probability of false detection. However, update time can be altered to suit specific requirements.
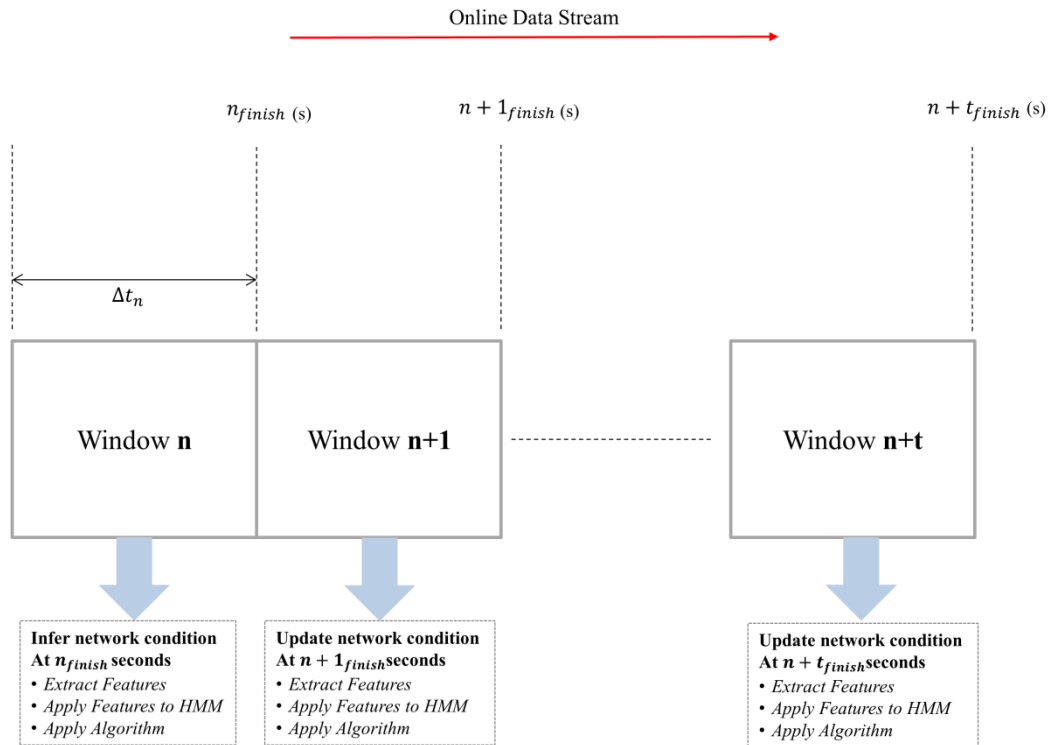
Figure 5-12: Basic example of IntelArc network condition updates after application of load current data windows

5.2.4 Feature Extraction

The importance of data feature extraction to the development and application of accurate fault diagnosis systems was introduced in Chapter 3. In ML based systems, the extracted features should be optimally discriminative between the different conditions/behaviours under consideration [30].

Consequently, the development of three separate HMM corresponding to three separate conditions modelled in IntelArc – nominal steady-state, nominal transient and series DC arc fault – required significant empirical research into the determination of optimally discriminative features. This section discusses and presents the research results for determining discriminative features from the data. The extracted features were in both time-frequency and time domains. Time-frequency domain feature extraction using the WT is presented before time domain extraction using statistical techniques is described.

5.2.4.1 Series DC arc fault time-frequency domain Feature Extraction Using the Wavelet Transform

The WT has been described throughout previous chapters. Chapter 4 elaborated on its ability to provide both time and frequency resolution to signals. Why is this resolution characteristic useful for feature extraction of series DC arc faults within an HMM based detection method? Consideration of the following elaborates on the benefits of using the WT.

Essentially, the use of HMMs for fault detection depends on signals being non-stationary across time periods – HMMs use changing states (state transitions) to model the non-stationary behaviour. Also, arc faults, as described in Chapter 4, exhibit highly transient, non-stationary behaviour, with expansive frequency spectra. While the FFT provides excellent frequency resolution [156], it does not provide any time resolution; as such, with respect to non-stationary signals, the FFT is not a powerful tool as there is no representation of how the frequency contributions change throughout time. On the other hand, the WT does provide information on both frequency and time.

So, specifically:

1) HMMs depend on signals changing across time (non-stationary signals);

2) Arc faults exhibit highly transient (time domain) behaviour with expansive frequency ranges;

3) The WT provides time and frequency resolution.

These three points emphasise that the marriage of the WT (for feature extraction) with HMM (for inferring what the features relate to) has the potential to be the basis for a robust arc fault detection method.

5.2.4.2 The Wavelet Transform

It is important to understand both the theory of WT, and the additional information the transform provides about a signal. The theory of WT is complex and extensive – refer to Appendix C for a complete overview of the WT[12].

The DWT changes the time and frequency resolutions by convolving the signals with high and low pass filters, and down sampling by two. The bandwidths of the resultant sub-bands are ultimately determined by the sampling frequency of the original signal. Within the application of IntelArc for diagnosis of intermittent arcing events the sampling frequency, f_s,

---

[12] This overview includes: discussion on the resolution properties of the transform, and its benefits over the FFT; descriptions of both the continuous WT and the discrete WT (DWT); and information on the extracted WT Detail and Approximate coefficients.

of the load current was 20 kHz. Frequency sub-bands relative to the extracted approximation and detail coefficients are outlined in Table 5-5.

Table 5-5: Frequency sub-bands of the DWT approximate and detailed coefficients

	Frequency Bandwidth	Bandwidth for 20KHz Sampled Signal
Original Time Domain Signal		
Load Current Signal	$0 - \dfrac{f_s}{2}$	0 – 10KHz
Time-Frequency WT Extractions		
Approximate 1	$0 - \dfrac{f_s}{4}$	0 – 5KHz
Approximate 2	$0 - \dfrac{f_s}{8}$	0 – 2.5KHz
Approximate 3	$0 - \dfrac{f_s}{16}$	0 – 1.25KHz
Approximate 4	$0 - \dfrac{f_s}{32}$	0 – 625Hz
Approximate 5	$0 - \dfrac{f_s}{64}$	0 – 312.5Hz
Detail 1	$\dfrac{f_s}{4} - \dfrac{f_s}{2}$	5kHz – 10KHz
Detail 2	$\dfrac{f_s}{8} - \dfrac{f_s}{4}$	2.5kHz – 5KHz
Detail 3	$\dfrac{f_s}{16} - \dfrac{f_s}{8}$	1.25kHz – 2.5KHz
Detail 4	$\dfrac{f_s}{32} - \dfrac{f_s}{16}$	625Hz – 1.25KHz
Detail 5	$\dfrac{f_s}{64} - \dfrac{f_s}{32}$	312.5Hz – 625Hz

The following sections describe selecting the WT coefficients that optimise series arc fault detection and discrimination.

5.2.4.3 DWT Approximate Coefficients – Determining Optimum Features

Feature selection as a formal technique determines the extracted features that provide sufficient difference across the range of conditions under consideration. Determination of such features optimises a detection methods discriminative capabilities and accuracy. This section details the extraction of the DWT approximate coefficients and shows how these features vary between arc fault conditions and nominal conditions[13].

Figure 5-13 (a) illustrates normalised load current sampled at 20 kHz across a 50ms window under nominal conditions (1000 samples for 20 kHz sampling frequency) and

---

[13] For clarity, only extracted DWT approximate coefficients under nominal steady-state and series arc fault conditions are described.

Figure 5-13 (b) shows the associated level 1, 3 and 5 WT approximate coefficient feature extractions (load current data was simulated using SimPower Systems and DWT approximation coefficients were extracted from load current data using MATLABs Wavelet toolbox [228]). DC ripple [229] is evident within the nominal load current – this ripple is a result of the upstream rectifier. Also, 5 kHz Gaussian measurement noise is present within the load current. The approximate coefficients extract the time-frequency response across the lower frequency sub-bands (see Table 5-5). The high frequency noise is filtered out as the levels increase and the frequency sub-bands get both lower and narrower.
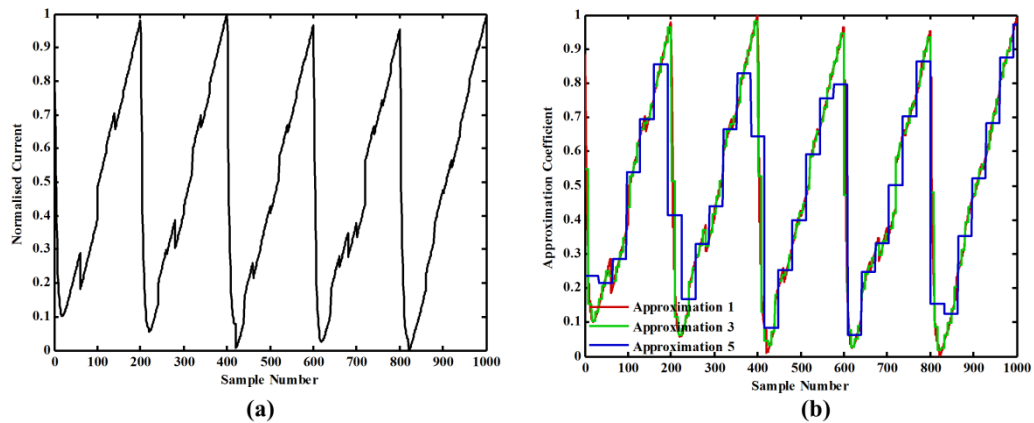
Figure 5-13: (a) Example of normalised load current signal across 50ms window during nominal conditions (b) Associated Level 1, 3 and 5 DWT approximate coefficients

In contrast, Figure 5-14 (a) shows an example of normalised load current under series DC arc fault conditions, and Figure 5-14 (b) shows the associated DWT approximate coefficients. The sudden decrease in load current is a result of an unsuccessful arc-quenching attempt – this decrease significantly changes the magnitude and shape of the approximate coefficients during arc fault conditions.
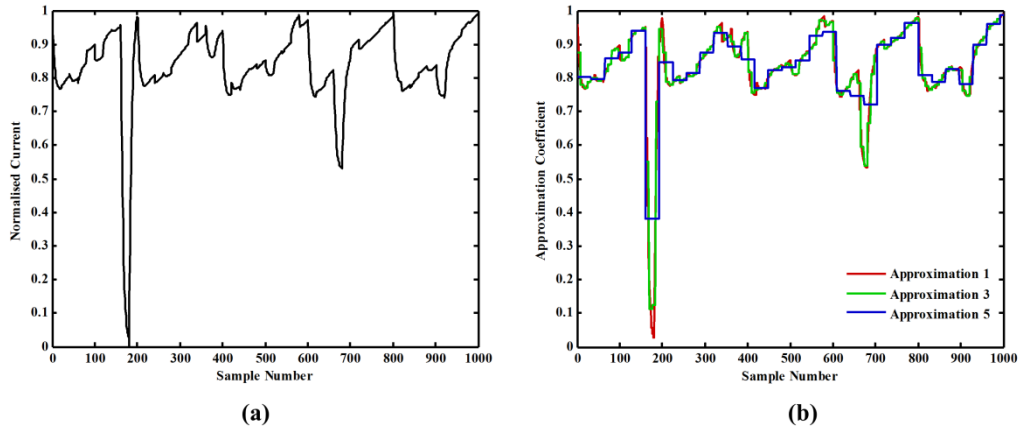
Figure 5-14: (a) Example of normalised load current signal across 50ms window during series DC arc fault conditions (b) Associated Level 1, 3, and 5 DWT approximate coefficients

The use of an empirical cumulative distribution function (CDF) highlights the difference in DWT approximate coefficients for nominal and fault conditions, with the CDF of approximation coefficients illustrated in Figure 5-15. The CDF was calculated across the training data sets for nominal and arc fault conditions. These training sets consisted of 350×50ms windows captured during nominal conditions and 131×50ms windows captured during fault conditions - generation of training data was described in Section 5.2.2.
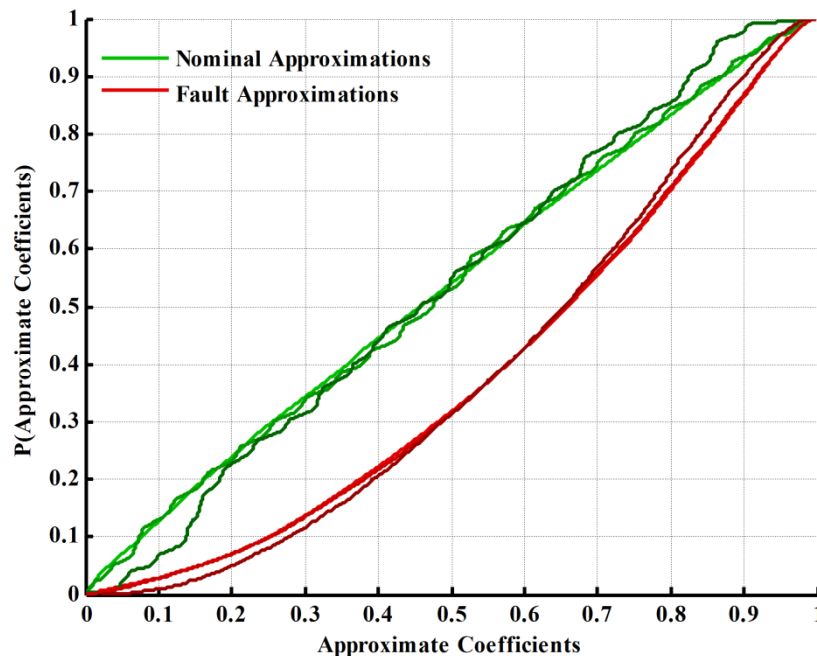
Figure 5-15: Illustration of CDFs of various levels of approximate coefficients for both nominal and arc fault conditions

138

The CDF details the probability that the magnitude of the approximate coefficients will be within a certain range of values. The difference in CDF's between nominal and fault conditions is evident from Figure 5-15. For example, the probability that the magnitude of approximate coefficients is >0.5 during arc fault conditions is roughly 70%, compared to roughly 45% during nominal conditions. The higher magnitudes of approximate coefficients under fault conditions are understandable when considering Figures 5-13 and 5-14.

The difference in magnitude of the approximate coefficients under nominal and fault conditions is useful for discrimination. However, detection systems based on HMM also rely on features that change across time. Modelling the distribution of these coefficients enables the dynamic element of each feature to be modelled.

Figure 5-16 illustrates the distribution of the Level 1, 3 and 5 approximations during nominal and fault conditions - non-parametric kernel density estimates [30] were used to model the basic distributions.
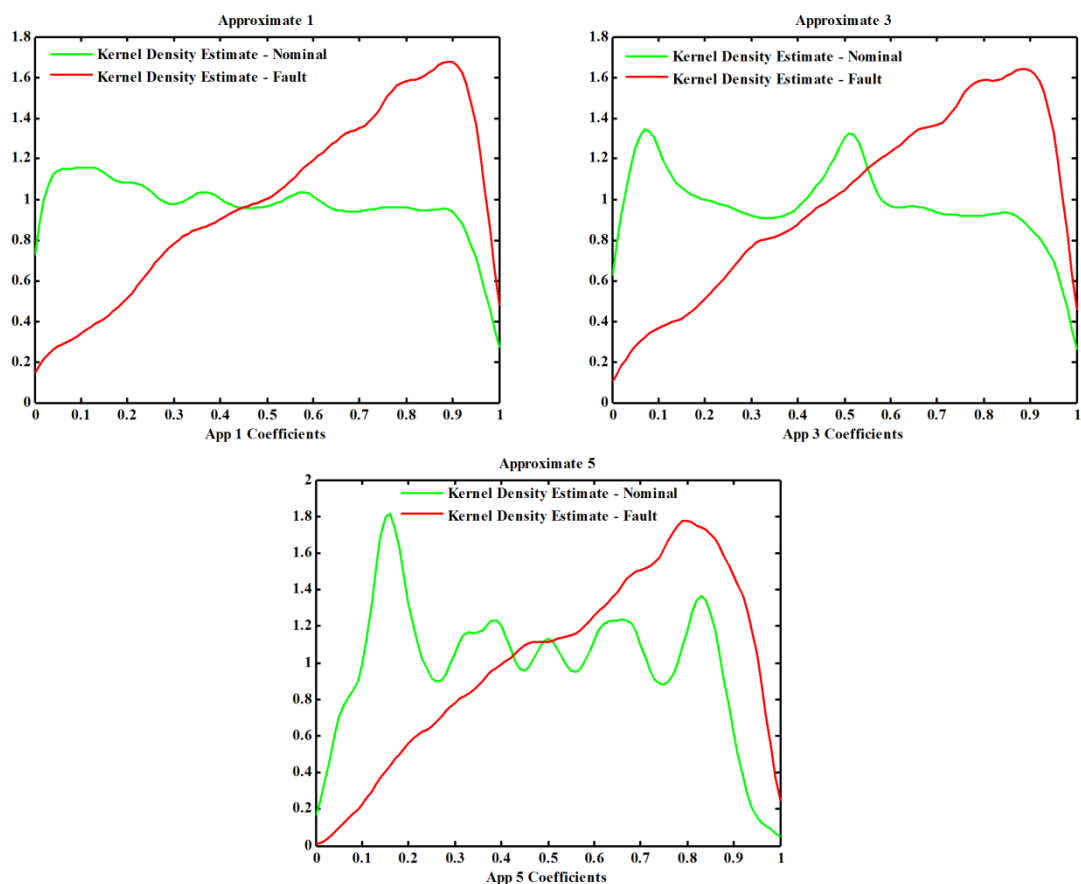
Figure 5-16: Kernel density estimates of Levels 1, 3 and 5 WT approximation coefficients

During nominal conditions, the coefficients are evenly distributed between 0 and 1. However, during arc fault conditions, the density at lower values is considerably smaller than the density at higher values i.e. the probability of approximate coefficients having greater magnitude throughout arcing conditions is increased.

A parametric GMM [30] is used to model how the approximate coefficients change throughout time. Consider the illustrative examples provided in Figure 5-17. Figure 5-17 (a) shows a GMM for the distribution of Level 1 coefficients under nominal conditions using four mixture components. Each Gaussian models the distribution of coefficients falling between specified ranges - the *blue* Gaussian models the distribution of coefficients between 0 and 0.25, the *red* Gaussian models coefficients between 0.25 and 0.5, the *green* Gaussian models coefficients between 0.5 and 0.75 and the *magenta* Gaussian models coefficients between 0.75 and 1.
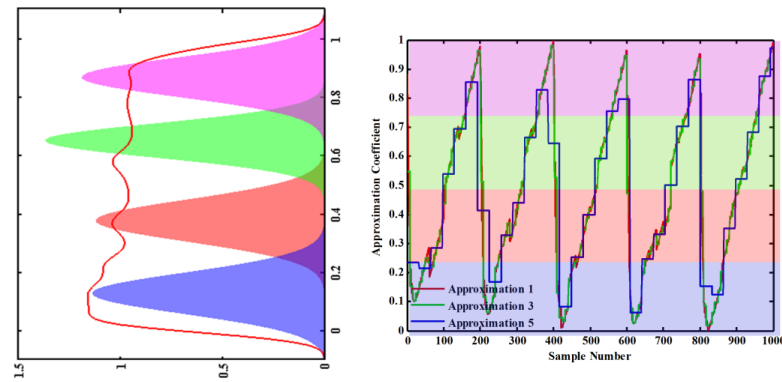
(a)
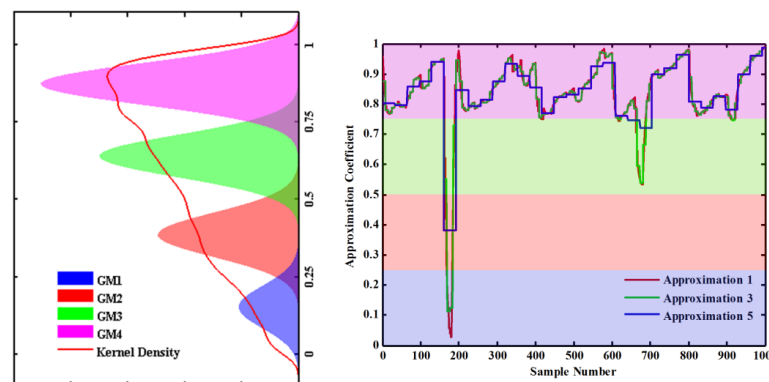
(b)

Figure 5-17: GMMs to model the distribution of WT approximate coefficients during (a) nominal conditions and (b) series arc fault conditions. Note the increased rate of transitions between each Gaussian under nominal conditions in comparison to the fault conditions.

The area under each Gaussian models the probability that a coefficient will be within each range. Under nominal conditions, the area under each Gaussian is roughly similar which indicates a uniform distribution between 0 and 1. Thus, as illustrated in Figure 5-17 (a), there will be numerous transitions between each Gaussian throughout time.

In contrast, Figure 5-17 (b) illustrates a GMM for Level 1 coefficients under arc fault conditions. The area under the Gaussian modelling the distribution of coefficients between 0 and 0.25 is significantly smaller in comparison to the Gaussian modelling the distribution between 0.75 and 1. This difference in area means that the probability of the coefficients being between 0.75 and 1 is significantly higher than the coefficients being between 0 and 0.25. Also, the number of transitions throughout time between each Gaussian is likely to be significantly less under arc fault conditions.

The differing rate of transitions between nominal and arc fault conditions shows that the extracted approximation coefficients are a useful feature for discriminating between each condition. It is also necessary to determine the levels of approximation coefficients that should be used – is there suitable benefits of using all levels, or should a subset be selected? It was evident from analysis that the coefficients begin to level out at certain magnitudes as the levels increase and the frequency sub-bands get closer to zero. This is not ideal as the distributions begin to become clustered within certain regions and reduces the number of transitions during nominal conditions - this concept is illustrated in Figure 5-13 where the level 5 coefficients are less sharp. These factors resulted in level 4 and level 5 coefficients not being selected for use within IntelArc whereas Levels 1 to 3 were selected as suitable features for arc fault detection. These features ensure the load current signal is decomposed into different frequency resolutions in the 0 to 5 kHz bandwidth (see Table 5-5) and also minimize the effect of extremely low frequency bands on detection accuracy.

5.2.4.4 DWT Detail Coefficients – Determining Optimum Features

The approximation coefficients extract low frequencies of the time domain signal at various resolutions. These approximate coefficients represent the original signal without the high frequency components. However, highly transient arc fault signals contain high frequency components that are potentially useful for detection purposes [85]. The DWT detail coefficients, which extract higher frequency components, were therefore an important feature to consider. Similar to the approximate coefficients, it was necessary to select detail coefficient features that optimally discriminate between the various conditions.

The bandwidths of various levels of detail coefficients for a 20 kHz sampled signal are outlined in Table 5-5. Figure 5-18 illustrates examples of Levels 1, 3 and 5 detail coefficients relative to 50ms windows of load current data during nominal and fault conditions.
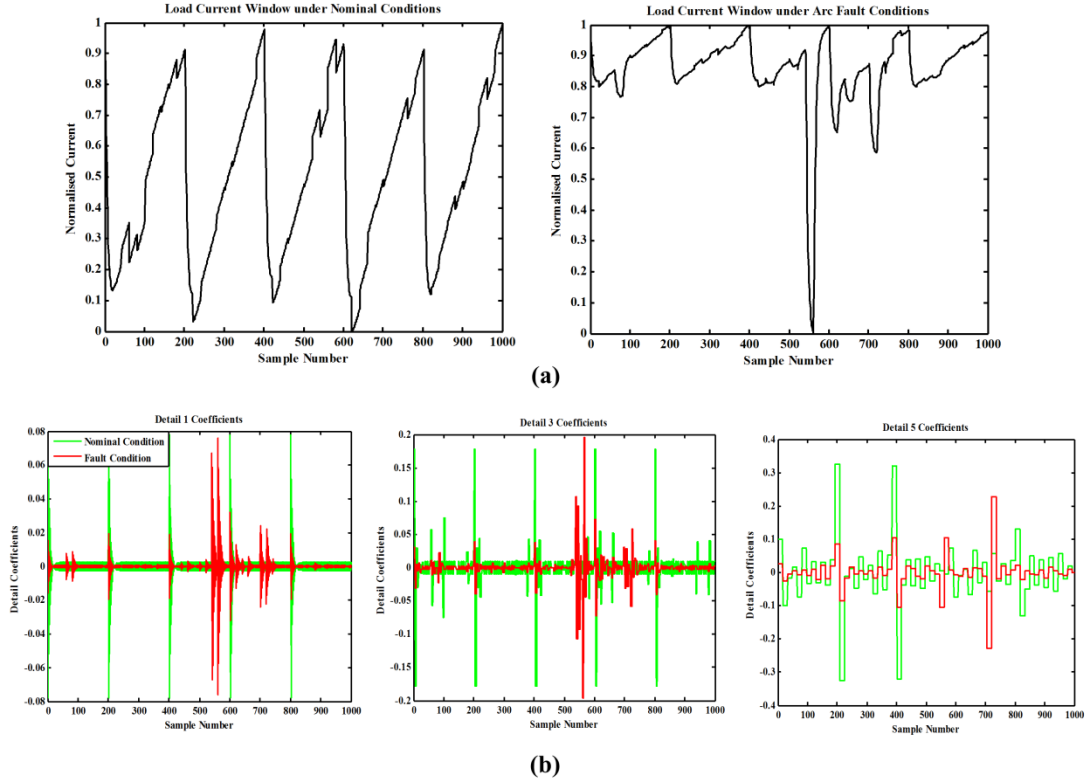
Figure 5-18: (a) Examples of 50ms load current windows during nominal and arc fault conditions. (b) Extraction of WT detail coefficient levels 1, 3 and 5 for corresponding nominal and fault load current windows. Note that there are a higher number of increases in coefficient magnitude at lower detail levels under fault conditions – these increases are evident by the spikes in Detail 1 and 3 coefficients in (b).

An increase in the magnitude of the detail coefficients indicates that the frequency bandwidth extracted by the particular level is present at that particular time. The load current during nominal conditions contains both DC ripple and measurement noise. The DC ripple results in increases in Level 1 and 3 coefficients roughly every 12.5ms (or 200 samples) under nominal conditions. The measurement noise also increases the magnitude of detail coefficients – as noise tends to be random, these increases are less predictable. The 5 kHz noise has a notable effect on detail levels 3-5, whereas levels 1-2 are less affected.

In comparison, the detail coefficients under fault conditions are mostly affected by the transient nature of the arcing events. Coefficient increases are evident in levels 1 and 3 when current suddenly decreases - these transients result in the presence of high frequency

components and thus an increase in coefficient magnitude. These increases tend to be less prominent at higher detail levels.

At lower level details, there tends to be a greater number of coefficient magnitude increases under series arc fault conditions in comparison to nominal conditions. The difference in coefficient increases between nominal and fault conditions was determined to be a useful feature for detection. As was the case with the approximation coefficients, the dynamics of the detail coefficients can be modelled using a GMM.

Figure 5-19 illustrates GMMs for level 1 details during both nominal and fault conditions. The majority of detail coefficients in both conditions are clustered around zero with minimal standard deviation. The main difference between each GMM is the probability of the coefficient magnitude being greater than the zero-mean cluster. The area under each Gaussian is relative to the probability of a coefficient value being within the range of values. The increased area of the *red* and *blue* Gaussians under fault conditions signifies a greater probability of higher magnitude coefficients.
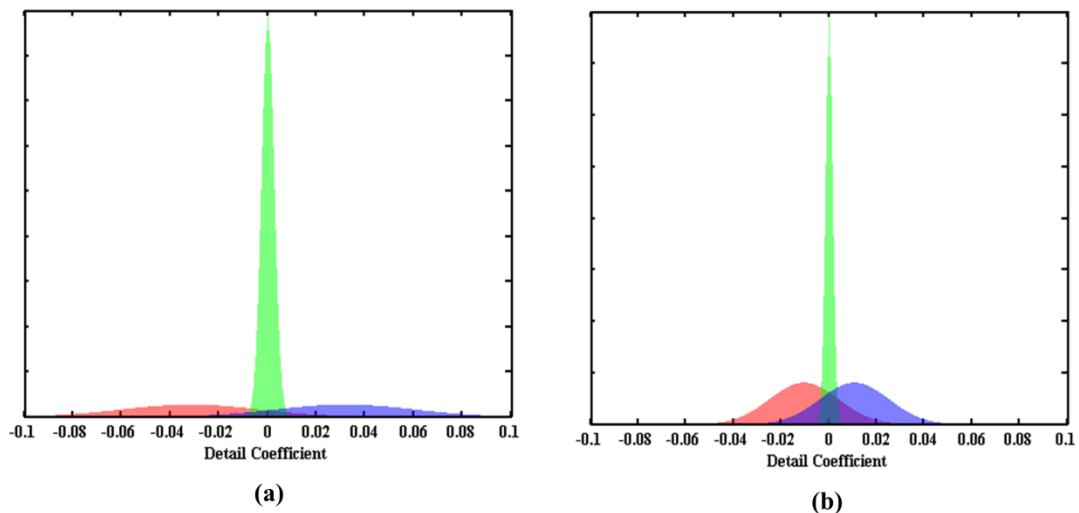
Figure 5-19: GMMs for level 1 detail coefficients during (a) nominal conditions and (b) fault conditions. Note the increased probability of increases in coefficient magnitude during fault conditions.

The increased probability of higher magnitude coefficients means that, in comparison to nominal conditions, there is likely to be greater transitions between each mixture during fault conditions. The differing rate of transitions between nominal and fault conditions ensure that DWT detail coefficients are a feature that will enhance the discrimination capabilities of the HMM based IntelArc system.

Again, it was necessary to select the levels of details that would optimise discrimination between each condition. Analysis of each detail level throughout each condition showed that Levels 3-5 were not suitable for discrimination. Level 3 coefficients were heavily distorted by the 5 kHz measurement noise whereas levels 4 and 5 did not capture the high frequency transients present throughout arc fault conditions (refer to Figure 5-18 (b) for illustrations of Levels 1, 3 and 5 detail coefficients). Consequently, detail levels 1 and 2 were selected as features for use in IntelArc.

In practice, noise from power electronic converters will not be limited to 5 kHz and may be present across the entire 0-10 kHz observable bandwidth. Noise between 5-10 kHz will have an effect on lower level detail extractions; however, the salient higher frequency signatures of arcing will still be present within these features and they will remain useful for diagnosis. This is not the case at increased detail levels as the higher frequency components are filtered out - their inclusion in IntelArc will likely impair detection. Consequently, the number of DWT detail extractions is limited to lower levels with only levels 1 and 2 being selected as suitable features.

5.2.4.5 Summary of time-frequency domain feature selection

The importance of selecting optimal features for the development of accurate fault detection systems has been emphasised in the previous sections. The process of modelling the probability distributions of extracted coefficients under different network conditions was critical for using HMM for AFD. Modelling the distribution enables appreciation of the coefficient dynamics under each network condition. This simplifies the HMM training stage (see Section 5.2.5). While previously proposed systems [219, 230] have used WT extracted features for AFD, the studies outlined here, to the best of knowledge, are not reported in literature.

After significant effort and research through modelling and analysing the distribution of coefficients extracted from load current data, the three approximate and two detail DWT coefficients extracted with a 20 kHz sampling frequency were deemed optimal for series DC arc fault detection within IntelArc.

5.2.4.6 Series DC arc fault time domain feature extraction

It was described in Section 5.2.2 that both time-frequency and time domain features were utilised within IntelArc. This section briefly describes the extraction of time domain features. The time domain features were, unlike the WT time-frequency domain features described in

the previous sections, extracted using more simplistic statistical analysis of the load current windows.

Specifically, a time domain feature based on a moving average [231] across the 50ms windows was extracted. Figure 5-20 illustrates examples of the moving average calculated for normalised windows of nominal and arc fault load current data. The moving average used a lag of 100 samples – hence, the moving average window contains only 900 samples.
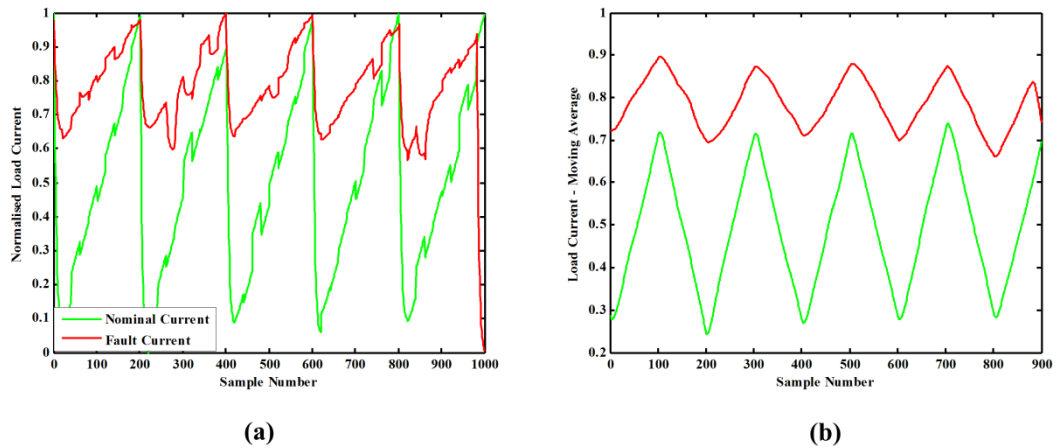
Figure 5-20: (a) Normalised 50ms window of load current data during nominal and series arc fault conditions (b) Moving averages of nominal and fault currents

Calculation of the moving average removes the extent of the DC ripple and separates the data into distinct regions for each condition. Both signals are generally smoother, with the majority of high frequency noise removed. The feature is complimentary to the WT approximate coefficients as the general shape of the signals, and distinctions between each condition, are highlighted.

The moving average time domain feature, in combination with the approximate and detail coefficients, was used for AFD within IntelArc.

Training of the HMM using these features is described in the following section.

5.2.5 HMM Training for IntelArc

Feature selection of DWT extracted coefficients determined that six feature vectors in total were used to train each HMM within IntelArc. These features included:

- WT approximation coefficient levels 1-3
- WT detail coefficient levels 1 and 2
- Moving Average

A separate HMM was developed corresponding to each condition; thus, one model was developed for nominal steady-state behaviour, one for nominal transient behaviour and one for series DC arc fault behaviour. For HMM theory, refer to Chapter 3.

Sections 5.2.4.3 and 5.2.4.4 illustrated the concept of modelling data using GMMs. Those sections also described the differing rate of transitions between mixtures throughout each condition. HMM development is analogous to these concepts. Modelling the observation space of HMM is similar to modelling the data using GMM, as illustrated in Figures 5-17 and 5-19. The training data in the context of HMM development was the six feature vectors and, therefore, has higher dimensionality than the GMM examples provided in these figures.

While the observation space is analogous to the GMMs of the data, the hidden state space relates the changes in mixtures across time to changes in hidden states i.e. changes in the observational data relates to changes in the hidden states (this was previously discussed in Section 5.1.3.1). It should be emphasised that the hidden states have no physical meaning – it is the trained parameters of the HMM that describe the behaviour of each modelled condition [41].

The feature selection process established the characteristics of each extracted feature under nominal and series DC arc fault conditions. These characteristics were useful in determining both the number of hidden states and mixture components within the observation space for each HMM prior to training. The EPSmart method, described in Sections 5.2, used the BIC to determine the optimal number of hidden states and mixture components of each HMM - the lack of training data for the ADAPT meant this methodology was used in an attempt to limit over fitting each HMM. However, the use of synthetic data simulated using software models meant that the volume of training data was not a concern during development of IntelArc; thus, the BIC formalism was not used throughout HMM training.

It was determined that the nominal steady-state HMM would have a greater number of hidden states and mixtures in comparison to the fault and nominal transient models. A greater number of states emphasises higher transition rates between each state (as described in Section 5.2.4.3), where the probabilities of transition are roughly uniform. The number of hidden states and mixture components for each HMM are summarised in Table 5-6.

Table 5-6: Number of hidden States and Gaussian mixtures of each HMM in IntelArc

HMM Model	Number of Hidden States	Number of Mixtures
Nominal Steady-State	10	10
Series DC arc fault	6	6
Nominal Transient	4	4

The increased number of hidden states in the nominal steady-state model is a consequence of the WT approximation features. Although the transition rate between the hidden states in the fault model are increased as a consequence of the WT detail features (refer to Section 5.2.4.4), it was considered unnecessary to include additional states to model these transitions. The nominal transient model will have the least number of transitions between hidden states as step changes in load current will dominate state dynamics. Limiting the number of hidden states and mixture components of the fault and nominal transient model also reduced the risk of over fitting the models [110] to the training data. Over fitting the nominal steady-state model is less of an issue as data under this condition is likely to be more consistent across a range of network scenarios.

The HMM parameters that were trained using the data are described in Table 5-7.

Table 5-7: Description of Trained HMM Parameters

HMM Trained Parameters
Mixture weights of Gaussian components modelling observation space
Variance between Gaussian mixture components
Mean of each Gaussian mixture components
Transition probabilities between each hidden state

These trained parameters are used for inference of new system data. As new system data is applied to a model, the trained parameters are used to determine the LL that the data was generated by said model – see (5.5) in Section 5.2.2.

The following sections further describe how the trained HMM are used within IntelArc to diagnose series DC arc faults.

5.2.6 IntelArc – Examples of Application

Two applications of the IntelArc method have previously been discussed in Section 5.2.3. The first application was for the diagnosis of sustained arc faults within aircraft representative networks, where a multitude of power converters and voltage distribution levels are present. The second application was for detection of highly intermittent arcing events. The use of IntelArc for diagnosis of sustained arc faults uses a reduced sampling frequency of 2 kHz while intermittent arc fault diagnosis uses a sampling frequency of 20 kHz. Sampling frequency is reduced in the sustained application to determine the effect this will have on diagnostic accuracy and detection time.

The different windowing techniques relevant to each application were discussed in Section 5.2.3.1. The use of HMM for AFD is dependent on correct interpretation of the LL outputs. LLs are calculated with the application of new test data to each trained HMM – this was

described in Section 5.2.3.2. Within IntelArc an algorithm assesses the LL values output from each HMM to infer network condition. The different times at which each new data window is analysed (i.e. applied to each trained HMM) within each application resulted in separate AFD algorithms being developed for each application. These algorithms are described in the following sub-sections.

The sub-sections also provide examples of the LL outputs from each HMM throughout certain arc fault conditions. This highlights how the IntelArc method can be used to accurately diagnose arcing conditions.

5.2.6.1 IntelArc – Diagnosis of Sustained Series DC Arc Faults

An example of load current sampled at 2 kHz during a sustained arcing event is illustrated in Figure 5-21 (a) and the corresponding LL outputs from each trained HMM are illustrated in Figure 5-21 (b).
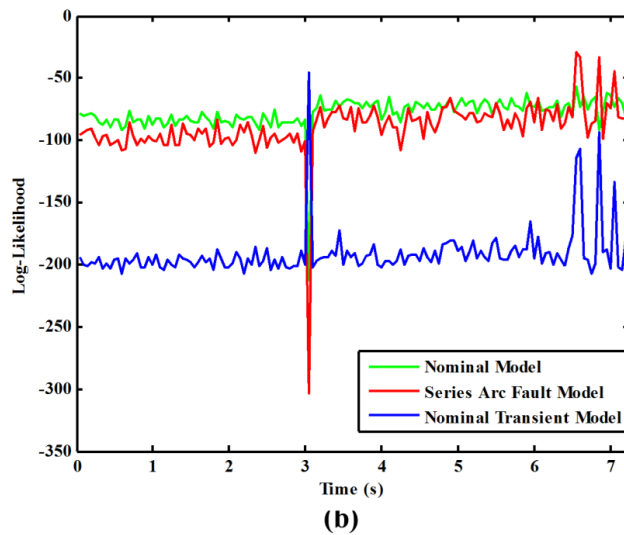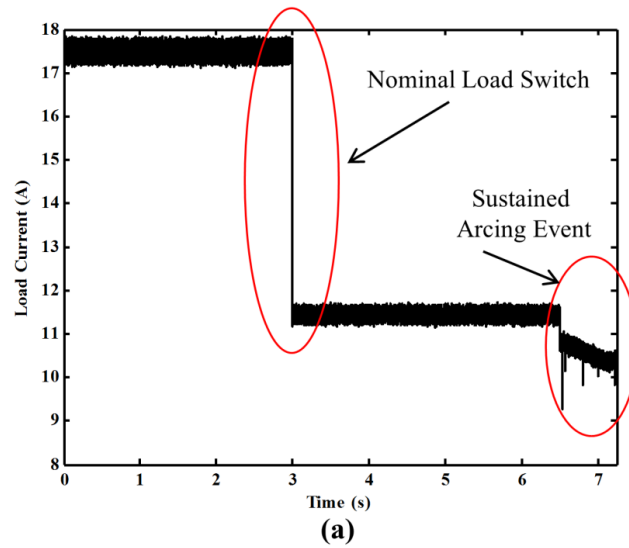
Figure 5-21: (a) Example of load current during a sustained series DC arcing event (b) Corresponding LL output from each HMM.

The LL outputs from each model change according to various dynamics in the load current. LL values closer to zero indicate higher probability. During relatively static nominal conditions the LL output of the nominal model, 'LL_Nom', is greater than the other two models.

During the load switching event ($\approx$ 3 seconds), 'LL_Nom' decreases - this could potentially indicate the presence of a fault. However, the simultaneous LL increase of the nominal transient model, 'LL_Switch', indicates that a normal load transient, as opposed to a fault, is present.

During the sustained arcing event (≈ 6.5 seconds) the LL of the series arc fault model, 'LL_Fault', increases beyond 'LL_Nom' ('LL_Switch' increases but not beyond 'LL_Nom' or 'LL_Fault') – this evidence suggests an increased probability of arc fault presence and an arc fault warning for the observational period should be issued.

Another measure that indicates an increased probability of fault presence is a likelihood ratio test [232]. This ratio expresses how many times more likely the data is under one hypothesis (model) compared to the other, and is defined as:

$$LL\_Ratio = -2 \ln \left(\frac{Nominal\ Likelihood}{Fault\ Likelihood} \right) = -2 \times (LL\_Nom) + 2 \times (LL\_Fault) \tag{5.7}$$

The corresponding likelihood ratio for the example outlined in Figure 5-21 is shown in Figure 5-22.
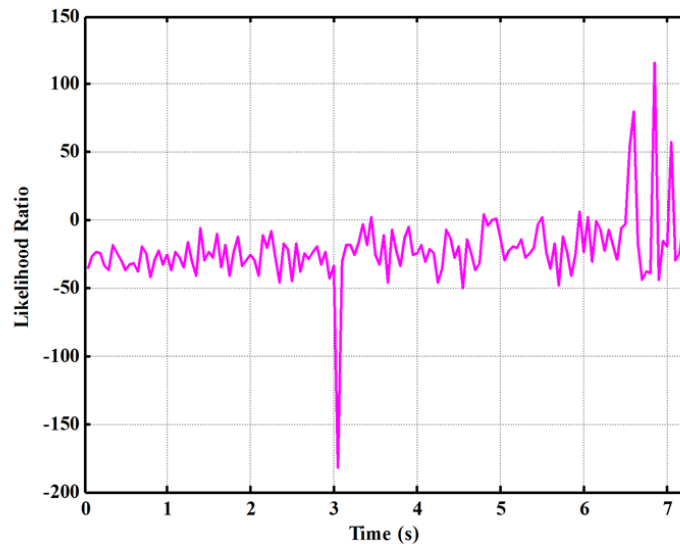
Figure 5-22: Likelihood ratio between nominal and fault model. Note the significant increase beyond zero at fault onset.

The likelihood ratio stays consistently below zero until onset of the sustained arcing event. During the load switching event, the decrease in 'LL_Fault' results in the likelihood ratio decreasing significantly. Throughout the sustained arc event, the increase in 'LL_Fault' beyond 'LL_Nom' results in the ratio becoming significantly greater than zero. Thus, there is an increased probability of series arc fault presence at points where the ratio increases beyond zero.

IntelArc was developed to infer network condition in real-time using both the HMM LL outputs and the likelihood ratio. With its application to the diagnosis of sustained arcing

events, the aim was to diagnose series DC arc fault presence across a range of load conditions and voltage distribution levels.

Figure 5-23 details operation of the IntelArc method applied for the diagnosis of sustained arc faults.

The method is split into three distinct stages:

- System Start Up
- Data Widowing and HMM application
- AFD Algorithm

These stages are summarised in Table 5-8.

IntelArc System – Sustained Arc Fault Application
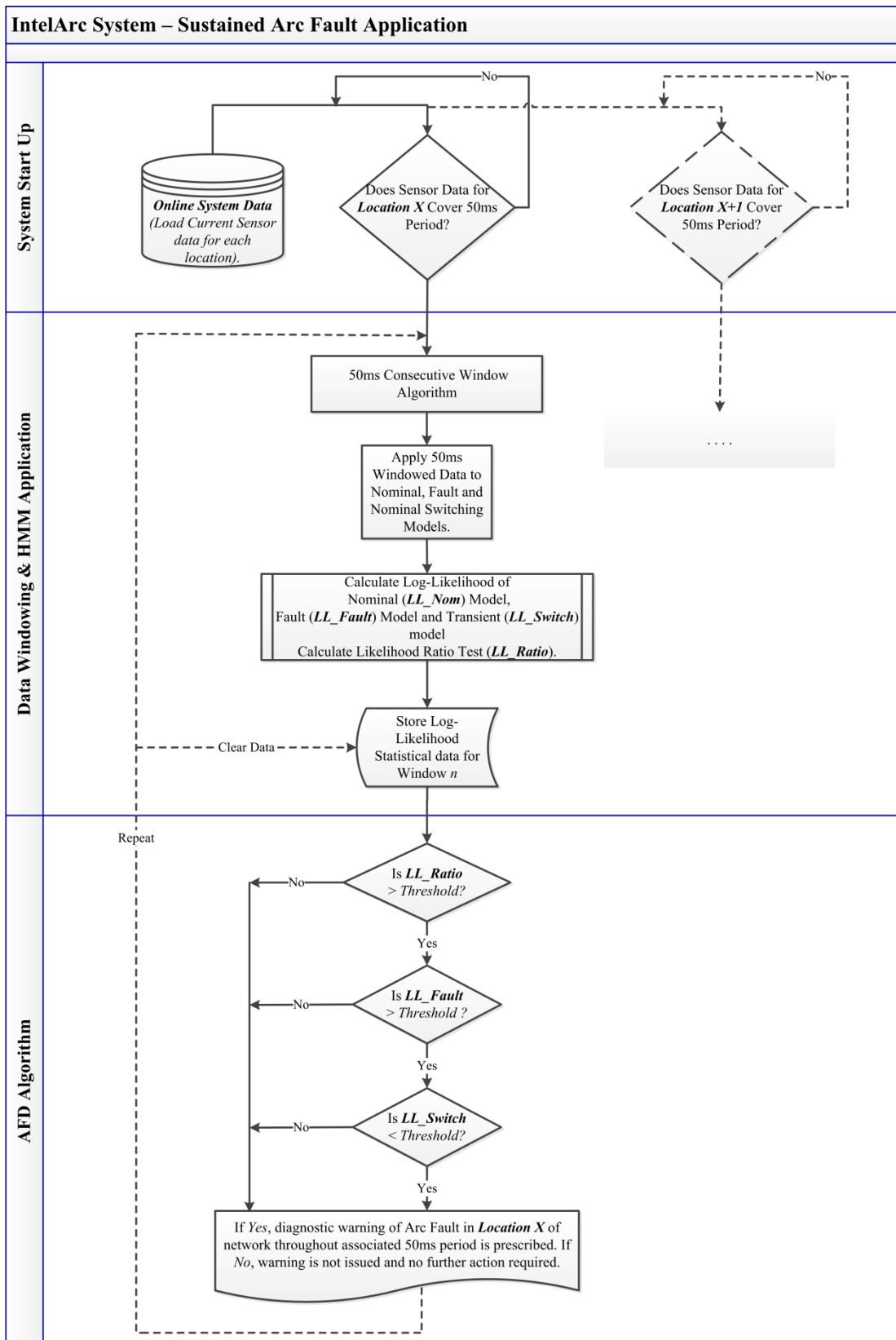
Figure 5-23: IntelArc for diagnosis of sustained arc faults

152

Table 5-8: Summary of separate stages of the IntelArc method for diagnosis of sustained arcing events

System Start-Up	The use of consecutive data windows requires a minimum of 50ms available data. Therefore, a 50ms delay is implemented between system start-up and algorithm initiation.
	System data are load current observations for loads at different locations (***Location X***, ***Location X+1***) throughout the network. Load Current is sampled at 2 kHz.
Data Windowing and HMM Application	System data is processed for application to each model. Using the consecutive window technique, windowed load current data covering the previous 50ms is recursively applied to the nominal steady-state model, fault model and nominal transient model every 50ms.
	All three log-likelihood HMM outputs for window *n* are stored and evaluated at the next stage.
AFD Algorithm	All HMM outputs are evaluated to determine if there is a significant probability of series arc fault presence during each 50ms observational period.
	The algorithm determines **if** the *LL_Ratio* output is > predetermined threshold **and** the *LL_Fault* output > predetermined threshold **and** the *LL_Switch* output < predetermined threshold **then** an arc fault diagnostic warning for the observational period of window *n* at ***Location X*** is issued. If all of these specifications are not met, nominal operation is assumed.
	This whole process is repeated every 50ms throughout system operation.

The consecutive window technique results in the load current data being analysed every 50ms. The pre-determined thresholds ensure there is sufficient evidence to diagnose a series DC arc fault. The three thresholds determine if:

1) 'LL_Fault' has increased
2) There is sufficient difference between 'LL_Nom' and 'LL_Fault' (the likelihood Ratio)
3) 'LL_Switch' has not increased beyond 'LL_Fault'

If all of these conditions are true, a diagnostic warning for window *n* at Location *X* is issued. The process is then repeated for window *n+1* to *n+N*.

5.2.6.2 IntelArc – Diagnosis of Intermittent Series DC Arc Faults

An example of load current during an intermittent series DC arcing event is illustrated in Figure 5-24. Within this application, load current is sampled at a frequency of 20 kHz. Intermittent arcing events were simulated using an intermittent arc fault model - this model is an adapted version of the sustained fault model, and is described fully in Appendix A.
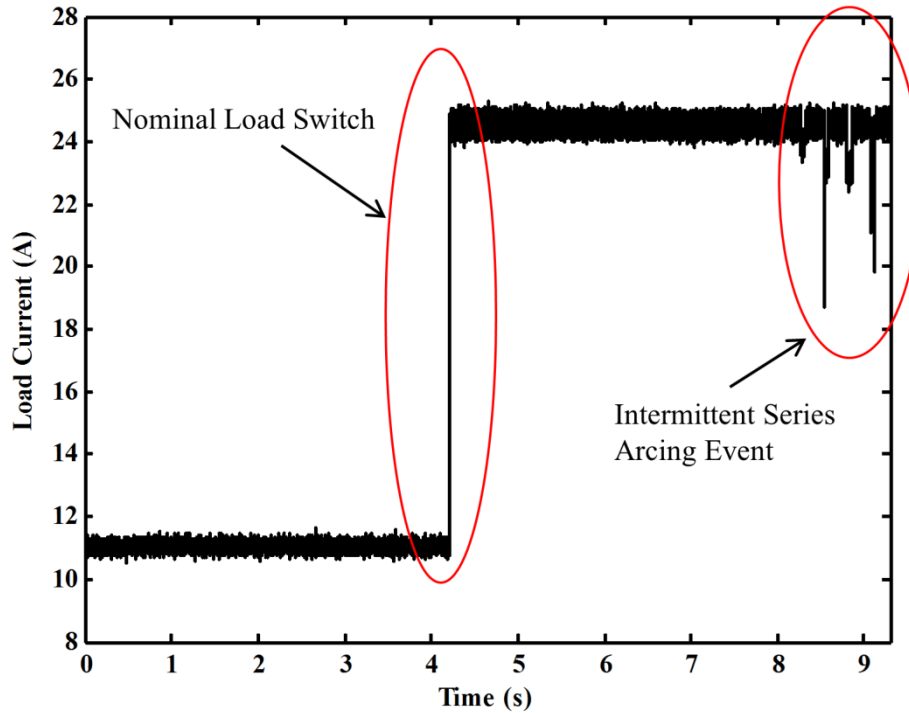
Figure 5-24: Example of load current during intermittent series DC arcing events

The intermittent fault develops at roughly 8 seconds and results in periods of decreased load current. The duration of each intermittent event, and the level of current decrease, are both variable. The aim of IntelArc is to accurately diagnose these highly variable events in real-time.

Application of IntelArc for diagnosis of these events follows a similar methodology as its application for diagnosis of sustained events, where the HMM LL outputs are analysed for evidence of fault presence. The main differences are the increased sampling frequency and the fact that a sliding window technique is used for application to the nominal and fault model; this means load current windows are analysed every 10ms as opposed to every 50ms in the sustained AFD algorithms.

The corresponding LL outputs of the nominal and fault models (for the load current of Figure 5-24) are illustrated in Figure 5-25 (a). The likelihood ratio is illustrated in Figure 5-25 (b). The only points at which the LLs are not relatively static are during the nominal load switching event and throughout the intermittent arcing events. At fault onset, 'LL_Fault' increases and 'LL_Nom' decreases – this change is emphasised in the likelihood ratio and indicates a high probability of fault presence.

The corresponding LL output of the nominal transient model is illustrated in Figure 5-26. Consecutively windowed data (as opposed to a sliding window) is applied to the switching model to minimise false positives – evaluating the LL of the switching model every 50ms, as opposed to every 10ms, allows a better representation of fast transient switching behaviour as the current remains constant across the majority of the data window.

During the nominal load switch (≈ 4.1 seconds), 'LL_Switch' increases while both 'LL_Nom' and 'LL_Fault' decrease indicating a high probability of a nominal transient event. Despite 'LL_Switch' increasing during the intermittent fault events, the fact that 'LL_Fault' also increases means that there is a higher probability of an arc fault event.

Figure 5-27 details operation of the IntelArc method applied for the diagnosis of intermittent arc faults. Each stage of the system is outlined in Table 5-9.

The LL outputs are again compared to various pre-determined thresholds to ensure there is sufficient evidence to diagnose the presence of series DC arc faults throughout each 50ms interval. The main difference between application of IntelArc for intermittent fault diagnosis and application for sustained diagnosis is there are five LL outputs from the nominal and fault models over the 50ms interval (compared to one in the sustained AFD algorithm). The algorithm determines if any of the five LL outputs over each 50ms observational period are greater than the pre-determined thresholds.

The predetermined thresholds were set through analysis of HMM LL outputs across different operational scenarios. Trade-offs between false detection, non-detection and detection time must be considered when selecting suitable thresholds – for example a LL threshold that accurately and quickly diagnoses an arc fault event may also provide too many false positives at nominal transient events. LL thresholds may be tuned to improve diagnosis in networks with particular operational scenarios or characteristics.
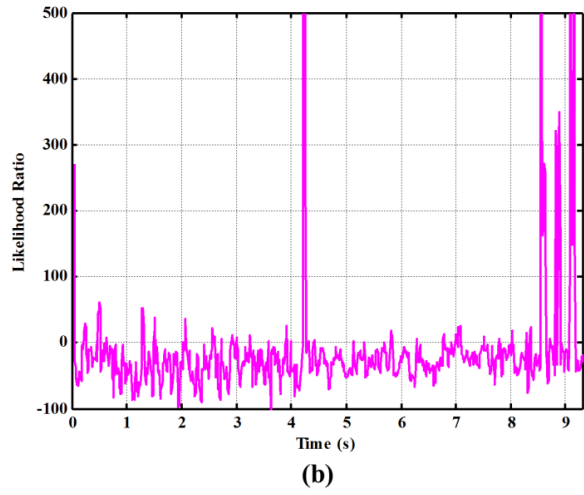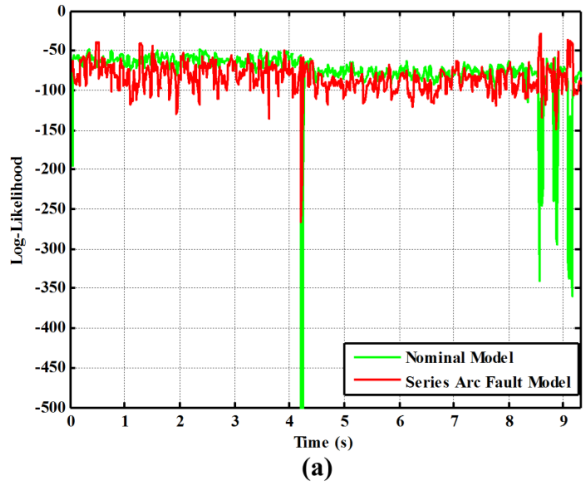
Figure 5-25: (a) LL outputs of nominal and fault models during intermittent arc event (b) Likelihood ratio between nominal and fault models.
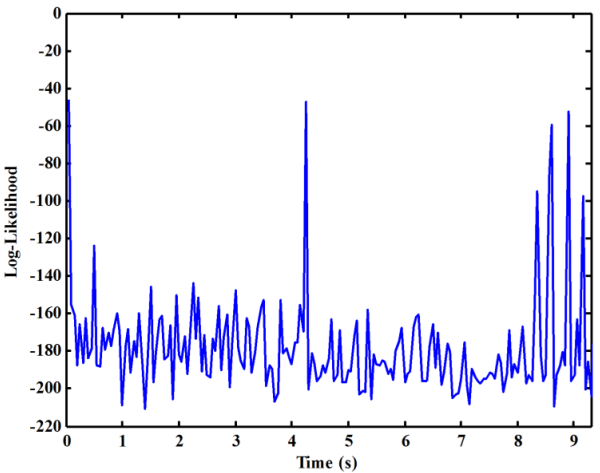
Figure 5-26: Corresponding LL output of nominal transient model.
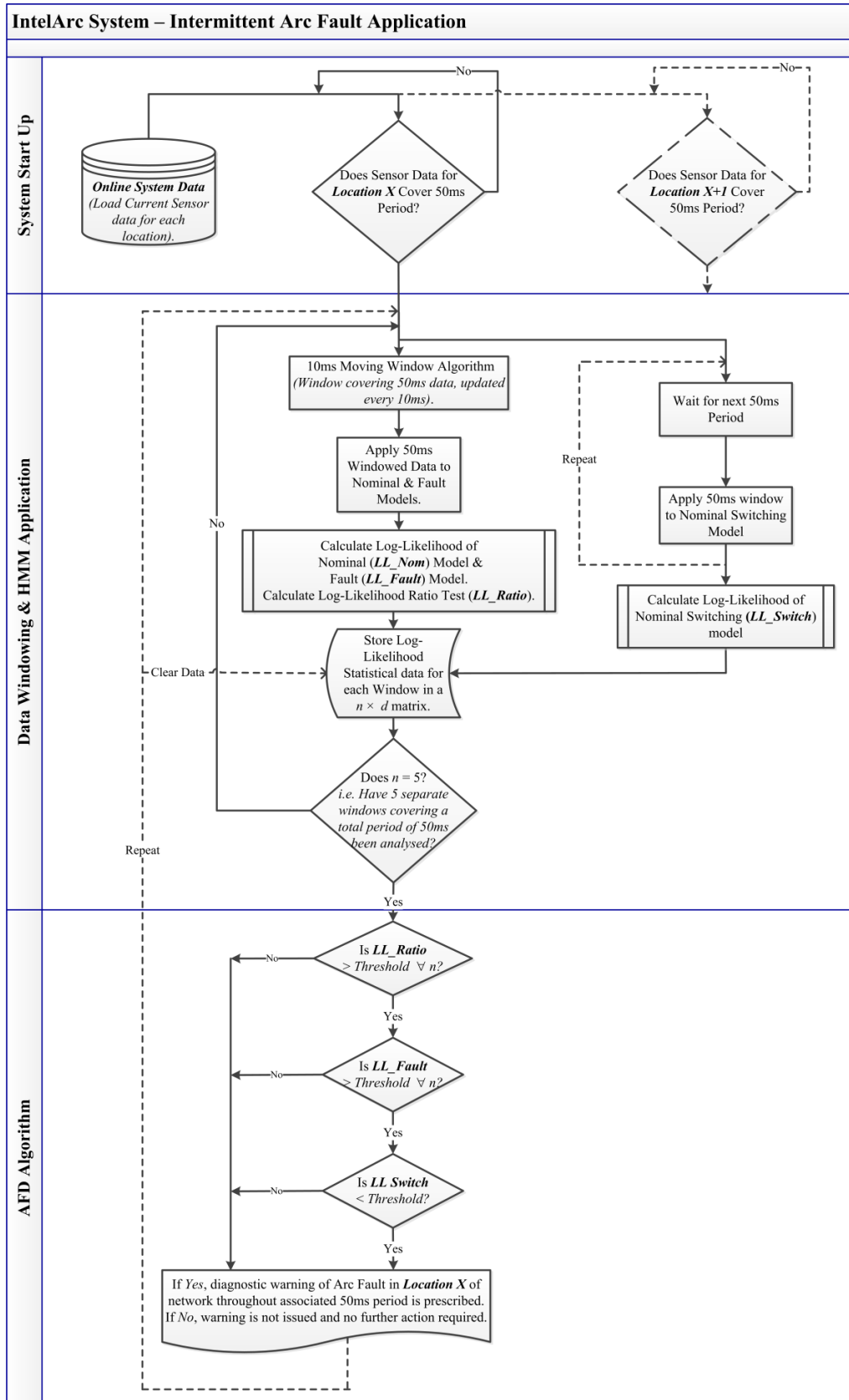
Figure 5-27: IntelArc for diagnosis of intermittent arc faults

Table 5-9: Summary of separate stages of the IntelArc method for diagnosis of intermittent arcing events

System Start-Up	The use of moving windows requires a minimum of 50ms available data. Therefore, a 50ms delay is implemented between system start-up and algorithm initiation. System data are load current observations for loads at different locations (**Location X**, **Location X+1**) throughout the network. Load Current is sampled at 20 kHz.
Data Windowing and HMM Application	System data is processed for application to each model. Using the moving window technique, windowed data covering the previous 50ms is recursively applied to the nominal model and fault model every 10ms. 50ms consecutive data windows are applied to the nominal switching model. All log-likelihood model outputs are evaluated every 50ms at the next stage – this includes $5\times LL\_ratio$ and $5\times LL\_fault$ (one every 10ms) and $1\times LL\_nominal\_switch$ (one every 50ms) for the nominal switching model. All LL statistical data is stored in an $n\times d$ matrix for each 50ms observational period, where n=number of windows analysed every 10ms=5 and d=number of different LL statistics calculated=4.
AFD Algorithm	All outputs are evaluated to determine if there is a significant probability of series arc fault presence during each 50ms observational period. The algorithm determines **if** *any* of the $5\times LL\_ratio$ outputs are > predetermined threshold **and** *any* of the $5\times LL\_fault$ outputs > predetermined threshold **and** the $1\times LL\_nominal\_switch$ output < predetermined threshold **then** an arc fault diagnostic warning for the observational period is issued for **Location X**. If all of these specifications are not met, nominal operation is assumed. This process is repeated consecutively every 50ms throughout system operation.

5.2.7 IntelArc - Summary

IntelArc is proposed to diagnose series arc faults within DC supplied systems in real-time using load current data. The method is based on a framework of trained HMM, where

models correspond to nominal steady-state, nominal transient and series arc fault conditions. All models were trained using synthetic data acquired through software simulations. Time-frequency and time domain features of the on-line load current data windows are applied to each HMM to generate LL statistics. An AFD algorithm analyses the LL outputs of each model to infer network conditions.

Two separate applications of IntelArc were described. The first application described generalised sustained arc fault diagnosis across a range operating conditions. The second application was concerned with the diagnosis of intermittent series arc fault events. The only methodological differences between the applications are current sensor sampling frequency and type of window used. The sustained AFD application uses a sampling frequency of 2 kHz and a *consecutive* data window, while the intermittent AFD application uses a higher sampling frequency of 20 kHz and a *sliding* data window.

Three case studies are provided in Chapter 6 to validate these applications of IntelArc. The first case study tests the accuracy of IntelArc for diagnosing sustained arc faults within aircraft representative EPS. The second case study tests the accuracy of AFD for diagnosing intermittent arc fault events. The third case study validates IntelArc using experimental data generated on a scaled DC testbed.

5.3 Chapter 5 Conclusions

The chapter has proposed two data driven FDI methods for application to EPS deployed within an aircraft environment. The aim of these methods is to improve network protection and control through diagnosis of critical and degraded network faults. Both methods are based on the use of trained HMM to detect a variety of different fault types.

EPSmart, presented throughout Section 5.1, is proposed to detect abrupt, intermittent and incipient fault modes in a hybrid AC/DC EPS. The two stage method primarily uses a framework of multiple trained HMM to classify network condition - classification of network condition includes both fault mode and location.

The second stage of the method determines the severity of any fault that has been classified. Fault severity can be either critical or degraded, and this is determined through utilising the optimal state sequence of an HMM to calculate time of fault onset and fault current levels. For the purposes of this thesis, EPSmart was developed using data from a sub-set of NASA's ADAPT test bed. A total of fifteen faults, including sensor failures, were modelled using the ADAPT data.

Feature extraction from data, and sensor fusion, are critical aspects of development – these were described in Section 5.1.3.2. Another significant aspect of development involved optimising the trained parameters of the HMM training with only limited training data available – this was described in Section 5.1.3.3.

IntelArc, a novel series DC AFD method, was presented throughout Section 5.2. IntelArc, like EPSmart, is also based on a framework of multiple trained HMM. The method uses time-frequency and time domain feature extraction from load current data. The main points of discussion in these sections included:

- Off-line development
- The selection of optimal time-frequency domain extracted features
- Two separate on-line applications of IntelArc

Off-line development used simulated training data to train each HMM; separate HMM corresponding to different network conditions were trained. Detection is based on interpretation of the LL outputs of each HMM as real-time system data is applied.

Optimal features were determined through analysis of the WT coefficients extracted from the training data. The time and frequency resolution properties of the WT were deemed useful for the HMM based IntelArc method. This study analysed the distribution of various WT coefficients under the different network conditions to determine optimal features. Various low frequency band (approximate coefficients) and high frequency band (detail coefficients) features were selected.

Two applications of IntelArc were described. The first application was for the generalised diagnosis of sustained arc events. The second application was for diagnosis of intermittent arc events. The only differences between these applications were the sampling frequency of load current and the type of data window used.

The following chapter describes case studies that were implemented to validate both EPSmart and IntelArc.

6. TESTING OF EPSMART & INTELARC FDI METHODS: CASE STUDIES

Chapter 5 detailed the design of two novel fault diagnosis and isolation (FDI) methods – *EPSmart* and *IntelArc* - for application to aircraft EPS. These two proposed FDI methods are the main contributions of this thesis. The aim of EPSmart is to provide autonomous, and accurate, diagnosis of various critical and degraded failure modes within a hybrid AC/DC EPS. IntelArc aims to diagnose series arcing events within DC supplied networks.

This chapter describes separate case studies that have been used to test the accuracy of these two methods. The first case study outlines application of EPSmart to NASA's advanced diagnostic and prognostic test bed (ADAPT), a representative aircraft EPS. The second case study tests application of IntelArc for diagnosis of sustained series DC arc fault events across a range of EPS operating conditions. The third case study tests application of IntelArc for diagnosis of intermittent series DC arc faults. A fourth case study validates IntelArc using experimental data captured on a scaled DC testbed. In each case study results

are presented and discussed. Chapters 2 and 4 discussed the difficulties in detecting and diagnosing these type of faults, as well as the dangers they pose to overall safety and reliability: preliminary evaluation of these two methods within these case studies allows their performance to be analysed and highlights their various attributes towards diagnosing such fault conditions within representative aircraft EPS.

6.1 Case Study 1: Application of EPSmart to the ADAPT Network

The case study to be investigated in this section tests the application of EPSmart to a subset of the ADAPT network, the ADAPT-Lite (ADL). Design and operation of EPSmart has been provided in Chapter 5. The format adopted for the presentation of this case study is to firstly outline the testing procedure before going on to describe and discuss test results in Sections 6.1.1 and 6.1.2. The performance of EPSmart is compared to other systems proposed for FDI on the ADL network in Section 6.1.3.

It was described previously in Chapter 5 that electrical system data from the ADAPT network was used to develop the EPSmart method. This data was publicly released for the International Diagnostic Competition in 2010 (DXC10) [139]. The complete dataset described 166 individual controlled experiments undertaken on the ADL network – 25 experiments outlined system data under nominal conditions, and 141 experiments outlined data during various fault conditions. Each individual experiment covered roughly four minutes of time, with sensor readings recorded at frequencies of 2-10Hz. There are a total of 12 sensors throughout the ADL network (see Chapter 5, Section 5.1.3.2).

For the purposes of this case study, the ADL data released by DXC10 was randomly divided into training and testing data. The number of data files used for training and testing each of the ADL conditions modelled within EPSmart are outlined in Table 6-1.

In total, 129 files were used for testing whereas only 37 were used for training the models; the reason for this disparity between training and testing data was to fully test the ability to develop an accurate EPSmart method using minimal faulty data, as well thoroughly test the method with a variety of test cases.

Testing the accuracy of EPSmart applied to the ADL network involved inputting each test file separately and observing the diagnostic outputs. The diagnostic outputs of EPSmart are compared to the 'true' network conditions labelled within each test case to quantify accuracy. EPSmart was tested in an off-line scenario, where only one set of diagnostic decisions was provided for each test case (as opposed to updating a diagnostic decision as new sensor data is received - refer to Section 6.1.3).

Table 6-1: Division of DXC10 data into training and test data sets

Fault Location	Fault Mode	# Training Files	# Test Files
No Fault	Nominal	5	20
DC Load Faults	Abrupt Resistance Offset	2	9
	Intermittent Resistance Offset	2	8
	Incipient Resistance	4	7
AC Load Faults	Abrupt Resistance Offset	2	9
	Intermittent Resistance Offset	2	8
	Incipient Resistance	3	8
	Fan Load Failed Off	2	2
Inverter Faults	Failed	1	2
Voltage Sensor Faults	Stuck	2	5
	Intermittent	2	5
	Incipient	3	4
Current Sensor Faults	Stuck	2	14
	Intermittent	2	14
	Incipient	3	14
	Total	**37**	**129**

The EPSmart method, which was described in Section 5.1.2, is based on two separate stages. The first stage uses the data to classify the condition of the network. If a fault condition is classified after Stage 1, Stage 2 of the method uses fault parameter calculation algorithms (FPA) to determine what time throughout the observation period the fault occurs, fault current levels and various other relevant parameters (see Chapter 5, Section 5.1.3.4). Information on fault parameters can then be used to determine the severity of the fault i.e. the effect it may have on system reliability. Fault severities were labelled within the DXC10 competition data as either *critical* or *degraded.*

Thus, with the input of ADL test data into EPSmart, there are three outputs:

- ADL Network Condition Classification
- Electrical Fault Parameters (void if nominal condition classified)
- Diagnostic decision – critical or degraded fault (again, void if nominal condition is classified)

The procedure of testing EPSmart using the ADL data is illustrated in Figure 6-1.
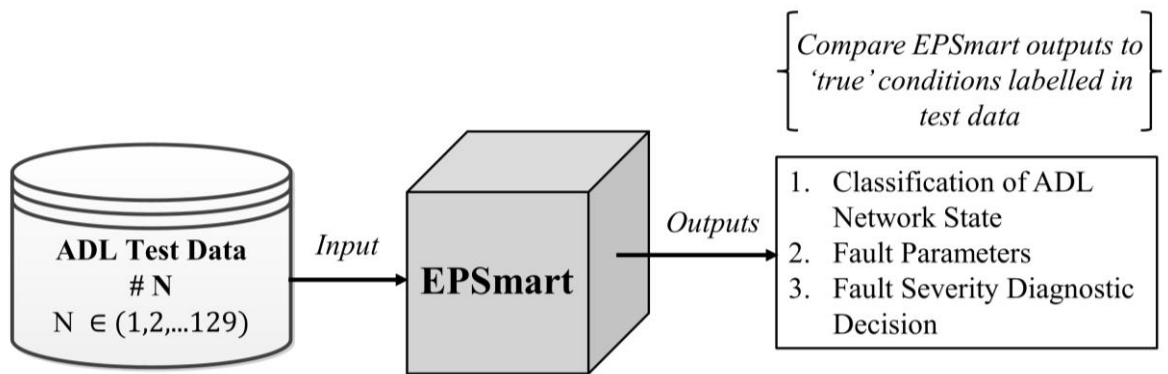
Figure 6-1: EPSmart testing procedure using ADL data

Accuracy of the three EPSmart outputs is quantified for each test case by determining:

1) If the network condition classified after Stage 1 matches the condition labelled in the test data

2) If the fault parameters calculated by the FPAs are within ± 5% of the parameters labelled in the test data

3) If the diagnostic decision on fault severity matches the severity labelled in the test data

Accuracy for the 129 test cases is outlined in Table 6-2. The following sections describe and discuss these test results.

6.1.1 EPSmart Test Results - Description

Results are described in terms of classification accuracy (Stage 1 of the method) and fault severity diagnosis accuracy (Stage 2 of the method):

- **Classification Accuracy**

The results in Table 6-2 show that EPSmart was 95.3% accurate at discriminating between the 15 different ADL network conditions. This equates to 6 misclassifications out of the 129 test cases presented to the system; of the six misclassifications, four of these are attributed to the misclassification of incipient faults. In all six misclassified test cases, the network was assumed to be in a nominal condition (false negatives).

- **Fault Severity Diagnosis Accuracy**

Severity diagnosis is based on the ability of EPSmart to accurately calculate fault parameters after a fault has been classified from Stage 1. Parameters of the fault, such as fault current

Table 6-2: Testing results of EPSmart applied to ADL test bed

Fault Location	Fault Mode	# Tests	Classification Accuracy (%)	Fault Parameter Calculation Accuracy (%)	# of Critical Faults labelled in Test Data	# of Critical Faults diagnosed by EPSmart	# of Degraded Faults labelled in Test Data	# of Degraded Faults diagnosed by EPSmart	Diagnostic Decision Accuracy for Critical Faults (%)	Diagnostic Decision Accuracy for Degraded Faults (%)
Nominal	N/A	20	100	N/A	0	0	0	0	100	100
DC Loads	Abrupt	9	100	100	5	5	4	4	100	100
	Intermittent	8	87.5	100	3	3	5	4	100	80
	Incipient	7	85.7	71.4	4	3	3	3	85.7	100
AC Loads	Abrupt	9	100	100	4	4	5	5	100	100
	Intermittent	8	100	91.6	4	4	4	4	100	100
	Incipient	8	87.5	81.25	4	4	4	3	100	75
	Fan Failed Off	2	100	100	1	1	1	1	100	100
Inverter	Failed Off	2	100	100	1	1	1	1	100	100
Voltage Sensors	Stuck	5	80	100	0	0	5	4	100	80
	Intermittent	5	100	100	0	0	5	5	100	100
	Incipient	4	75	50	0	0	4	3	100	75
Current Sensors	Stuck	14	100	100	0	0	14	14	100	100
	Intermittent	14	100	100	0	0	14	14	100	100
	Incipient	14	92.8	64.28	0	0	14	13	100	92.9
	Total	**129**	**95.3**	**89.89**	**26**	**25**	**83**	**78**	**96.2**	**93.98**

levels, determine the severity of the fault to the network - for complete descriptions of the FPAs refer to Section 5.1.3.4. In the majority of fault test cases, the calculation of parameters was accurate (i.e. within the ± 5% margin). For abrupt and intermittent fault cases the calculation accuracies were high.

The main instance where accuracy was limited was when calculating parameters for incipient faults, which, in some cases was as low as 50%. The reduced overall accuracy of 89.89% for parameter calculation accuracy can mainly be accredited to the inaccuracies of incipient parameter calculations. Despite the relative inaccuracies of the FPAs, all faults that were classified correctly at Stage 1 and assessed at Stage 2 were correctly diagnosed as either degraded or critical - incorrect diagnoses were mainly a result of inaccuracies at Stage 1. The main parameter incorrectly calculated was the time of fault onset.

There were a total of 26 critical faults within the labelled ADL test data – EPSmart correctly identified 25 of them, resulting in a critical fault diagnosis of 96.2%. The critical DC load incipient fault condition was not identified as it was incorrectly classified as a degraded current sensor fault at Stage 1.

There were a total of 83 degraded faults within the test data, and EPSmart correctly identified 78 of them (93.98% accuracy). The five inaccuracies (intermittent DC load, incipient AC load and incipient/stuck voltage and current sensor faults) were a result of them being misclassified as a nominal condition at Stage 1.

EPSmart correctly identified all 20 nominal condition tests.

6.1.2 EPSmart Test Results – Discussion

The test results described in the previous section validate that EPSmart has the potential to utilise system data to diagnose and isolate a multitude of critical and degraded fault modes. In particular, diagnosis of abrupt and intermittent conditions was achieved with very high accuracy. The accurate discrimination of sensor failures from faults in the underlying system was evident from the test results, with only 2 out of 56 (3.5%) sensor failure tests inaccurately diagnosed.

In terms of network degradations, EPSmart managed to correctly identify 93.98% of all test cases. The main reason this is not higher is because of complications in dealing with incipient fault conditions. The previous section touched upon the fact that the trained HMM within EPSmart were not accurately classifying incipient fault conditions: four of the six misclassifications at Stage 1 were incipient conditions. This suggests that the HMM for

incipient conditions were not responding to dynamics within the system data. This concept is illustrated in Figure 6-2, which shows the optimal state sequence of the relevant HMM for examples of abrupt, intermittent and incipient ADL fault conditions.

State changes within the hidden sequences of the abrupt and intermittent HMMs correspond to changes in the sensor data – hence these models have a high probability of accurately diagnosing and isolating the respective fault conditions. However, this is not the case for incipient faults (Figure 6-2 (c)), where the onset of current drift, evident in the sensor data at roughly 50s, does not result in a change in hidden state of the associated HMM. Indeed, within this example, there is roughly a 50s delay between fault onset and a change in hidden state.

These issues highlight that the lack of hidden state dynamics may result in incipient fault conditions being misdiagnosed as nominal conditions. This is backed up in the results, where all four incorrectly diagnosed incipient faults were attributed to be in a nominal condition by the EPSmart system.

One solution to this problem would be to increase the number of hidden states within incipient condition models. This alteration would increase the probability of discriminating between marginal incipient conditions and nominal behaviour as increasing the number of states enhances sensitivity to slight changes in data, albeit with a trade off with model complexity. The volume of available training data must also be considered when attempting to improve the diagnosis capabilities of HMM through increasing the number of states. A drawback of data driven approaches is that, compared with cases involving nominal condition data, there is significantly less data available describing fault conditions.

The lack of data can result in fault condition models being over fitted with poor performance when inferring new instances of the same condition. In this case study of EPSmart, the BIC [30] was used to optimise each HMM based on various parameters, including the number of training cases available (see Chapter 5, Section 5.1.3.3). Test results outlined in Table 6-2 have shown that the abrupt and intermittent fault models accurately inferred test cases, even though some models were trained using only two separate examples. The incipient models were not as accurate, despite being trained using a similar number of training examples.
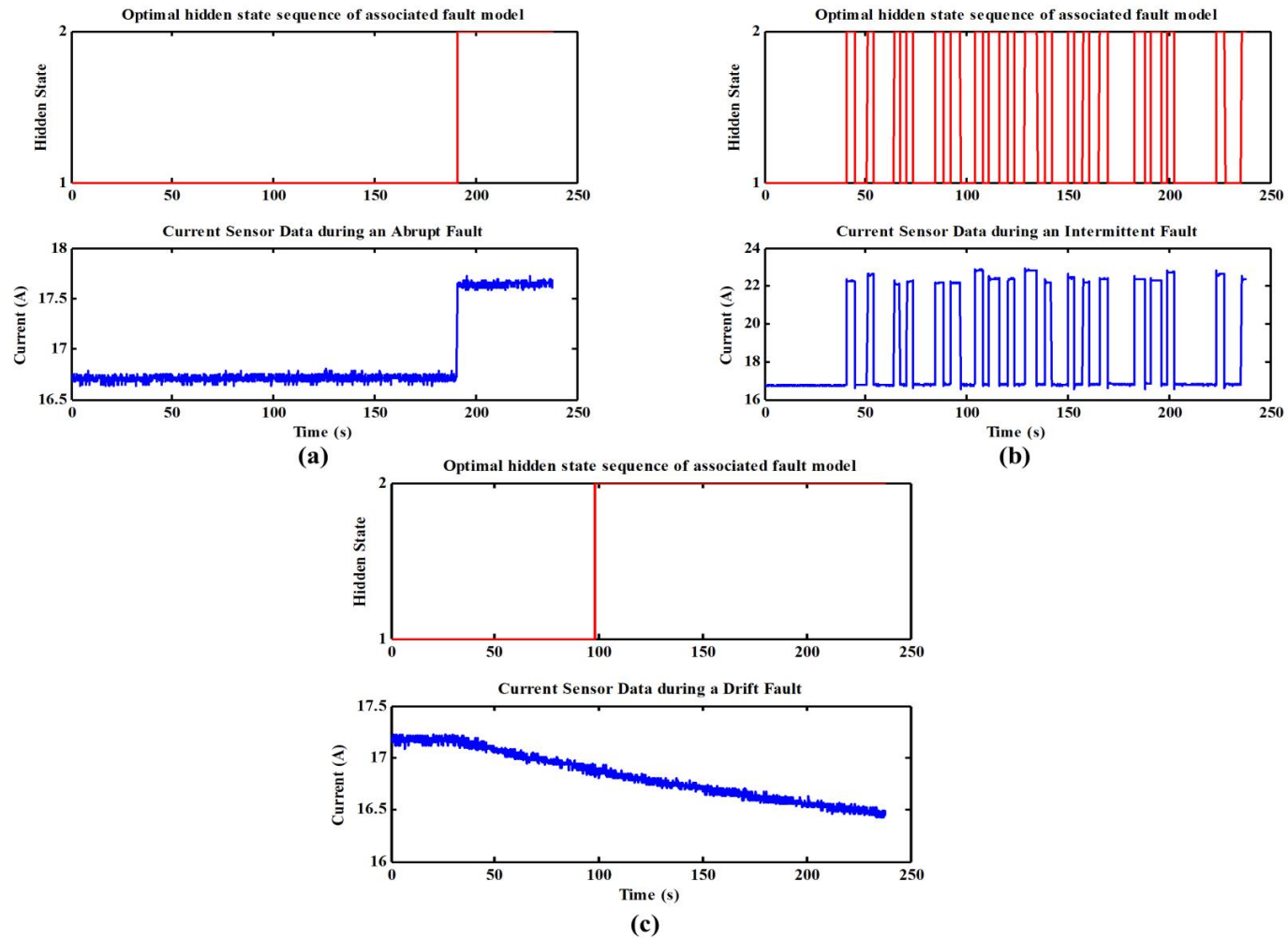
Figure 6-2: Optimal State Sequences of relevant HMMs for examples of (a) abrupt (b) intermittent and (c) incipient ADL fault conditions.

The solution to improving the performance of incipient fault models by increasing the number of hidden states is dependent on the number of training cases available. Without more training examples, increasing the number of hidden states will simply result in a model over fitted to the training examples. Such issues highlight that, while increasing the volume of training data will lead to a better generalisation within all fault models, certain fault conditions are more dependent on the quantity of training cases for accurate inference of unseen data.

Overall, case study results have shown that EPSmart can diagnose and isolate a range of critical and degraded faults within a hybrid AC/DC aircraft representative EPS. There is a wide range of distinct fault conditions within aircraft EPS and, it is imperative that system dynamics are monitored and evaluated throughout flight to enable early and accurate diagnosis of anomalies. Application of the proposed EPSmart method to the ADL network has shown that it has the ability to determine and quantify complex system dynamics from network data, and has the potential to aid system health monitoring and improve network protection.

6.1.3 EPSmart Test Results – Comparison with DXC10 Systems

EPSmart was developed and tested for application to the ADL network using data from the DXC10 competition [139]. This section compares the performance of EPSmart against other ADL FDI methods proposed within the DXC10 competition. These methods were all discussed in detail in Chapter 3, Section 3.11.2.1.

Figure 6-3 shows test results of the DXC10 systems alongside results of EPSmart. These results show the percentage of accurately diagnosed test cases (true positives), the percentage of false negatives and the percentage of false positives for each FDI method. The number of test cases varied between each system – these are outlined in Table 6-3.

The comparison in Figure 6-3 shows that the EPSmart provided the highest overall diagnostic accuracy with 95.3% true positives, 4.7% false negatives and zero false positives. However, there is a caveat: testing of EPSmart, described in the previous sections, was conducted in an off-line environment. In this scenario, a complete test case, describing roughly four minutes of ADL network data, was input. EPSmart then returned a diagnostic decision for the associated four-minute observational period. This was not the case during testing of the DXC10 methods, which was conducted in an on-line scenario i.e. the diagnostic decisions were updated when new sensor data was received, with the time between updates governed by the sampling rates of the sensors.

This issue does not negate EPSmart – its methodology for FDI would be similar for on-line application, where diagnostic decisions would be updated using windows of data. Similar on-line application issues were discussed with regards to the IntelArc FDI method throughout Chapter 5. EPSmart is not bound to a four-minute observational window – length of the window can be adjusted accordingly within an on-line application of the method.
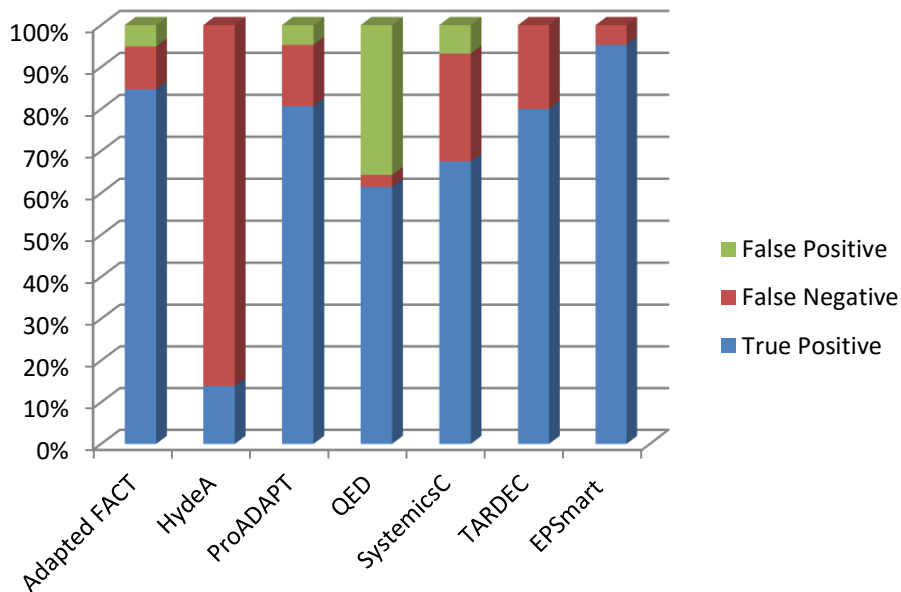
Figure 6-3: Test results of the ADL FDI methods proposed in DXC10 and the EPSmart method

Table 6-3: Number of separate test cases applied to each FDI Method

FDI Method	# of Test Cases
AdaptedFACT	98
HydeA	137
ProADAPT	171
QED	70
SystemicsC	74
TARDEC	60
EPSmart	129

The ProADAPT [33], AdaptedFACT [140] and Tardec [139] methods all provided relatively high overall accuracy, with each method returning roughly 80% true positives. TARDEC was the overall winner as it incurred the least cost. Costs were calculated by determining the diagnostic output of each method to the actual case. For example, if the method determines the UAV mission should abort due to a system fault, when in actual fact it should not (a false positive), the cost incurred is the cost of losing the mission. Likewise, if the diagnostic method determines the mission should not be aborted, when in actual fact it should (a false

negative), the cost incurred is the cost of the mission plus the cost of the UAV itself [139]. Similar to the EPSmart method proposed as part of this thesis, TARDEC did not provide any false positive diagnoses. Other methods, notably HydeA and QED, struggled with diagnosing a variety of different failure modes. In [139] a complete breakdown of the DXC10 results is provided.

In general, incipient faults presented the most difficulty to the FDI methods proposed in DXC10 - indeed, the AdapatedFACT system did not even consider incipient faults [139]. In some incipient fault scenarios, the faults were isolated to the incorrect component or incorrect failure mode, while in other scenarios the isolation was correct but estimation of the slope or fault injection time was inaccurate. Test case results presented in Section 6.1.1 showed that diagnosis and isolation of incipient faults was also particularly challenging for EPSmart. These results, along with the DXC10 competition results, show that handling incipient faults is one area where future research and development should be focused.

Overall, the EPSmart method has shown excellent potential for diagnosing and isolating a range of fault modes and locations. Basic testing has shown that the method out performs all FDI methods proposed in the DXC10. However, more rigorous, on-line testing is required before its application to more advanced systems.

6.1.4 Case Study 1 - Summary

This case study has tested the application of the proposed EPSmart method to NASA's ADL test bed. A total of 129 test cases were conducted. Accuracy of EPSmart for diagnosing and isolating faults within the ADL network was quantified by comparing the fault modes, locations and severity labelled in the test cases to the outputs of EPSmart.

The method managed to correctly identify 123 (95.6%) cases, including 25 out of 26 (96.2%) critical faults, and 78 out of 83 (93.98%) degraded faults. Fault modes included abrupt, intermittent and incipient. The case study identified incipient faults to be the most challenging to diagnose; procedures for potentially improving the trained incipient fault HMMs were discussed.

The case study also compared the test results of EPSmart to results of FDI methods proposed in DXC10. These comparisons showed that EPSmart had the highest diagnostic accuracy. However, more rigorous on-line testing of EPSmart should be conducted.

Overall, the case study showed the potential for the proposed EPSmart method to diagnose and isolate a multitude of degraded and critical faults within aircraft EPS.

6.2 Case Study 2: Application of the IntelArc for diagnosis of sustained DC Arc Faults

This case study is used to test and analyse application of the proposed IntelArc method for diagnosis of sustained series DC arc fault events. IntelArc was described in Chapter 5; its application for diagnosis of sustained DC arc faults was described in detail in Chapter 5, Section 5.2.6.1.

A general outline of this case study is provided in Section 6.2.1. Results of the case study are presented in Section 6.2.2 and analysed in Section 6.2.3. Results are used to determine the ability of IntelArc to provide generalised diagnosis of sustained arc events within a representative DC aircraft EPS network.

6.2.1 Case Study 2 - Outline

The case study involved development of a representative aircraft DC EPS network model using MATLAB Simulink [227]. Arc fault conditions within the network were simulated using the arc fault model described and validated in Chapter 4. The EPS network model was used for generation of arc fault, nominal steady-state and nominal transient test data – this data was used to test the arc fault diagnostic capabilities of IntelArc.

6.2.1.1 EPS Model

The general topology of the modelled DC EPS network used for generation of test data is illustrated in Figure 6-4. Network architecture is similar to the system described in Chapter 2, Section 2.3.3.2.

The network consists of 270VDC and 28VDC distribution levels. A passive 6 pulse rectifier converts main 230VAC power to 270VDC. The output of the rectifier is connected to the 270VDC bus. Two separate high power (≈ 2.7 - 8 kW) 270VDC load banks are powered from this bus; the two areas between the 270VDC bus bar and load banks are designated as Zones 1 and 2 respectively.

A DC/DC buck converter is also connected to the 270 VDC bus. The DC/DC converts the 270VDC power to 28VDC, and its output is connected to the 28VDC bus. A lower power (≈ 0.3 - 0.9 kW) load bank is connected to the 28VDC bus; the area between the 28VDC bus and load bank is designated as Zone 3.

A 28VDC battery system provides power to a Battery Bus. A standby load bank is connected to the battery bus and this area is designated as Zone 4. The battery bus is also connected to the 28VDC bus through a CB, which is nominally open.
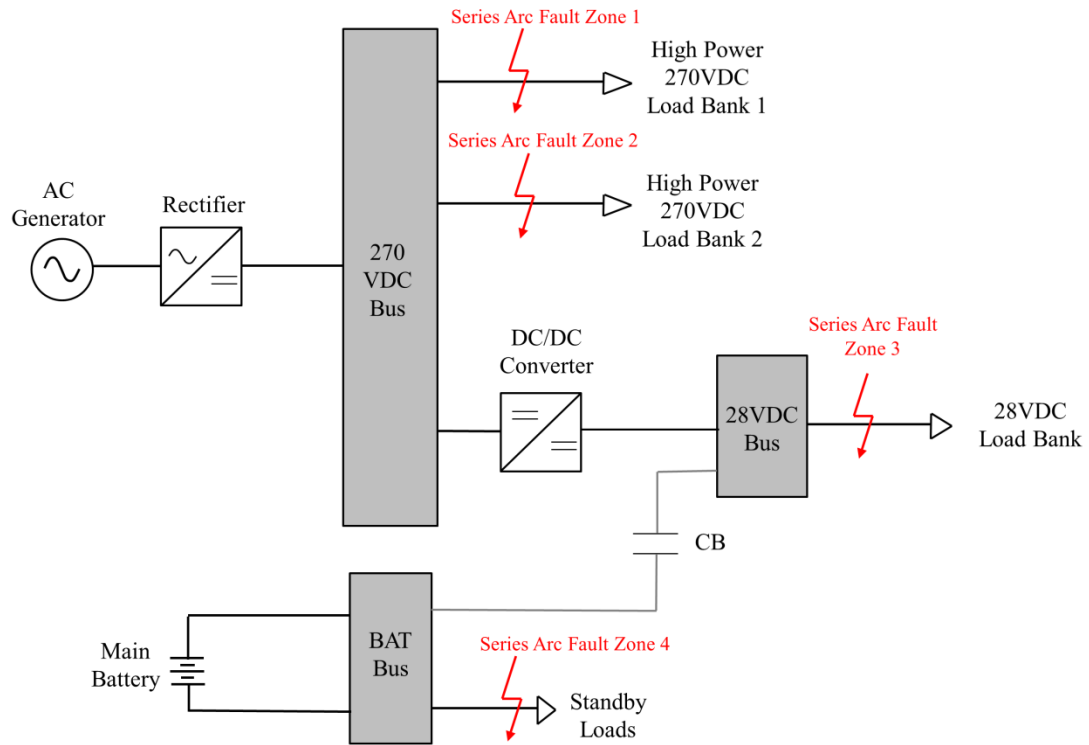
Figure 6-4: Topology of aircraft EPS network model developed for generation of test data in Case Study 2

The modelled network has a variety of distribution levels, converter interfaces and load locations. This allowed testing of IntelArc's ability to provide generalised diagnostic performance. IntelArc uses load current data from the four different zones for inference of network condition.

Model parameters are summarised in Table 6-4. A complete description of the network model is provided in Appendix A.

6.2.1.2 Types of Load and Load switching

Both inductive and capacitive loads were included in the model to test the IntelArc's capability of diagnosing sustained arc faults in a variety of reactive power scenarios. Lumped element models consisting of inductors, resistors and capacitors were used to model the reactive loads. Typically, capacitive loading reduces transients within the load current during arcing conditions. This can potentially impact diagnostic performance.

Maximum and minimum values of inductance, capacitance and resistance for each type of load are summarised in Table 6-5.

Table 6-4: Summary of Case Study 2 network model parameters

DC Line Impedances	
Resistance	0.641Ω/km
Inductance	0.34mh/km
Capacitance	1mF
Battery	
Type	Lithium-Ion
Nominal Voltage	28V
Rated Capacity	60Ah
Initial State of Charge	100%
Battery Response Time	30s
Current Measurements	
Gaussian noise generator mean value	0
Gaussian noise generator variance	0.0001
Gaussian noise generator sample time	0.001s
Passive Rectifier	
Input Voltage	230VAC
Output Voltage	270VDC
Input Frequency	400Hz
Number of Bridge Arms	3
Snubber Resistance	0.1MΩ
Snubber Capacitance	Inf.
Diode Forward Impedance	1mΩ
Forward Voltage	0.7V
Filter Capacitance	1mF
270/28VDC Buck Converter	
Inductance	250µH
Capacitance	100µF
Switching Frequency	20 kHz
Duty Cycle	0.12
DC Loads	
Load Resistance	Ranged between 2 and 25Ω
Load Inductance	Ranged between 1.25 and 7mH
Load capacitance	Ranged between 0.1 and 7µF
Series Arc Fault Model	
Parameters varied between simulations as described in Appendix A	

Table 6-5: Maximum and minimum values of impedance for each type of load

Type of Load	Inductance	Capacitance	Resistance
270VDC	Max: 7 mH	Max: 7 µF	Max: 25 Ω
	Min: 1.5 mH	Min: 1 µF	Min: 10 Ω
28 VDC	Max: 4.5 mH	Max: 0.7 µF	Max: 6.5 Ω
	Min: 1.25 mH	Min: 0.1 µF	Min: 2 Ω

Values were randomised between the maximum and minimum for each simulation run. The different maximum and minimum values for 270 VDC and 28 VDC loads resulted in similar load current ranges of 10A – 25A across both 270VDC and 28VDC levels (the increased power in the 270VDC loads is a result of the higher voltage).

Switching of loads in each zone was used to model nominal transient behaviour. Load switching resulted in either increased or decreased current levels. The presence of transient conditions within the simulated load current data was used to evaluate the percentage of false positives diagnosed by IntelArc.

6.2.1.3 Case Study 2 Methodology

Numerous simulations of the EPS network model described in Section 6.2.1.1 were undertaken for generation of test data; these are summarised in Table 6-6.

Table 6-6: Summary of simulations used to generate test data

Fault Location	No. of Simulations	Load Types: (No. of simulations)	Nominal Transient Behaviour	Feeder Length & Fault Location along Feeder
No Fault	20	Inductive: 12 Capacitive: 8	*Load Switching at various Times & Locations*	*Line lengths ranged from 20 to 120m*
Zone 1	25	Inductive: 20 Capacitive: 5		
Zone 2	25	Inductive: 20 Capacitive: 5		
Zone 3	25	Inductive: 20 Capacitive: 5		
Zone 4	25	Inductive: 20 Capacitive: 5		

A total of 120 model simulations were executed, resulting in a total of 120 test cases where duration of each test case was 10s; arc faults were introduced at a variety of locations and times throughout the 10s duration. The arc fault model described in Chapter 4 was used for simulating series arc fault conditions. Load switching events were also introduced at a variety of locations and times throughout each 10s test case. Feeder length refers to the length of the feeder between each bus and load. These were varied between 20-120m throughout simulations – the short feeder lengths characterised the compactness of aircraft EPS. The location of the arc fault along the feeder was also varied.

These simulations produced load current test data for the four separate zones. Load current was sampled at 2 kHz. 5 kHz Gaussian noise was added to simulate sensor and switching

noise. This data was applied to IntelArc which outputs a decision on network condition every 50ms; hence 200 decisions are output for each 10s simulation period. The output is either:

1) Network is in Nominal Condition – No Fault

   or,

2) A Series Arc Fault has been Diagnosed in Zone X (where $X \in (1, 2, 3, 4)$)

As the various conditions throughout each test case were known, it was possible to assess the accuracy of IntelArc.

Fault detection time is a critical factor and, as test results were being assessed, the detection time of IntelArc was compared against a maximum detection time, T_{dtect}, proposed in Underwriters Laboratory 1699B standard [191]. This time is defined as:

$$T_{detect} \leq \frac{750}{V_{arc}I_{arc}}$$

(6.1)

where V_{arc} is arc voltage and I_{arc} is arc current.

Consequently, each test result also included a '% of max detection time' metric that signified whether IntelArc had, or had not, detected arcing within a suitable timeframe. Complete test results for Case Study 2 are presented in the following section.

6.2.2 Case Study 2 Results

The accuracy of IntelArc for diagnosis of sustained arcing events was quantified using the test cases. In total there were 120 test cases generated using the model simulations described in the previous section, the results of which are outlined in Table 6-7.

Of the 120 test cases, a total of 116 were diagnosed correctly, resulting in 96.67% diagnostic accuracy. The four cases incorrectly diagnosed were all at 28VDC levels; these included three false negatives i.e. non-detection of the arcing event and only one false positive. The average detection time was 0.4673 seconds. It is desirable to reduce this average time, despite the majority of detection times being below the max detection times. Note that the % of average max detection times were not calculated for 28VDC levels as the low voltage, and hence power, meant the times were well within the maximum (see (6.1)).

The complete results of Case Study 2 are provided in Appendix B. Full analysis of these results is provided in the following section.

Table 6-7: Case Study 2 Test Results

Fault Location	Load Type	Load Interface/ Source	No. of Tests	No. of correct diagnoses	Diagnosis Accuracy (%)	Summary of Incorrect Diagnoses	Average Detection Time (s)	Average % of Max Detection Time
-	-	-	20	20	100	-	-	-
Zone 1	Inductive	Rectifier	20	20	100	-	0.385	34.149
(270VDC)	Capacitive	Rectifier	5	5	100	-	0.6	34.147
Zone 2	Inductive	Rectifier	20	20	100	-	0.4725	52.193
(270VDC)	Capacitive	Rectifier	5	5	100	-	0.82	29.72
Zone 3	Inductive	DC/DC	20	19	95	1×false negative	0.2394	N/A
(28VDC)	Capacitive	DC/DC	5	5	100	-	0.29	N/A
Zone 4	Inductive	Battery	20	18	90	2×false negative	0.494	N/A
(28VDC)	Capacitive	Battery	5	4	80	1×false positive	0.4375	N/A
		Totals	**120**	**116**	**96.67**	**-**	**0.4673**	**37.55**

6.2.3 Analysis of Case Study 2 Test Results

IntelArc testing resulted in 96.67% of the test cases being accurately diagnosed. This level of accuracy proved that a FDI method based on HMM, and using time and time-frequency domain features, could potentially be used for on-line detection of series DC arc faults. However, there were other issues which arose from the test results; in particular, the overall detection time was too high.

The conditions within the test cases were suitably varied (e.g. different levels of load switching and different load power/current ratings) to fully test the generalisation capabilities of IntelArc. The method handled the nominal load transients well, with only 1 false positive out of 120 tests (0.83%). This was considered very successful since some of the load transient's involved small decreases in current that could easily be misinterpreted as an arc fault condition using less advanced detection methods.

Testing was particularly successful at 270VDC distribution levels, where the system was 100% accurate. All four incorrectly diagnosed test cases were at the 28VDC levels, and three were at the battery powered Zone 4. Three of the incorrect diagnoses did not detect the presence of an arc fault (false negative). This was probably a consequence of a reduced LL output of the fault model during 28VDC arcing events. A smaller LL value will result in the threshold condition not being met and non-diagnosis of a fault event. This is one aspect where the sustained AFD algorithm did not generalise particularly well, although it was only in three instances.

Testing showed that IntelArc could successfully handle different types of load reactance – the system misdiagnosed three inductive load scenarios and one capacitive load scenario. These results are misconstrued by the fact that only 20 arc faults under capacitive loading were tested, in comparison to 80 inductive test cases. Detection under capacitive loading is generally considered more challenging as the load capacitance resists changes in load voltage resulting in limited arcing noise signatures. However, there was sufficient diagnostic accuracy (95%) in the capacitive test cases, albeit with a higher detection time at the 270VDC distribution zones.

The issue of high overall detection time is a result of the reduced sampling frequency. Ideally, sampling frequency would be minimised to reduce computational overheads. The 2 kHz sampling frequency, despite providing enough data for accurate diagnosis, meant that arcing conditions had to be relatively prolonged to reach the pre-determined threshold values. Thus, overall detection time of IntelArc was increased. The thresholds could be

reduced to minimise detection times of true arcing events. However, reducing thresholds would also result in an increase of false positives. Essentially, a significantly reduced, and (perhaps) ambitious, sampling frequency means there is significant trade-off between detection time and accuracy.

Although the average detection times were well within the max detection time quantified by (6.1), this trade off must be minimised for the IntelArc to be applied in an aircraft EPS environment. Sustained arc faults are unlikely at higher altitude [36], meaning detection time must be reduced without sacrificing accuracy. This case study has shown that a sampling frequency greater than 2 kHz is required to enable accurate detection within a suitable time frame.

Overall, the case study has proven that IntelArc is capable of accurately diagnosing arc faults within a range of different conditions. However, the applicability potential to aircraft EPS is limited due to the reduced sampling frequency and overlong detection time.

6.2.4 Case Study 2 - Summary

This case study tested application of IntelArc for generalised diagnosis of sustained DC arc faults within representative aircraft EPS. This application of IntelArc was discussed extensively in Chapter 5, Section 5.2.6.1.

A power systems model of an aircraft DC EPS was developed and used to generate arc fault, nominal steady-state and nominal transient test data. The system consisted of: 270VDC and 28VDC distribution levels; various power converter interfaces; capacitive and inductive loads, and different load feeder lengths. These variables were randomised within the test data to fully test the generalisation capabilities of IntelArc.

A total of 120 individual test cases were generated; 100 cases contained arc fault conditions at different locations throughout the network and 20 included nominal steady-state behaviour. All test cases included load switching transients. Test results showed IntelArc had a 96.67% diagnostic accuracy, with an average detection time of 0.467 seconds. Overall, the case study has shown the potential for IntelArc to provide accurate diagnosis of series DC arc faults across a range of operating conditions. Despite the fact that detection times in the majority of test cases were well within a max detection time quantified by UL1699B, it was concluded that, for practical application, load current sampling must be increased beyond 2 kHz.

6.3 Case Study 3: Application of IntelArc for diagnosis of intermittent DC Arc Faults

This case study is used to test and analyse application of IntelArc for diagnosis of intermittent series DC arc faults. The use of IntelArc to diagnose intermittent arc events was discussed in detail in Chapter 5, Section 5.2.6.2.

The case study is outlined in Section 6.3.1, and results are described and analysed in Sections 6.3.2 and 6.3.3 respectively.

6.3.1 Case Study 3 - Outline

The case study focuses on diagnosis of intermittent arcing events at 270VDC and 28VDC distribution levels. An EPS model was developed in Simulink for generation of intermittent arc fault data. This data was input to IntelArc to test its capabilities of diagnosing intermittent arc faults.

6.3.1.1 EPS Model

The basic model topology is illustrated in Figure 6-5.
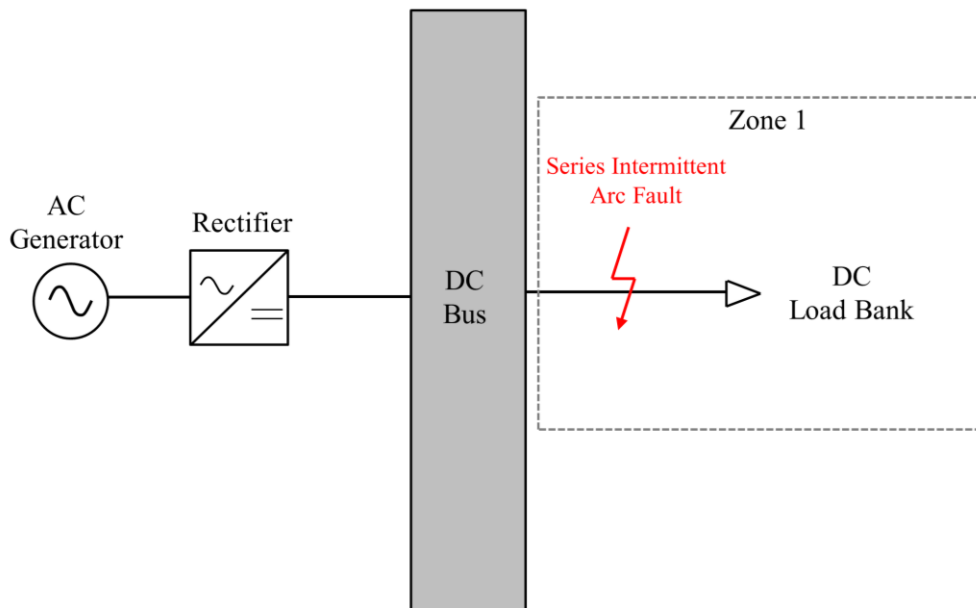
Figure 6-5: Topology of network model developed for generation of test data in Case Study 3

The model consisted of a passive rectifier that converts either 230VAC into 270VDC or 115VAC to 28VDC. The output of the rectifier is connected to a DC distribution bus. A single load bank is connected to the distribution bus and series intermittent arc faults are introduced on the feeder between the load bank and bus bar. The load bank is directly interfaced and does not include additional conversion stages.

Lumped element models consisting of inductors, resistors and capacitors were used to model the reactive loads. The same maximum and minimum impedance values for each voltage level outlined in Table 6-5 in Case Study 2 were applicable. Length of the feeder between the bus and loads, and fault location along the feeder, were also variable. Parameters for the network model are summarised in Table 6-8.

Table 6-8: Summary of Case Study 3 network model parameters

DC Line Impedances	
Resistance	0.641Ω/km
Inductance	0.34mh/km
Capacitance	1mF
Current Measurements	
Gaussian noise generator mean value	0
Gaussian noise generator variance	0.0001
Gaussian noise generator sample time	0.001s
Passive Rectifier	
Input Voltage	230VAC / 115VAC
Output Voltage	270VDC / 28VDC
Input Frequency	400Hz
Number of Bridge Arms	3
Snubber Resistance	0.1MΩ
Snubber Capacitance	Inf.
Diode Forward Impedance	1mΩ
Forward Voltage	0.7V
Filter Capacitance	1mF
DC Loads	
Load Resistance	Ranged between 2 and 25Ω
Load Inductance	Ranged between 1.25 and 7mH
Load capacitance	Ranged between 0.1 and 7μF
Intermittent Series Arc Fault Model	
Parameters varied between simulations as described in Appendix A	

6.3.1.2. Case Study 3 - Methodology

The model simulations used for generation of intermittent arc fault test data are summarised in Table 6-9. A modified version of the sustained arc fault model described in Chapter 4 was used for simulating intermittent arc faults. This modified intermittent fault model is described in detail in Appendix A.

Table 6-9: Summary of simulations used to generate intermittent test fault data

Load Type	Load Interface	Voltage Level (VDC)	No. of Tests	Nominal Transient behaviour	Feeder Lengths
Inductive	Rectifier	270	30	*Load Switching at various times*	*Lengths ranged from 45 to 90m*
		28	10		
Capacitive	Rectifier	270	10		
		28	10		
		Total	60		

A total of 60 test cases were simulated - each of the 60 simulations lasted 10 seconds. 40 simulations were conducted at 270VDC and 20 simulations were conducted at 28VDC. Each test case includes: periods of nominal steady-state behaviour; a nominal transient event; and the onset of intermittent arc faults. An example load current during a 10 second test case is illustrated in Figure 6-6.
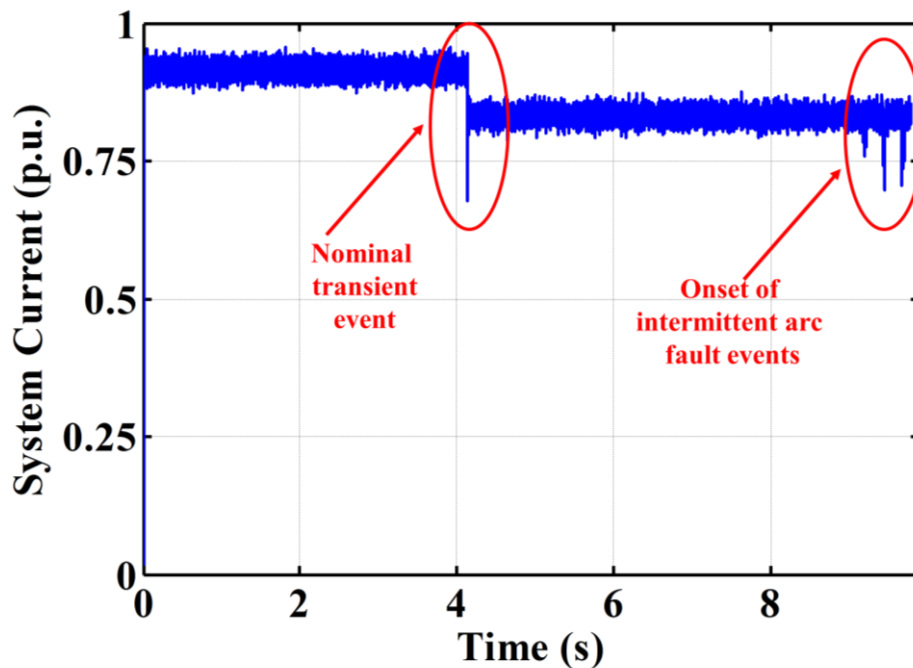
Figure 6-6: Example load current during 10 second test case

Load current was sampled at 20 kHz and 5 kHz Gaussian noise was used to simulate sensor/switching noise. The case study does not consider noise from active power converters. Similar to the methodology followed in Case Study 2, the test cases were applied to IntelArc to determine accuracy of the system. IntelArc outputs a decision on network state

every 50ms; hence 200 decisions were output for each 10s simulation. Outputs of IntelArc were outlined in Case Study 2, Section 6.2.1.3.

The onset and duration of intermittent fault events across each test case was variable. To determine accuracy of IntelArc, it was necessary to first establish when an intermittent arc event occurred throughout each test case. This information was compared to IntelArc outputs to quantify accuracy.

Test results are presented in the following section.

6.3.2 Case Study 3 -Test Results

The accuracy of IntelArc for diagnosis of intermittent arcing events was quantified using the test cases. Testing results are outlined in Table 6-10.

In total, 56 out of the 60 test cases were correctly diagnosed resulting in 93.3% accuracy – this included 37 out of 40 (92.5%) test cases at 270 VDC and 19 out of 20 (95%) at 28VDC. IntelArc accurately identified all intermittent fault events i.e. no false negatives were prescribed. The four incorrectly diagnosed test cases were a result of false positives induced at nominal transient events under inductive loading. The average time for detection of intermittent arcing events is 0.0571 seconds – significantly lower than detection time results outlined in Case Study 2. Another metric outlined in Table 6-10 includes the average duration of intermittent arcing events in each scenario.

Full discussion and analysis of these results is provided in the following section, and the complete results are provided in Appendix B.

6.3.3 Analysis of Case Study 3 Test Results

Testing resulted in 93.3% of all test cases being accurately diagnosed, with an average fault detection time of 0.0571 seconds. This case study has highlighted various attributes of the IntelArc method. These include:

- Detection of variable duration intermittent arcing events
- Detection of arcing events with variable decreases in load current magnitude
- Detection across a range of load currents
- Detection across two different distribution voltages
- Accurate identification of all intermittent fault events (no false negatives)
- Minimal impact from nominal transients
- Minimal detection time
- Minimal computational overheads

Table 6-10: Summary of Case Study 3 Test Results

Load Type	Load Interface	Voltage Level (VDC)	No. of Tests	No. of correct diagnoses	Diagnosis Accuracy (%)	Summary of incorrect diagnoses	Average Detection Time (ms)	Average Duration of arcing event (ms)
Inductive	Rectifier	270	30	27	90	3xfalse positives	56.9	97
		28	10	9	90	1xfalse positive	55.5	89
Capacitive	Rectifier	270	10	10	100	-	62.4	104.4
		28	10	10	100	-	53.7	101.2
		Totals	**60**	**56**	**93.3**	**-**	**57.1**	**97.905**

The preliminary test results, coupled with these characteristics, show that the method has the potential to be both accurate and practically applicable. The main limitation with the preliminary testing is that only a limited number of test cases were considered, particularly under capacitive loading.

Analysis of results shows that all four misdiagnosed cases were false positives induced by nominal switching events. The main reason for this was accredited to the LL of the nominal model significantly decreasing at nominal switching events (as expected) before increasing to a value more associated with arc fault events just after the switching event. This increase to a value more associated with arcing events causes IntelArc to incorrectly diagnose the presence of an arc fault. To attempt to alleviate this problem, it is proposed that diagnosis of a fault event cannot be made for a predetermined time (say 50ms) after a significant reduction in likelihood of the nominal model - for an example of LL outputs across a test case, refer to Chapter 5, Section 5.2.6.2.

IntelArc diagnosed effectively under different types of inductive and capacitive loads; further testing should be undertaken under capacitive loading to fully assess the impact it may have on intermittent detection. Also, the average duration of arcing events (97ms), should be reduced further to assess impact of even shorter arcing events.

The reduced detection time (in comparison to Case Study 2) was a result of the increased 20 kHz sampling frequency and also the analysis of data windows every 10ms (as opposed to every 50ms). 20 kHz sampling does not result in significant computational overheads. These initial results prove that the combination of wavelet transform extracted features (across the 0-10 kHz bandwidth) with HMM enables accurate intermittent arc fault diagnosis within acceptable detection times.

Overall, testing proved both the capabilities and applicability of the IntelArc method. Case Study results show that IntelArc can protect DC networks from arcing events by detecting intermittent faults with high accuracy and within short time frames. The difficulty of accurate series arc fault detection, particularly in DC systems, was discussed throughout Chapters 2 and 4. Although the IntelArc method, proposed as part of the work of this thesis, has only been tested at basic levels, its potential has been proven within this case study.

6.3.4 Case Study 3 - Summary

This case study was used to test the ability of IntelArc to diagnose series DC intermittent arc fault events. A basic EPS model was used to generate intermittent arc fault test data – the

model consisted of a passive rectifier converting AC power to 270VDC or 28VDC which is distributed to a single load bank.

A total of 60 individual test cases were generated where intermittent arcing events were randomly injected into the load feeder using an intermittent arc fault model– IntelArc managed to accurately diagnose 56 test cases (93.3%) with an average detection time of 0.0571 seconds. All four misdiagnosed test cases were a result of false positives at nominal transient events – IntelArc did not provide false negatives and accurately identified all intermittent fault events.

This case study showed the potential for accurate intermittent series DC arc fault diagnosis within an acceptable time frame. It highlighted that a sampling frequency of 20 kHz and the use of a sliding window technique will significantly reduce detection time and can maintain diagnostic accuracy.

6.4 Case Study 4: Experimental Application of IntelArc

This case study was used to validate the accuracy of the IntelArc for diagnosing series arc faults within a scaled DC testbed setup. Fault data was generated within the testbed and was used to test the accuracy of the method that was trained using data simulated with the arc model described in Chapter 4. This case study allows further assessment of the generalisation capabilities of IntelArc and also identifies the effects that system noises will have on diagnostic accuracy.

6.4.1 Case Study 4 - Outline

Data was generated within a DC testbed that has means of inducing series DC arc faults. A one-line diagram of the experimental setup is shown in Figure 6-7 and photographs depicting various system elements are provided in Figure 6-8 (a).

The set-up consists of a four-quad active rectifier providing DC power to a main busbar through two SSPCs. Two separate loads, a directly interfaced resistive load bank and two parallel motors interfaced using a buck-boost DC/DC converter, are connected to the main busbar. Two current measurements are taken at each respective feeder and a voltage measurement is taken at the main bus bar. This equipment and configuration is limited to a maximum of 40V, 320W which allows representation of low voltage DC networks. As part of the case study, series arc faults were induced between the source and busbar with use of a fault throwing unit that consists of a stepper motor intermittently separating two contacts –

this is shown in Figure 6-8 (b). This form of series arc fault generation has also been described in [171].
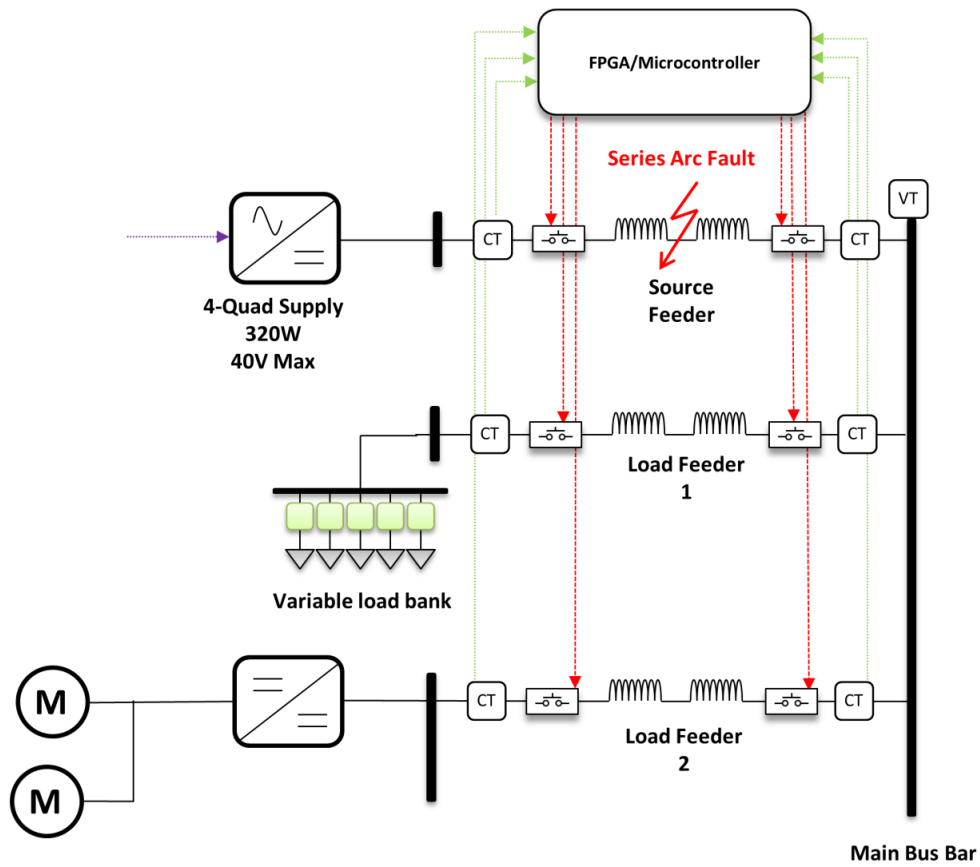
Figure 6-7: One-line diagram of DC testbed set-up

(a)   (b)
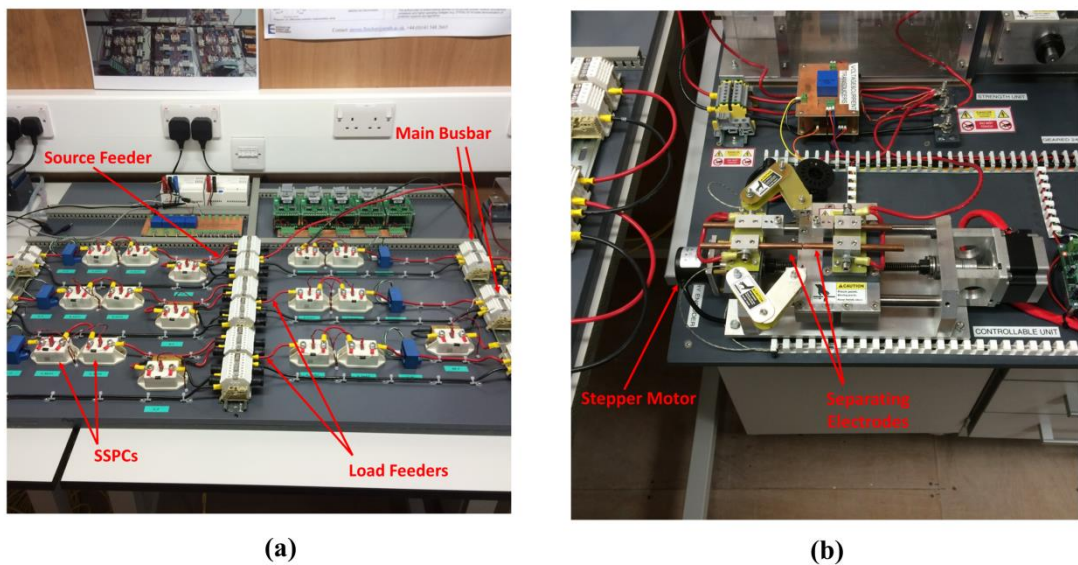
Figure 6-8: (a) Depiction of various components within the experimental DC testbed configuration and (b) Series arc fault throwing unit

Switching within the variable load bank was used to capture nominal transient behaviour. Electrical current data sampled at 20 kHz was captured at the source feeder using an oscilloscope during steady-state, series arc fault and nominal load switching behaviours. This data was used to test the accuracy of the IntelArc method that was trained using data generated from the software model described in Chapter 4.

6.4.2 Case Study 4 – Test Results

An example of the experimental data and the corresponding diagnostic outputs of the IntelArc method are illustrated in Figure 6-9. Within this test example, the nominal load switch at 0.4s did not result in false diagnosis, while the onset of intermittent fault conditions at 2.4s were accurately diagnosed by IntelArc.
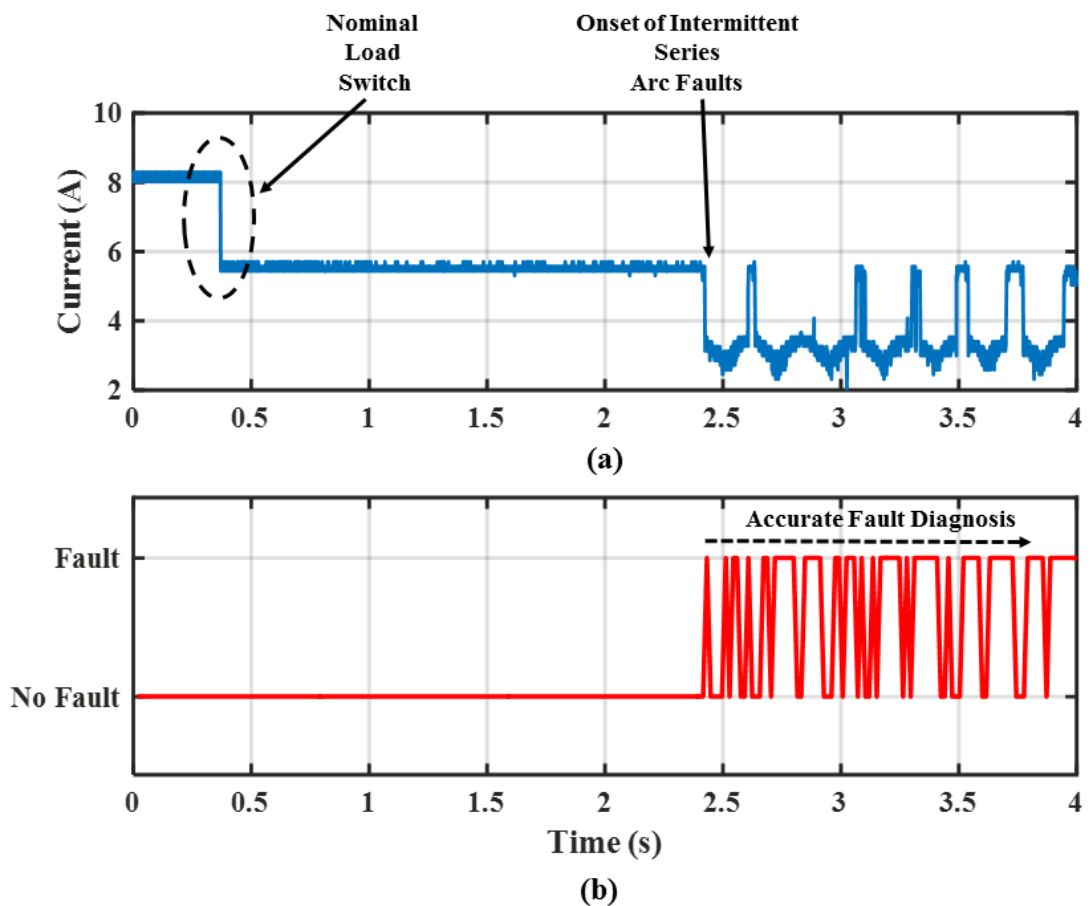
Figure 6-9: (a) Experimental data captured using the DC testbed. Within the experiment, a nominal load switch occurred at 0.4 s and the onset of intermittent series arcing occurred at 2.4s (b) Corresponding diagnostic outputs of the IntelArc outputs. IntelArc is not affected by the nominal load switch and accurately detects arcing at the appropriate time.

188

Five tests were conducted with the onset of arcing occurring at two different power levels outlined in Table 6-11. Accuracy was quantified by comparing the time of fault onset with the diagnostic decision provided by IntelArc; the ability of IntelArc to not provide false positives during both nominal steady-state and nominal transient conditions was also used for accuracy validation. IntelArc accurately diagnosed series arc fault conditions in each test case and load switching behaviour did not result in FPs.

Table 6-11: Summary of Case Study 4 Results

Voltage Level (V)	Current Level (A)	No. of Tests	IntelArc Accuracy (%)
33	5.5	3	100
28	8	2	100

These results have shown the capability of IntelArc to accurately diagnose series arc faults in the presence of active converter and system noise. Test case data presented here were generated on a testbed which had not previously been presented throughout model training - this highlights the robustness of IntelArc to provide diagnosis across a range of network conditions.

6.4.3 Case Study 4 – Summary

This case study was used to test the ability of IntelArc to diagnose series arc faults within the presence of active converter and switching noises. Data throughout nominal and fault conditions was generated within a scaled DC testbed that included an active rectifier, a DC/DC converter and various resistive and motor loads. Five test cases were presented across different power levels, and diagnostic results have shown the capability of IntelArc to provide accurate fault detection within this environment. These results prove the method can provide generalised fault diagnosis despite the presence of system noise and varying network conditions.

6.5 Chapter 6 Conclusions

The purpose of this chapter was to test the application and accuracy of the two novel FDI methods proposed as part of the work of this thesis. Testing was described with the use of four separate case studies.

The first case study applied EPSmart to a subset of NASA's ADAPT network, the ADL. The ADL is a basic network representing an aircraft EPS and consists of a single 24V DC

battery source directly powering a DC load and two AC loads through an inverter. Application of EPSmart to ADL tested its ability to provide FDI of multiple failure modes within hybrid AC/DC networks, as well as to diagnose both critical and degraded faults.

Testing showed EPSmart accurately diagnosed 123 out of 129 (95.3%) intermittent, abrupt and incipient fault mode test cases. This included 25 out of 26 (96%) critical faults, 78 out of 83 (93%) degraded faults and 20 out of 20 (100%) nominal conditions. The main drawback of the EPSmart method identified throughout testing was the misdiagnosis of incipient fault conditions; various procedures for improving this aspect were proposed and discussed. In general, case study results proved the potential of EPSmart to improve network protection through autonomous diagnosis of multiple critical and degraded fault modes.

The test results were compared to previously proposed FDI methods applied to the ADAPT – comparisons showed EPSmart provided the highest diagnostic accuracy. However, it was explained that EPSmart testing was conducted in an off-line scenario, whereas the other methods were tested in an on-line setting. Hence, the next progression of EPSmart development is testing its ability to provide on-line FDI.

The second case study tested the ability of IntelArc to provide generalised diagnosis of sustained series DC arc faults. The case study involved development of an EPS model for generation of test data – the model represented an aircraft DC EPS and consisted of 270VDC and 28VDC distribution zones, various converters, inductive and capacitive load types and different feeder lengths. The arc fault model described in Chapter 4 was used for simulating series arc fault conditions. This model is capable of producing a wide range of conditions and, as such, enabled the generalisation capabilities of the method to be tested.

IntelArc managed to correctly diagnose 116 out of 120 (96.67%) test cases with an average detection time of 0.4673s. Although the majority of test cases in the second case study diagnosed faults within the acceptable time frame stipulated in [191], the average detection time was deemed too long for the detection of faults that are either sustained over shorter time frames or intermittent in nature. The overlong detection was reasoned to be a result of the limited 2 kHz sampling frequency: although discriminative features for fault diagnosis are present within the observable bandwidth of the 2 kHz sampled signal, a higher sampling frequency would also enable the use of salient higher frequency signatures for fault detection and would thus present further evidence and allow for fault detection reduced timeframes. Significant conclusions from the Case Study were that IntelArc provided highly accurate, generalised series DC arc fault diagnosis; however, an increased load current sampling

frequency would be required to reduce overall detection time and make IntelArc more suitable for practical application.

The third case study challenged the ability of IntelArc to diagnose series DC intermittent arc fault events. A basic EPS model was used for generation of intermittent arc test data – the model included a single passive rectifier converting AC power to 270VDC or 28VDC which is distributed to a single load bank. Intermittent arc fault conditions were simulated on the load feeder using a modified version of the arc fault model. Intermittent arcing events exhibited both variable duration and variable reduction in load current.

IntelArc accurately diagnosed 56 out of 60 (93.3%) test cases with an average detection time of 0.0571s. The case study showed that this application IntelArc, which utilises a higher load current sampling frequency of 20 kHz as well as a sliding window method, is able to maintain high diagnostic accuracy and significantly reduce detection time. Significant conclusions were that practical application of IntelArc would require the increased 20 kHz sampling frequency and use of a sliding window technique.

The fourth case study used test data generated within a scaled DC testbed setup to assess the capability of IntelArc to diagnose series arc faults in the presence of system noise. The system comprised different active converters, resistive and motor loads, and a stepper motor based fault throwing unit for the creation of intermittent series arc faults. Five test cases were generated that included series arcing and nominal switching behaviour within the load banks.

Each test case was presented to IntelArc and diagnostic results showed that it had the ability to accurately detect intermittent arcing events. These results also showed that active converter noise and load transients did not result in false positives. This case study has provided further evidence of the robustness of IntelArc for providing accurate, generalised diagnosis within environments and conditions that were not presented throughout model training.

Overall, these case studies have shown that the EPSmart and IntelArc methods have the potential to aid real-time fault management and improve EPS protection and health management systems.

7. CONCLUSIONS & FURTHER WORK

This thesis has focused on the design of intelligent data-driven FDI methods to improve real-time fault protection and health management systems within MEA aircraft EPS. In particular, two novel methods have been proposed: EPSmart, that can accurately diagnose the onset of degraded faults prior to critical failure; and IntelArc, that can accurately detect series arc faults. The thesis has established the need to develop intelligent FDI methods by emphasising the limitation of conventional protection methods in detecting and isolating these types of fault – limitations include fault currents being well below relay trip curves and intermittency reducing fault energy.

Motivations for developing data-driven FDI methods within the EPS of MEA were established; these included accurately determining network behaviour/operational status across large volumes of system data and removing the requirement for advanced system knowledge associated with model-driven approaches. The absence of fault data was identified as being a significant hurdle to overcome throughout development of such methods. The thesis presented and described discriminative fault features that minimised the impact the lack of data may have on diagnostic accuracy.

The main contributions of the thesis were the design of the *EPSmart* and *IntelArc* methods. EPSmart was developed for detection and diagnosis of intermittent, incipient, abrupt and sensor faults within hybrid AC/DC aircraft EPS. Significant benefits of this method were determined to be the autonomous diagnosis of multiple critical and degraded fault modes and the ability to accurately discriminate between faults in the underlying system and sensor failures. IntelArc was developed for diagnosis of self-sustained and intermittent series DC arc faults, where its main benefits lie in its ability to provide generalised diagnosis across a range of operating conditions.

Significant conclusions from each chapter within the thesis are detailed in the following.

7.1 Conclusions

Chapter 2 introduced aircraft EPS in general, outlined the motivations for the shift to MEA, and described the effect this wholesale change will have on the EPS of future aircraft – the significant challenge of maintaining high reliability standards within more complex and demanding MEA EPS was underlined. A particular aim of the chapter was to describe relevant limitations of the conventional protection methods, and hence justify the requirement for the development of advanced FDI methods to assist protection and health management within more complex EPS. Accordingly, there was a discussion on the inability of conventional methods to accurately detect fault conditions where there is an absence of significant overcurrent beyond nominal levels. Conditions where this type of behaviour is evident were elaborated, including: intermittent, incipient, high impedance, and arcing faults. Accurate detection and isolation of these degraded conditions prior to critical failure in future aircraft, where high EPS reliability will be even more of a necessity, is extremely difficult through conventional means. Thus, the main conclusions from this chapter was that there is motivation for the development of intelligent FDI methods for application to future aircraft EPS to accurately detect degraded fault conditions and improve network protection and reliability.

Chapter 3 discussed intelligent fault diagnosis and its application to the aircraft EPS domain. The chapter established the relative advantages and disadvantages of each subset of FDI techniques to explain why the methods proposed in the thesis utilised a data-driven approach. The increased volumes of EPS data expected to be generated within MEA, along with a limited requirement for specific domain/system knowledge throughout design and

development, were deemed critical factors for adopting the data based approach. In particular, the chapter reasoned that methods utilizing ML techniques have the potential to autonomously, and accurately, diagnose system status through analysis of the extensive volumes of data. After the description of various ML techniques, certain characteristics of HMM were outlined that make them an excellent candidate for meeting requirements of the proposed FDI methods. These characteristics included, but are not limited to: suitability for detection of transient signals; ability to provide metrics that quantifies the probability of various fault hypotheses; and, inherent scalability that allows systems to be readily updated to include models of emergent system conditions. Previous applications of HMM for anomaly detection and fault diagnostics within various domains were summarised. Although these applications showed their suitability for reaching these goals, their use within EPS has so far been limited to main grid transmission and distribution networks, and thus focused only on AC distribution. The chapter also reviewed general FDI within the aircraft EPS domain, including NASA's ADAPT testbed. This review established that there is a lack of FDI methods specific to this domain, and the majority of aircraft EPS still rely on local control and basic overcurrent fault protection methods.

Chapter 4 was dedicated to series arc faults, including: validation of a fault model that was used for synthetic generation of arc fault data; consequences and hazards of their presence within aircraft EPS; and, description of the difficulties in detecting them. Design of the arc fault model in Simulink, which had previously been proposed by Uriarte *et. al* [171], was outlined. A particular goal of this chapter was to compare simulated outputs from this model with previous studies that had attempted to characterise electrical arcing. Overall there was relatively good agreement between the Simulink model outputs and arc characterisations described in the previous studies. The main inconsistency concerned V-I characteristics at very low current levels; as such, the model should not be used for conditions where arcing current is significantly less than 10A. The chapter reviewed previously proposed series arc FDI methods. It was explained how major challenges still exist with regards to developing generalised FDI methods that can accurately detect series arc faults across a range of network configurations, voltage levels and loads. A main conclusion from the chapter was that basic FDI methods, which rely on simple thresholds, will not suffice in meeting these challenges. Hence, there is motivation for the development of intelligent FDI methods to provide accurate, generalised series arc FDI within aircraft EPS.

Chapter 5 described the proposed EPSmart and IntelArc FDI methods, which are the main contributions of the thesis. EPSmart is a two-stage method, whereby a framework of trained

HMM is primarily used to classify EPS condition – classification of network condition includes both fault mode and location. The second stage of EPSmart determines the severity of any fault that has been classified from the first stage. For the purposes of this thesis, EPSmart was developed using data from a subset of NASAs aircraft EPS representative ADAPT testbed. A total of 15 separately trained HMMs relating to various ADAPT nominal operating and fault conditions constituted the classification framework. Challenges of HMM training were discussed, including optimising the number of model parameters and extracting discriminative features when only limited volumes of fault data are available. There was discussion on statistical based feature extractions and sensor fusion techniques that allowed discrimination between nominal conditions; intermittent, incipient and abrupt fault modes; and, sensor failures. Using HMM to decipher state changes, and thus determine fault severity, was also described.

IntelArc, a series DC arc FDI method, is also based on a framework of multiple trained HMM. The method uses time-frequency and time domain features extracted from EPS current data. IntelArc design and development centered on training HMMs relating to nominal, transient and arc fault conditions - series arc fault data, generated from the arc fault model described in Chapter 4, was used to develop the fault condition HMM. An algorithm was also developed to analyse each of the LL outputs of the trained HMM as real-time network data is applied and thus infer network condition. IntelArc is designed to operate with a sampling rate in the kHz range, and updates inference of network condition every 50ms. A major contribution of this chapter was determining time-frequency domain features, extracted using the DWT that enhance series arc FDI within the HMM based IntelArc. Presentation of DWT coefficients, including GMMs of their temporal characteristics, highlighted that approximate coefficient levels 1-3 and detail coefficient levels 1-2, extracted using a 20 kHz sampling frequency, were optimal for diagnosis.

Chapter 6 used four separate case studies to test application and accuracy of EPSmart and IntelArc. The first case study used test data from a subset of the ADAPT network to test the ability of EPSmart to provide FDI of multiple failure modes within hybrid AC/DC networks. Testing showed EPSmart accurately diagnosed 95.3% of 129 test cases. This included 25 out of 26 (96.1%) critical faults, 78 out of 83 (93.9%) degraded faults and 20 out of 20 (100%) nominal conditions. The majority of inaccuracies were accredited to misdiagnosis of incipient faults – it was described how increasing the number of hidden states within incipient HMM may improve detection of these types of faults. Results of EPSmart were compared to other systems proposed for FDI within ADAPT – these comparisons showed

EPSmart to have the highest diagnostic accuracy. However, EPSmart was limited to off-line testing (where volumes of data covering roughly four minutes of network operation were used for each test case) as opposed to a simulated on-line testing scenario used by the other systems.

Case Study 2 tested the ability of IntelArc to provide generalised diagnosis of sustained series DC arc faults. A representative aircraft MEA EPS model with various converters, load types and feeders was used for generation of arc fault test data at different DC voltage levels. Current sampling in this case study was limited to 2 kHz to test accuracy of IntelArc with reduced data resolution. Of the 120 individual sustained series arc fault test cases, IntelArc accurately diagnosed and isolated 96.67% of test cases, with an average detection time of 0.4673 seconds. This case study showed the suitability of applying IntelArc for FDI of sustained series DC arc faults. However, the increased detection time also highlighted that an increased current sampling frequency would be required to reduce overall detection time and make IntelArc more suitable for practical application.

Case Study 3 tested the ability of IntelArc to accurately diagnose intermittent series DC arc faults. A basic aircraft EPS model was used for generation of intermittent fault test data and network current was sampled at 20 kHz. IntelArc accurately diagnosed 56 out of 60 test cases with an average detection time of 57.1 milliseconds. The case study showed the potential for diagnosis of intermittent arc faults within an acceptable time frame. In particular, the ability of IntelArc to diagnose variable duration intermittent arcing, where reductions in load current magnitude are also variable, was demonstrated. It also highlighted that a sampling frequency of 20 kHz using a sliding window technique will significantly reduce detection time and maintains diagnostic accuracy.

Case Study 4 used test data generated within a scaled DC testbed to assess the performance of IntelArc for diagnosing intermittent series arc faults in the presence of active converter and system noises. Main components of the testbed system included an AC/DC active rectifier, a DC/DC converter, and motor and resistive load banks – current was sampled at 20 kHz at the main busbar in the system using an oscilloscope. Intermittent series arc faults were created using a fault throwing unit consisting of a stepper motor separating two contacts apart. Five test cases that included fault behaviour as well as load switching and steady-state behaviours were generated and presented to IntelArc. Results showed the capability of the method to accurately detect the onset of intermittent arcing while nominal load switching and converter and system noises did not result in false positive diagnoses.

This case study further highlighted the robustness of the method to provide accurate diagnosis within a variety of DC systems and conditions.

Overall conclusions from the thesis are that this work has progressed the knowledge and ability to diagnose a variety of critical and degraded EPS faults through analysis of system data. FDI methods have been designed that possess autonomous and accurate diagnostic characteristics – these methods will improve overall aircraft safety and operational reliability through isolation of hazardous fault conditions. Possessing detailed knowledge of network behaviour, conditions and trends will also ease maintenance procedures and assist scheduling. Implementation of these methods on-board operational aircraft is constrained by the strict certification standards that dictate the suitability, or 'readiness', of new technologies – accelerating the methods through technology readiness levels (TRL) is required before these novel methods will be utilised within protection and health management systems. It is envisaged that IntelArc will function to provide primary protection from DC arc faults whereas EPSmart will supplement health management through the identification of EPS degradations and will provide backup protection from critical faults.

Volumes of EPS data will steadily progress in future platforms that possess greater complexity and dependence, and it is imperative to implement such autonomous methods whereby end-users are not overloaded with information – determining what is important within the data is critical, and this work has developed diagnostic methods that rely on sensor fusion and feature extraction to focus on informative data and minimize redundancy.

Previous research has established methods for the diagnosis of arcing and degraded faults (see Chapters 3 and 4) – often these methods are deployed in systems that possess specific characteristics, and accuracy out with these limited conditions is questionable. This thesis has developed scalable, generalised methods based on machine learning techniques that can be implemented across a variety of EPS configurations and operating conditions. EPSmart highlighted the scalability and computational simplicity of HMM for EPS diagnostic purposes. It also showcased the ability to diagnose difficult to detect intermittent and incipient fault conditions. The work of this thesis analysed and presented DWT arc fault features that are useful for providing generalised diagnosis and significant discrimination between fault and nominal conditions – use of these features within IntelArc has shown they can provide accurate arc fault diagnosis and reduce the impact of nominal transient behaviour on system performance. The generalisation capabilities of IntelArc means it is not

limited to aircraft environments and may also be introduced to shipboard, photovoltaic and building networks.

The following section describes further work that is required to build upon this thesis and progress these novel methods.

7.2 Further Work

Based on the experienced gained from working in this research area, four aspects of further work are recommended and outlined in the following sections.

7.2.1 Scaled hardware on-line implementation of FDI methods.

The case studies in Chapter 6 have proven the potential of EPSmart and IntelArc –these case studies should be used as a basis in which to proceed towards hardware implementation. In particular, Case Study 4 described a DC testbed on which series arc faults were created. The case study described the use of the testbed to generate system data under various nominal and fault conditions; this data was then applied to the IntelArc method to test its diagnostic accuracy.

The next main ambition of this research would be to test IntelArc in a real-time manner on this testbed. In this context, development of IntelArc would remain software based. This would involve using data to train the different HMM and coding of the algorithms. Trained HMMs and associated algorithms would be integrated onto a micro-controller/field programmable gate array (FPGA) [234] ready for use within the testbed. Data would be collected, processed an analysed using the integrated microcontroller/FPGA to allow diagnosis of series arc faults in real-time. In the event of fault detection, control signals would be communicated to SSPCs to isolate the fault and thus test time between fault onset and isolation.

Similarly, the EPSmart method could be implemented in hardware by initiating intermittent short circuit faults and incipient faults at various locations within the testbed. An intermittent short circuit fault throwing unit could be developed that vibrates positive and negative feeders with exposed conductors together, while incipient faults would be created by applying an artificial offset to sensor data. EPSmart, integrated onto an FPGA/microcontroller, would receive data measurements across the testbed to diagnose the different fault types and their location.

In the longer term, the EPSmart and IntelArc methods could be combined to create a complete FDI method that diagnoses intermittent short circuits, incipient degradations, sensor failures and series DC arc faults within hybrid AC/DC testbed. Combining the two

methods highlights the inherent scalability of HMM based methods and is one of the motivations for their use. Furthermore, implementing the FDI methods into an operational UAV with fault throwing capabilities would be integral for testing EPSmart and IntelArc within an actual flight environment. A flying demonstrator is envisaged as a move beyond TRL6.

7.2.2 Application of IntelArc to other DC systems & further consideration of PE Devices

An anticipated benefit of IntelArc is its ability to provide accurate series arc fault diagnosis across a range of system conditions and operating environments. In particular, IntelArc has the potential to be applied within utility microgrids, photovoltaic systems, shipboard systems and building networks - further work would include method implementation within these respective environments. The intelligent nature of IntelArc means that its detection capabilities are agnostic to distribution voltage and current magnitudes although progression of IntelArc to different environments will determine certain unique system characteristics that may result in inaccurate fault diagnosis. One such unique system characteristic is power electronics. The majority of DC systems and microgrids rely on PE devices for conversion functionality, and further studies are recommended to determine the effect that control systems of different power electronic devices, particularly devices that use constant power control, will have on detection accuracy. A voltage decrease at the output terminals of a constant power controlled converter as the result of a series arc fault may cause the converter to increase current to achieve power balancing – this current increase will mask the current signatures required by IntelArc for diagnosis.

7.2.3 Use of voltage measurements to detect series arc faults

Another avenue of potentially fruitful future research involves the use of voltage measurements for series DC arc fault detection. Nominally, line voltage should remain minimal with only line impedance causing small voltage drops. In the presence of series arcing, there will be a significant increase in line voltage. This increase in voltage could potentially be used as a fault signature. The main obstacle to this concept would be obtaining accurate, non-obtrusive, voltage measurements across live conductors between loads and busbars. With measurements of this type being already available within the testbed setup illustrated in Figure 7-1, it would be interesting to establish the extent to which this effect could influence the diagnosis of series arc faults.

7.2.4 Assessment of methods when system data is missing

The methods developed as part of this thesis have been tested so far with the assumption that the data required for diagnosis is available at all times. In practice this may not always be the case – sensors could fail, systems could be compromised, new and emergent use cases may manifest themselves. Further research work is recommended to consider the effect that missing data may have on the diagnostic performances of EPSmart and IntelArc. Here missing data are characterised by a percentage of null readings across observed time windows and may be a result of hardware or communication failure. These studies would establish the robustness of classification and diagnostic accuracy when null readings are present. Furthermore, they would support the development of remedial strategies in the absence complete information.

7.2.5 Co-existence of Sustained and Intermittent IntelArc applications

The vast majority, if not all, arcing conditions on-board aircraft are intermittent in nature; although the thesis presented two applications of IntelArc for both sustained and intermittent arcing conditions, it is likely that the intermittent application will be of greater importance within aircraft EPS. This does not negate the sustained application, and the potential does exist for both applications to co-exist within a single system and provide diagnosis of sustained and intermittent series DC arc faults. There are certain practicalities that must be overcome before this can be realised: each application utilises different sampling frequencies and will therefore require different types of current sensors throughout the monitored system while the greater volume of data required by the intermittent application will result in increased computational requirements.

7.2.6 Exploration of Number of Features within IntelArc

Six feature vectors have been proposed for detection within IntelArc. Future work could include sensitivity studies on the effect that reducing the number of features has on diagnostic accuracy. Using a reduced number of feature vectors that does not negatively impact accuracy will improve computational complexity and benefit practical application of IntelArc.

7.3 Concluding Remarks

This thesis has established the shortcomings of aircraft EPS that rely on conventional protection methods and has proposed novel intelligent FDI methods that have the potential to address these issues. The advantages of using data driven FDI methods for accurate, and autonomous, diagnosis of network health is apparent in an age where volumes of operational data continue to increase. Despite the fact that EPSmart and IntelArc are currently at an early stage of development, the thesis has shown some of the benefits they offer with respect to network protection and health management. The enhanced knowledge these systems will elicit to improve management and maintenance of the EPS is a significant advantage of their implementation. Although challenges do still exist with regards to development and validation of both methods, the contributions of this thesis are a step toward intelligent protection and health management systems that would be integral within future aircraft EPS.

BIBLIOGRAPHY

[1] 'Airbus - Future Journeys - Global Market Forecast 2013'. [Online]. Available: http://www.airbus.com/company/market/forecast/. [Accessed: 02-Mar-2015]

[2] R.E.J. Quigley, 'More Electric Aircraft', in *Proc. of 8th Applied Power Electronics Conference and Exposition*, San Diego, USA, 1993, pp. 906–911

[3] J.A. Rosero *et al.*, 'Moving towards a more electric aircraft', IEEE Aerosp. and Electr. Syst. Mag., vol. 22, no. 3, pp. 3–9, 2007

[4] R.I Jones, 'The more electric aircraft – assessing the benefits', Proc. of the Inst. of Mechanical Engineers, Part G: Journal of Aerosp. Eng., vol. 216, no. 5, pp.259-269, 2002

[5] R.I. Jones, 'The More Electric Aircraft: the past and the future?', in *IEE Colloquium on Electrical Machines and Syst. for the More Electric Aircraft*, London, UK, 1999, pp. 1/1–1/4

[6] R. Abdel-Fadil *et al.*, 'Electrical Distribution Power Systems of Modern Civil Aircrafts', *Proc. 2nd Int. Conf. on Energy Systems and Technologies*, Cairo, Egypt, 2013

[7] A.A. AbdElhafez and A.J. Forsyth, 'A review of more-electric aircraft', in *Proc. 13th Int. Conf. on Aerospace Science and Aviation Technology,* Cairo, Egypt, 2009

[8] M. Sinnett, '787 No-Bleed systems', Boeing Aero Quarterly, 2007, no. 4

[9] L. Faleiro, 'Beyond the more electric aircraft', Aerospace America, vol. 43, no. 9, pp.35-40, 2005

[10] M. Maldonado and G.J. Korba, 'Power management and distribution system for a more-electric aircraft (MADMEL)', IEEE Aerosp. and Electr. Syst. Mag., vol. 14, no. 12, pp. 3–8, 1999

[11] 'Power optimised aircraft (POA)', [Online]. Available: http://www.2020-horizon.com/POA-Power-optimised-aircraft (POA)-s16028.html. (Accessed: 05-Sep-2014)

[12] S.J. Cutts, 'A collaborative approach to the More Electric Aircraft', in *Proc. Int. Conf. Power Electronics*, *Machines and Drives,* Bath, UK, 2002, pp. 223–228

[13] C.R. Spitzer, 'The all-electric aircraft: A systems view and proposed NASA research programs', IEEE Trans. Aerosp. and Electr. Syst., vol. 20, no. 3, pp.261-266, 1984

[14] C.A. Luongo *et al.*, 'Next generation more-electric aircraft: A potential application for HTS superconductors', IEEE Trans. App. Supercon., vol. 19, no. 3, pp.1055-1068, 2009

[15] US Department of Defense, 'MIL-STD-756B: Reliability Modeling and prediction', 1981

[16] A. Emadi, A and A. Eshani, 'Aircraft power systems: technology, state of the art and future trends', IEEE Aerosp. and Electr. Syst. Mag., vol. 15, no. 1, pp.28-32, 2000

[17] M, Blanke *et al.*, 'Fault tolerant control systems – A holistic view', *Control Eng. Practice*, vol. 5, no. 5, pp.693-702, 1997

[18] '787 Airplane health management overview'. [Online]. Available:

http://www.boeing.com/787-media-resource/docs/AHM-overview.pdf. [Accessed: 06-Oct-2014]

[19] D. Izquierdo *et al*., 'Protection Devices for Aircraft Electrical Power Distribution Systems: State of the Art', IEEE Trans. Aerosp. and Electronic Syst*.,* vol. 47, no. 3, pp. 1538–1550, 2011

[20] K. Keller *et al.*, 'Aircraft electrical power system prognostics and health management', in *Proc. IEEE Aerospace Conference*, Montana, USA, 2006, doi: 10.1109/AERO.2006.1656087

[21] N.J. Sharma *et al*., 'Review of Artificial Intelligence Techniques Application to Dissolved Gas Analysis on Power Transformer', Int. Jour. of Comp. and Electr. Eng., vol.3, no.4, pp. 577-582, 2011

[22] M.A. Awadallah and M.M. Morcos, 'Application of AI tools in fault diagnosis of electrical machines and drives – an overview', IEEE Trans. on Energy Conv., vol. 18, no. 2, pp.245-251, Jun. 2003

[23] J. Lee, F. Wu, W. Zhao, M. Ghaffari, L. Liao and D. Siegel, 'Prognostics and health management design for rotary machinery systems—Reviews, methodology and applications', *Mechanical Syst. and Signal Processing*, vol. 42, no. 1–2, pp. 314-334, 2014

[24] C. Booth, 'The use of artificial intelligence based systems for the summarisation and diagnosis of events on electrical power networks', in *IEE Col. on AI for Network Management Systems,* London, UK*,* 1997, doi: 10.1049/ic:19970540

[25] S. Rudd *et al.*, 'Intelligent monitoring of the health and performance of distribution automation', in Int. *Conf. on Intelligent System Application to Power Systems*, Hersonissos, Greece, 2012, doi: 10.1109/ISAP.2011.6082220

[26] 'Diagnosing faults in electrical power systems of spacecraft and aircraft', [Online]. Available: http://repository.cmu.edu/cgi/viewcontent.cgi?article=1047&context=silicon_valley [Accessed: 02-Mar-2015]

[27] R. Glass *et al*., 'An artificial intelligence approach for the verification of requirements for aircraft electrical power systems', in *Aerospace and Electronics Conference,* Ohio, USA, 1991, pp.455-461

[28] V. Venkatasubramanian *et al.*, 'A review of process fault detection and diagnosis: Part III: Process history based methods', Comp. and Chem. Eng., vol. 27, no. 3, pp. 327-346, Mar. 2003

[29] D. Granados-Lieberman *et al.*, 'Techniques and methodologies for power quality analysis and disturbances classification in power systems: a review', IET Gen. Trans. and Dist*.,* vol. 5, no. 4, pp.519–529, 2011

[30] K.P. Murphy, 'Machine Learning: A probabilistic approach', MIT Press, 2012

[31] J. Qi *et al*., 'Fault Detection Design for RUAV with an Adaptive Threshold Neural-Network Scheme', in *Proc. of IEEE Int. Conf. on Control and Automation*, Guangzhou, China, 2007, pp.554-559

[32] M. Sarlak and S.M. Shahrtash, 'High impedance fault detection in distribution networks using support vector machines based on wavelet transform', in *Proc. Electric Power Conf*., Vancouver, Canada, 2008, doi: 10.1109/EPC.2008.4763380

[33] O.J. Mengshoel *et al*., 'Probabilistic Model-Based Diagnosis: An Electrical Power System Case Study', *IEEE Trans. Syst. Man and Cybernetics, Part A: Syst. and Humans*, vol. 40, no. 5, pp.874-885, 2010

[34] T. Abdel-Galil *et al*., 'Disturbance classification using Hidden Markov Models and vector quantization', *IEEE Trans. Power Delivery*, vol. 20, no. 3, pp.2129-2135, 2005

[35] S. Fletcher, 'Protection of physically compact multiterminal DC power systems', Ph.D. dissertation, Dept. Electron. Eng., Strathclyde Univ., Glasgow, UK, 2013

[36] R. Spyker *et al.*, 'An evaluation of diagnostic techniques relevant to arcing fault current interrupters for direct current power systems in future aircraft', in *Proc. 2005 Electrical Insulation Conf.*, Indiana, USA, 2005, pp.146-150

[37] 'Swissair 111, TWA 800 and Electromagnetic Interference', [Online]. Available: http://www.nybooks.com/articles/archives/2000/sep/21/swissair-111-twa-800-electromagnetic-interference/. [Accessed: 06-Mar-2015]

[38] C. Furse and R. Haupt, 'Down to the Wire', IEEE Spectrum, vol.38, iss.2, pp. 34-39, 2001

[39] W.G. Fenton *et al.*, 'Fault diagnosis of electronic systems using intelligent techniques: A review', IEEE Trans. Syst. Man Cybern. C, Appl. Rev., vol. 31, no. 3, pp. 269-281, Aug. 2001

[40] J. Hu and M.K. Bown, 'HMM based on-line handwriting recognition', IEEE Trans. Pattern Anal., vol. 18, no. 10, pp. 1039-1045, Oct. 1996

[41] L.R. Rabiner, 'A tutorial on hidden Markov models and selected applications in speech recognition', Proc. IEEE, vol. 77, no. 2, pp. 257-286, Feb. 1989

[42] Q. Miao and V. Makis, "Condition monitoring and classification of rotating machinery using wavelets and hidden Markov models", Mechanical Systems and Signal Processing, vol.21, no.2, pp.840-855, Feb.2007

[43] 'Electric Drones: unmanned aerial vehicles (UAV) 2015-2025', [Online]. Available: http://www.idtechex.com/research/reports/electric-drones-unmanned-aerial-vehicles-uavs-2015-2025-000430.asp. [Accessed: 02-Aug-2016]

[44] R. Telford and S. Galloway, 'Fault classification and diagnostic system for unmanned aerial vehicles based on hidden Markov models', IET Electr. Syst. Transp., vol. 5, no. 3, pp. 103-111, Sep. 2015

[45] R. Telford, S. Galloway, B. Stephen and I. Elders, 'Diagnosis of series DC arc faults: A machine learning approach' IEEE. Trans. on Indust. Info., accepted for publication Nov. 2016, to be published

[46] I. Moir and A. Seabridge, *Aircraft systems: mechanical, electrical and avionics subsystems integration*, vol. 21. John Wiley & Sons, 2008.

[47] A. Tantawy *et al.*, 'Aircraft AC generators: Hybrid system modeling and simulation', in *International Conference on Prognostics and Health Management,* Colorado, USA, 2008, pp. 1–11.

[48] R. J. Kennett, 'Integrated drive generators for aircraft', *Electron. Power*, vol. 17, no. 2, pp. 73–76, 1971.

[49] J. C. Lee, 'Aircraft transformer-rectifier units', *Stud. Q. J.*, vol. 42, no. 169, pp. 69–71, 1972.

[50] D. G. Vutetakis, 'Current status of aircraft batteries in the U.S. Air Force', in *Proc. of Battery Conf. on Applications and Advances,* California, USA, 1994, pp. 1–6.

[51] R. Bojoi *et al.*, 'Analysis and survey of multi-phase power electronic converter topologies for the more electric aircraft applications', in *2012 Int. Symp. on Power Electronics, Electrical Drives, Automation and Motion (SPEEDAM)*, Sorrento, Italy, 2012, pp. 440–445.

[52] 'Intergovernmental Panel on Climate Change'. [Online]. Available: http://www.ipcc.ch/pdf/special-reports/spm/av-en.pdf. [Accessed: 19-Dec-2014].

[53] 'European Aeronautics: A vision for 2020'. [Online]. Available: http://www.acare4europe.org/sites/acare4europe.org/files/document/Vision%202020_0.pdf. [Accessed: 19-Dec-2014].

[54] 'Aircraft Engine Emissions'. [Online]. Available: http://www.icao.int/environmental-protection/Pages/aircraft-engine-emissions.aspx. [Accessed: 19-Dec-2014].

[55] K. Rajashekara, 'Power Electronics for More Electric Aircraft', in *Power Electronics for Renewable Energy Systems, Transportation and Industrial Applications*, H. Abu-Rub, Riuszlinowski, and K. Al-Haddad, Eds. John Wiley & Sons, Ltd, 2014, pp. 365–386.

[56] J. Clare, 'Examples of More Electric Research in the Aerospace Research Centre'.

[57] J. S. Cloyd, 'Status of the United States Air Force's More Electric Aircraft initiative', IEEE Aerosp. Electron. Syst. Mag., vol. 13, no. 4, pp. 17–22, Apr. 1998.

[58] M. J. J. Cronin, 'The all-electric aircraft', IEE Rev., vol. 36, no. 8, pp. 309–311, Sep. 1990.

[59] A. J. Mitcham and N. Grum, 'An integrated LP shaft generator for the more electric aircraft', in *1998/260), IEE Colloquium on All Electric Aircraft (Digest No*, 1998, pp. 8/1–8/9.

[60] 'Towards More Electric Airplanes', *SAFRAN magazine*, Mar-2008.

[61] K. J. Karimi, 'Future Aircraft Power Systems - Integration Challenges', 2007.

[62] '"POA" – research project works to optimise aircraft power use'. [Online]. Available: http://ec.europa.eu/research/transport/projects/items/_poa____research_project_works_to_optimise_aircraft_power_use_en.htm. [Accessed: 19-Dec-2014].

[63] M. Hirst *et al.*, 'Demonstrating the more electric engine: a step towards the power optimised aircraft', IET Electr. Power Appl., vol. 5, no. 1, pp. 3–13, Jan. 2011.

[64] 'The more electric aircraft: Why aerospace needs power electronics?', in *13th European Conference on Power Electronics and Applications, 2009. EPE '09*, 2009, pp. 1–30.

[65] I. Cotton and A. Nelms, 'Higher voltage aircraft power systems', IEEE Aerosp. Electron. Syst. Mag., vol. 23, no. 2, pp. 25–32, Feb. 2008.

[66] 'F-22 Flight Critical Systems'. [Online]. Available: http://www.globalsecurity.org/military/systems/aircraft/f-22-fcas.htm. [Accessed: 19-Dec-2014].

[67] D. Schlabe and J. Lienig, 'Energy management of aircraft electrical systems – state of the art and further directions', in Electrical Systems for Aircraft, Railway and Ship Propulsion (ESARS), doi: 10.1109/ESARS.2012.6387387

[68] Y. Isik, 'ARINC 629 data bus standard on aircraft',in Proc. 9th Int. Conf. on circuits, systems, electronics, control and signal processing, Athens, Greece, pp. 191-195

[69] 'Boeing: Airplane Health Management: Monitoring the airplane in flight', [Online]. Available: http://www.boeing.com/features/2013/07/bca-airplane-health-mgmt-07-30-13.page. [Accessed: 14-Apr-2015]

[70] 'Airbus and IBM to help aircraft operators optimise fleet management and operations', [Online]. Available: http://www.airbus.com/presscentre/pressreleases/press-release-detail/detail/airbus-and-ibm-to-help-aircraft-operators-optimize-fleet-management-and-operations/. [Accessed: 14-Apr-2015].

[71] 'EMC and functional safety in the Aerospace Industry', IEE Guidance Document, Annex A, pp.1-12

[72] 'Standard Practice for System Safety', MIL-STD-882D, Feb. 2000

[73] 'System Design and Analysis', FAA Advisory Circular AC25-1309-1A, Jun. 1988

[74] 'ETA introduces first remote control circuit breaker to exceed MIL-PRF-83383', [Online]. Available: http://www.automation.com/automation-news/industry/e-t-a-introduces-first-remote-control-circuit-breaker-to-exceed-mil-prf-83383. [Accessed: 16-Apr-2015]

[75] 'Network protection and automation guide, chapter 2: Fundamentals of protection practice', [Online]. Available: http://electrical-engineering-portal.com/download-center/books-and-guides/electrical-engineering/automation-guide. [Accessed: 23-Apr.-2015].

[76] S. Fletcher et al., 'Solid state circuit breakers enabling optimised protection of DC aircraft power systems', in Proc. 14th European Conf. on Power Electronics and Applications, Birmingham, UK, 2011

[77] M. Tooley and D. Wyatt, 'Aircraft electrical and electronic systems: Principles, maintenance and operation', 1st ed., Oxford, UK, Butterworth-Heinemann, 2009, pp.142-146

[78]'Energy based discrimination for low voltage protective devices', [Online]. Available: http://www.schneider-electric.co.uk/documents/technical-publications/en/shared/electrical-engineering/dependability-availability-safety/low-voltage-minus-1kv/ect167.pdf. [Accessed: 23-Apr.-2015].

[79] D.Izquierdo et al., 'Modeling methods for solid state power controllers', in Compatability and power electronics, Badajoz, Spain, 2009, pp. 265-270

[80] M.S. Revely, 'Assessement of the state of the art integrated health management technologies as applicable to damage conditions', NASA, Technical Memorandum 2010-216911, Dec. 2010

[81] B.M. Aucoin et al., 'Detection of incipient and low current faults in electric distribution systems (of spacecraft)', in Proc. of 24th Energy Conversion Eng. Conf., Washington DC, USA, 1989, pp. 153-158

[82] 'Aircraft wiring system integrity issues', [Online]. Available: http://wire.arc.nasa.gov/participating_orgs/RTO%20BF%20on%20Aging%20Wiring%20final%20PA%20approved.pdf. [Accessed: 23-Apr.-2015]

[83] D. Galler and G. Slenski, 'Causes of aircraft failures', IEEE Aerosp. Electron. Syst. Mag, vol.6, no.8, pp.3-8

[84] B.G. Moffat *et al.*, 'Failure mechanisms of legacy aircraft wiring and interconnects', IEEE Trans. Deielctr. Electr. Insul., vol. 15, no. 6, pp. 808-822

[85] G.W. Scott and K.B. Wong, 'Arc fault detection for aircraft', U.S. Patent 6 625 550, Sep. 23, 2003

[86] P.L. Cahill and J.H. Dailey, 'Aircraft electrical wet-wire arc tracking', Fed. Aviation Admin., Atlantic City, NJ, Tech. Rep., DOT/FAA/CT-88/4

[87] S.D.A. Fletcher *et al.*, 'Determination of protection system requirements for DC unmanned aerial vehicle electrical power networks for enhanced capability and survivability', IET Electr. Syst. Transp., vol. 1, no. 4, pp. 137-147

[88] A. Fekih, 'Fault diagnosis and fault tolerant control design for aerospace systems: A bibliographical review', in *American Control Conf.*, Portland, OR, 2014, pp. 1286-1291

[89] R.J. Patton *et al.*, 'Artificial intelligence approaches to fault diagnosis', in *IEE Colloq. on Condition monitoring: Machinery, external structures and health*, London, UK, 1998, doi: 10.1049/ic:19981029

[90] G. Heredia and A. Ollero, 'Virtual sensor for failure detection, identification and recovery in the transition phase of a morphing aircraft', Sensors, vol. 10, no.3, pp. 2188-2201, 2010, doi: 10.3390/s100302188

[91] V. Venkatasubramanian *et al.*, 'A review of process fault detection and diagnosis: Part I: Quantitative model based methods', Comp. and Chem. Eng., vol. 27, no.3, pp. 293-311, Mar. 2003

[92] Y. Zhiang and J. Jiang, 'Bibliographical review on reconfigurable fault-tolerant control systems', Annual Reviews in Control, vol. 32, no. 2, pp. 229-252, Dec. 2008

[93] G. Ducard and H.P. Geering, 'Efficient non-linear actuator fault detection and isolation system for unmanned aerial vehicles', J. of Guidance, Control and Dynamics, vol. 31, no. 1, pp. 225-237, Jan. 2008

[94] Y.M. Zhang and J. Jiang, 'Active fault-tolerant control system against partial actuator failures', IEE Proc. of Cont. Theory and App., vol. 149, no. 1, pp. 95-104, Jan. 2002

[95] D. Shore and M. Bodson, 'Flight testing of a reconfigurable control system on an unmanned aircraft', J. of Guidance, Control and Dynamics, vol. 28, no. 4, pp. 698-707, Jul. 2005

[96] R. Duan and H. Zhou, 'A new fault diagnosis method based on fault tree and Bayesian networks', in *Int. Conf. on Future Electrical Power and Energy Systems*, Madrid, Spain, 2012, pp. 1376-1382

[97] V. Venkatasubramanian *et al.*, 'A review of process fault detection and diagnosis: Part II: Qualitative models and search strategies', Comp. and Chem. Eng., vol.27, no.3, pp. 313-326, Mar 2003

[98] R.J. Patton *et al.*, 'Issues for fault diagnosis for dynamic systems', London, UK, Springer, 2000

[99] P.C. Shutte *et al.*, 'An evaluation of a real-time fault diagnosis expert system for aircraft', in *IEEE Conf. on Decision and Control*, Los Angeles, CA, 1987, pp. 1941-1947

[100] H. Long and X. Wang, 'Aircraft fuel system diagnostic fault detection through expert system', in *World Congr. on Intelligent control and automation*, Chongqing, China, 2008, pp. 7104-7107

[101] M.P. Lishke and K.L. Mayer, 'TEAMS: technical expert aircraft maintenance system', in *Aerospace and Electronics Conf.*, Dayton, OH, 1992, pp. 960-964

[102] K.P. Tripathi, 'A review on knowledge-based expert system: Concept and architecture', Int. J. of Comp. App. Special Issue on Artificial Intelligence Techniques, vol. 4, pp. 19-23, 2011

[103] K.K. Gautam and V. Bhuria, 'Fuzzy logic application in power system fault diagnosis', J. of Comp. Sci. and Eng., vol. 2, no.4, pp. 554-558, Aug. 2011

[104] L.A. Zadeh, 'The role of fuzzy logic in modelling, identification and control', Modelling, Identification and Control, vol. 15, no. 3, pp. 191-203, 1994

[105] H. Wu *et al.*, 'Fault diagnosis expert system for modern commercial aircraft', Aircraft Eng. and Tech., vol. 76, no.4, pp. 398-403, 2004

[106] S. Moziful Islam *et al.*, 'A novel fuzzy logic approach to transformer fault diagnosis', IEEE Trans. Dielectr. Elecr. Insul., vol. 7, no. 2, pp. 177-186, Apr. 2000

[107] Y. Yamashita, 'Qualitative trend analysis for the monitoring of process plant', in *IEEE Int. Conf. on Modeling, Simulation and Applied Optimisation*, Kuala Lumpur, Malaysia, 2011, doi: 10.1109/ICMSAO.2011.5775647

[108] M.R. Mauraya *et al.*, 'Fault diagnosis by qualitative trend analysis of the principal components', Chem. Eng. Research and Design, vol. 83, no. 9, pp. 1122-1132, Sep. 2005

[109] N.H.W Eklund, 'Using synthetic data to train an accurate real-world fault detection system', in *IMACS Multiconf. on Computational Engineering in Systems Applications*, Beijing, China, Oct. 2006, pp. 483-488

[110] C.M. Bishop, 'Pattern recognition and machine learning', New York, Springer, 2006

[111] K.C. Kwon and J.H. Kim, "Accident identification in nuclear power plants using hidden Markov models", Eng. App. of Artificial Intelligence, vol.12, no.4, pp.491-501, Aug.1999

[112] H.M. Ertunc *et al.*, "Tool wear condition monitoring in drilling operations using hidden Markov models (HMMs)", Int. J. of Machine Tools and Manufacture, vol.41, no.9, pp.1363-1384, Jul.2001

[113] W. Khreich *et al.*, "A survey of techniques for incremental learning of HMM parameters", Information Sciences, vol. 197, pp. 105-130, Aug. 2012

[114] C.H. Lo, 'Bayesian network for fault diagnosis', in *IEEE European Control Conf.*, Cambridge, UK, Sep. 2003, pp. 1381-1386

[115] D. Nikovski, 'Constructing Bayesian networks for medical diagnosis from incomplete and partially correct statistics', IEEE Trans. Knowl. Data. Eng., vol. 12, no. 4, pp. 509-516, Jul. 2000

[116] J. Zhu, 'Intelligent condition diagnosis method for rotating machinery using relative ratio symptom parameter and Bayesian network' in *Int. Symp. on Signals Systems and Electronics*, Nanjing, China, doi: 10.1109/ISSSE.2010.5607088

[117] Y. Huang *et al.*, 'Probability based fault diagnosis: Bayesian network method', J. of Intelligent Manufacturing, vol. 19, no. 3, pp. 301-311, Jan. 2008

[118] T. Sorsa and H.N. Koivo, 'Application of artificial neural networks in process fault diagnosis', Automatica, vol. 29, no. 4, pp. 843-849, 1993

[119] S. Khomofi and L.M. Tolbert, 'Fault diagnostic system for a multilevel inverter using a neural network', IEEE Trans. Power Electron., vol. 22, no. 3, pp. 1062-1069, May 2007

[120] I. Dabbaghchi *et al.*, 'AI application areas in power systems', IEEE Expert, vol. 12, no. 1, pp. 58-66, Jan. 1997

[121] C.J.C. Burges, 'A tutorial on support vector machines for pattern recognition', Data Mining and Knowledge Discovery, vol. 2, no. 2, pp. 121-167, 1998

[122] U.B. Parikh *et al.*, 'Combined wavelet-SVM technique for fault zone detection in a series compensated transmission line', IEEE Trans. on Power Del., vol. 23, no. 4, pp. 1789-1794, Oct. 2008

[123] J. Ni *et al.*, 'An adaptive approach based on KPCA and SVM for real-time fault diagnosis of HVCBs', IEEE Trans. on Power Del., vol. 26, no. 3, pp. 1960-1971, Jul. 2011

[124] M. Sarlak and S.M. Shahrtash, 'SVM based method for high impedance fault detection in distribution networks', Int. Journal for Comp. and Math. in Electr. And Electronic Eng., vol. 30, no. 2, pp. 431-450, 2011

[125] J. Lee *et al.*, 'Prognostics and health management design for rotary machine systems – Reviews, methodology and applications', Mechanical Systems and Signal Processing, vol. 42, no. 1-2, pp. 314-334, Jan. 2014

[126] S.B. Kostiris *et al.*, 'Machine learning: A review of classification and combining techniques', Artificial Intelligence Rev., vol. 26, no. 3, pp. 159-190, 2006

[127] L. Rabiner and B.H. Juang, 'An introduction to hidden Markov models', IEEE ASSP Mag., vol. 3, no. 1, pp. 4-16, Jan. 1986

[128] M.J. Roemer *et al.*, 'Assessment of data and knowledge fusion strategies for prognostics and health management', in *IEEE Proc. of Aerospace Conf.*, Big Sky, MT, 2001, pp. 2979-2988

[129] H. Bhavsar and A. Ganatra, 'A comparative study of training algorithms for supervised machine learning', J. of Soft Computing and Eng., vol. 2, no. 4, Sep. 2012

[130] C.Doll *et al.*, 'IMMUNE project: An overview', in *Proc. of Automatic Control in Aerospace Symp.*, Nara, Japan, Sep. 2010, pp. 434-439

[131] W. Yin *et al.*, 'A SVM based multiple faults classification scheme design in flight control FDI system', in *Int. Conf. on Innovative Computing, Information and Control*, Kunamoto, Japan, 2007, doi: 10.1109/ICICIC.2007.100

[132] D. Berdjag *et al.*, 'Fault detection and isolation for redundant aircraft sensors', in *Conf. on Control and Fault-Tolerant Systems*, Nice, France, pp. 137-142

[133] M. Jayakumpur and B.B. Das, 'Isolating incipient sensor faults and system reconfiguration in a flight control actuation system', Proc. of the Inst. of Mechanical Engineers, Part G: J. of Aerosp. Eng., vol. 224, no. 1, pp. 101-111, 2010

[134] D. Dasgupta *et al.*, 'Negative selection algorithm for aircraft fault detection', in *Artificial Immune Systems*, Berlin, Germany: Springer, 2004

[135] F. Bateman *et al.*, 'Fault Diagnosis and fault-tolerant control strategy for the aerosonde UAV', IEEE Trans. Aerosp. Electron. Syst., vol.47, no.3, pp. 2119-2137, 2011

[136] J. Marzat *et al.*, 'Model based fault diagnosis for aerospace systems: A survey', Proc. of the Inst. of Mechanical Engineers, Part G: J. of Aerosp. Eng., doi: 10.1177/0954410011421717

[137] S. Poll *et al.*, 'Evaluation, selection and application of model-based diagnosis tools and approaches', in *Proc. of American Institute of Aeronautics and Astronautics Infotech*, Rohnert Park, CA, 2007

[138] T. Kurtoglu *et al.*, 'Benchmarking diagnostic algorithms on an electrical power system testbed' in *Proc. of Prognostics and Health Management Conf.*, San Diego, CA, 2009

[139] S. Poll *et al.*, 'Second International Diagnostic Competition – DXC'10', in *Proc. of Prognostics and Health Management Conf.*, Portland, OR, 2010

[140] M.J. Daigle *et al.*, A comprehensive diagnosis methodology for complex hybrid systems: A case study on spacecraft power distribution systems', IEEE Trans. Syst. Man Cybernet. A., Syst. Humans, vol. 40, no. 5, pp. 917-931, Sep. 2010

[141] S. Narasimhan and L. Brownston, 'HyDE – A general framework for stochastic and hybrid model based diagnosis', in Proc. of Principles on Diagnosis, Nashville, TN, 2007, pp. 186-193

[142] D. Gorinevsky *et al.*, 'Estimation of faults in DC electrical power system', in *American Control Conf.*, St. Louis, MO, Jun. 2009, pp. 4334-4339

[143] J. De Kleer and B.C. Williams, 'Diagnosing multiple faults', Artificial Intelligence, vol. 32, no. 1, pp. 97-130, 1987

[144] K. Keller *et al.*, 'Aircraft electrical power systems prognostics and health management', in *IEEE Aerospace Conf.*, Big Sky, MT, Mar. 2006, doi: 10.1109/AERO.2006.1656087

[145] Z. Liu *et al.*, 'Intelligent built-in test fault diagnosis based on wavelet analysis and neural networks', in *World Congr. on Intelligent Control and Automation*, Dalian, China, Jun. 2006, pp. 5610-5614

[146] D.W. Richards, 'Smart BIT: A plan for intelligent built-in test', IEEE Aerosp. Electron. Syst. Mag., vol. 4, no. 1, pp. 26-29, Jan. 1989

[147] J.B. Cao *et al.*, 'Design of fault diagnosis expert system for certain types of aircraft electrical power', Advanced Materials Research, vol. 466-467, pp. 1186-1190, Feb. 2012

[148] L. Liu *et al.*, 'Fault detection, diagnostics and prognostics: Software agent solutions', IEEE Trans. Veh. Technol., vol. 56, no. 4, pp. 1613-1622, Jul. 2007

[149] W. Li *et al.*, 'Fault detection and classification in medium voltage DC shipboard power systems with wavelets and artificial neural networks', IEEE Trans. Instrum. Meas., vol. 63, no. 11, pp. 2651-2665, Nov. 2014

[150] N.K. Chanda and Y. Fu, 'ANN-based fault classification and location in MVDC shipboard power systems', in *North American Power Symp.*, Boston, MA, Aug. 2011, doi: 10.1109/NAPS.2011.6025172

[151] E. Christopher *et al.*, 'Fault location in a zonal DC marine power system using active impedance estimation', IEEE Trans. Ind. Appl., vol. 49, no. 2, pp. 860-865, Mar. 2013

[152] A.J. Gonzalez *et al.*, 'Model-based, real-time control of electrical power systems', IEEE Trans. Syst. Man Cybernet. A., Syst. Humans, vol. 26, no. 4, pp. 470-482, Jul. 1996

[153] M.E. Baran and N.R. Mahajan, 'Overcurrent protection on voltage-source-converter based multi-terminal DC distribution system', IEEE Trans. Power Del., vol. 22, no. 1, pp. 406-412, Jan. 2007

[154] O. Rashid *et al.*, 'A framework for the integration of gesture and posture recognition using HMM and SVM', in *Proc. IEEE Conf. on Intelligent Computing and Intelligent Systems*, Shanghai, China, Nov. 2009, pp. 572-577

[155] A.D. Kenyon *et al.*, 'An agent-based implementation of hidden Markov models for gas turbine condition monitoring', IEEE Trans. Syst. Man Cybernet. A., Syst. Humans, vol. 44, no. 2, pp. 186-195, Feb. 2014

[156] R.X. Gao and R.Yan, 'From Fourier Transform to Wavelet Transform: a historical perspective' in *Wavelets: Theory and Applications for Manufacturing*, Springer Science, 2011, ch. 2, pp. 17-32

[157] B. Stephen *et al.*, 'The use of hidden Markov models for anomaly detection in nuclear core condition monitoring', IEEE Trans. Nucl. Sci., vol. 56, no. 2, pp. 453-461, Apr. 2009

[158] N. Perera and A.D. Rajapakse, 'Development and hardware implementation of a fault transients recognition system', IEEE Trans. Power Deliv., vol. 27, no. 1, pp. 40-52, Jan. 2012

[159] J. Chung *et al.*, 'Power disturbance classifier using a rule based method and wavelet packet-based hidden Markov model', IEEE Trans. Power Deliv., vol. 17, no. 1, pp. 233-241, Jan. 2002

[160] M. Jannati *et al.*, 'A novel algorithm for fault type fast diagnosis in overhead transmission lines using hidden Markov models', J. of Electr. Eng. and Technol., vol. 6, no. 6, pp. 742-749, 2011

[161] L.E. Baum and T. Petrie, 'Statistical inference for probabilistic functions of finite state Markov chains', Ann. Math. Statist., vol. 37, no. 6, pp. 1554-1563, 1966

[162] F. Jelinek, 'Continuous speech recognition by statistical methods', Proc. IEEE, vol. 64, no. 4, pp. 532-556, Apr. 1976

[163] 'The wavelet tutorial', [Online]. Available: http://person.hst.aau.dk/enk/ST8/wavelet_tutotial.pdf [Accessed: 16-Jul-2015]

[164] J. Xu *et al.*, 'PHM-oriented integrated fusion prognostics for aircraft engines based on sensor data', IEEE Sensors J., vol. 14, no. 4, pp. 1124-1132, Apr. 2014

[165] R.F. Ammerman *et al.*, 'DC arc models and incident-energy calculations', IEEE Trans. Ins. App., vol. 46, no.5, pp.1810-1819, Sep. 2010

[166] A. Parizad *et al.*, 'Optimization of arc model parameters using genetic algorithm', in Int. Conf. on Electric power and energy conversion, Sharjah, UAE, 2009

[167] 'Electric Arc – properties of the arc'. [Online]. Available: http://science.jrank.org/pages/2295/Electric-Arc-Properties-arc.html. [Accessed: 05-May-2015].

[168] F. Dricot and H.J. Reher, 'Survey of arc tracking on aerospace cables', IEEE Trans. Dielectr. Electr. Insul., vol.1, no.5, pp. 896-903, Oct. 1994

[169] V.V. Terzija and H.J. Koglin, 'On the modelling of long arc in still air and arc resistance calculation', IEEE Trans. Power Del., vol.19, no.3, pp. 1012-1017, Jul. 2004

[170] D. Li, 'A method for residential series arc fault detection and identification', in Proc. of IEEE conf. on Electrical Contacts, Vancouver, BC, 2009, pp. 8-14

[171] F.M. Uriarte, 'A DC arc model for series faults in low voltage microgrids', IEEE Trans. Smart Grid, vol.3, no.4, pp2063-2070, Dec. 2012

[172] K. Koziy *et al.*, 'A low cost power-quality meter with series arc fault detection capability for smart grid', IEEE Trans. Power Del., vol. 28, no. 3, pp. 1584-1591, Jul. 2013

[173] P. Muller *et al.*, 'Characteristics of series and parallel low current arc faults in the time and frequency domain', in Proc. of IEEE conf. on Electrical Contacts, Charlestown, SC, 2010, doi: 10.1109/HOLM.2010.5619539

[174] X. Yao, 'A series DC arc fault detection method and hardware implementation', in IEE Applied Power Electronics Conf. and Expo., Long Beach, CA., 2013, pp. 2444-2449

[175] S.Y. Guo *et al.*, 'DC arc detection and prevention circuit and method', U.S. Patent 6 683 766, Jan. 27 2004

[176] C. E. Restrepo, 'Arc fault detection and discrimination methods', in Proc. of IEEE conf. on Electrical Contacts, Pittsburgh, PA, 2007, pp. 115-122

[177] F. Karetta and M. Lindmayer, 'Simulation of the gas dynamic and electromagnetic processes in low voltage switching arcs', IEEE Trans. Compon. Packag. Manuf. Technol., vol. 21, pp. 96-103, Mar. 1998

[178] J. Andrea *et al.*, 'A new DC and AC arc fault electrical model', in Proc. of IEEE conf. on Electrical Contacts, Charlestown, SC, 2010, doi: 10.1109/HOLM.2010.5619541

[179] A.P. Strom, 'Long 60-cycle arcs in air', Trans. Amer. Inst. Elect. Eng., vol. 65, pp. 113-117, Mar. 1946

[180] A.D. Stokes and W.T. Oppenlander, 'Electric arcs in open air', Journal of Physics D: Applied Physics, vol.24, no.1, pp.26-35, Jan. 1991

[181] J. Paukert, 'The arc voltage and arc resistance of LV fault arcs', in Proc. Int. Switching Arc Phenomenon Symp., Lodz, Poland, 1993

[182] P.M. Hall *et al.*, 'Arcing faults on direct trolley systems', in Proc. of Coal Mine Electro technology, Morgantown, WV, 1978, pp. 1-19

[183] M.T. Parker *et al.*, 'Electric arc monitoring systems', U.S. Patent 6 772 0777, Aug. 3 2004

[184] T.E. Browne, 'The electric arc as a circuit element', Journal of the Electrochemical Soc., vol.102, no.1, pp. 27-37, 1955

[185] H. Ayrton, 'The electric arc', Cambridge University Press, 1902

[186] C.P. Steinmetz, 'Transformation of electric power into light', Proc. of Amer. Inst. of Electr. Eng., vol. 25, no.11, pp. 755-779, Nov. 1906

[187] W.B. Nottingham, 'A new equation for the static characteristic of the normal arc', Amer. Inst. of Electr. Eng., vol. 42, no.1, pp. 12-19, Jan. 1923

[188] F.M. Uriarte *et al.*, 'Development of a series fault model for DC microgrids', in IEEE Innovative Smart Grid Technologies, Washington D.C., 2012 doi: 10.1109/ISGT.2012.6175802

[189] 'DC arc fault'. [Online]. Available: https://www.utexas.edu/research/cem/dc_arc.html. [Accessed: 06-May-2015].

[190] J. Li *et al.*, 'DC series arc generation and characteristic and modelling with arc demonstrator and shaking table', in Int. Conf. on Developments in Power System Protection, Copenhagen, Denmark, doi: 10.1049/cp.2014.0129

[191] 'Outline of investigation for photovoltaic (PV) DC arc fault circuit protection' Underwriters Laboratories 1699B, 2013

[192] J. Johnson and K. Armijo, 'Parametric study of PV arc-fault generation methods and analysis of conducted DC spectrum', in Photovoltaic Specialist Conf., Denver, CO., 2014, pp. 3543-3548

[193] G. Liu *et al.*, 'A survey on arc fault detection and wire fault location for aircraft wiring systems', SAE Int. Journ. Aerosp., vol.1, no. 1, pp. 903-914, Jan. 2008

[194] G. Friberg and G.J. Pietsch, 'Calculation of pressure rise due to arcing faults', IEEE Trans. Power Del., vol. 14, no.2, pp. 365-370, Apr. 1999

[195] T.S. Sidhu *et al.*, 'Microprocessor based instrument for detecting and locating electric arcs', IEEE Trans. Power Del., vol. 13, no.4, pp. 1079-1085, Oct. 1998

[196] H.B. Land, 'Sensing switchboard arc faults', IEEE Power Eng. Rev., vol.22, no.4, pp. 18-27, Apr. 2002

[197] R.A. Bax, 'Aircraft applicable current imbalance detection and circuit interrupter and packaging thereof', US Patent 6 618 229, Sep. 9, 2003

[198] E.C. Senger *et al.*, 'Broken conductors protection system using carrier communication', IEEE Trans. Power Del., vol. 15, no.2, pp. 525-530, Apr. 2000

[199] C.V. Pellon *et al.*, 'Low cost arc fault detection technique', US Patent 7 400 481, Jul. 15, 2008

[200] J.C. Zeurcher and D.L. McClanahan, 'Apparatus and method for real-time determination of arc fault energy, location and type', US Patent 7 068 045, Jun. 27, 2006

[201] F.K. Blades, 'Series arc fault diagnostic for aircraft wiring', US Patent 6 882 158, Apr. 19, 2005

[202] D.G. Kilroy and W.H. Oldenburg, 'DC arc fault detection and protection' US Patent 2007/0 133 135, Dec. 5, 2006

[203] J. Andrea *et al.*, 'Principle of arc fault detection for solid state power controller', in IEEE Conf. on Electrical Contacts, Portland, OR., 2012, doi: 10.1109/HOLM.2012.6336556

[204] D. Lazarovich *et al.*, 'Arc fault detection for SSPC based electrical power distribution systems', US Patent 7 1777 125, Feb. 13, 2007

[205] C. Xiaochen *et al.*, 'AC arc fault detection based on Mahalanobis distance', in Power Electronics and Motion Control Conf., Novi Sad, Serbia, 2012, doi: 10.1109/EPEPEMC.2012.6397333

[206] W.H. Kwon *et al.*, 'High impedance fault detection utilizing incremental variance of normalized even order harmonic power', IEEE Trans. Power Del., vol. 6, no. 2, pp. 557-564, Apr. 1991

[207] A.R. Sedighi *et al.*, 'High impedance fault detection based on wavelet transform and statistical pattern recognition', IEEE Trans. Power Del., vol. 20, no. 4, pp. 2414-2421, Oct. 2005

[208] M. Michalik *et al.*, 'High impedance fault detection in distribution networks with use of wavelet based algorithm', IEEE Trans. Power Del., vol. 21, no. 4, pp. 1793-1802, Oct. 2006

[209] A.A. Girgis *et al.*, 'Analysis of high-impedance fault generated signals using a Kalman filter approach', IEEE Trans. Power Del., vol. 5, no. 4, pp. 1714-1724, Nov. 1990

[210] I. Nikoofekr *et al.*, 'Detection and classification of high impedance faults in power distribution networks using ART networks', in Iranian Conf. on Electrical Engineering, Mashhad, Iran, 2013, doi: 10.1109/IranianCEE.2013.6599760

[211] C.J. Kim and B.D. Russell, 'High impedance fault detection system using an adaptive element model', IEE Proc. C: Gen., Trans. and Dist., vol. 140, no. 2, pp. 153-159, Mar. 1993

[212] A. Yaramasu *et al.*, 'Aircraft electrical system intermittent arc fault detection and location', IEEE Trans. Aerosp. Electron. Syst., vol. 51, no. 1, pp. 40-51, Jan. 2015

[213] M. Dargatz and M. Fornage, 'Method and apparatus for detection and control of dc arc faults', U.S. Patent 8 179 147, May 15, 2012

[214] J. Zeurcher *et al.*, 'Detection of arcing in dc electrical systems' U.S. Patent 2004/0 027 749, Feb. 12, 2004

[215] H. Kojori, 'Method and apparatus for generalized arc fault detection', U.S. Patent 2006/ 0 203 401, Sep. 14, 2006.

[216] Y. Ohta and H. Isoda, 'Arc detecting device and aircraft equipped therewith', E.U. Patent 2 120 306, Nov. 18, 2009

[217] J.A. Momoh and R. Button, 'Design and analysis of aerospace dc arcing faults using fast Fourier transformation and artificial neural network', in IEEE Power Eng. and Soc. General Meeting, Toronto, Canada, 2003, doi: 10.1109/PES.2003.1270407

[218] L. Yuan *et al.*, 'Simulation of fault arc using conventional arc models', Energy and Power Eng., vol. 5, no. 4, pp. 833-837, Jul. 2013

[219] X. Yao *et al.*, 'Characteristic study and time-domain discrete wavelet transform based hybrid detection of series DC arc fault', IEEE Trans. Power Electron., vol. 29, no. 6, pp. 3103-3115, Jun. 2014

[220] D. Saxena *et al.*, 'Power quality event classification: an overview and key issues', Int. Jour. of Eng. Sci. and Tech., vol.2, no.3, pp. 186-199, 2010

[221] G. Yunmei *et al.*, 'Wavelet packet analysis applied in detection of low voltage dc arc fault', in IEEE Conf. on Industrial Electronics and Applications, Xi'an, China, 2009, pp. 4013-4016

[222] J.W. Cooley *et al.*, 'Application of the fast Fourier transform to computation of Fourier integrals, Fourier series and convolution integrals', IEEE Trans. Audio Electroacoust., vol.15, no.2, pp. 79-84, Jun. 1967

[223] G.D. Forney Jr., 'The Viterbi algorithm', Proc. IEEE, vol. 61, no. 3, pp. 268-278, 1973

[224] T.P. Minka, 'Automatic choice of dimensionality for PCA', MIT Laboratory Perceptual Computing Section, Tech. Rep. 514, 2000

[225] W. Khreich *et al.*, 'A survey of techniques for incremental learning of HMM parameters', Inf. Sci., vol. 197, pp. 105-130, 2012

[226] 'Machine learning, Part II: Supervised and unsupervised learning', [Online]. Available: http://www.aihorizon.com/essays/generalai/supervised_unsupervised_machine_learning.htm. [Accessed: 16-Jul-2015]

[227] 'SimPowerSystems: Model and simulate electrical power systems', [Online]. Available: http://uk.mathworks.com/products/simpower/?refresh=true. Accessed [16-Jul-2015].

[228] 'Wavelet toolbox', [Online]. Available: http://uk.mathworks.com/products/wavelet/?refresh=true [Accessed: 24-Jul-2015]

[229] 'Diodes, Rectifiers and Power Supplies', [Online.] Available: http://uav.ece.nus.edu.sg/~bmchen/courses/EG1108_Rectifiers.pdf. [Accessed: 24-Jul-2015]

[230] Z. Wang *et al.*, 'Arc fault signal detection – Fourier transformation vs. wavelet decomposition techniques using synthesized data', in Photovoltaic Specialist Conf., Denver, CO, 2014, pp. 3239-3244

[231] 'Moving Averages – Simple and Exponential', [Online.] Available: http://stockcharts.com/school/doku.php?id=chart_school:technical_indicators:moving_averages [Accessed: 24-Jul-2015]

[232] 'Likelihood Ratio Test', [Online.] Available: http://uk.mathworks.com/help/econ/lratiotest.html#bt1v951-3 [Accessed: 24-Jul-2015]

[233] X. Hu *et al.*, 'Multivariate change detection for time series data in aircraft engine fault diagnostics', in *IEEE Int. Conf. on Systems, Man and Cybernetics*, Montreal, Canada, Oct. 2007, pp. 2484-2489

[234] 'Field Programmable Gate Array (FPGA)', [Online.], Available: http://www.xilinx.com/training/fpga/fpga-field-programmable-gate-array.htm [Accessed: 24-Jul-2015]

[235] 'Mobile Vibration System', [Online.] Available: http://www.copernicustechnology.com/index.php/products/mobile-vibration-system-copernicus-technology [Accessed: 24-Jul-2015]

APPENDIX A: SIMULINK MODELS

A description of the Simulink based models used throughout the work of this thesis. Section A.1 describes the sustained series arc fault model developed for generation of synthetic fault data and Section A.2 describes the intermittent series arc fault model. Section A.3 describes the DC network model used in Case Study 2 and Section A.4 describes the DC network model used in Case Study 3.

A.1 Sustained Series Arc Fault Model

Figure A-1 illustrates the referenced fault model block. This block can be implemented within any *SimPowerSystems* parent model, providing the +VE, GND and –VE terminals are properly connected.

The referenced model block should be implemented in series with electrical loads - the –VE port should NOT be connected directly to modelled ground/neutral return.

The first layer in the model hierarchy is illustrated in Figure A-2. User defined variable *Fault Time* determines simulation time, in seconds, of fault onset. There is zero voltage across +VE and –VE ports prior to fault onset i.e. there is an ideal conductor between source and load.

At onset, voltage between the +VE and –VE port begins to increase – this voltage effectively models a gap in the conductor, with the +VE port representing the positive electrode and the –VE port representing the negative electrode. The voltage between the two electrodes, V_{gap}, increases at arc fault onset.

There are five distinct subsystems that determine V_{gap}, summarised as follows:
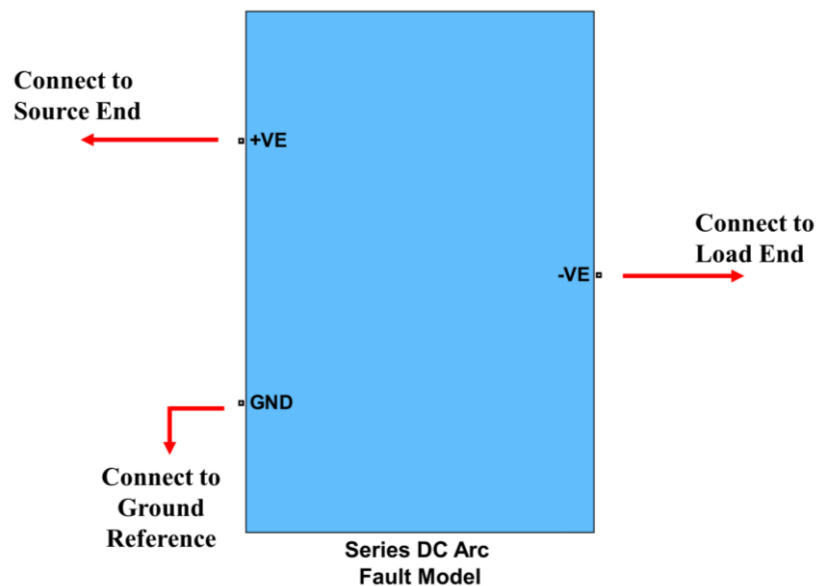
Figure A-1: Referenced series DC arc fault model
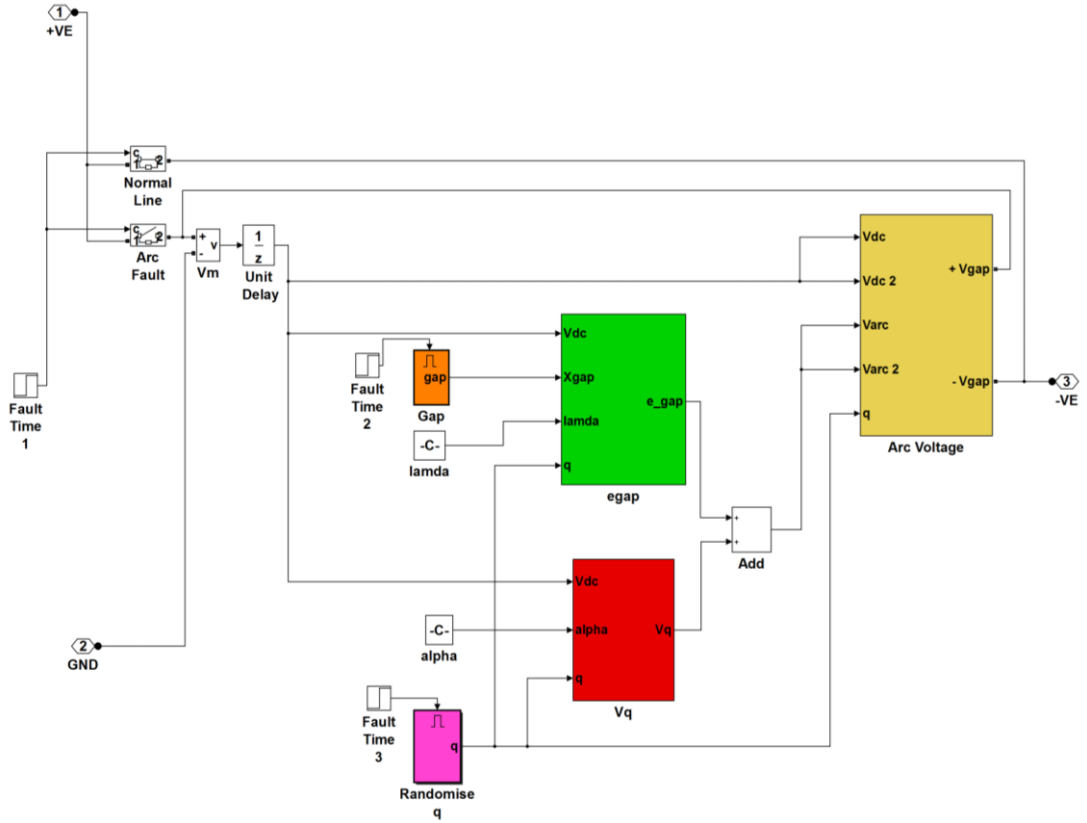
Figure A-2: First layer of hierarchical series DC arc fault model

A.1.1 Gap

Increments the electrode gap distance, X_{gap}, in mm/s. Sub-system enabled at *Fault Time,* with initial value of $X_{gap} = 0$. The rate of increase is determined by the following user inputs.

User Inputs

- *Gap* – Constant, G, that determines speed of electrode gap separation. X_{gap} is incremented at each simulation step and is a product of G and the elapsed time since fault onset, F_{time}

$$X_{gap} = G \times F_{time}$$

(A.1)

    where

$$F_{time} = \frac{Time\ Since\ Fault\ Onset}{Simulation\ Time\ Step}$$

(A.2)

- *Gap Dwell* – Constant that determines distance at which electrode gap is fixed. The electrode gap dwells at a pre-determined distance for fixed distance faults - conditional logic is used at each simulation step to determine whether electrode gap > predetermined distance.

218

- X_{gap}

A.1.2 Randomise q

This sub-system models the distance ratio, q. Sub-system enabled at *Fault Time*, with a random initial value, q_{init}, where $0 \leq q_{init} \leq 1$. q randomly increases incrementally (q_{inc}) from q_{init} at each simulation time-step. Also, random spikes, q_{rand}, are added to q at each time-step to model unsuccessful arc quenches, where $0 \leq q_{rand} \leq 1$. Accordingly:

$$q_i = q_{i-1} + q_{inc} + q_{rand}$$

(A.3)

where i is the ith time step from *Fault Time*.

When $i = 1$,

$$q = q_{init} + q_{inc} + q_{rand}$$

(A.4)

Sub-system Outputs

- q

A.1.3 e_{gap}

This sub-system models the step function, e_{qgap}. The function contributes to arc voltage, V_{arc}, and is described in Chapter 5, section $(5.3.1.1)$[14].

Sub-system Inputs

- X_{gap} – Electrode gap distance
- q – Distance ratio
- V_{dc} – DC supply voltage magnitude
- $Lamda, \lambda$ – This user-defined constant determines the rate at which the slope of the step function rises (see (A.2) for typical values).

Sub-system Outputs

- e_{gap}

---

[14] In Chapter 4, V_{gap} is used as opposed to V_{arc} – strictly speaking, V_{arc} should be used as V_{gap} is equal to equal to open circuit V_{dc} upon arc extinction (see (A.1.5))

A.1.4 V_q

This sub-system models the hyperbolic tangent function, V_q. The function contributes to V_{arc} and is described in Chapter 5, Section (5.3.1.1).

Sub-system Inputs

- V_{dc} – DC supply voltage magnitude
- *Alpha,* α – This constant determines the effect of distance ratio q on V_q. Higher values of α increase voltage disparity between low and high values of q. α is approximated by:

$$\alpha = \left(\frac{-1}{2}\right) ln\left(\frac{R_{closed}I_{load}}{V_{dc}}\right) \tag{A.5}$$

  Where R_{closed} is impedance when $X_{gap} = 0$ (R_{closed} is $\approx 0.001\Omega$ and is relative to the closed-state impedance of a circuit breaker) and I_{load} is the nominal load current.
- q – Distance ratio

Sub-system Outputs

- V_q

A.1.5 Arc Voltage

This sub-system uses conditional logic to determine if the arc has extinguished, and hence the magnitude of voltage across the electrode gap, V_{gap}. The sub-system executes the following:

while $q_i < 1$
  $V_{gap} = V_{arc}$
break
end
  $V_{gap} = V_{dc}$

   This logic is used to determine if $q < 1$ at each time step after fault onset; if this is true, the arc is still burning, $V_{gap} = V_{arc}$, and voltage continues to dynamically change. At the point in time where q is greater than or equal to one, the arc has extinguished, the gap is an open circuit, and $V_{gap} = V_{dc}$ for the remainder of the simulation time.

   A controlled voltage source block is used to model V_{gap}.

Sub-system Inputs

- V_{dc} – DC supply voltage magnitude
- V_{arc} – This is the combination of e_{gap} and V_q where $V_{arc} = e_{gap} + V$

- V_{gap} − Voltage across the electrode gap

A.1.6 Model Parameters

Model parameters for the sustained series DC arc fault model are summarised in Table A-1.

Table A-1: Summary of model parameters

Parameter	Description	Value (Typical)
q_{init}	Initial Value of distance ratio	Random number between 0 and 1
q_{inc}	Increments distance ratio at each time step	Random number that depends on sample time (between 0 and 0.001 for 0.01s sample)
q_{rand}	Additional random value to distance ratio	Random number between 0 and 1
Fault Time	Time of arc fault onset	User defined (in seconds)
V_{arc}	Arc voltage	Sum of e_{gap} and V_q
α	Determines the effect of V_q across different distance ratios	Approximated by eq. (A.5)
X_{gap}	Electrode gap distance	Determined by G and sample time
G	Constant that determines speed of electrode gap separation	User Defined
Gap Dwell	Constant that determines distance at which electrode gap remains constant	User Defined (in mm)
V_q	Hyperbolic tangent contribution to V_{arc}	Defined in Chapter 5, eq. (5.4)
e_{gap}	Step function contribution to V_{arc}	Defined in Chapter 5, eq. (5.5)
λ	Determines rate step function rises	User Defined (nominal value of 100)
V_{dc}	DC supply voltage magnitude	Dependent on implementation
I_{load}	Nominal load current magnitude	Dependent on implementation
R_{closed}	Gap Impedance when $X_{gap} = 0$	0.001Ω (typical impedance of closed CB)

A.2 Intermittent Series Arc Fault Model

The intermittent arc fault model is an extension of the sustained arc fault model. The main design of the intermittent model is identical to the sustained model with the exception of some additional functionality to model fault intermittency. Figure A-3 outlines design of the intermittent fault model and highlights this additional functionality.
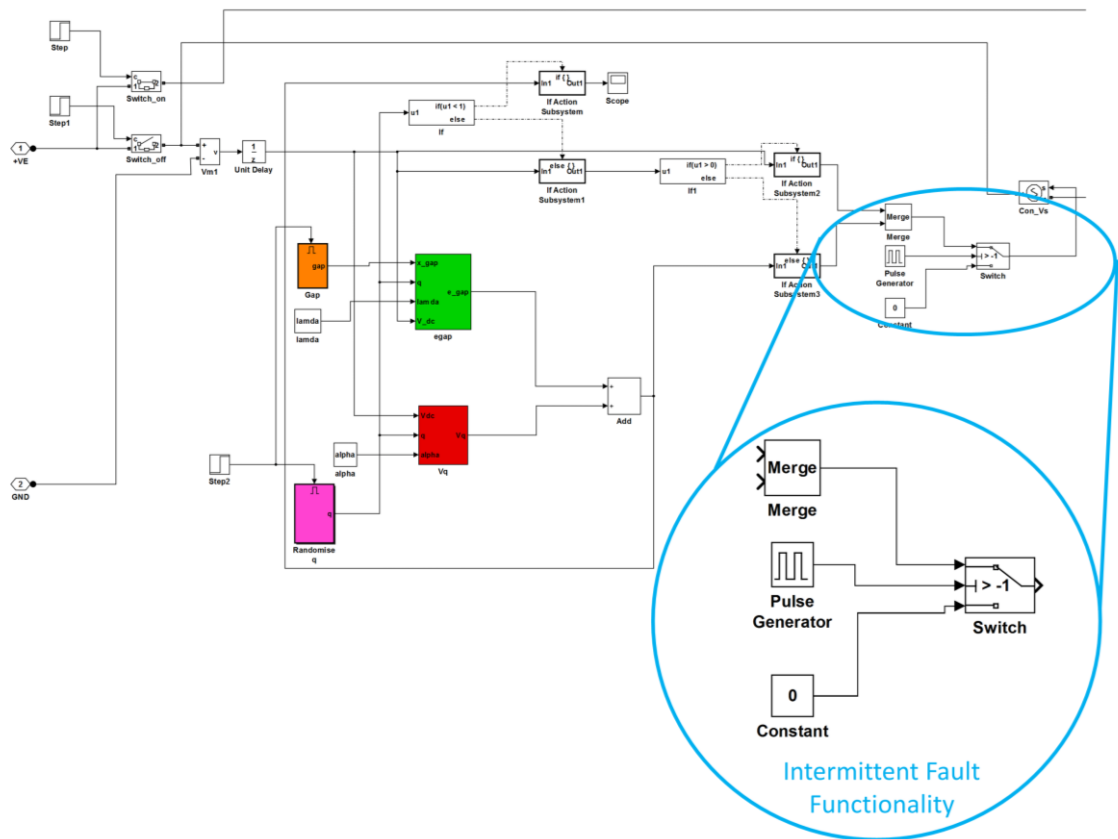
Figure A-3: Intermittent Series Arc Fault Model.

The additional functionality that enables modelling of fault intermittency includes Simulink switch and pulse generator blocks. The output of the switch block is conditional on the pulse generator block: if the output of pulse generator block is greater than a threshold specified in the switch block, the modelled arc voltage, V_{gap}, is equal to V_{arc}; otherwise, V_{gap} is zero. This method allows fault intermittency to be determined by the pulse generator block i.e. the period where the pulse is greater than the threshold is when an arc fault is present and the period where the pulse is less than a threshold is when no fault is present.

The block parameters outlined in Table A-2 are required to provide this functionality.

Table A-2: Parameters of additional blocks for modelling intermittent faults.

Parameter	Description	Value
Pulse Generator Block		
Amplitude	Amplitude of the pulse signal. This must be set to a negative value.	-1
Pulse Type	Time based as opposed to sample based.	Time Based
Time		Use Simulation Time
Period	Total period of pulse.	User Defined (ms)
Pulse Width (%)	Determines period of each intermittent fault event	User Defined (ms)
Phase Delay (secs)	Determines delay of block from beginning of simulation time. This must be set to equal the time of intermittent fault onset.	*Fault Time* (s)
Switch Block		
Threshold	Used to determine whether Input 1 or Input 2 should be passed to the Output.	-1
Criteria for Passing Input 1	Set threshold criteria	Input 2 > Threshold
Input 1	Input 1 to the Switch block.	V_{arc}
Input 3	Input 3 to the Switch block.	0
Input 2	Input 2 to the Switch Block that determines whether arc voltage is V_{arc} or zero.	Connected to Pulse Generator Output.

A.3 Case Study 2 - DC Network Model

Model parameters for the DC network model used in Case Study 2 are summarised in Table
A-3.

Table A-3: Case Study 2 DC network model parameters.

DC Line Impedances	
Resistance	0.641Ω/km
Inductance	0.34mh/km
Capacitance	1mF
Battery	
Type	Lithium-Ion
Nominal Voltage	28V
Rated Capacity	60Ah
Initial State of Charge	100%
Battery Response Time	30s
Current Measurements	
Gaussian noise generator mean value	0
Gaussian noise generator variance	0.0001
Gaussian noise generator sample time	0.001s
Passive Rectifier	
Input Voltage	230VAC
Output Voltage	270VDC
Input Frequency	400Hz
Number of Bridge Arms	3
Snubber Resistance	0.1MΩ
Snubber Capacitance	Inf.
Diode Forward Impedance	1mΩ
Forward Voltage	0.7V
Filter Capacitance	1mF
270/28VDC Buck Converter	
Inductance	250µH
Capacitance	100µF
Switching Frequency	20 kHz
Duty Cycle	0.12
DC Loads	
Load Resistance	Ranged between 2 and 25Ω
Load Inductance	Ranged between 1.25 and 7mH
Load capacitance	Ranged between 0.1 and 7µF
Series Arc Fault Model	
Parameters varied between simulations as described in Section A.1.	
Model Configuration	
Solver	Ode23tb(stiff/TR-BDF2)
Type	Variable-step

Figure A-4 illustrates the model as developed in Simulink.
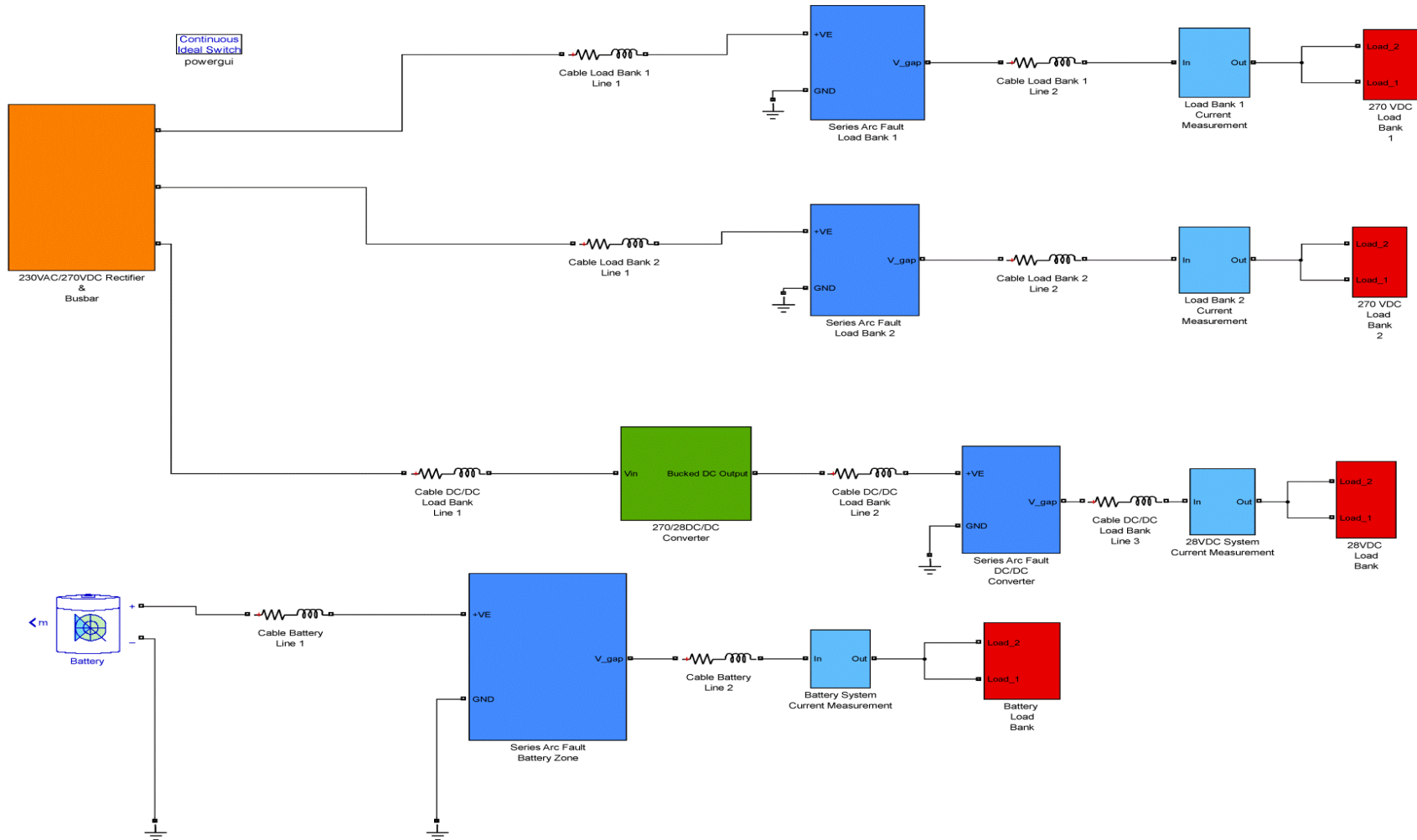
Figure A-4: DC network model used for Case Study 2.

A.4 Case Study 3 - DC Network Model

Model parameters for the DC network model used in Case Study3 are summarised in Table A-4.

Table A-4: Case Study 3 DC network model parameters.

DC Line Impedances	
Resistance	0.641Ω/km
Inductance	0.34mh/km
Capacitance	1mF
Current Measurements	
Gaussian noise generator mean value	0
Gaussian noise generator variance	0.0001
Gaussian noise generator sample time	0.001s
Passive Rectifier	
Input Voltage	230VAC / 115VAC
Output Voltage	270VDC / 28VDC
Input Frequency	400Hz
Number of Bridge Arms	3
Snubber Resistance	0.1MΩ
Snubber Capacitance	Inf.
Diode Forward Impedance	1mΩ
Forward Voltage	0.7V
Filter Capacitance	1mF
DC Loads	
Load Resistance	Ranged between 2 and 25Ω
Load Inductance	Ranged between 1.25 and 7mH
Load capacitance	Ranged between 0.1 and 7μF
Intermittent Series Arc Fault Model	
Parameters varied between simulations as described in Section A.1 & Section A.2.	
Model Configuration	
Solver	Ode23tb(stiff/TR-BDF2)
Type	Variable-step

Figure A-5 illustrates the model as developed in Simulink.
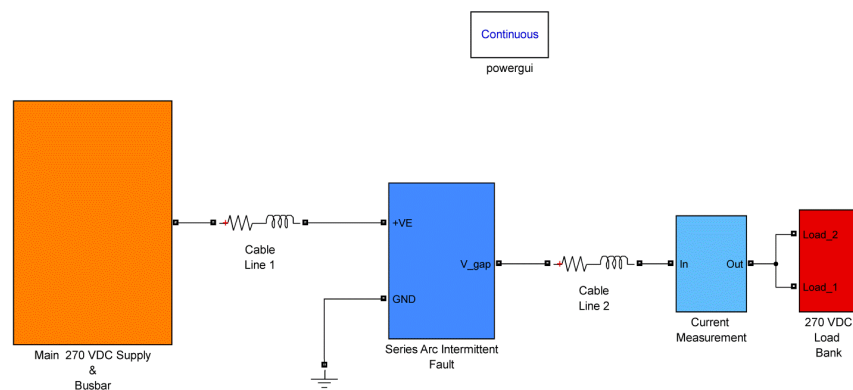
Figure A-5: DC network model used for Case Study 3.

APPENDIX B: INTELARC TESTING – CASE STUDY RESULTS

The complete results of the case studies described in Chapter 6 are presented.

B.1 Case Study 2 Results

NETWORK CONDITION: NO FAULT – NOMINAL CONDITIONS						
Test #	Cable Length (m)	Load Switching Times (s)	Load Switching Levels (W)	Fault Times (s)	IntelArc System Output	Detection Time (s)
1	Z1: 120 Z2: 120 Z3: 135 Z4: 150	Z1: - Z2: - Z3: - Z4: -	Z1: - Z2: - Z3: - Z4: -	Z1: - Z2: - Z3: - Z4: -:	*No Fault*	N/A
2	Z1: 120 Z2: 120 Z3: 135 Z4: 150	Z1: 2 Z2: - Z3: 8 Z4: -	Z1: 391.5 Z2: - Z3: -95.2 Z4: -	Z1: - Z2: - Z3: - Z4: -	*No Fault*	N/A
3	Z1: 120 Z2: 120 Z3: 135 Z4: 150	Z1: 3.53 Z2: - Z3: 8.267 Z4: -	Z1: -405 Z2: - Z3: -143.64 Z4: -	Z1: - Z2: - Z3: - Z4: -:	*No Fault*	N/A
4	Z1: 120 Z2: 120 Z3: 135 Z4: 150	Z1: - Z2: 8.53 Z3: - Z4: 5.66	Z1: - Z2: -729 Z3: - Z4: -46.48	Z1: - Z2: - Z3: - Z4: -	*No Fault*	N/A
5	Z1: 120 Z2: 120 Z3: 135 Z4: 150	Z1: - Z2: 7 Z3: - Z4: 6	Z1: - Z2: 1188 Z3: - Z4: 67.2	Z1: - Z2: - Z3: - Z4: -:	*No Fault*	N/A
6	Z1: 42 Z2: 60 Z3: 78 Z4: 67.5	Z1: 5.253 Z2: 4.126 Z3: - Z4: -	Z1: -108 Z2: -297 Z3: - Z4: -	Z1: - Z2: - Z3: - Z4: -:	*No Fault*	N/A
7	Z1: 42 Z2: 60 Z3: 78 Z4: 67.5	Z1: - Z2: 6.5 Z3: 8.22 Z4: -	Z1: - Z2: 1269 Z3: -13.16 Z4: -	Z1: - Z2: - Z3: - Z4: -	*No Fault*	N/A
8	Z1: 42 Z2: 60 Z3: 78 Z4: 67.5	Z1: 1 Z2: - Z3: - Z4: 5	Z1: -108 Z2: - Z3: - Z4: -46.2	Z1: - Z2: - Z3: - Z4: -	*No Fault*	N/A
9	Z1: 42 Z2: 60 Z3: 78 Z4: 67.5	Z1: 4.2 Z2: 6.5 Z3: 8.22 Z4: 8.1	Z1: 1188 Z2: 567 Z3: 61.04 Z4: 43.4	Z1: - Z2: - Z3: - Z4: -	*No Fault*	N/A
10	Z1: 80 Z2: 60 Z3: 40 Z4: 40	Z1: 1.22 Z2: - Z3: 5.33 Z4: 5.66	Z1: 391.5 Z2: - Z3: 95.48 Z4: -19.6	Z1: - Z2: - Z3: - Z4: -	*No Fault*	N/A
11	Z1: 80 Z2: 60 Z3: 40 Z4: 40	Z1: 1.22 Z2: - Z3: 5.33 Z4: 5.66	Z1: 270 Z2: - Z3: 89.88 Z4: -29.4	Z1: - Z2: - Z3: - Z4: -	*No Fault*	N/A

12	Z1: 80 Z2: 60 Z3: 40 Z4: 40	Z1: 1.22 Z2: - Z3: 5.33 Z4: 5.66	Z1: 256.2 Z2: - Z3: 89.6 Z4: 85.4	Z1: - Z2: - Z3: - Z4: -	*No Fault*	N/A
13	Z1: 80 Z2: 60 Z3: 40 Z4: 40	Z1: 6.24 Z2: 2.54 Z3: 6.95 Z4: 7.83	Z1: -486 Z2: -661.5 Z3: -30.24 Z4: 84	Z1: - Z2: - Z3: - Z4: -	*No Fault*	N/A
14	Z1: 80 Z2: 60 Z3: 40 Z4: 40	Z1: 7.4 Z2: 5.63 Z3: - Z4: -	Z1: -486 Z2: -1188 Z3: - Z4: -	Z1: - Z2: - Z3: - Z4: -	*No Fault*	N/A
15	Z1: 130 Z2: 120 Z3: 110 Z4: 100	Z1: - Z2: - Z3: 6 Z4: 8	Z1: - Z2: - Z3: 69.16 Z4: 84	Z1: - Z2: - Z3: - Z4: -	*No Fault*	N/A
16	Z1: 130 Z2: 120 Z3: 110 Z4: 100:	Z1: - Z2: 4 Z3: 6 Z4: -	Z1: - Z2: 283.5 Z3: -106.4 Z4: -	Z1: - Z2: - Z3: - Z4: -	*No Fault*	N/A
17	Z1: 130 Z2: 120 Z3: 110 Z4: 100	Z1: 5.22 Z2: - Z3: - Z4: -	Z1: 3604 Z2: - Z3: - Z4: -	Z1: - Z2: - Z3: - Z4: -	*No Fault*	N/A
18	Z1: 130 Z2: 120 Z3: 110 Z4: 100:	Z1: - Z2: 7.65 Z3: - Z4: -	Z1: - Z2: -2389.5 Z3: - Z4: -	Z1: - Z2: - Z3: - Z4: -	*No Fault*	N/A
19	Z1: 130 Z2: 120 Z3: 110 Z4: 100:	Z1: - Z2: - Z3: 4.88 Z4: -	Z1: - Z2: - Z3: -175.76 Z4: -	Z1: - Z2: - Z3: - Z4: -	*No Fault*	N/A
20	Z1: 130 Z2: 120 Z3: 110 Z4: 100	Z1: - Z2: - Z3: - Z4: 6	Z1: - Z2: - Z3: - Z4: 161	Z1: - Z2: - Z3: - Z4: -	*No Fault*	N/A
					100% Accurate	

				NETWORK CONDITION: SERIES DC ARC FAULT - ZONE 1			
Test #	Cable Lengths (m)	Load Switching Times (s)	Load Switching Level (W)	Fault Time Onset (s)	Arc Power (W) & Max Detection Time (s)	IntelArc System Output	Detection Time (s)	% of Max Detection Time
1	Z1: 120 Z2: 120 Z3: 135 Z4: 150	Z1: - Z2: - Z3: - Z4: -	Z1: - Z2: - Z3: - Z4: -	Z1: 6 Z2: - Z3: - Z4: -	976.313W & **0.7682s**	*Z1 Fault, 6.35s*	0.35	45.56
2	Z1: 120 Z2: 120 Z3: 135 Z4: 150	Z1: - Z2: 6.5 Z3: 8.25 Z4: -	Z1: - Z2: 567 Z3: 61.6 Z4: -	Z1: 8 Z2: - Z3: - Z4: -	809.684W & **0.9263s**	*Z1 Fault, 8.15s*	0.15	16.19
3	Z1: 120 Z2: 120 Z3: 135 Z4: 150	Z1: - Z2: 6.5 Z3: 8 Z4: -	Z1: - Z2: 270 Z3: -66.4 Z4: -	Z1: 8 Z2: - Z3: - Z4: -	767.314W & **0.9774s**	*Z1 Fault, 8.75s*	0.75	76.73
4	Z1: 120 Z2: 120 Z3: 135 Z4: 150	Z1: 4 Z2: 6.5 Z3: 8.25 Z4: -	Z1: -486 Z2: -918 Z3: -86.8 Z4: -	Z1: 8 Z2: - Z3: - Z4: -	435.243W & **1.7232s**	*Z1 Fault, 8.25s*	0.25	14.51
5	Z1: 120 Z2: 120 Z3: 135 Z4: 150	Z1: - Z2: 6.89 Z3: 8.44 Z4: 7.25	Z1: - Z2: -2943 Z3: -13.16 Z4: -67.2	Z1: 8 Z2: - Z3: - Z4: -	568.196W & **1.32s**	*Z1 Fault, 8.75s*	0.75	56.8
6	Z1: 120 Z2: 120 Z3: 135 Z4: 150	Z1: 5 Z2: 2.1 Z3: 4 Z4: 6	Z1: -918 Z2: 4171.5 Z3: -61.6 Z4: -22.4	Z1: 7 Z2: - Z3: - Z4: -	1221W & **0.6142s**	*Z1 Fault, 7.25s*	0.25	40.7
7	Z1: 120 Z2: 120 Z3: 135 Z4: 150	Z1: - Z2: 6.25 Z3: 8.25 Z4: -	Z1: - Z2: 3658.5 Z3: -52.92 Z4: -	Z1: 8 Z2: - Z3: - Z4: -	910.514W & **0.8237s**	*Z1 Fault, 8.6s*	0.6	72.84
8	Z1: 120 Z2: 120 Z3: 135 Z4: 150	Z1: 3.33 Z2: 6.5 Z3: 7.25 Z4: 6	Z1: -1431 Z2: 999 Z3: -9.24 Z4: 74.2	Z1: 8 Z2: - Z3: - Z4: -	1290.5W & **0.5812s**	*Z1 Fault, 8.1s*	0.1	17.21
9	Z1: 120 Z2: 120 Z3: 135 Z4: 150	Z1: 3.58 Z2: 6.5 Z3: 3.24 Z4: 4.65	Z1: Min* Z2: -499.5 Z3: -66.64 Z4: -11.2	Z1: 8 Z2: - Z3: - Z4: -	1176.6W & **0.6374s**	*Z1 Fault, 8.3s*	0.3	47.07
10	Z1: 120 Z2: 120 Z3: 135 Z4: 150	Z1: - Z2: 6.89 Z3: 5.25 Z4: 4.44	Z1: - Z2: 1944 Z3: -61.6 Z4: Min*	Z1: 8 Z2: - Z3: - Z4: -	1140.4W & **0.6577s**	*Z1 Fault, 8.15s*	0.15	22.81
11	Z1: 120 Z2: 120 Z3: 135 Z4: 150	Z1: 4 Z2: 2.12 Z3: 3.56 Z4: 1.21	Z1: 1782 Z2: -634.5 Z3: -204.96 Z4: 40.6	Z1: 8 Z2: - Z3: - Z4: -	545.887W & **1.3739s**	*Z1 Fault, 8.35s*	0.35	25.47
12	Z1: 120 Z2: 120 Z3: 135 Z4: 150	Z1: 5.23 Z2: 6.13 Z3: 7.11 Z4: 2.69	Z1: -4482 Z2: -1917 Z3: 16.52 Z4: -24.08	Z1: 8 Z2: - Z3: - Z4: -	394.840W & **1.8995s**	*Z1 Fault, 8.1s*	0.1	5.26
13	Z1: 42 Z2: 60 Z3: 78 Z4: 67.5	Z1: 4.4 Z2: 6.5 Z3: 8.25 Z4: -	Z1: 2251.5 Z2: 972 Z3: 68.8 Z4: -	Z1: 7 Z2: - Z3: - Z4: -	499.454W & **1.5016s**	*Z1 Fault, 8.15s*	1.15	76.58

14	Z1: 42 Z2: 60 Z3: 78 Z4: 67.5	Z1: 4.24 Z2: 5.5 Z3: 2.25 Z4: 3.1	Z1: 2538 Z2: -2673 Z3: -178.36 Z4: 58.8	Z1: 7 Z2: - Z3: - Z4: -	346.105W & **2.167s**	*Z1 Fault, 7.4s*	0.4	18.46
15	Z1: 42 Z2: 60 Z3: 78 Z4: 67.5	Z1: 3.25 Z2: 1.12 Z3: - Z4: -	Z1: -1633.5 Z2: 769.5 Z3: - Z4: -	Z1: 7 Z2: - Z3: - Z4: -	269.815 W & **2.7797s**	*Z1 Fault, 7.1s*	0.1	3.598
16	Z1: 42 Z2: 60 Z3: 78 Z4: 67.5	Z1: - Z2: - Z3: 4.42 Z4: 3.2	Z1: - Z2: - Z3: -173.6 Z4: -56	Z1: 7 Z2: - Z3: - Z4: -	384.621 W & **1.95s**	*Z1 Fault, 7.95s*	0.95	48.72
17	Z1: 130 Z2: 120 Z3: 110 Z4: 100	Z1: 5.65 Z2: - Z3: 2.12 Z4: 2.36	Z1: -1093.5 Z2: - Z3: -9.52 Z4: Min*	Z1: 7 Z2: - Z3: - Z4: -	524.422 W & **1.4301s**	*Z1 Fault, 7.25s*	0.25	17.48
18	Z1: 130 Z2: 120 Z3: 110 Z4: 100	Z1: 5.65 Z2: - Z3: 2.12 Z4: 2.36	Z1: -1512 Z2: - Z3: 163.8 Z4: 36.4	Z1: 7 Z2: - Z3: - Z4: -	501.426W & **1.4957s**	*Z1 Fault, 7.1s*	0.1	6.69
19	Z1: 130 Z2: 120 Z3: 110 Z4: 100	Z1: 3.45 Z2: 1.22 Z3: 0.95 Z4: -	Z1: -216 Z2: -1998 Z3: -54.6 Z4: -	Z1: 7 Z2: - Z3: - Z4: -	610.248W & **1.229s**	*Z1 Fault, 7.35s*	0.35	28.48
20	Z1: 130 Z2: 120 Z3: 110 Z4: 100	Z1: - Z2: 4.23 Z3: 5.25 Z4: -	Z1: - Z2: -756 Z3: 45.64 Z4: -	Z1: 7 Z2: - Z3: - Z4: -	1045.5 W & **0.7173s**	*Z1 Fault, 7.3s*	0.3	41.82
21	Z1: 40 Z2: 52 Z3: 35 Z4: 40	Z1: 4.2 Z2: 6.5 Z3: 5 Z4: 9	Z1: -1498.5 Z2: 1026 Z3: 11.48 Z4: 462	Z1: 9 Z2: - Z3: - Z4: -	420.061W & **1.7855s**	*Z1 Fault, 9.75s*	0.75	42
22	Z1: 40 Z2: 52 Z3: 35 Z4: 40	Z1: 5.19 Z2: 4.22 Z3: 6.12 Z4: 8.21	Z1: 310.5 Z2: -494.5 Z3: -15.68 Z4: 291.2	Z1: 9 Z2: - Z3: - Z4: -	459.984W & **1.6305s**	*Z1 Fault, 9.65s*	0.65	47.48
23	Z1: 40 Z2: 52 Z3: 35 Z4: 40	Z1: 5 Z2: 6 Z3: 7.22 Z4: 4.36	Z1: -1755 Z2: -321.3 Z3: 46.76 Z4: 520.8	Z1: 9 Z2: - Z3: - Z4: -	352.478 W & **2.1278s**	*Z1 Fault, 9.6s*	0.6	28.2
24	Z1: 40 Z2: 52 Z3: 35 Z4: 40	Z1: 7 Z2: 8 Z3: 5.2 Z4: 1.24	Z1: -783 Z2: -216 Z3: 18.48 Z4: 53.2	Z1: 9 Z2: - Z3: - Z4: -	379.869W & **1.9744s**	*Z1 Fault, 9.10s*	0.1	5.06
25	Z1: 40 Z2: 52 Z3: 35 Z4: 40	Z1: 7.26 Z2: 4.20 Z3: 7.45 Z4: 6.21	Z1: 2403 Z2: 378 Z3: 80.64 Z4: 229.6	Z1: 9 Z2: - Z3: - Z4: -	397.471W & **1.8869s**	*Z1 Fault, 9.90s*	0.9	47.697
					100% Accurate		**0.428**	**34.1486**

NETWORK CONDITION: SERIES DC ARC FAULT - ZONE 2							
Test #	Cable Length (m)	Load Switching Time (s)	Load Switching Level (W)	Fault Times (s)	Arc Power (W) & Max Detection Time (s)	IntelArc System Output	Detection Time (s)	% of Max Detection Time
1	Z1: 80 Z2: 125 Z3: 60 Z4: 75	Z1: - Z2: - Z3: - Z4: -	Z1: - Z2: - Z3: - Z4: -	Z1: - Z2: 6 Z3: - Z4: -	417.894W & **1.794s**	*Z2 Fault, 6.1s*	0.1	5.57
2	Z1: 80 Z2: 125 Z3: 60 Z4: 75	Z1: 3.5 Z2: 2.22 Z3: - Z4: -	Z1: 1039.5 Z2: -256 Z3: - Z4: -	Z1: - Z2: 7 Z3: - Z4: -	550.983W & **1.3612s**	*Z2 Fault, 7.3s*	0.3	22.04
3	Z1: 80 Z2: 125 Z3: 60 Z4: 75	Z1: - Z2: 4.23 Z3: 5.25 Z4: -	Z1: - Z2: Min* Z3: -34.44 Z4: -	Z1: - Z2: 7 Z3: - Z4: -	1290W & **0.5814s**	*Z2 Fault, 7.4s*	0.4	68.79
4	Z1: 80 Z2: 125 Z3: 60 Z4: 75	Z1: 2.22 Z2: 6.2 Z3: 6.65 Z4: 1.91	Z1: -3604 Z2: 1053 Z3: -145.04 Z4: Min*	Z1: - Z2: 7 Z3: - Z4: -	702.906W & **1.067s**	*Z2 Fault, 7.6s*	0.6	60.9
5	Z1: 80 Z2: 125 Z3: 60 Z4: 75	Z1: - Z2: - Z3: 4.55 Z4: 2.36	Z1: - Z2: - Z3: 24.36 Z4: 123.2	Z1: - Z2: 7 Z3: - Z4: -	891.754W & **0.841s**	*Z2 Fault, 7.5s*	0.5	59.4
6	Z1: 80 Z2: 125 Z3: 60 Z4: 75	Z1: - Z2: 4.25 Z3: 2.65 Z4: -	Z1: - Z2: 270 Z3: -46.76 Z4: -	Z1: - Z2: 7 Z3: - Z4: -	1258.2W & **0.5961s**	*Z2 Fault, 7.4s*	0.4	67.1
7	Z1: 80 Z2: 125 Z3: 60 Z4: 75	Z1: - Z2: 1.24 Z3: 4.24 Z4: 5.21	Z1: - Z2: 1431 Z3: -99.4 Z4: 23.8	Z1: - Z2: 7 Z3: - Z4: -	1015.6W & **0.7385s**	*Z2 Fault, 7.65s*	0.65	88.02
8	Z1: 80 Z2: 125 Z3: 60 Z4: 75	Z1: - Z2: 1.54 Z3: - Z4: 3.21	Z1: - Z2: 2916 Z3: - Z4: -61.6	Z1: - Z2: 7 Z3: - Z4: -	468.425W & **1.601s**	*Z2 Fault, 7.45s*	0.45	28.1
9	Z1: 80 Z2: 125 Z3: 60 Z4: 75	Z1: - Z2: - Z3: - Z4: -	Z1: - Z2: - Z3: - Z4: -	Z1: - Z2: 8 Z3: - Z4: -	1202.1W & **0.6239s**	*Z2 Fault, 8.45s*	0.45	72.13
10	Z1: 95 Z2: 160 Z3: 50 Z4: 100	Z1: 1.11 Z2: 4.23 Z3: 3.9 Z4: -	Z1: -1809 Z2: -229.5 Z3: 102.2 Z4: -	Z1: - Z2: 8 Z3: - Z4: -	772.065W & **0.9714s**	*Z2 Fault, 8.15s*	0.15	15.44
11	Z1: 95 Z2: 160 Z3: 50 Z4: 100	Z1: 5.2 Z2: 3.21 Z3: - Z4: -	Z1: Min* Z2: -675 Z3: - Z4: -	Z1: - Z2: 7 Z3: - Z4: -	938.260W & **0.7994s**	*Z2 Fault, 7.70s*	0.7	87.5
12	Z1: 95 Z2: 160 Z3: 50 Z4: 100	Z1: - Z2: - Z3: 7.4 Z4: 6.1	Z1: - Z2: - Z3: 29.68 Z4: 9.24	Z1: - Z2: 8 Z3: - Z4: -	794.104W & **0.9445s**	*Z2 Fault, 8.70s*	0.7	74.11
13	Z1: 95 Z2: 160 Z3: 50 Z4: 100	Z1: - Z2: 3.2 Z3: - Z4: 6.91	Z1: - Z2: 54 Z3: - Z4: 7	Z1: - Z2: 7 Z3: - Z4: -	778.408W & **0.9635s**	*Z2 Fault, 7.10s*	0.1	10.37

14	Z1: 95	Z1: -	Z1: -	Z1: -	1055.3W	*Z2 Fault,*	0.7	97.6
	Z2: 160	Z2: -	Z2: -	Z2: 7	&	*7.70s*		
	Z3: 50	Z3: 5.2	Z3: 109.48	Z3: -	**0.7107s**			
	Z4: 100	Z4: -	Z4: -	Z4: -				
15	Z1: 80	Z1: 5.69	Z1: -81	Z1: -	704.898W	*Z2 Fault,*	0.4	37.59
	Z2: 105	Z2: -	Z2: -	Z2: 8	&	*8.40s*		
	Z3: 40	Z3: 2.12	Z3: -31.36	Z3: -	**1.064s**			
	Z4: 145	Z4: -	Z4: -	Z4: -				
16	Z1: 80	Z1: -	Z1: -	Z1: -	1326.9W	*Z2 Fault,*	0.25	44.23
	Z2: 105	Z2: 1.29	Z2: 378	Z2: 8	&	*8.25s*		
	Z3: 40	Z3: 4.21	Z3: -8.96	Z3: -	**0.5632s**			
	Z4: 145	Z4: 7.84	Z4: -29.4	Z4: -				
17	Z1: 80	Z1: -	Z1: -	Z1: -	735.325W	*Z2 Fault,*	0.55	53.92
	Z2: 105	Z2: 6.12	Z2: -	Z2: 7	&	*7.55s*		
	Z3: 40	Z3: -	3307.5	Z3: -	**1.02s**			
	Z4: 145:	Z4: 2.14	Z3: -	Z4: -				
			Z4: 160.44					
18	Z1: 80	Z1: -	Z1: -	Z1: -	1613.7W	*Z2 Fault,*	0.35	75.3
	Z2: 105	Z2: -	Z2: -	Z2: 7	&	*7.35s*		
	Z3: 40	Z3: -	Z3: -	Z3: -	**0.4648s**			
	Z4: 145:	Z4: 5	Z4: -	Z4: -				
			115.08					
19	Z1: 80	Z1: 4.12	Z1: -769.5	Z1: -	429.9647W	*Z2 Fault,*	1.5	85.99
	Z2: 105	Z2: 5.96	Z2: -248.5	Z2: 7	&	*8.50s*		
	Z3: 40	Z3: 4.44	Z3: 22.12	Z3: -	**1.7443s**			
	Z4: 145	Z4: -	Z4: -	Z4: -				
20	Z1: 80	Z1: 5.4	Z1: -	Z1: -	208.379W	*Z2 Fault,*	0.15	4.167
	Z2: 105	Z2: 6.6	3793.5	Z2: 7	&	*7.15s*		
	Z3: 40	Z3: -	Z2: Min*	Z3: -	**3.5992s**			
	Z4: 145	Z4: 3.16	Z3: -	Z4: -				
			Z4: 36.12					
21	Z1: 40	Z1: 7	Z1: -432	Z1: -	391.799W	*Z2 Fault,*	0.45	23.51
	Z2: 52	Z2: 4	Z2: 1498.5	Z2: 9	&	*9.45s*		
	Z3: 35	Z3: 1	Z3: 27.72	Z3: -	**1.9142s**			
	Z4: 40	Z4: 6	Z4: -291.2	Z4: -				
22	Z1: 40	Z1: 4	Z1: 1809	Z1: -	399.169W	*Z2 Fault,*	0.75	39.92
	Z2: 52	Z2: 5	Z2: -1674	Z2: 9	&	*9.75s*		
	Z3: 35	Z3: 3	Z3: -42.84	Z3: -	**1.878s**			
	Z4: 40	Z4: 2	Z4: 229.6	Z4: -				
23	Z1: 40	Z1: 6.25	Z1: -459	Z1: -	267.376W	*Z2 Fault,*	0.4	14.26
	Z2: 52	Z2: 7.4	Z2: 1560.6	Z2: 9	&	*9.4s*		
	Z3: 35	Z3: 1.25	Z3: 216.6	Z3: -	**2.8050s**			
	Z4: 40	Z4: 4.28	Z4: -614.6	Z4: -				
24	Z1: 40	Z1: 8.12	Z1: Min*	Z1: -	382.328W	*Z2 Fault,*	0.75	38.23
	Z2: 52	Z2: 2.14	Z2: -229.5	Z2: 9	&	*9.75s*		
	Z3: 35	Z3: 6.23	Z3: -35.84	Z3: -	**1.9617s**			
	Z4: 40	Z4: 3.14	Z4: 789.6	Z4: -				
25	Z1: 40	Z1: 5.23	Z1: -	Z1: -	326.830W	*Z2 Fault,*	0.75	32.68
	Z2: 52	Z2: 5.65	1687.5	Z2: 9	&	*9.75s*		
	Z3: 35	Z3: 2.26	Z2: 526.5	Z3: -	**2.294s**			
	Z4: 40	Z4: 4.87	Z3: 151.76	Z4: -				
			Z4: -387.8					
					100% Accurate		**0.502**	**48.27**

NETWORK CONDITION: SERIES DC ARC FAULT - ZONE 3					
Test #	Cable Lengths (m)	Load Switching Times (s)	Load Switching Levels (W)	Fault Times (s)	IntelArc System Output	Detection Time (s)
1	Z1: 120 Z2: 100 Z3: 70 Z4: 115	Z1: - Z2: - Z3: - Z4: -	Z1: - Z2: - Z3: - Z4: -	Z1: - Z2: - Z3: 5 Z4: -	*Z3 Fault, 5.15s*	0.15
2	Z1: 120 Z2: 100 Z3: 70 Z4: 115	Z1: - Z2: - Z3: 3.9 Z4: -	Z1: - Z2: - Z3: 160.72 Z4: -	Z1: - Z2: - Z3: 6 Z4: -	*Z3 Fault, 6.40s*	0.4
3	Z1: 120 Z2: 100 Z3: 70 Z4: 115	Z1: 7.12 Z2: 6.35 Z3: - Z4: -	Z1: 3267 Z2: 3483 Z3: - Z4: -	Z1: - Z2: - Z3: 8 Z4: -	*Z3 Fault, 8.30s*	0.3
4	Z1: 120 Z2: 100 Z3: 70 Z4: 115	Z1: - Z2: - Z3: 2.12 Z4: 4.03	Z1: - Z2: - Z3: -213.64 Z4: -7.56	Z1: - Z2: - Z3: 8 Z4: -	*Z3 Fault, 8.10s*	0.1
5	Z1: 120 Z2: 100 Z3: 70 Z4: 115	Z1: 3.65 Z2: 6.54 Z3: 2.12 Z4: 4.03	Z1: -1093 Z2: 2322 Z3: 73.08 Z4: -51.24	Z1: - Z2: - Z3: 8 Z4: -	*Z3 Fault, 8.10s*	0.1
6	Z1: 120 Z2: 100 Z3: 70 Z4: 115	Z1: 6 Z2: 7.45 Z3: 5.41 Z4: 6.22	Z1: 504.9 Z2: 2241 Z3: -148.4 Z4: 71.4	Z1: - Z2: - Z3: 8 Z4: -	*Z3 Fault, 8.40s*	0.4
7	Z1: 120 Z2: 100 Z3: 70 Z4: 115	Z1: 1.24 Z2: 6.25 Z3: 2 Z4: 4	Z1: -918 Z2: -216 Z3: -38.92 Z4: 23.8	Z1: - Z2: - Z3: 8 Z4: -	*Z3 Fault, 8.10s*	0.1
8	Z1: 120 Z2: 100 Z3: 70 Z4: 115	Z1: 4.75 Z2: 3.66 Z3: - Z4: 1.29	Z1: -2578.5 Z2: 94.68 Z3: - Z4: -109.2	Z1: - Z2: - Z3: 8 Z4: -	*Z3 Fault, 8.10s*	0.1
9	Z1: 80 Z2: 80 Z3: 65 Z4: 100	Z1: - Z2: 2.14 Z3: 4.68 Z4: -	Z1: - Z2: 140.84 Z3: -2.8 Z4: -	Z1: - Z2: - Z3: 8 Z4: -	*Z3 Fault, 8.15s*	0.15
10	Z1: 80 Z2: 80 Z3: 65 Z4: 100	Z1: 6 Z2: 5 Z3: - Z4: -	Z1: 521.1 Z2: 3186 Z3: - Z4: -	Z1: - Z2: - Z3: 8 Z4: -	*Z3 Fault, 8.20s*	0.2
11	Z1: 80 Z2: 80 Z3: 65 Z4: 100	Z1: - Z2: 5.32 Z3: 1.11 Z4: -	Z1: - Z2: 4704 Z3: 378 Z4:	Z1: - Z2: - Z3: 8 Z4: -	*Z3 Fault, 8.30s*	0.3
12	Z1: 80 Z2: 80 Z3: 65 Z4: 100	Z1: - Z2: 3.65 Z3: - Z4: -	Z1: - Z2: -688.5 Z3: - Z4: -	Z1: - Z2: - Z3: 7 Z4: -	*Z3 Fault, 7.10s*	0.1
13	Z1: 80 Z2: 80 Z3: 65 Z4: 100	Z1: - Z2: - Z3: - Z4: -	Z1: - Z2: - Z3: - Z4: -	Z1: - Z2: - Z3: 7 Z4: -	*Z3 Fault, 7.10s*	0.1

14	Z1: 80 Z2: 80 Z3: 65 Z4: 100	Z1: - Z2: 1.87 Z3: 3.54 Z4: -	Z1: - Z2: 1628.1 Z3: -107.8 Z4: -	Z1: - Z2: - Z3: 7 Z4: -	*Z3 Fault,* *7.25s*	0.25
15	Z1: 80 Z2: 80 Z3: 65 Z4: 100	Z1: - Z2: - Z3: 4.65 Z4: 3.74	Z1: - Z2: - Z3: 250.6 Z4: 77	Z1: - Z2: - Z3: 7 Z4: -	*Z3 Fault,* *7.60s*	0.6
16	Z1: 150 Z2: 140 Z3: 90 Z4: 120	Z1: - Z2: 6.25 Z3: 4.12 Z4: -	Z1: - Z2: 1039.5 Z3: -43.68 Z4: -	Z1: - Z2: - Z3: 7 Z4: -	*Z3 Fault,* *7.40s*	0.4
17	Z1: 150 Z2: 140 Z3: 90 Z4: 120	Z1: 3.25 Z2: 5 Z3: 6 Z4: 4.7	Z1: 1674 Z2: 837 Z3: 43.4 Z4: -8.96	Z1: - Z2: - Z3: 7 Z4: -	***No Fault***	N/A
18	Z1: 150 Z2: 140 Z3: 90 Z4: 120	Z1: 5 Z2: 4.1 Z3: 4.8 Z4: 4.2	Z1: -1620 Z2: 3631.5 Z3: -49 Z4: 37.8	Z1: - Z2: - Z3: 7 Z4: -	*Z3 Fault,* *7.25s*	0.25
19	Z1: 150 Z2: 140 Z3: 90 Z4: 120	Z1: - Z2: - Z3: 3 Z4: 1.24	Z1: - Z2: - Z3: -185.05 Z4: 26.6	Z1: - Z2: - Z3: 7 Z4: -	*Z3 Fault,* *7.45s*	0.45
20	Z1: 150 Z2: 140 Z3: 90 Z4: 120	Z1: 3.11 Z2: - Z3: 1.78 Z4: 2.87	Z1: -796.5 Z2: - Z3: 22.68 Z4: 81.76	Z1: - Z2: - Z3: 7 Z4: -	*Z3 Fault,* *7.10s*	0.1
21	Z1: 35 Z2: 30 Z3: 20 Z4: 45	Z1: 7.2 Z2: 6 Z3: 3.9 Z4: 4.25	Z1: -661.5 Z2: 1938.6 Z3: -154.84 Z4: Min*	Z1: - Z2: - Z3: 8 Z4: -	*Z3 Fault,* *8.40s*	0.4
22	Z1: 35 Z2: 30 Z3: 20 Z4: 45	Z1: 7.2 Z2: 6 Z3: 3.9 Z4: 4.25	Z1: -1269 Z2: -337.5 Z3: 35 Z4: -23.8	Z1: - Z2: - Z3: 8 Z4: -	*Z3 Fault,* *8.25s*	0.25
23	Z1: 35 Z2: 30 Z3: 20 Z4: 45	Z1: 8 Z2: 7.45 Z3: 6 Z4: 5	Z1: 1809 Z2: -558.9 Z3: -80.64 Z4: 415.8	Z1: - Z2: - Z3: 9 Z4: -	*Z3 Fault,* *9.25s*	0.25
24	Z1: 35 Z2: 30 Z3: 20 Z4: 45	Z1: 4.52 Z2: 1.22 Z3: 3.15 Z4: -	Z1: 81 Z2: 1714.5 Z3: 30.24 Z4: -	Z1: - Z2: - Z3: 9 Z4: -	*Z3 Fault,* *9.30s*	0.3
25	Z1: 35 Z2: 30 Z3: 20 Z4: 45	Z1: - Z2: 6.5 Z3: 5 Z4: 8	Z1: - Z2: -1431 Z3: 260.4 Z4: -714	Z1: - Z2: - Z3: 9 Z4: -	*Z3 Fault,* *9.25s*	0.25
					95.8% **Accurate**	**0.25**

NETWORK CONDITION: SERIES DC ARC FAULT - ZONE 4					
Test #	Cable Length (m)	Load Switching Times (s)	Load Switching Levels (W)	Fault Times (s)	AFD System Output	Detection Time (s)
1	Z1: 150 Z2: 150 Z3: 80 Z4: 160	Z1: - Z2: - Z3: - Z4: -	Z1: - Z2: - Z3: - Z4: -	Z1: - Z2: - Z3: - Z4: 7	*Z4 Fault, 7.85s*	0.85
2	Z1: 150 Z2: 150 Z3: 80 Z4: 160	Z1: - Z2: - Z3: - Z4: 4	Z1: - Z2: - Z3: - Z4: 16.8	Z1: - Z2: - Z3: - Z4: 6	*Z4 Fault, 6.45s*	0.45
3	Z1: 150 Z2: 150 Z3: 80 Z4: 160	Z1: 3.2 Z2: 6.1 Z3: - Z4: -	Z1: -1444.5 Z2: 40.5 Z3: - Z4: -	Z1: - Z2: - Z3: - Z4: 7	*Z4 Fault, 7.25s*	0.25
4	Z1: 150 Z2: 150 Z3: 80 Z4: 160	Z1: - Z2: - Z3: 3.1 Z4: 5.4	Z1: - Z2: - Z3: Z4:	Z1: - Z2: - Z3: - Z4: 7	*Z4 Fault, 7.35s*	0.35
5	Z1: 150 Z2: 150 Z3: 80 Z4: 160	Z1: - Z2: 2.33 Z3: 5.31 Z4: -	Z1: - Z2: 1190.7 Z3: 184.52 Z4: -	Z1: - Z2: - Z3: - Z4: 7	*Z4 Fault, 7.1s*	0.1
6	Z1: 150 Z2: 150 Z3: 80 Z4: 160	Z1: - Z2: 3.1 Z3: - Z4: 2.5	Z1: - Z2: 1053 Z3: - Z4: -133	Z1: - Z2: - Z3: - Z4: 7	*Z4 Fault, 7.3s*	0.3
7	Z1: 150 Z2: 150 Z3: 80 Z4: 160	Z1: 4.25 Z2: - Z3: 1.23 Z4: -	Z1: -1336.5 Z2: - Z3: 118.44 Z4: -	Z1: - Z2: - Z3: - Z4: 7	*Z4 Fault, 7.5s*	0.5
8	Z1: 150 Z2: 150 Z3: 80 Z4: 160	Z1: 4.25 Z2: - Z3: - Z4: 6.2	Z1: 3604.5 Z2: - Z3: - Z4: -93.8	Z1: - Z2: - Z3: - Z4: 8	***No Fault***	N/A
9	Z1: 150 Z2: 150 Z3: 80 Z4: 160	Z1: - Z2: - Z3: - Z4: 6.1	Z1: - Z2: - Z3: - Z4: 88.2	Z1: - Z2: - Z3: - Z4: 8	*Z4 Fault, 8.95s*	0.95
10	Z1: 150 Z2: 150 Z3: 80 Z4: 160	Z1: 1.5 Z2: 5.4 Z3: 4.25 Z4: -	Z1: -227.5 Z2: -1593 Z3: 80.08 Z4: -	Z1: - Z2: - Z3: - Z4: 8	*Z4 Fault, 8.15s*	0.15
11	Z1: 120 Z2: 130 Z3: 60 Z4: 140	Z1: - Z2: 4.25 Z3: - Z4: 6.24	Z1: - Z2: 2146.5 Z3: - Z4: 106.4	Z1: - Z2: - Z3: - Z4: 8	*Z4 Fault, 8.75s*	0.75
12	Z1: 120 Z2: 130 Z3: 60 Z4: 140	Z1: 3.25 Z2: 6.11 Z3: - Z4: -	Z1: 1269 Z2: 1766.4 Z3: - Z4: -	Z1: - Z2: - Z3: - Z4: 8	*Z4 Fault, 8.15s*	0.15
13	Z1: 120 Z2: 130 Z3: 60 Z4: 140	Z1: 3.2 Z2: - Z3: 5.21 Z4: -	Z1: -2335.5 Z2: - Z3: -49.84 Z4: -	Z1: - Z2: - Z3: - Z4: 8	*Z4 Fault, 8.55s*	0.55
14	Z1: 120 Z2: 130	Z1: 7.12 Z2: 2.56	Z1: -67.5 Z2: -2943	Z1: - Z2: -	*Z4 Fault, 9.3s*	1.3

	Z3: 60	Z3: 1.56	Z3: 346.36	Z3: -		
	Z4: 140	Z4: 3.22	Z4: 141.4	Z4: 8		
15	Z1: 120	Z1: 6.21	Z1: 2727	Z1: -	*No Fault*	N/A
	Z2: 130	Z2: 3.45	Z2: 2092.5	Z2: -		
	Z3: 60	Z3: 7.12	Z3: 103.2	Z3: -		
	Z4: 140	Z4: 1.2	Z4: 32.2	Z4: 8		
16	Z1: 120	Z1: 4.56	Z1: 275.4	Z1: -	*Z4 Fault,*	0.8
	Z2: 130	Z2: 1.89	Z2: 2205.9	Z2: -	*8.80s*	
	Z3: 60	Z3: -	Z3: -	Z3: -		
	Z4: 140	Z4: -	Z4: -	Z4: 8		
17	Z1: 100	Z1: -	Z1: -	Z1: -	*Z4 Fault,*	0.5
	Z2: 110	Z2: -	Z2: -	Z2: -	*7.5s*	
	Z3: 70	Z3: -	Z3: -	Z3: -		
	Z4: 90	Z4: 3.11	Z4: 62.44	Z4: 7		
18	Z1: 100	Z1: 3.67	Z1: 2430	Z1: -	*Z4 Fault,*	0.3
	Z2: 110	Z2: -	Z2: -	Z2: -	*7.3s*	
	Z3: 70	Z3: -	Z3: -	Z3: -		
	Z4: 90	Z4: 4.12	Z4: -162.4	Z4: 7		
19	Z1: 100	Z1: 2.56	Z1: -472.5	Z1: -	*Z4 Fault,*	0.5
	Z2: 110	Z2: 7.12	Z2: -1957.5	Z2: -	*8.5s*	
	Z3: 70	Z3: 3.62	Z3: -24.08	Z3: -		
	Z4: 90	Z4: 2.24	Z4: 176.68	Z4: 8		
20	Z1: 100	Z1: -	Z1: -	Z1: -	*Z4 Fault,*	0.15
	Z2: 110	Z2: -	Z2: -	Z2: -	*8.15s*	
	Z3: 70	Z3: 6.45	Z3: 97.16	Z3: -		
	Z4: 90	Z4: 7.02	Z4: -43.4	Z4: 8		
21	Z1: 30	Z1: 4.25	Z1: -108	Z1: -	***Z1 Fault,***	N/A
	Z2: 40	Z2: 1.22	Z2: 1633.5	Z2: -	***4.3s***	
	Z3: 40	Z3: 6.11	Z3: 177.8	Z3: -		
	Z4: 20	Z4: 7.30	Z4: 667.8	Z4: 8		
22	Z1: 30	Z1: 4.25	Z1: -1107	Z1: -	*Z4 Fault,*	0.05
	Z2: 40	Z2: 1.22	Z2: -513	Z2: -	*8.05s*	
	Z3: 40	Z3: 6.11	Z3: 86.52	Z3: -		
	Z4: 20	Z4: 7.3	Z4: -658	Z4: 8		
23	Z1: 30	Z1: 5.25	Z1: 445.5	Z1: -	*Z4 Fault,*	0.65
	Z2: 40	Z2: -	Z2: -	Z2: -	*8.65s*	
	Z3: 40	Z3: -	Z3: -	Z3: -		
	Z4: 20	Z4: 6.11	Z4: 278.6	Z4: 8		
24	Z1: 30	Z1: 4.12	Z1: 1155.6	Z1: -	*Z4 Fault,*	0.3
	Z2: 40	Z2: 6.56	Z2: -54	Z2: -	*8.30s*	
	Z3: 40	Z3: -	Z3: -	Z3: -		
	Z4: 20	Z4: -	Z4: -	Z4: 8		
25	Z1: 30	Z1: -	Z1: -	Z1: -	*Z4 Fault,*	0.75
	Z2: 40	Z2: 7.45	Z2: -918	Z2: -	*8.75s*	
	Z3: 40	Z3: 6.24	Z3: -188.72	Z3: -		
	Z4: 20	Z4: -	Z4: -	Z4: 8		
					88% Accurate	**0.484**

B.2 Case Study 3 Results

Key

Accurate Detection of Arcing
Inaccurate Detection of Arcing

INTERMITTENT SERIES DC ARC FAULT - ZONE X						
Test #	Cable Length (m)	Load Switch Time (s)	Load Switch Level (W)	Initial Intermittent Arc Fault Onset (s)	Further Intermittent Arc Fault |Onsets (s)	Average Arcing Time (ms)	IntelArc System Outputs (s)
1	60 (30)	8.12	1080	8.5	8.98, 9.5	171.3	Arcing - 8.60, 8.70, 9.6
2	60 (30)	5.54	-1147.5	8.85	9.43	89.2	Arcing - 8.90, 9.00, 9.45, 9.50
3	60 (30)	6.54	1512	9.58	--	156.2	Arcing - 9.75
4	60 (30)	2.28	202.5	9.25	9.59, 9.93	46.3	Arcing - 2.35, 9.95
5	60 (30)	3.65	-864	9	9.47	110.4	Arcing - 9.05, 9.15, 9.50
6	60 (30)	6.53	108	9.03	9.29	97.3	Arcing - 9.05, 9.10, 9.20, 9.35
7	60 (30)	4.27	243	9.02	9.35	49.5	Arcing - 9.05, 9.10, 9.40, 9.45
8	60 (30)	6.96	-2430	9.12	9.35, 9.58, 9.82	31.8	Arcing - 9.15, 9.40, 9.60
9	60 (30)	5.4	-945	9.5	--	213.6	Arcing - 9.65
10	60 (30)	2.98	-904.5	9.18	9.51, 9.84	88.8	Arcing - 9.20, 9.35, 9.65, 9.95
11	60 (30)	5.94	2403	8.69	9, 9.64,	122.4	Arcing - 8.75, 8.85, 9.10, 9.20, 9.70, 9.75, 9.80
12	60 (30)	4.7477	378	9.05	9.34, 9.62, 9.9	39.8	Arcing - 9.10, 9.15, 9.35, 9.40, 9.45, 9.65, 9.70, 9.95
13	60 (30)	2.922	-1593	9.3	9.8	133.5	Arcing - 9.35, 9.85, 10
14	60 (30)	6.5	-3226.5	9.01	9.3, 9.6, 9.88	90.4	Arcing - 9.05, 9.45, 9.65, 9.70, 9.75, 9.95, 10
15	60 (30)	6.78	2187	9.03	--	94.7	Arcing - 9.10, 9.20, 9.80
16	60 (30)	3.51	1485	9	9.4, 9.83	130.8	Arcing - 9.05, 9.15
17	60 (30)	4.46	1039.5	8.74	9.15, 9.58	167.9	Arcing - 8.80, 8.95, 9, 9.60
18	60 (30)	6.89	162	8.98	9.42, 9.85	76	Arcing - 6.90, 9.45, 9.55, 9.90, 10

19							Arcing - 8.75, 8.90, 9.15, 9.25, 9.40, 9.70, 9.85,
	60 (30)	5.22	-1512	8.71	9.04, 9.38, 9.71	117	9.90
20							Arcing - 8.55, 8.85, 8.90, 8.95,
	60 (30)	5.98	1728	8.5	8.8, 9.12, 9.45, 9.77	76.3	9.15, 9.50, 9.85
21							Arcing - 9.25, 9.35, 9.60, 9.70,
	45 (20)	3.57	-1512	9.2	9.52, 9.84	86.9	9.90, 10
22							Arcing - 8.60, 8.65, 8.80, 9.05, 9.10, 9.15, 9.25, 9.50, 9.65, 9.95,
	45 (20)	2.59	-553.5	8.55	9.02, 9.45, 9.9	162.4	10
23							Arcing - 8.75, 8.85, 9.15, 9.25, 9.55, 9.65, 9.90,
	45 (20)	7.47	-553.5	8.71	9.1, 9.49, 9.88	81.3	9.95
24						8.85, 9.13, 9.42,	
	45 (20)	4.06	2767.5	8.58	9.7	67.4	Arcing - 8.65
25							Arcing - 8.65, 8.80, 8.95, 9, 9.05, 9.10, 9.40, 9.65, 9.70, 9.90,
	45 (20)	2.38	-756	8.63	8.94, 9.25, 9.55, 9.87	94.4	9.95
26							Arcing - 9.05,
	45 (20)	6.95	2146.5	8.99	--	134.1	9.15, 9.20
27							Arcing - 9.10,
	45 (20)	3.2	-2214	9.08	9.58	60.9	9.15, 9.20, 9.65
28							Arcing - 8.85, 8.9, 9, 9.3, 9.35, 9.40, 9.70, 9.75,
	45 (20)	7.4	-2565	8.84	9.26, 9.69	72	9.85
29							Arcing - 9.10,
	45 (20)	1.7	2254.5	9	9.4, 9.1	134.3	9.40, 9.95
30							Arcing - 9.10, 9.20, 9.30, 9.45,
	45 (20)	2.12	-607.5	9	9.17, 9.4, 9.62, 9.83	60.5	9.65, 9.85, 9.95
31							Arcing - 3.50, 8.65, 9.20, 9.25,
	50 (35)	3.42	540	8.62	9.18, 9.79	100.6	9.85
32							Arcing - 8.65,
	50 (35)	3.47	2956.5	8.58	9.12, 9.38	79.3	8.75, 9.20, 9.45
33							Arcing - 9.20, 9.40, 9.60, 9.65,
	50 (35)	3.01	486	9.16	9.37, 9.56, 9.77	39.9	9.70, 9.80, 9.90
34							Arcing - 9.35,
	50 (35)	4.41	715.5	9.28	--	48.4	9.40
35							Arcing - 9.25,
	50 (35)	4.88	769.5	9.22	--	102.7	9.30, 9.40
36							Arcing - 9.05,
	50 (35)	5.27	-588.6	8.98	9.5	58.2	9.10, 9.55, 9.65
37							Arcing - 1.65,
	50 (35)	1.6	-175.5	9	9.5	102	9.05, 9.15, 9.6
38							Arcing - 9.65, 9.75, 9.85, 9.90,
	50 (35)	4.14	-1876.5	9.5	9.73, 9.97	92.3	10
39							Arcing - 9.25,
	50 (35)	3.63	1336.5	9.18	9.52	75.9	9.35, 9.55
40	50 (35)	2.78	580.5	9.77	--	56.6	Arcing - 9.85

#							
41	80 (50)	3.14	1012.5	9.29	9.68	49.5	Arcing - 9.30, 9.35, 9.40, 9.70
42	80 (50)	6.2	-378	8.78	9.17, 9.58	122.5	Arcing - 9.65
43	81 (50)	2.49	-162	9.3	9.74	70.7	Arcing - 9.40, 9.75, 9.80, 9.85
44	82 (50)	4.7	2700	8.53	8.92, 9.32, 9.71	46	Arcing - 8.60, 8.65, 8.95, 9, 9.05, 9.45, 9.75, 9.80, 9.85
45	83 (50)	4.16	405	8.7	9.08, 9.43, 9.82	139.9	Arcing - 8.75, 8.90, 9.10, 9.15, 9.20, 9.45, 9.55, 9.85, 9.90, 9.95
46	84 (50)	4.31	729	9.5	9.9	76.3	Arcing - 9.55, 9.65, 9.95
47	85 (50)	4.86	1660.5	9.47	--	109	Arcing - 9.55, 9.60, 9.65
48	86 (50)	4.41	-2754	9.2	9.43, 9.69, 9.91	22.8	Arcing - 9.25, 9.30, 9.45, 9.75, 9.95
49	87 (50)	4.95	2740.5	8.67	9.57	139.2	Arcing - 8.75, 9.60
50	88 (50)	3.23	521.1	9.45	--	107.3	Arcing - 9.45, 9.50, 9.55
51	75 (20)	7.5	-837	9.5	--	141.5	Arcing - 9.55, 9.70
52	75 (20)	5.5	-486	9.3	9.86	195.9	Arcing - 9.35, 9.60, 9.90, 9.95
53	75 (20)	6.93	-270	9.14	9.37, 9.58, 9.8	32.8	Arcing - 9.15, 9.20, 9.25, 9.40, 9.45, 9.65, 9.85, 9.90
54	75 (20)	2.6	Min*	8.57	9.34, 9.72	50.2	Arcing - 8.60, 9.45, 9.75, 9.80
55	75 (20)	--	--	8.5	9.14, 9.58	59.1	Arcing - 8.55, 9.20, 9.50, 9.60
56	75 (20)	2.39	-828.9	8.77	9.21, 9.76	70.8	Arcing - 8.80, 8.90, 9.30, 9.80
57	75 (20)	1.5	1336.5	9.58	--	163	Arcing - 9.65, 9.70
58	75 (20)	1.53	2119.5	8.68	9.15	123.3	Arcing - 8.70, 8.90, 9.20, 9.25
59	75 (20)	5.18	1944	8.55	9.15, 9.77	113.2	Arcing - 8.75, 9.20, 9.25, 9.85, 9.90
60	75 (20)	5.57	972	9.08	9.82	78.3	Arcing - 9.15, 9.85
							93.3% Accurate

APPENDIX C: WAVELET TRANSFORM - THEORY

The *IntelArc* system uses the wavelet transform (WT) to extract time-frequency domain features from load current data. Determining optimal WT features for series DC arc fault diagnosis was described in detail in Chapter 5, Section 5.2.4. The background and theory of the WT, in the context of its use within IntelArc, is provided in the following.

C.1 Wavelet Transform

It is important to understand both the theory of the WT and the additional information the transform provides about a signal. The theory of WT is complex and extensive – this overview only provides a high level introduction. For further information, refer to the excellent introduction provided by Polikar [C.1].

The use of the fast Fourier transform (FFT) for transforming time domain signals into the frequency domain is well documented. The WT was first developed in the early 1980's to overcome the lack of time resolution provided by the FFT and provide a multi-resolution transformation of a time domain signal.

Prior to the WT, the short time Fourier transform (STFT) [C.2] was used to resolve signals in both time and frequency domains. The STFT basically splits a time-domain signal into separate windows and calculates the FFT at each window. This process assumes a non-stationary signal can be split into windows of stationary signals – calculating the FFT at each stationary window enables an accurate representation of what frequencies occur at what time.

However, the main issue with STFT arises when attempting to choose a window that provides good time and frequency resolution. A narrow window will provide good time resolution but poor frequency resolution, whereas a wide window will provide good frequency resolution but a poor time resolution.

C.2 Continuous Wavelet Transform

The continuous WT (CWT) was developed as an alternative to the STFT to overcome the problems involved with choosing a suitable window function. The CWT operates by multiplying a time-domain signal with a wavelet window function that is scaled (change of wavelet window width and hence frequency resolution) and shifted (window moved through time).

The CWT is defined as

$$C\big(a, b; f(t), \Psi(t)\big) = \int\limits_{-\infty}^{\infty} f(t) \frac{1}{\sqrt{a}} \Psi^* \left(\frac{t - b}{a} \right) dt \qquad \text{(C.1)}$$

where C are the wavelet coefficients, $\Psi(t)$ is the mother wavelet, $f(t)$ is the time-domain signal, a is the scaling parameter and b is the shifting parameter. In short, scaled and shifted versions of the

mother wavelet are compared against the original signal- the wavelet coefficients are obtained through continuously changing the scaling and shifting in time.

This results in significantly improved resolution in both frequency and time domains. Figure C-1 illustrates this concept – Figure C-1 (a) shows time frequency plane for a CWT and Figure C-1 (b) shows the same time-frequency plane for the STFT.
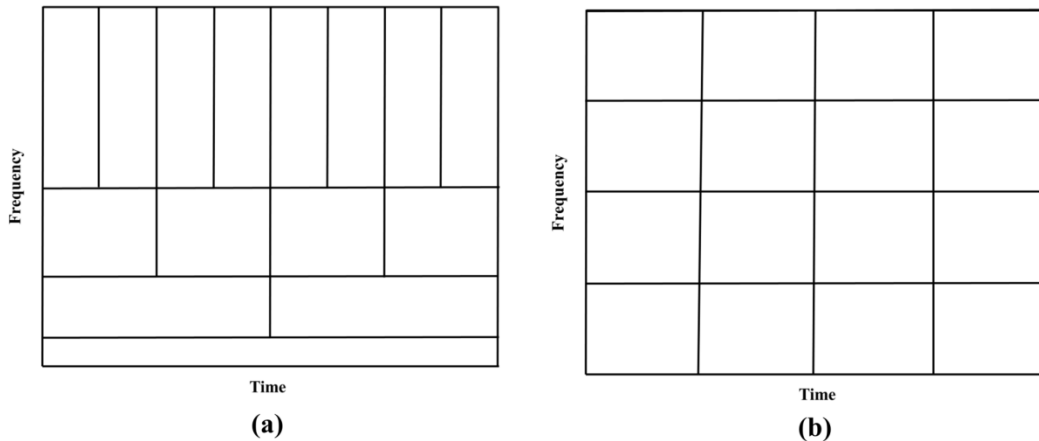
Figure C-1: Time-frequency planes of (a) the CWT and (b) the STFT. The different dimensions of the boxes in the CWT time-frequency plane illustrate the different resolution provided by various scales of a mother wavelet. At higher frequencies, the mother wavelet is shrunk resulting in poorer frequency resolutions with better time resolution. At lower frequencies, the mother wavelet is dilated providing better frequency resolution with poorer time resolution. The fixed window of the STFT results in fixed time-frequency resolutions.

Each box in Figure C-1 (a) relates to a scaled and shifted wavelet function that provides a certain time and frequency resolution. At shorter frequencies, the height of the boxes are shorter, which corresponds to better frequency resolution (as there is less ambiguity regarding the value of the exact frequency) but their widths are longer (which correspond to poor time resolution as there is more ambiguity regarding the value of the exact time). At higher frequencies the width of the boxes decreases and the heights increase i.e. lower frequency resolution and better time resolution.

Compare the varying resolutions provided by the CWT with that of the STFT, illustrated in Figure C-1 (b). The constant width of the analysis window means that both time and frequency resolutions are the same across the entire time-frequency plane; hence, unlike the CWT, the choice of window used in STFT significantly affects the results.

The improved time-frequency resolution provided by the CWT is extremely useful for feature extraction of arc fault signatures as there is the ability to accurately analyse the contribution of various frequency bandwidths of the time-domain load current signal across the entire sampled time period without having to consider the type of window used.

However, the fact that the CWT shifts and scales the mother wavelet in a continuous fashion to calculate the coefficients makes it impractical in terms of increased computational time and resources. Also, there is significant redundancy involved with shifting and scaling continuously. The *discrete*

wavelet transform (DWT) improves the computational and redundancy issues and is generally more suited for practical applications (where signals are discretely sampled).

C.3 Discrete Wavelet Transform

The DWT assesses both frequency and time at discrete intervals as opposed to continuously. To summarise, the CWT is a correlation between a wavelet at different scales and a time-domain signal, with the scale (or frequency) being used as a measure of similarity. The CWT is computed by changing the scale of the wavelet window, shifting the window in time, multiplying by the signal, and integrating over all times. In the DWT, filters of different cut-off frequencies are used to analyse the signal at different, discrete scales. The signal is passed through a series of high pass filters to analyse the high frequencies, and it is passed through a series of low pass filters to analyse the low frequencies.

It is easier to understand the DWT process by considering Figure C-2.
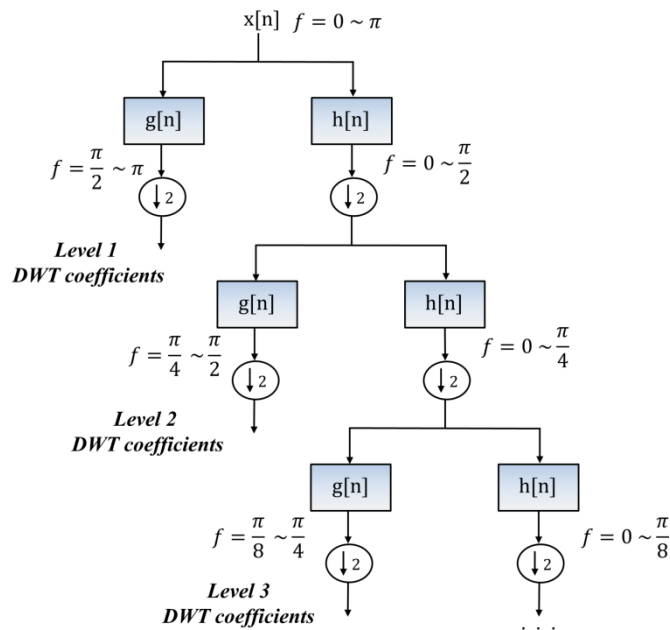
Figure C-2: Illustration of the DWT processes. The discretely sampled signal is applied to successive high and low pass filters and down sampled at each level. The filtering and down sampling processes vary the time and frequency resolution.

The sampled time-domain signal $x[n]$ is decomposed into different frequency bands by successive high pass and low pass filtering. The bandwidth of $x[n]$ is, according to the Nyquist theorem [C.3], limited to half the sampling frequency; therefore $\pi = \frac{f_s}{2}$ [15]. $x[n]$ is first passed through a half-band high pass filter $g[n]$ and a low pass filter $h[n]$. The filtering process results in level 1 detailed and

---

[15] In discrete signals, frequency is expressed in terms of radians.

approximate coefficients respectively. The level 1 low pass signal is decomposed further into low pass and high pass frequency contributions to generate further levels of detailed and approximate coefficients.

An important feature of decomposing the low pass frequencies is the *down sampling* of the signal. Down sampling refers to discarding every other sample. The process of dropping samples can be undertaken as only half the frequencies are being assessed, and the Nyquist criterion can still be met. Down sampling reduces the time-resolution as the number of samples covering the same time periods has reduced by half.

To avoid further confusion, the filtering and down sampling processes essentially vary time and frequency resolution across all scales. Analogous to the CWT, the filter banks basically compute the wavelet coefficients for a discrete set of child wavelets.

Importantly, applying the DWT to load current signals generates approximate and detail coefficients that represent various time-frequency responses of the signal. These coefficients can be incredibly important in terms of arc fault diagnosis (AFD).

A significant step towards development of the IntelArc AFD system was determining discriminative features from within the approximate and detailed coefficients. This *feature selection* process was described in Chapter 5, Section 5.2.4.

C.4 Choice of Mother Wavelet

The time and frequency resolution properties of the WT have been described in terms of a *mother wavelet* – changing the scale of the mother wavelet and shifting in time enables the multi-resolution transform. There are a variety of mother wavelets available [C.4]. Conceptually, changing the mother wavelet changes the *dimensions* of the time-frequency boxes illustrated in Figure C-1 (a), albeit with similar time and frequency trade-offs (i.e. the *area* of the boxes remain the same). Significant discussion on the various types of mother wavelets is beyond the scope of this thesis.

The type of mother wavelet used for time-frequency DC arc fault feature extraction was determined qualitatively. This qualitative process assessed the similarity between the time-domain load current signal and the different types of mother wavelet. The load current signal throughout arcing events possessed highly transient and rapidly changing features. It was therefore desirable to choose a mother wavelet that possessed sharp characteristics without excessive smooth features. The lower orders of the Daubechies (db) wavelet family [C.4] possessed sharp characteristics ideal for extracting the transient features within the load current signal. Consequently, db level 2 (db2) was selected as the mother wavelet.

C.5 Relating DWT Approximation and Detail Coefficients to frequency sub-bands

Figure C-2 illustrated how the DWT changed the time and frequency resolutions by convolving the signals with high and low pass filters, and down sampling by two. The bandwidths of the resultant sub-bands are ultimately determined by the sampling frequency of the original signal. Within the application of IntelArc for diagnosis of intermittent arcing events the sampling frequency, f_s, of the load current was 20 kHz. This value meant the wavelet decompositions were within the main frequency sub-bands of interest. Recall from Chapter 5 the description of the research conducted by Parker [C.5] which stated that sub-bands within the 200-3500Hz range would be optimal for AFD. A sampling frequency of 20 kHz[16] enabled full coverage of this frequency range. Frequency sub-bands relative to the extracted approximation and detail coefficients are outlined in Table C-1.

Table C-2: Frequency sub-bands of the DWT approximate and detailed coefficients

	Frequency Bandwidth	Bandwidth for 20KHz Sampled Signal
Original Time Domain Signal		
Load Current Signal	$0 - \dfrac{f_s}{2}$	0 – 10KHz
Time-Frequency WT Extractions		
Approximate 1	$0 - \dfrac{f_s}{4}$	0 – 5KHz
Approximate 2	$0 - \dfrac{f_s}{8}$	0 – 2.5KHz
Approximate 3	$0 - \dfrac{f_s}{16}$	0 – 1.25KHz
Approximate 4	$0 - \dfrac{f_s}{32}$	0 – 625Hz
Approximate 5	$0 - \dfrac{f_s}{64}$	0 – 312.5Hz
Detail 1	$\dfrac{f_s}{4} - \dfrac{f_s}{2}$	5kHz – 10KHz
Detail 2	$\dfrac{f_s}{8} - \dfrac{f_s}{4}$	2.5kHz – 5KHz
Detail 3	$\dfrac{f_s}{16} - \dfrac{f_s}{8}$	1.25kHz – 2.5KHz
Detail 4	$\dfrac{f_s}{32} - \dfrac{f_s}{16}$	625Hz – 1.25KHz
Detail 5	$\dfrac{f_s}{64} - \dfrac{f_s}{32}$	312.5Hz – 625Hz

---

[16] The 20 kHz load current sampling frequency referred to here was only employed in the application of IntelArc for diagnosing intermittent arcing events. The application of IntelArc for diagnosis of sustained arcing events used a limited sampling frequency of 2 kHz. After analysis of testing results (see Chapter 6), it was concluded that the 2 kHz sampling frequency led to increased detection times and, as such, feature extraction is explained in terms of 20 kHz sampling.

C.6 Bibliography for Appendix C

[C.1] 'The wavelet tutorial', [Online]. Available: http://person.hst.aau.dk/enk/ST8/wavelet_tutotial.pdf [Accessed: 16-Jul-2015]

[C.2] R.X. Gao and R. Yan, 'From Fourier Transform to Wavelet Transform: a historical perspective' in *Wavelets: Theory and Applications for Manufacturing*, Springer Science, 2011, ch. 2, pp. 17-32

[C.3] 'Nyquist theorem', [Online.] Available: http://whatis.techtarget.com/definition/Nyquist-Theorem. [Accessed: 16-Jul-2015]

[C.4] Z. Wang *et al.*, 'Arc fault signal detection – Fourier transformation vs. wavelet decomposition techniques using synthesized data', in Photovoltaic Specialist Conf., Denver, CO, 2014, pp. 3239-3244

[C.5] M.T. Parker *et al.*, 'Electric arc monitoring systems', U.S. Patent 6 772 0777, Aug. 3 2004

APPENDIX D: CONVENTIONAL & MORE-ELECTRIC AIRCRAFT SYSTEMS

D.1 Pneumatic/Bleed Air Distribution System

In many civil aircraft, the largest amount of secondary power is extracted in the form of bleed air, and the largest continual user of this power is the Environmental Control System (ECS) [D.2]. The ECS undertakes a number of functions including; the regulation of cabin pressure (maintained to levels similar to that experienced at 8000ft above sea level [D.3]), oxygen, temperature and contaminants to requisite levels; and the removal of heat from undercarriage bays, electrical equipment and flying control areas. The bleed air taken from the compressor to provide ECS function is reduced in pressure and cooled through a series of heat exchangers and an air cycle machine to provide cool air for the cockpit and avionics cooling system. Military aircraft use ECS systems working on the same principles as those for civil aircraft, albeit the pressurised cabin is smaller in volume and the avionics are more complex, produce comparatively more heat, and require additional levels of cooling.

Bleed air also supplies the provision of power for engine and wing anti-icing/de-icing functions. Despite the fact that dangerous icing conditions are rarely encountered on modern aircraft, protection from the development of intolerable ice on the lifting surfaces of the airframe and the engine in-takes is required. Protection can be obtained in two forms – *de-icing* allows ice to form to a certain extent and then periodically removes it, while *anti-icing* is a system which is activated when icing conditions are likely and prevents ice formation. The operation of anti/de-icing systems depend upon the type of aircraft engine. It is possible for turbo-fan engines to provide the main form of protection for both engine and airframe. However, turbo-prop powered aircraft have insufficient bleed for thermal anti-icing, and alternative forms of protection are required [D.1]. An example of the main components and structure of the bleed air system in an Airbus-310 is illustrated in Figure D-1.
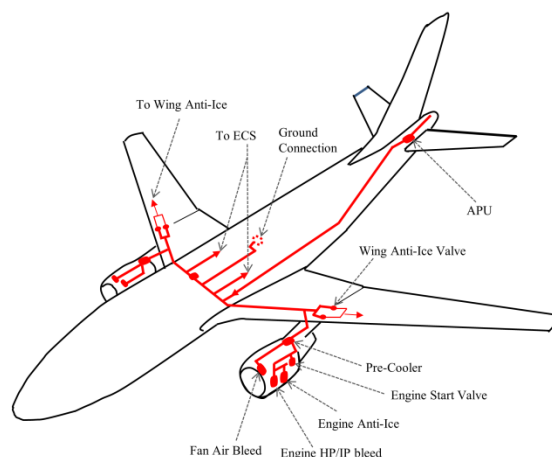
Figure D-1: Example of main components and structure of a conventional bleed air system

D.2 Hydraulic Distribution System

Hydraulic systems first appeared on aircraft in the early 1930's when retractable undercarriages were introduced– since then, the number of tasks performed using hydraulics, and the corresponding power demand, has increased significantly. Benefits of using hydraulic systems include; their efficient amplification ability, where high pressures or forces can be achieved with a small volume of fluid (hydraulic oil); and their precision control of load rate, position and magnitude [D.4]. As such, hydraulic systems have an important part to play in today's civil and military aircraft. Figure D-2 outlines the main operations performed using hydraulic power in a typical aircraft system [D.1].

❑ **Primary Flight Controls**
- Elevators – (1)
- Rudders – (2)
- Ailerons – (3)
- Flaperons – (4)

❑ **Secondary Flight Controls**
- Flaps – (5)
- Slats – (6)
- Spoilers – (7)
- Airbrakes – (8)
- Stabilizer Trim – (9)

❑ **Utilities**
- Landing gear
- Brakes
- Gear Steering
- Aerial Refuelling Probes (Military)
- Cargo Doors
- Loading Ramp (Military)
- Passenger Stairs
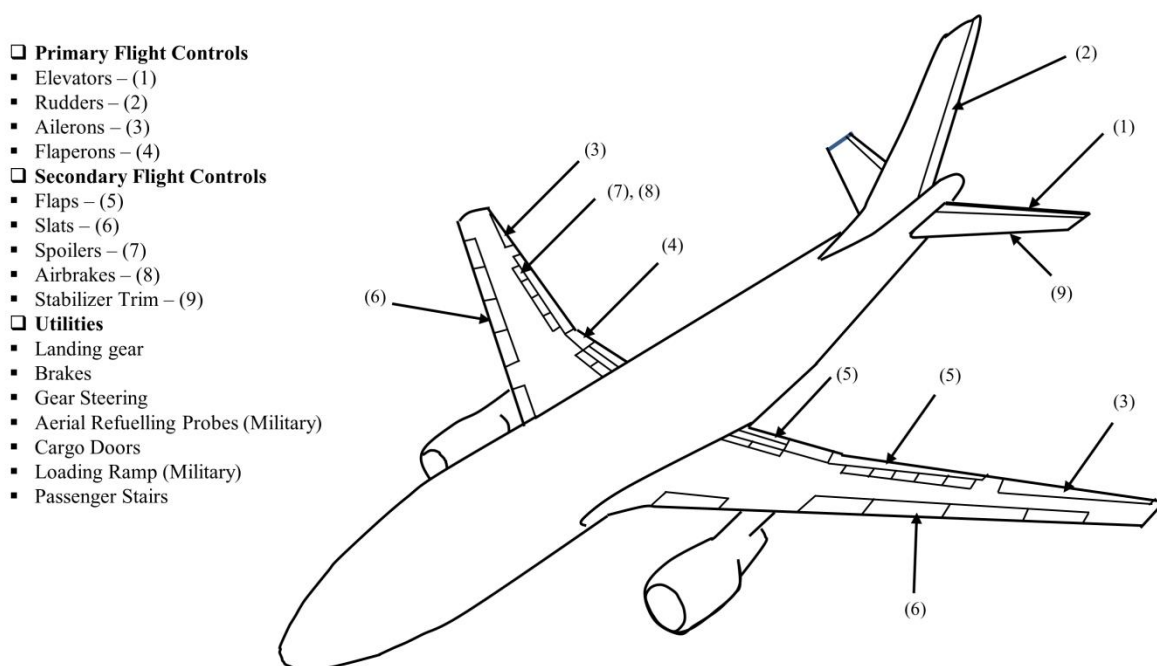
Figure D-2: Hydraulic power functions in a typical aircraft

Primary flight control of pitch, roll and yaw and secondary flight control of various trim devices and flaps is conventionally provided using hydraulically powered mechanical actuators (mechanical manual signalling from the pilot to the actuators was predominantly overtaken with the advent of automated electrical signalling, or 'fly-by-wire' systems); similarly, retractable landing gear deployment and steering, breaking and anti-skid systems and a number of other utility functions are hydraulically powered [D.5].

The majority of these operations are safety critical, where high supply reliability is required and single failure events should not prevent, or even momentarily interrupt, operation. The reliability requirements primarily dictate the design of the hydraulic system, where redundancy measures ought to be considered. Also, the type of aircraft and their mission profiles have a role to play in system design (where a crude categorisation of type is either civil or military). However, generally speaking, hydraulic distribution architectures would be of the simplified form illustrated in Figure D-3. This is

an example of a dual channel system where hydraulic pumps are connected to the engine gearboxes. The pumps cause a pressurised flow of fluid through stainless steel pipes to various actuating devices, and a reservoir ensures that sufficient fluid is available under all conditions of demand. Typically, military aircraft would have dual channel redundancy whilst large civil transport systems would invariably have three or more separate systems.
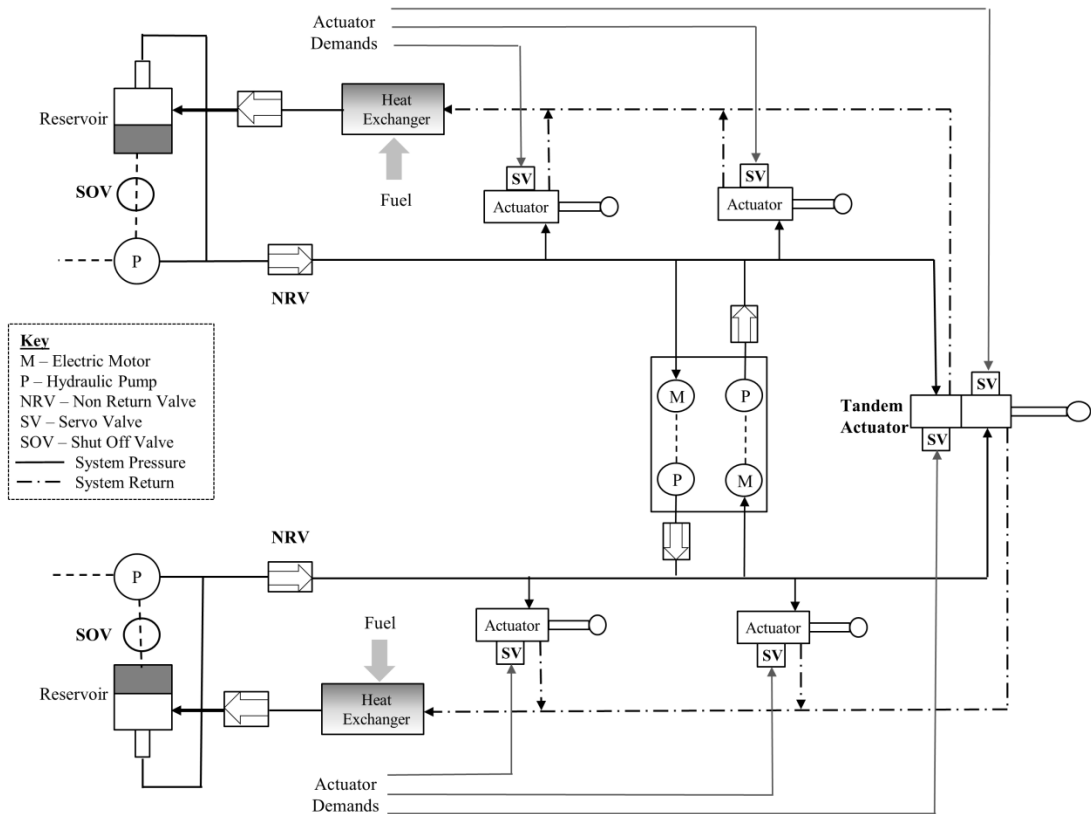
Figure D-3: Dual Channel hydraulic distribution system

D.3 Alternative Generation Sources

Aside from the main engines of the aircraft, other sources of secondary power generation are available throughout certain operational periods [D.6]. One such period where alternative sources are required is during ground operation. Ground power may be generated by means of a ground power unit (GPU) – GPUs generate electricity by means of a motor generator set, where a prime motor drives a dedicated generator. The usual standard for ground power is 115VAC three-phase 400Hz, which is the same as the power supplied by the aircraft AC generators. In some cases, 115VAC three- phase power can be derived and converted from the national electricity grid.

Ground power can also be sourced independently from GPUs through the use of auxiliary power units (APU). APU's are gas turbine engines located in the tail of the aircraft which are primarily used

during ground operation to provide compressed air for cabin air conditioning, electricity for the basic instruments and shaft power and pressurised air for main engine start-up (in some aircraft, the APU also aids hydraulic functions, allowing pilots to operate flight control surfaces). Engine start-up requires a large jolt of energy that cannot be provided by the battery alone - APU sourced compressed air provides the additional energy required. The APU may also operate in flight to relight engines that have failed or to provide back-up power for the main flight instruments in the event of a mid-air total engine failure. To achieve this, the APU may be left running throughout the flight (usually only during long-haul, overwater journeys), or started mid-flight.

In the event that the majority of conventional power generation has failed and an emergency situation has developed, additional backup power may be provided by a ram air turbine (RAT). The RAT is confined to function as a source of sufficient power to fly the aircraft while attempting to restore the primary generators or carry out a diversion to the nearest airfield, and is not intended to provide significant amounts of power for a lengthy period of operation. A RAT is an air driven turbine normally located in the nose section which is extended either automatically or manually; the passage of air over the turbine is used to power a small emergency generator ordinarily rated between 5-15 kVA which supplies essential flight instruments and other critical services. The RAT also powers a small hydraulic power generator for similar hydraulic system emergency power provision.

The deployment of the RAT should only occur during extreme emergency conditions, and aircraft certification directives dictate that additional methods of backup electrical power supply should be implemented prior to the RAT [D.7]. The hierarchical form of generation redundancy involves backup generators for AC load provision which are driven by the same engine accessory gearboxes as the main engines (but independent of the main generators[17]), and permanent magnet generators (PMG) rated in the order 10^2 Watts for backup DC load provision.

D.4 Conventional EPS Example

To illustrate the design and operation of conventional aircraft EPS, the complete electrical distribution system of the B777 is described in the following.

D.4.1 B777 Electrical Power System

The Boeing 777 is a large twin engine jet designed for regional and longer range operations [D.8]. The B777's first flight was completed in 1994 before its introduction to the market in 1995. A simplified schematic of the complete B777 EPS [D.9, D.10, D.11, D.12] is provided in Figure D-4. There are two electrical generation systems, a main system and a backup system. Within the main system, the two propulsion engines each drive a 120kVA IDG, which output three phase 115VAC, 400Hz power. The two IDGs serve their respective primary bus through GCBs. Generator control units (GCUs)

---

[17] ~20kVA variable frequency generators with backup constant frequency converters.

control the operation of the GCBs by closing them when all operating parameters are satisfactory and opening them when generator fault conditions prevail. The two primary buses are connected through BTB. In the event of the loss of one IDG, the BTB automatically closes, powering both primary buses from the operational IDG. Each 120kVA rated IDG has the capacity to power all electrical loads.

In addition to the two IDGs, a 120kVA generator is connected to the APU (there is no requirement for an IDG as the APU operates at constant RPM). This generator is connected between the BTB through an auxiliary power breaker (APB). With an IDG inoperative, the APU generator can supply the respective primary bus through the APB and BTB (whilst the other BTB remains open). The aircraft can therefore be dispatched with only one IDG operative. During ground operation, an external power receptacle provides 115VAC 400HZ to the primary buses.

The backup generation system comprises one 20kVA variable frequency generator on each engine. Backup generators are directly connected to the engine gearbox with no speed conversion. The purpose of the backup system is to provide equivalent redundancy in the event of main generation system failure. The generator outputs are directly connected to a solid-state variable speed constant frequency (VSCF) converter, which outputs the nominal 115VAC, 400Hz to respective transfer buses. Power from the backup generator can then be distributed through the transfer bus. Backup sources supply power during IDG failure, although only in the event that the APU is not servicing the primary bus of the failed IDG. In emergency situations, the RAT generator will supply up to 7.5kVA to the transfer buses.
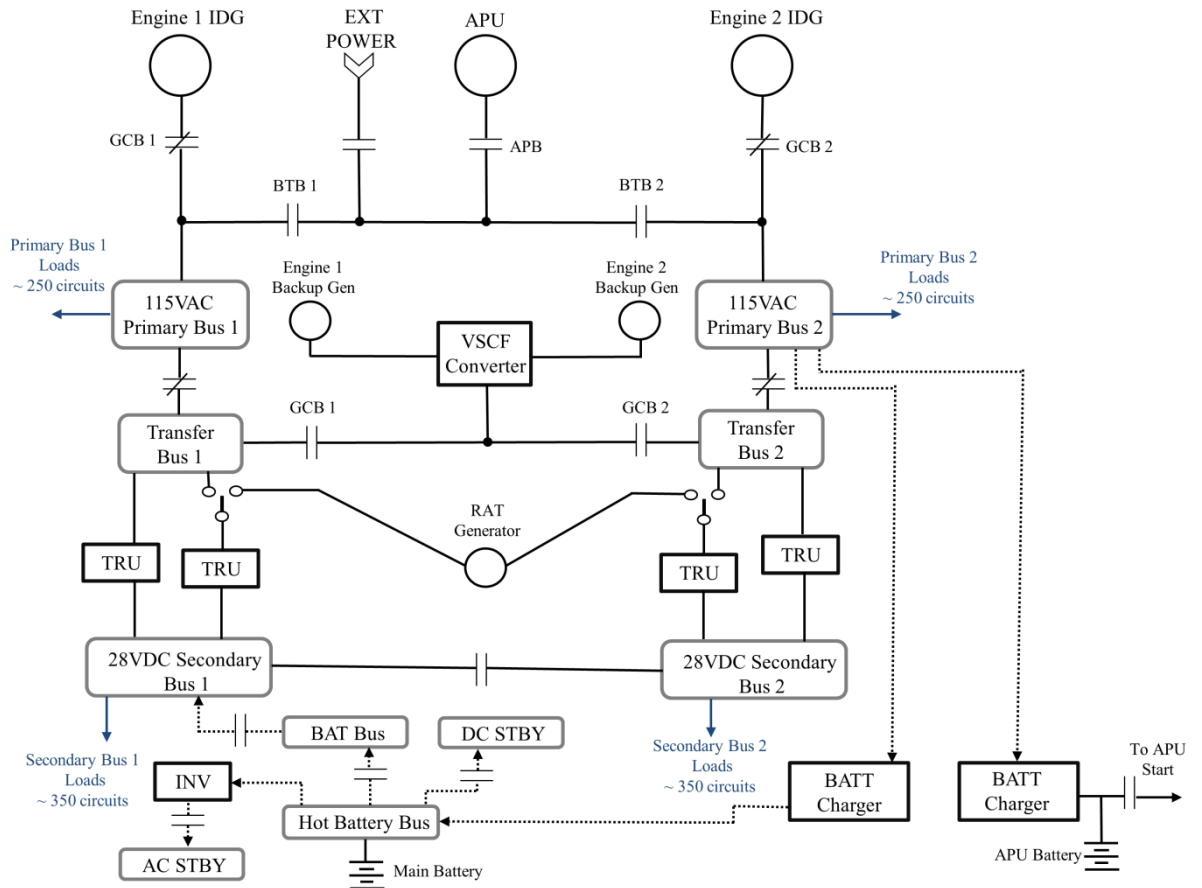
Figure D-4: Simplified schematic of the B777 EPS

The function of the transfer buses is to distribute power to the DC system through TRUs. Power is supplied to the transfer buses from the primary buses or, in the event of IDG/APU failure, from the backup converters or RAT generator. TRUs convert the three phase AC power supplied by the transfer bus into 28VDC power for distribution to the secondary power DC buses. DC bus ties enable power to flow between the two buses in the event of TRU or transfer bus failure.

The battery system is located in the DC network. Battery chargers connect directly to a hot battery bus and maintain the battery charge. The battery powers a standby electrical system during primary electrical system failures. The standby system powers critical DC loads such as flight instruments as well as an inverter for the provision of power to critical AC loads. The B777 main battery has a 47 A/h capacity and can supply critical standby loads for up to 30 minutes. The system also consists of an APU battery which is connected to a separate battery charger through an APU battery bus. The APU battery is a source of dedicated power for the APU electric starter.

D.5 Conventional Electrical Loads

The electrical distribution system supplies the generated power to the aircraft services. Electrically powered services in conventional systems are spread geographically throughout the aircraft and can be broadly subdivided into four categories [D.1]:

- Motors and actuation
- Lighting services
- Heating services
- Subsystem controllers and avionics

Higher power services will be located and supplied by the primary distribution bus while the lower rated services will be supplied by lower voltage levels at the secondary buses. Generally speaking, utility and galley loads such as lighting and heating services are often located at the primary bus, while avionic loads are serviced by the secondary bus. Further information on the function of each electrical service category is provided in the following sections.

D.5.1 Motors and Actuation

Motors are used to drive and position valves and actuators throughout the aircraft. The major motor driven sub-systems include:

- Starter motors for provision of starting power for engine, APU and other systems that require assistance for self-sustaining operation
- Pumps - The provision of motive force for fuel and hydraulic pumps
- Control valve operation – electrical operation of fuel, hydraulic and air control valves
- Fan motors for provision of cooling power to both passengers and equipment
- Gyroscope motors – power to run gyroscopes for flight instruments and auto pilot

These sub-systems use a combination of AC and DC motors. DC motors are used for operations which operate for a small proportion of flight time while AC motors are typically used in continuously operational functions like fan and gyroscope motors.

D.5.2 Lighting Services

Lighting is essential for the safe operation of aircraft during night or low visibility conditions. Conventional filament bulbs, powered from either 28VDC or transformed 26VAC from the primary AC bus, are typically used to provide this service. Lighting systems are categorised as either external or internal. External lighting services function to provide:

- Navigation lights
- Landing/Taxi lights
- Formation lights
- Inspection lights for wings and engine anti-icing
- Emergency evacuation lights
- Searchlights

Internal lighting services provide:

- Cockpit/flight deck lighting
- General Cabin lighting
- Emergency/evacuation lighting
- Bay lighting for servicing cargo or equipment bays

D.5.3 Heating Services

Electrical heating is used in various areas of the aircraft. The highest power usage (often 10s of kVAs) is in anti/de-icing systems for the tail plane and fin leading edges, intake cowls and propellers. Electrical heating is combined with bleed air de-icing and are controlled to ensure optimum operation periods and avoid overheating. Electrical heating is also used in windshield de-icing in the cockpit and air heating of cargo compartments and passenger cabins.

D.5.4 Subsystem Controllers and Avionics

The aircraft avionic systems comprise display, communication and navigation functions. Avionics are lower power loads supplied from the 28VDC secondary bus. These loads contain internal dedicated controllers for specific control functions and are packaged into line replaceable units (LRUs). The internal controllers allow power to be further conditioned according to the type of electronics - usually, this involves converting the 28VDC to ±15VDC or +5VDC. The LRUs enable increased modularity and hence rapid replacement and turnaround in the event of faults. There are hundreds of LRUs throughout the aircraft, the majority of which are critical for safe operation. Consequently, the critical LRUs should be distributed across several busbars to ensure sufficient supply redundancy. The provision of emergency power to LRUs should also be guaranteed to maintain critical services during emergency situations.

D.6 MEA Electrical Loads

A fundamental aspect of MEA concerns the different loads which the increased generation and distributed power will service. In essence, a high proportion of novel electrical loads in MEA will be motor loads, with the remainder functioning as power supplies for avionics and radar systems. This section briefly introduces the type and function of new electrical loads which demand significant levels of highly reliable electrical power. To illustrate, two systems expected to consume additional electrical load in future aircraft, actuation systems and environmental control systems (ECS), are summarised.

D.6.1 More-Electric Actuation

Conventionally, actuation processes of flight control surfaces were controlled mechanically through mechanical cables and activated hydraulically through a central hydraulic system. *Fly-by-wire* technology, where actuators are controlled electrically as opposed to mechanically, was developed in the 1980's and became the industry standard for modern jetliners [D.13].

The concept of using electrical power for actuation as well as control is attractive in terms of potential aircraft level weight reductions through the elimination of the centralised hydraulic network. Ultimately, it is perceived that aircraft will integrate electro-mechanical actuators (EMA) [D.14] to realise the complete elimination of all on-board hydraulic devices along with the centralised network. However, in the intermediate time, electro-hydrostatic actuator (EHA) technology [D.15] is the preferred choice for air framers as they retain many of the characteristics and advantages of conventional hydraulic actuators and their implementation requires minimal change in system definition [D.16].

EHAs drive control surfaces using localised hydraulic power transformed from electrical power. This *power-by-wire* concept utilises an electrical motor to drive a hydraulic pump which controls fluid pressure and an actuator. The self-contained nature of the hydraulic fluid within this configuration means that significant pressure is only required for movement, resulting in an energy saving over the conventional hydraulic servo actuator which maintains pressure when holding [D.16]. Also, safety advantages entail from the utilisation of less hazardous fluids in localized systems. Indeed, the A380 has employed the use of EHA for the ailerons and elevators and back-up for the rudders and spoilers [D.17].

EHA technology is considered a stop gap for pure electrical actuation. The EMA – an electric motor, gearbox and mechanical actuator – has the potential to be more compact and weight saving than the EHA through the elimination of the hydraulic reservoir. Their adoption on aircraft has been hampered by their relatively poor power density and reliability concerns over jamming [D.17]. EMA are present in the A380 slat actuation and the B777 flap/slat actuation, albeit operating redundantly with hydraulic motors – also, flap/slat systems are not safety critical as continued flight and safe landing is guaranteed in the event of a failure.

The reliability and fault tolerance issues of EMA highlight that the integration of electrical actuation systems across primary and secondary flight controls is dependent on technological maturation in both motor and power electronics. However, it is also evident that actuation is a particular area of the aircraft where novel electrical loading will significantly increase throughout future generations.

D.6.2 Environmental Control Systems

The reduction/elimination of bleed air (BA) extraction from the aircraft's engines requires the environmental control system (ECS), the largest user of BA, to be alternatively sourced via electrical power [D.1, D.18]. Conventionally[18], BA enters the ECS where it is cooled by an air cycle machine which outputs pressured air to the cabin equivalent to 6000ft altitude. Within more-electric ECS (MECS), permanent magnet motors drive air compressors (in the B787 there are four separate compressors) where each motor drive is a high rated load in the order of 100-125kVA. The compressed air is fed to primary and secondary heat controllers which use external RAM air as a heat sink. The resultant cold air is mixed with recirculation air to maintain the desired cabin temperature.

---

[18] ECS design is dependent on the aircraft type and mission profile. This is only a general outline.

Despite the high power demand of MECS, there are significant benefits associated with its adoption. Conventional systems draw bleed air at ~400ºF and 30 psi[19] – the conditioned air output to the cabin is ~60ºF and 11.8 psi. In comparison, MECS inputs compressed air at roughly half the temperature (~200ºF) and half the pressure (15 psi) whilst outputting similarly conditioned air. The difference in energy expended between the two systems is marked – this difference represents energy loss and waste [D.1].

In other words, the replacement of BA derived ECS with electrically powered ECS culminates in a potentially more energy efficient system. However, again, caveats concerning the efficiency at aircraft level should be issued. The MECS will likely introduce additional weight to the system. The management of such efficiency and weight trade-offs are beyond the scope of this particular discussion. What can be dissected from this brief summary is that motor dives in MECS will represent significant additional load within modern aircraft EPS.

D.7 More Electric Aircraft EPS Architectures

The MEA concepts and technologies previously described are illustrated with a discussion of the A380 and B787 electrical systems – two MEA currently in service. Comparing these two systems with the conventional B777 system highlights the increased capacity and criticality of EPS within the MEA.

D.7.1 Airbus A380 EPS

The A380 was the first modern aircraft to re-adopt VF distribution. The simplified EPS architecture is illustrated in Figure D-5. The four main engine driven generators are rated at 150kVA each and provide 230VAC VF power to their respective primary distribution bus. Two 120kVA rated CF APU's constitute the main generation system. A 70kVA RAT functions as emergency power provision. The VF supply dictates that the four primary AC buses cannot be paralleled. Galley loads with a typical total demand ranging between 120-240kVA are split across the AC buses.

The AC buses feed the main DC system power conversion units. These units include three battery charge regulator units (BCRU) for supply to each of the three 50Ah batteries, one TRU and one static inverter. The DC system has a no-break power capability whereby key aircraft systems operate without power interruptions. The architecture of this system is such that the AC1/AC4 buses feed the DC ESS and the AC2 and AC3 respectively feed the DC1 and DC2 buses that are regulated to 28VDC by the BCRUs. The DC ESS bus feeds the AC EMER bus through a static inverter. The AC EMER bus can also be supplied by the RAT through an AC ESS bus. There is a dedicated APU starter subsystem provided by charging the 50Ah battery from the AC4 bus through the APU TRU.

System segregation allows three independent channels of power, each with an associated main generator, BCRU and battery. Segregation maximises EPS redundancy.

---

[19] Pounds per square inch

Figure D-5: Simplified A380 EPS Architecture

The switching and protection of loads is undertaken in separate electrical panels throughout the aircraft. These are summarised as follows:

- 1 × integrated primary power distribution centre
- 2 × secondary electrical power distribution centres to distribute power to loads rated < 5kVA
- 6 × secondary electrical power distribution boxes for power to non-critical domestic loads. These loads include galleys, cabin lighting (~ 15kVA), galley cooling ~ 90kVA and in-flight entertainment ~ 50-60kVA
- SSPCs for switching and protection are preferred to thermal circuit breakers within the secondary power distribution centres and boxes

D.7.2 Boeing 787 EPS

The B787 entered service in 2011. Its design is widely regarded as being a significant step towards the AEA where bleed air systems have essentially been eliminated and a large number of hydraulic actuators are powered electrically.

The B787 EPS is outlined in Figure D-6. The two main engines each have two VF 250kVA rated generators, resulting in 500kVA of generated power per engine and the APU engine drives two 225kVA starter/generators. Total electrical generation on the B787 accumulates to 1.5MW, significantly higher than any previous civil aircraft.
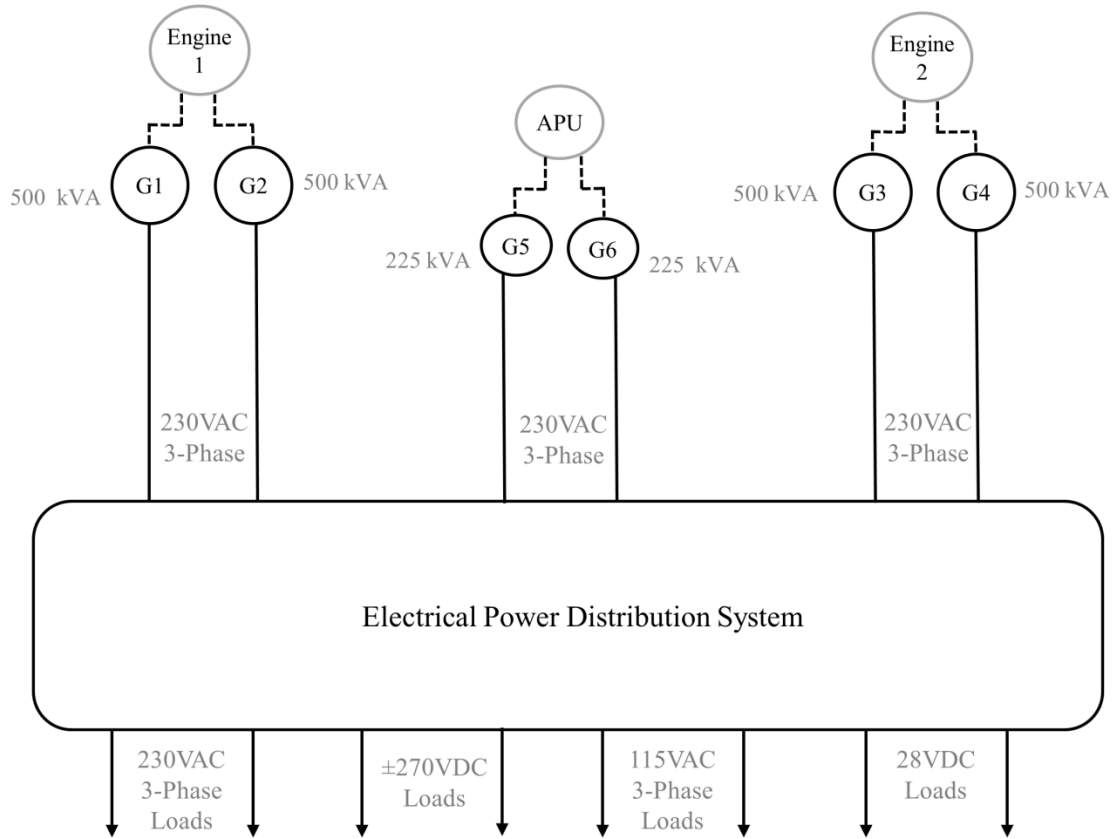
Figure D-6: Outline of the B787 EPS

Each main generator feeds its own primary 230VAC bus, where loads are either directly connected or power is converted for further distribution. The large loads driven from the 230VAC bus are usually interfaced with DC link converters to convert the VF to CF for speed control of load motors. Legacy distribution levels of 115VAC and 28VDC levels are attained through autotransformers and TRUs respectively.

A unique feature of the B787 is the conversion of 230VAC into ±270VDC using an ATRU. The ±270VDC levels have an additional zero volt return cable equating to a total potential difference of 540VDC. The ±270VDC levels power large variable speed loads such as the ECS compressor.

The main advancement of the B787 SPDS is the removal of bleed air for supply to the ECS, cabin pressurisation systems and wing anti-icing systems – the only bleed air taken from the engine is used for anti-icing of the engine cowl. The BA systems have largely been replaced with electrically driven systems. The main novel electrical loads within the B787 system include:

- *Environmental Control System and Pressurisation* – four large electrically driven compressors are required for ECS and cabin pressurisation. The compressors consume a total of ~ 500kVA.
- *Wing Anti Icing* – provided by electrical heating mats and requiring ~ 100kVA.
- *Electric Motor Pumps* – four electrical motors replace some of the accessory driven hydraulic pumps. Each pump is rated at 100kVA

The electrical system has a geographically distributed architecture. Four main primary distribution panels (two in the forward and two in the aft electrical bays) contain the electrical motor pumps and the main engine and APU starter motor controllers. Electrically powered air conditioning packs and motor compressors are located in the centre section of the aircraft while twenty-one separate remote power distribution units provide secondary power distribution.

This brief summary of the B787 highlights the more electric features of the SPDS. The removal of bleed air systems is the predominant feature of this revolutionary aircraft. This redesign impacts significantly on electrical system generation, demand, and topology. The B787 has set the more-electric benchmark from which future aircraft will evolve.

D.8 Bibliography for Appendix D

[D.1] I. Moir and A. Seabridge, *Aircraft systems: mechanical, electrical and avionics subsystems integration*, vol. 21. John Wiley & Sons, 2008.

[D.2] M. Dechow and C. A. H. Nurcombe, 'Aircraft environmental control systems', in *Air Quality in Airplane Cabins and Similar Enclosed Spaces*, pp.3-24, Springer, 2005.

[D.3] 'Aircraft environmental control system'. [Online]. Available: http://webserver.dmt.upm.es/~isidoro/tc3/Aircraft%20ECS.pdf. [Accessed:17-Dec-2014].

[D.4] P. Stricker, 'Aircraft Hydraulic System Design', 2010.

[D.5] 'SKYbrary - Hydraulic Systems'. [Online]. Available: http://www.skybrary.aero/index.php/Hydraulic_Systems. [Accessed: 18-Dec-2014].

[D.6] M. Koerner, 'Recent developments in aircraft emergency power', in *Energy Conversion Engineering Conference and Exhibit, 2000. (IECEC) 35th Intersociety*, Nevada, USA, 2000, pp. 12–19.

[D.7] X. Roboam *et al.*, 'Hybrid power generation system for aircraft electrical emergency network', IET Electr. Syst. Transp., vol. 1, no. 4, pp. 148–155, 2011.

[D.8] 'Boeing: 777'. [Online]. Available: http://www.boeing.com/boeing/commercial/777family/. [Accessed: 19-Dec-2014].

[D.9] L. Andrade and C. Tenning, 'Design of Boeing 777 electric system', *IEEE Aerosp. Electron. Syst. Mag.*, vol. 7, no. 7, pp. 4–11, 1992.

[D.10] 'Boeing B777 - Systems Summary (Electrical)'. [Online]. Available: http://www.smartcockpit.com/plane/BOEING/B777.html. [Accessed: 05-Dec-2014].

[D.11] 'Boeing 777 Specifications'. [Online]. Available: http://www.brandweerschiphol.nl/luchtvaart/instructie-aircraft-crash-recovery-guide/boeing/boeing_777_03.pdf. [Accessed: 02-Dec-2014].

[D.12] 'Lufthansa Technical Training Manual - B777'. [Online]. Available: https://www.scribd.com/doc/105499684/75/RAT-Generator. [Accessed: 02-Dec_2014].

[D.13] 'Fly-By-Wire'. [Online]. Available: http://www.airbus.com/innovation/proven-concepts/in-design/fly-by-wire/. [Accessed: 09-Apr-2015]

[D.14] 'More electric aircraft are not without their challenges'. [Online]. Available: http://articles.sae.org/11465/. [Accessed: 09-Apr-2015]

[D.15] K. Rongjie et.al, 'Design and simulation of Electro-hydrostatic actuator with a built in power regulator', Journal of Aeronautics, vol.22, no.6, pp.700-706, 2009.

[D.16] P.M. Churn et.al, 'Electro-hydraulic actuation of primary flight control surfaces', *IEE coll. All electric aircraft, London*, UK, 1998

[D.17] J.W. Bennett et.al, 'Safety critical design of electromechanical actuation systems in commercial aircraft', IET Electric Power Applications, vol.5, no.1, pp.37-47, 2011.

[D.18] L.B. Buss, 'Electric aeroplane environmental control systems energy requirements', IEEE Trans. Aerosp. Electron. Syst., vol.20, no.3, pp.250-256, 1984.